Summer 2013

Novel Computational Methods for Solving High-Dimensional Random Eigenvalue Problems

Vaibhav Yadav
University of Iowa

NOVEL COMPUTATIONAL METHODS FOR SOLVING HIGH-DIMENSIONAL RANDOM EIGENVALUE PROBLEMS

by

Vaibhav Yadav

A thesis submitted in partial fulfillment of the
requirements for the Doctor of Philosophy
degree in Mechanical Engineering
in the Graduate College of
The University of Iowa

August 2013

Thesis Supervisor: Professor Sharif Rahman

Graduate College
The University of Iowa
Iowa City, Iowa

CERTIFICATE OF APPROVAL

PH.D. THESIS

This is to certify that the Ph.D. thesis of

Vaibhav Yadav

has been approved by the Examining Committee for the thesis requirement for the Doctor of Philosophy degree in Mechanical Engineering at the August 2013 graduation.

Thesis Committee: _____
Sharif Rahman, Thesis Supervisor

_____
Salam Rahmatalla

_____
Osnat Stramer

_____
Shaoping Xiao

_____
Olesya I. Zhupanska

To Vaidehi

ACKNOWLEDGEMENTS

It gives me immense pleasure to thank a number of people who contributed to the completion of this thesis. First and foremost, I offer my sincerest gratitude to my supervisor, Prof. Sharif Rahman, for his constant guidance and support. He has the unique quality of letting you work in your own way and bringing the best out of you. I am proud to have had Prof. Rahman as my advisor and mentor.

My deepest gratitude goes to the members of my committee, Prof. Salam Rahmatalla, Prof. Osnat Stramer, Prof. Shaoping Xiao, and Prof. Olesya I. Zhupanska, for their valuable insights and suggestions to make this thesis better.

I am thankful to the staff members of the Department of Mechanical Engineering, and the staff members of the Center for Computer Aided Design for their help during the last five years. Special thanks goes to Ms. Melanie Laverman for making editorial corrections to refine this thesis.

No words can express my gratitude towards my parents who have supported me all throughout my life and even more strongly during the course of this thesis. This thesis is only a manifestation of their lifelong dreams. A very special thanks goes to my brother Akshay for being a constant source of cheer and optimism. My mother-in-law and father-in-law deserve a distinct gratitude for their overwhelming support and encouragement. Last but not least, I am deeply thankful to my wonderful wife Kalyani for always being a rock solid source of strength and inspiration to me, when all I could do for her was explain random eigenvalues.

I would like to acknowledge the financial support for this work from the US National Science Foundation under Grant Nos. CMMI-0653279 and CMMI-1130147.

ABSTRACT

The primary objective of this study is to develop new computational methods for solving a general random eigenvalue problem (REP) commonly encountered in modeling and simulation of high-dimensional, complex dynamic systems. Four major research directions, all anchored in polynomial dimensional decomposition (PDD), have been defined to meet the objective. They involve: (1) a rigorous comparison of accuracy, efficiency, and convergence properties of the polynomial chaos expansion (PCE) and PDD methods; (2) development of two novel multiplicative PDD methods for addressing multiplicative structures in REPs; (3) development of a new hybrid PDD method to account for the combined effects of the multiplicative and additive structures in REPs; and (4) development of adaptive and sparse algorithms in conjunction with the PDD methods.

The major findings are as follows. First, a rigorous comparison of the PCE and PDD methods indicates that the infinite series from the two expansions are equivalent but their truncations endow contrasting dimensional structures, creating significant difference between the two approximations. When the cooperative effects of input variables on an eigenvalue attenuate rapidly or vanish altogether, the PDD approximation commits smaller error than does the PCE approximation for identical expansion orders. Numerical analysis reveal higher convergence rates and significantly higher efficiency of the PDD approximation than the PCE approximation. Second, two novel multiplicative PDD methods, factorized PDD and logarithmic PDD, were

developed to exploit the hidden multiplicative structure of an REP, if it exists. Since a multiplicative PDD recycles the same component functions of the additive PDD, no additional cost is incurred. Numerical results show that indeed both the multiplicative PDD methods are capable of effectively utilizing the multiplicative structure of a random response. Third, a new hybrid PDD method was constructed for uncertainty quantification of high-dimensional complex systems. The method is based on a linear combination of an additive and a multiplicative PDD approximation. Numerical results indicate that the univariate hybrid PDD method, which is slightly more expensive than the univariate additive or multiplicative PDD approximations, yields more accurate stochastic solutions than the latter two methods. Last, two novel adaptive-sparse PDD methods were developed that entail global sensitivity analysis for defining the relevant pruning criteria. Compared with the past developments, the adaptive-sparse PDD methods do not require its truncation parameter(s) to be assigned a priori or arbitrarily. Numerical results reveal that an adaptive-sparse PDD method achieves a desired level of accuracy with considerably fewer coefficients compared with existing PDD approximations.

TABLE OF CONTENTS

LIST OF TABLES

Table

LIST OF FIGURES

Figure

CHAPTER 1
INTRODUCTION

1.1 Background and Motivation

Random eigenvalue problems (REPs) are concerned with determining the probabilistic characteristics of eigenvalues and eigenvectors of random matrices [2]. First introduced by Wishart [3] in 1928, random matrices are the matrices that are completely defined by statistical distributions. The study of random matrices gained prominence in the 1950s, spurred by Wigner's [4] pioneering work in nuclear physics. The mathematical foundation of the random matrix theory was later established in a series of landmark papers by Wigner [5], Mehta [6], and Dyson [7]. A comprehensive account of random matrices can be found in Mehta's seminal work [8]. Random matrices have far-reaching applications in fields as diverse as quantum physics [9–11], number theory [12–14], multivariate statistics [15–17], graph theory [18, 19], signal processing and communication [20, 21], finance [22, 23], computational biology [24], and, of course, mechanics [25–38].

In mechanics, random matrices prominently appear in structural dynamics and structural stability, among others. The solutions may represent oscillatory modes of a mechanical system, bifurcation and instability of a structure, disposition of electrons around an atom or a molecule, acoustic modes of a concert hall, and numerous other physical quantities of interest. The evaluation of modal frequencies and buckling capacity of mechanical systems involves solution of eigenvalue problems for stochastic

differential operators and stochastic matrices. The randomness in these operators or matrices comes from the statistical variability of material properties, system geometry, and boundary conditions. The texts by Boyce [29] and Scheidt and Purkert [26], as well as the papers by Ibrahim [32], Benaroya [27], Manohar and Ibrahim [34], and others [28, 37, 38], are useful information sources on early work in this research area and also provide a systematic account of various approximate methods for solving REPs. Some later works, for example those by Nair and Keane [36], Pradlwarter and Schuëller [39], Adhikari [25] and Rahman [40–42], summarize current progress, including developments of new computational methods. Indeed, studying REP has been identified as an important research topic in the field of stochastic mechanics [43].

For practical problems, an REP may encounter very large matrices. Due to domain discretization by the finite element method (FEM), random matrices containing millions to billions of degrees of freedom are not uncommon. Such systems also depend on a very large number, say 100 or 1000, of random input parameters. Dealing with such large-dimensional input parameters involves encountering the curse of dimensionality, the phenomenon in which the computational effort grows exponentially with respect to the dimension. Most of the existing methods for solving REPs have major limitations in handling such large and complex systems. Taylor series or perturbation methods [29,37,38] and the polynomial chaos expansion (PCE), introduced by Wiener [44], are the two most popular methods among the existing approximation methods for solving REPs. The perturbation methods involve first- or second-order Taylor series expansions of the eigenvalue or eigenvector in terms of the input random

parameters. These methods have two major limitations: the variability or randomness in the input parameters should be small, and the non-linearity of the random eigenvalues and eigenvectors with respect to the input parameters must also be small. These two limitations pose a major hurdle in applying the perturbation method to large-scale REPs, since the engineering problems could have both: input parameters with large variability and a system with high non-linearity. The PCE method is a promising method available today for dealing with engineering REPs. This method is based on the expansion of the eigenvalue and eigenvector with respect to the input parameters with increasing order. For a high-dimensional problem, again, this method succumbs to the curse of dimensionality, as its computational requirements increase at a prohibitively fast pace with respect to the dimension. Furthermore, most existing methods, including the Taylor expansion and PCE method, delve into calculating only the second moment statistics of eigensolutions. The resultant tail probabilistic characteristics, highly important for reliability analysis and design, have not been adequately scrutinized. The major motivation for this work is to develop methods of solving REPs that can address the two biggest limitations of the present methods: (1) countering the curse of dimensionality to some extent, and (2) calculating the statistical moments as well as rare event probabilities of eigenvalues and eigenvectors with high accuracy and/or high efficiency.

1.2 Objective of the Study

The primary objective of this study is to develop new computational methods for solving a general REP commonly encountered in modeling and simulation of high-dimensional complex dynamic systems. Four major research directions, all anchored in polynomial dimensional decomposition (PDD), have been defined to meet the objective. They involve: (1) a rigorous comparison of accuracy, efficiency, and convergence properties of the PCE and PDD methods; (2) development of two novel multiplicative PDD methods for addressing multiplicative structures in REPs; (3) development of a new hybrid PDD method to account for the combined effects of the multiplicative and additive structures in REPs; and (4) development of adaptive and sparse algorithms in conjunction with the PDD methods.

1.3 Overview of the Thesis

The thesis proposal is organized as follows. Chapter 2 presents the preliminaries of probability theory. This chapter also discusses the state-of-the-art review of the existing methods for solving REPs. A brief review of the cutting-edge numerical algorithms of eigenvalue analysis is also presented. Finally, the needs for fundamental research are outlined.

Chapter 3 presents a rigorous comparison of the PCE and PDD methods for solving REPs. Five numerical examples are presented to illustrate the differences in accuracy, efficiency, and convergence properties of the two methods.

Chapter 4 introduces two novel multiplicative decomposition methods for solv-

ing REPs. Two variants of the multiplicative decomposition were developed: the factorized PDD (F-PDD) method and the logarithmic PDD (L-PDD) method. Three numerical examples were solved by the proposed methods, and the results are compared with the existing additive PDD (A-PDD) method. The proposed method was applied to obtain random eigensolutions of a high-dimensional vehicle dynamics problem.

Chapter 5 presents a new hybrid PDD method, developed as a linear combination of additive PDD and multiplicative PDD. Two numerical examples were solved by the proposed method, and the performance of hybrid PDD in determining the probabilistic characterisitics of random functions was compared with the performance of additive and multiplicative PDD methods. The proposed method was applied for stochastic eigenvalue analysis entailing high-dimensional coupled acoustic-structural behavior of a pickup truck.

Chapter 6 presents a new adaptive-sparse PDD method. This chapter also presents an efficient sparse-grid integration technique for performing high-dimensional numerical integrations encountered in calculating the PDD expansion coefficients. Three numerical examples were solved to illustrate the accuracy, efficiency, and covergence of the new method. The proposed method was applied for stochastic eigenvalue analysis of a high-dimensional disk brake system.

Finally, conclusions are drawn and future research directions are suggested in Chapter 7.

CHAPTER 2
STATE-OF-THE-ART REVIEW

This chapter presents existing mathematical theories, methods, and algorithms, elucidating those widely employed for solving REPs, and then discusses the need for fundamental research. Section 2.1 presents the preliminaries of probability theory. The REP is defined along with its applications in dynamical systems in Section 2.2. Section 2.3 contains the state-of-the-art review of the existing methods for solving REPs. A brief review of the cutting-edge numerical algorithms of eigenvalue analysis is presented in Section 2.4. Finally, the needs for fundamental research are outlined in Section 2.5.

2.1 Mathematical Preliminaries

Modeling of any engineering phenomenon while incorporating the inherent randomness requires a thorough understanding of probability theory. This section presents some fundamentals of probability theory that are imperative and relevant for solving any REP.

2.1.1 Probability space

Each time a random experiment is performed, there are a number of possible outcomes. The sample space Ω of a random experiment is a collection of all possible outcomes of the random experiment. The σ-field (or σ-algebra) $\mathcal{F}$ is a non-empty collection of subsets of Ω that satisfy the following:

1. The empty set $\varnothing \in \mathcal{F}$.

2. Any event $A \in \mathcal{F}$, then $A^C \in \mathcal{F}$.

3. If $A_i \in \mathcal{F}$ is a countable sequence of sets, then $\cup_i A_i \in \mathcal{F}$.

The probability measure P is a set function defined on $\mathcal{F}$ that has the following properties:

1. For any event A in $\mathcal{F}$, $0 \leq P(A) \leq 1$.

2. $P(\Omega) = 1$, and $P(\phi) = 0$, where ϕ denotes the empty set.

The probability space is defined as a triple $(\Omega, \mathcal{F}, P)$ where Ω is the set of outcomes, $\mathcal{F}$ is the set of events, and $P : \mathcal{F} \to [0, 1]$ is a function that assigns probabilities to the events. A special case of σ-field $\mathcal{F}$ is the Borel σ-field $\mathcal{B}$ that is generated by the collection of open sets of a space Ω [31].

2.1.2 Random variable

Consider a probability space $(\Omega, \mathcal{F}, P)$; then every elementary event $\omega \in \Omega$ has an associated real number $X(\omega)$ called the random variable in $(\Omega, \mathcal{F}, P)$. For a continuous random variable X, the cumulative distribution function (CDF), or just the distribution function, denoted by $F_X(x)$, describes the probability that the real-valued random variable X will be found at a value less than or equal to x, i.e., $F_X(x) := P(X \leq x)$, and the probability density function (PDF) $f_X(x) := dF_X(x)/dx$. The probability for the random variable to fall within a particular region is given by the integral of this variable's PDF over the region, i.e., $P[a \leq X \leq b] = \int_a^b f_X(x)\,dx$ where $a \in \mathbb{R}$, $b \in \mathbb{R}$, $b \geqslant a$. The probability density function is

nonnegative everywhere, and its integral over the entire space is equal to one. The l^{th} statistical moment of a random variable is defined as

$$m_l = \mathbb{E}\left[X^l\right] = \int_{\mathbb{R}} x^l \, f_X(x) \, dx, \tag{2.1}$$

where $\mathbb{E}$ is the expectation operator, and the integral is a definite integral taken for x over the range of X. The first moment m_1 of a random variable X is called its mean $\mu_X := \mathbb{E}[X] := \int_{\mathbb{R}} x \, f_X(x) \, dx$. The variance of X, σ_X^2 is its second moment about the mean μ_X and is defined as $\sigma_X^2 := \mathbb{E}\left[(X - \mu_x)^2\right] := \int_{\mathbb{R}} (x - \mu_x)^2 \, f_X(x) \, dx$; here σ_X is called the standard deviation of X. Generally, the first two moments along with the PDF define the probability distribution of a random variable. This research involves systems with random input parameters following a variety of probability distributions like uniform, normal, lognormal, beta, etc., details of which can be found in the literature [45].

2.1.3 Random vectors

A random vector, also known as a multivariate random variable, is a column vector $\boldsymbol{X} = \{X_1, \ldots, X_N\}^{\mathrm{T}}$, whose components $X_1, \ldots, X_N$ are scalar-valued random variables on the same probability space $(\Omega, \mathcal{F}, P)$. The joint CDF, denoted by $F_{\boldsymbol{X}}(\boldsymbol{x})$, of $\boldsymbol{X}$ is defined by the mapping $\boldsymbol{X} : \Omega \to \mathbb{R}^N$ and the probability measure P, i.e., $F_{\boldsymbol{X}}(\boldsymbol{x}) := P\left(\cap_{i=1}^{N} \{X_i \leq x_i\}\right)$. If $F_{\boldsymbol{X}}(\boldsymbol{x})$ is such that $f_{\boldsymbol{X}}(\boldsymbol{x}) = \partial^N F_{\boldsymbol{X}}(\boldsymbol{x}) / \partial x_1 \cdots \partial x_N$ exists, then $f_{\boldsymbol{X}}$ is called the joint PDF of $\boldsymbol{X}$. The random variables belonging to a random vector are said to be independent when their joint PDF $f_{\boldsymbol{X}}(\boldsymbol{x})$ is a product of their marginal PDFs, i.e., $f_{\boldsymbol{X}}(\boldsymbol{x}) = \prod_{i=1}^{N} f_{X_i}(x_i)$. The expected value or mean $\boldsymbol{\mu}_{\boldsymbol{X}}$

of a random vector $\boldsymbol{X}$ is a fixed vector $\mathbb{E}(\boldsymbol{X})$ whose elements are the expected values of the respective random variables.

The covariance matrix, $\boldsymbol{\Sigma}_{\boldsymbol{X}} := \mathbb{E}\left[(\boldsymbol{X} - \boldsymbol{\mu}_X)(\boldsymbol{X} - \boldsymbol{\mu}_X)^{\mathrm{T}}\right]$, of a random vector is an $N \times N$ matrix whose i, j element is the covariance between the i^{th} and the j^{th} random variables. The covariance between the i^{th} and the j^{th} random variables is defined as $\mathrm{Cov}(X_i, X_j) := \mathbb{E}[(X_i - \mu_i)(X_j - \mu_j)]$. The variance of X_i is the i^{th} diagonal element of $\boldsymbol{\Sigma}_{\boldsymbol{X}}$. The correlation coefficient, $\rho_{ij} := \Sigma_{ij}/(\sigma_i \sigma_j)$, where $\sigma_i \neq 0$, $\sigma_j \neq 0$, between two random variables X_i and X_j measures the extent to which, as one variable increases, the other variable tends to increase. When X_i and X_j are independent, then X_i and X_j are uncorrelated, i.e., $\rho_{ij} = 0$. But if X_i and X_j are uncorrelated, then X_i and X_j are not necessarily independent.

2.1.4 Hilbert space

A Hilbert space is an abstract vector space possessing the structure of an inner product that allows length and angle to be measured. Hilbert spaces arise naturally and frequently in mathematics, physics, and engineering, typically as infinite-dimensional function spaces. A particular type of Hilbert space is the $\mathcal{L}_2$-space, which is defined as the set of all functions $f : \mathbb{R}^N \to \mathbb{R}$ such that the integral of the square of the absolute value of the function is finite, i.e., $\int_\Omega |f(\boldsymbol{x})|^2 f_{\boldsymbol{X}}(\boldsymbol{x}) d\boldsymbol{x} < \infty$. In this case, the inner product $\langle f, g \rangle := \int_\Omega f(\boldsymbol{x}) g(\boldsymbol{x}) f_{\boldsymbol{X}}(\boldsymbol{x}) d\boldsymbol{x}$ exists and is finite. In other words, in vectorial space $\mathcal{L}_2(\Omega, \mathcal{F}, P)$, the real random variables $\boldsymbol{X} \in \mathcal{L}_2$ exist with a finite second moment, i.e., $\mathbb{E}[X_i^2] < \infty$, $i = 1, \ldots, N$, and $\mathbb{E}[X_i X_j] < \infty$, $i, j = 1, \ldots, N$.

2.1.5 Random field

Consider a probability space $(\Omega, \mathcal{F}, P)$, where Ω is the sample space, $\mathcal{F}$ is the σ-field of subsets of Ω, and P is the probability measure. A random field $\alpha(\boldsymbol{x})$ on the probability space $(\Omega, \mathcal{F}, P)$, is a collection of random variables indexed by a k-dimensional continuous parameter $\boldsymbol{x} \in \mathcal{D} \subset \mathbb{R}^k$, where $\mathcal{D}$ is an open set describing the system geometry. For a given point $\boldsymbol{x}$ in $\mathcal{D}$, $\alpha(\boldsymbol{x})$ is a random variable. A random field is called weakly homogeneous if the mean and the standard deviation are constant and the covariance function is only a function of the difference, $\boldsymbol{x}_2 - \boldsymbol{x}_1$, between two points $\boldsymbol{x}_1$ and $\boldsymbol{x}_2$.

One of the major requirements for incorporating a random field in a discrete model like the finite element (FE) model is to discretize the continuous random field. Such discretization is commonly achieved by the Karhunen-Loève (K-L) representation of the random field. Let $(\Omega, \mathcal{F}, P)$ be a probability space. Defined on the probability space and indexed by a spatial coordinate $\boldsymbol{x} \in \mathcal{D} \subset \mathbb{R}^K$, $K = 1, 2$, or 3, consider a real-valued random field $\alpha(\boldsymbol{x})$ with mean *zero* and covariance function $\Gamma(\boldsymbol{x}_1, \boldsymbol{x}_2) \equiv \mathbb{E}[\alpha(\boldsymbol{x}_1)\alpha(\boldsymbol{x}_2)]$, which is continuous over $\mathcal{D}$. Denote by $\mathcal{L}_2(\Omega, \mathcal{F}, P)$, or simply $\mathcal{L}_2$, a collection of random variables α for each $\boldsymbol{x} \in \mathcal{D}$ such that $\mathbb{E}[|\alpha|^2] < \infty$. If α is in $\mathcal{L}_2$, then $\Gamma(\boldsymbol{x}_1, \boldsymbol{x}_2)$ is a square integrable and hence a bounded function.

Let $\{\beta_i, g_i(\boldsymbol{x})\}, i = 1, 2, \ldots, \infty$, be the eigenvalues and eigenfunctions of $\Gamma(\boldsymbol{x}_1, \boldsymbol{x}_2)$, which satisfy the integral equation

$$\int_{\mathcal{D}} \Gamma(\boldsymbol{x}_1, \boldsymbol{x}_2) g_i(\boldsymbol{x}_2) d\boldsymbol{x}_2 = \beta_i g_i(\boldsymbol{x}_1), \ \forall i = 1, 2, \ldots, \infty. \tag{2.2}$$

The eigenfunctions are orthogonal in the sense that

$$\int_{\mathcal{D}} g_i(\boldsymbol{x}) g_j(\boldsymbol{x}) d\boldsymbol{x} = \delta_{ij}, \ \forall i, j = 1, 2, \ldots, \infty, \tag{2.3}$$

where δ_{ij} is the Kronecker delta. The K-L representation of $\alpha(\boldsymbol{x})$ is

$$\alpha(\boldsymbol{x}) = \sum_{i=1}^{\infty} V_i \sqrt{\beta_i} g_i(\boldsymbol{x}), \tag{2.4}$$

where $V_i, i = 1, \ldots, \infty$ is an infinite sequence of uncorrelated random variables, each of which has *zero* mean and *unit* variance. In practice, the infinite series of Equation (2.4) must be truncated, yielding a K-L approximation or expansion

$$\hat{\alpha}_N(\boldsymbol{x}) = \sum_{i=1}^{N} V_i \sqrt{\beta_i} g_i(\boldsymbol{x}), \tag{2.5}$$

which approaches $\alpha(\boldsymbol{x})$ in the mean square sense for $\boldsymbol{x} \in \mathcal{D}$ as $N \to \infty$. According to Equation (2.5), the K-L expansion provides a parametric representation of a random field with N random variables.

The K-L expansion requires solution of an integral eigenvalue problem (Equation (2.2)), which is not an easy task in general. Closed-form solutions are only available when the covariance kernel has simpler functional forms, such as exponential and linear functions, or when domain $\mathcal{D}$ is rectangular [46–48]. Appendix A, for instance, describes the analytical solution for univariate random field and exponential covariance function. For arbitrary covariance functions or arbitrary domains, the FEM is often used to solve the eigenvalue problem. More recently, mesh-free and wavelet methods have been exploited in solving the integral eigenvalue problem [47, 48].

2.2 What is an REP?

Let $(\Omega, \mathcal{F}, P)$ be a complete probability space, where Ω is a sample space, $\mathcal{F}$ is a σ-field on Ω, and $P : \mathcal{F} \to [0, 1]$ is a probability measure. Let $\mathbb{R}^N$ and $\mathbb{C}^N$ be N-dimensional real and complex vector spaces, respectively, and $\mathbb{R}^{N\times N}$ a set of all $N \times N$, real-valued matrices. With $\mathcal{B}^N$ representing a Borel σ-field on $\mathbb{R}^N$ and $\mathbb{E}$ the expectation operator on $(\Omega, \mathcal{F}, P)$, consider an $\mathbb{R}^N$-valued, independent, input random vector $\{\boldsymbol{X} = \{X_1, \cdots, X_N\}^T : (\Omega, \mathcal{F}) \to (\mathbb{R}^N, \mathcal{B}^N)\}$, which has mean vector $\boldsymbol{\mu_X} := \mathbb{E}[\boldsymbol{X}] \in \mathbb{R}^N$, covariance matrix $\boldsymbol{\Sigma_X} := \mathbb{E}[(\boldsymbol{X} - \boldsymbol{\mu_X})(\boldsymbol{X} - \boldsymbol{\mu_X})^T] \in \mathbb{R}^{N\times N}$, and joint probability density function $f_{\boldsymbol{X}}(\boldsymbol{x}) = \Pi_{i=1}^{i=N} f_i(x_i)$, where $f_i(x_i)$ is the marginal probability density function of X_i defined on the probability triple $(\Omega_i, \mathcal{F}_i, P_i)$. In most dynamic systems, the vector $\boldsymbol{X}$ represents uncertainties in material parameters (*e.g.*, mass, damping, stiffness), geometry (*e.g.*, size, shape, topology), and constraints (*e.g.*, initial and boundary conditions). If some or all input variables are modeled as random fields, then $\boldsymbol{X}$ includes random variables due to their discretization.

Consider a family of $L \times L$, real-valued, random coefficient matrices $\boldsymbol{A}_j(\boldsymbol{X}) \in \mathbb{R}^{L\times L}$, $j = 1, \cdots, J$, where J is a positive integer and a general nonlinear function f . The probabilistic characteristics of $\boldsymbol{A}_j(\boldsymbol{X})$ can be derived from the known probability law of $\boldsymbol{X}$. A non-trivial solution of

$$f\left(\lambda(\boldsymbol{X}); \boldsymbol{A}_1(\boldsymbol{X}), \cdots, A_J(\boldsymbol{X})\right) \boldsymbol{\phi}(\boldsymbol{X}) = \boldsymbol{0}, \tag{2.6}$$

if it exists, defines the random eigenvalue $\lambda(\boldsymbol{X}) \in \mathbb{R}$ or $\mathbb{C}$ and the random eigenvector $\boldsymbol{\phi}(\boldsymbol{X}) \in \mathbb{R}^L$ or $\mathbb{C}^L$ of a general eigenvalue problem. Depending on the type of application, a wide variety of functions f and, hence, eigenvalue problems exist.

Table 2.1 lists a few examples of REPs frequently encountered in dynamic systems.

Table 2.1: Random eigenvalue problems in stochastic dynamical systems

Eigenvalue problem[(a)]	Problem type and application(s)
$[-\lambda(\boldsymbol{X})\boldsymbol{M}(\boldsymbol{X}) + \boldsymbol{K}(\boldsymbol{X})]\,\boldsymbol{\phi}(\boldsymbol{X}) = \boldsymbol{0}$	*Linear*; undamped or proportionally damped systems [49–53]
$\left[\lambda^2(\boldsymbol{X})\boldsymbol{M}(\boldsymbol{X}) + \lambda(\boldsymbol{X})\boldsymbol{C}(\boldsymbol{X}) + \boldsymbol{K}(\boldsymbol{X})\right]\boldsymbol{\phi}(\boldsymbol{X}) = \boldsymbol{0}$	*Quadratic*; non-proportionally damped systems, singularity problems [54–62]
$\left[\lambda(\boldsymbol{X})\boldsymbol{M}_1(\boldsymbol{X}) + \boldsymbol{M}_0(\boldsymbol{X}) + \boldsymbol{M}_1^T(\boldsymbol{X})/\lambda(\boldsymbol{X})\right]\boldsymbol{\phi}(\boldsymbol{X}) = \boldsymbol{0}$	*Palindromic*; acoustic emissions in high-speed trains [63–66]
$\left[\sum_k \lambda^k(\boldsymbol{X})\boldsymbol{A}_k(\boldsymbol{X})\right]\boldsymbol{\phi}(\boldsymbol{X}) = \boldsymbol{0}$	*Polynomial*; control and dynamics problems [56, 66–68]
$\left[\lambda(\boldsymbol{X})\boldsymbol{M}(\boldsymbol{X}) - \boldsymbol{K}(\boldsymbol{X}) + \sum_k \frac{\lambda^q(\boldsymbol{X})\boldsymbol{C}_k(\boldsymbol{X})}{a_k - \lambda(\boldsymbol{X})}\right]\boldsymbol{\phi}(\boldsymbol{X}) = \boldsymbol{0}$	*Rational*; plate vibration (q=1), fluid-structure vibration (q=2), vibration of viscoelastic materials [69–74]

[(a)] $\boldsymbol{M}(\boldsymbol{X})$, $\boldsymbol{C}(\boldsymbol{X})$, and $\boldsymbol{K}(\boldsymbol{X})$ are mass, damping, and stiffness matrices, respectively; $\boldsymbol{M}_0(\boldsymbol{X})$, $\boldsymbol{M}_1(\boldsymbol{X})$, $\boldsymbol{A}_k(\boldsymbol{X})$, and $\boldsymbol{C}_k(\boldsymbol{X})$ are various coefficient matrices.

In general, the eigensolutions depend on the random input $\boldsymbol{X}$ via solution of

the matrix characteristic equation

$$\det\left[f\left(\lambda(\boldsymbol{X}); \boldsymbol{A}_1(\boldsymbol{X}), \cdots, \boldsymbol{A}_J(\boldsymbol{X})\right)\right] = 0, \tag{2.7}$$

and subsequent solution of Equation (2.6). A major objective in solving an REP, linear or nonlinear, is to find the probabilistic characteristics of eigenpairs $\{\lambda_i(\boldsymbol{X}), \boldsymbol{\phi}_i(\boldsymbol{X})\}$, $i = 1, \cdots, L$, when the probability law of $\boldsymbol{X}$ is arbitrarily prescribed.

2.3 Methods of Random Eigenvalue Analysis

Existing methods for solving REPs can be grouped into five major classes: (1) asymptotic methods; (2) classical or elementary approximate methods; (3) dimensional decomposition methods; (4) polynomial chaos expansion methods; and (5) simulation and sampling methods. A brief review of each class of methods is presented as follows.

2.3.1 Asymptotic methods

Ever since the publication of Dyson's paper, the physics community has devoted much attention to three important Gaussian (also known as Hermite) ensembles: orthogonal, unitary, and symplectic [9]. If an $L \times L$ random matrix $\boldsymbol{G}$, comprising independent and identically distributed standard Gaussian elements $[G_{ij}]$, defines a Gaussian random matrix, then the symmetric $L \times L$ random matrix $\boldsymbol{A} = (\boldsymbol{G} + \boldsymbol{G}^T)/2$ is called the Gaussian orthogonal ensemble. There are complex and quaternion analogs of the Gaussian orthogonal ensemble, known as Gaussian unitary ensemble and Gaussian symplectic ensemble, respectively. For all three Gaussian ensembles, the joint probability density of eigenvalues can be derived asymptotically when $L \to \infty$ [8].

Asymptotic solutions also exist for other classical ensembles associated with the Wishart (or Laguerre) and the multivariate analysis of variance (or Jacobi) random matrices [75]. These important ensembles, also known as β-Hermite, β-Laguerre, β-Jacobi ensembles, are identified with discrete values of $\beta = 1$ (real), $\beta = 2$ (complex), and $\beta = 3$ (quaternion), respectively. Moreover, Dumitriu and Edelman [75] have advanced the idea that a unified, general β-theory exists from which discrete β-ensembles can be generated as special cases, a theory which researchers are only beginning to explore.

The success of the random matrix theory is due to the breakthrough discovery that the statistical properties of eigenvalues and eigenvectors are to a large extent independent of the underlying distribution of input random parameters $\boldsymbol{X}$ when the matrix has a special structure and the size of the matrix is large, and are dependent only on global symmetry properties of the random matrix. It appears that there is a "central limit theorem" for large random matrices defined by classical ensembles. While these classical solutions provide significant insight, random matrices encountered in engineering unfortunately do not follow specific matrix structures or probability distributions of classical β-ensembles. For example, the matrices $\boldsymbol{M}(\boldsymbol{X})$, $\boldsymbol{K}(\boldsymbol{X})$, and $\boldsymbol{C}(\boldsymbol{X})$ in solving mechanical vibration problems [49–56] can be symmetric, skew-symmetric or non-symmetric, can be positive-definite or semi-positive definite, can include random parameters that come from a variety of sources, and can have a wide range of probability distributions. Classical methods of random matrix theory are either inapplicable or highly nontrivial to apply in solving REPs addressed

in this work. Therefore, approximate methods involving a sound theoretical foundation and advanced computational techniques are required to solve a general REP addressed in this study.

2.3.2 Classical or elementary approximate methods

Current approximate methods for solving REPs in dynamics are heavily dominated by perturbation methods [26–29,31,32,34,37,38]. These methods involve either first- or second-order Taylor series expansions of the eigenvalue or eigenvector in terms of basic input random parameters and application of standard stochastic operators to obtain second-moment properties and probability density functions of eigensolutions. The popular use of perturbation methods is primarily attributed to the ease of implementation and computational efficiency. However, there are two major limitations of these methods – both the uncertainty of the random input and the nonlinearity of the random eigenvalue or eigenvector with respect to the random input must be small. The errors in these methods can be bounded if higher-order partial derivatives of the eigenvalue or eigenvector variable exist and are available. However, such bounds are rarely used in engineering applications since they require expensive calculation of higher-order partial derivatives. Methods other than perturbation methods include the iteration method [29], a direct matrix product [33], the Ritz method [35], the crossing theory [30], a stochastic reduced basis [36], and an asymptotic method [25]. The iteration method invokes a heuristic assumption of local independence to provide statistical moments of eigenvalues and eigenvectors. The direct matrix product, pro-

posed by Lee and Singh [33], has been demonstrated to accurately calculate only the first two moments of eigenvalues for simple structures. Mehlhose *et al.* [35] applied the Ritz approximation to obtain probability densities of eigenvalues of a continuous vibrating beam under bending. Applications of the direct matrix product or the Ritz method in solving large-scale REPs have yet to be demonstrated. Grigoriu [30] evaluated zeros of random polynomials and employed the well-established crossing theory of stochastic processes to determine probability densities of eigenvalues for real-valued symmetric matrices. The stochastic reduced basis formulation, developed by Nair and Keane [36], involves discretization of the governing equation in space together with the random dimension leading to a linear algebraic system of equations with random coefficients. The numerical results of large-scale systems indicate that more accurate statistics are obtained by the stochastic reduced basis formulation than those obtained by low-order perturbation methods. However, the method loses accuracy for systems with large uncertainties of random input. Recently, a method based on asymptotics of multi-dimensional integral analysis was developed by Adhikari [25], but it requires expensive calculation of eigenvalue derivatives, similar to perturbation methods, and has been illustrated to solve both moments and probability densities of eigenvalues of simple dynamic systems.

2.3.3 Dimensional decomposition methods

Dimensional decomposition of a multivariate function is a finite sum of simpler component functions of input variables with increasing dimensions. This decomposi-

tion, first presented by Hoeffding [76] in relation to his seminal work on U-statistics, has been studied by many other researchers [77]: Sobol [78] used it in the study of quadrature methods, calling it the "decomposition into summands of different dimensions," and also for analysis of variance (ANOVA) [79]; Efron and Stein [80] applied it to prove their famous lemma on jackknife variances; Owen [81] presented a continuous space version of the nested ANOVA; Hickernell [82] developed a reproducing kernel Hilbert space version; and Rabitz and Alis [83] made further refinements, referring to it as high-dimensional model representation (HDMR). More recently, Rahman and his associates introduced this decomposition from the perspective of Taylor series expansion, solving a number of stochastic-mechanics problems [84–86].

Consider a continuous, differentiable, real-valued eigenvalue $\lambda(\mathbf{X}) : \mathbb{R}^N \mapsto \mathbb{R}$ that depends on random input vector $\mathbf{X} = \{X_1, \ldots, X_N\}^T \in \mathbb{R}^N$. A dimensional decomposition of $\lambda(\mathbf{X})$ is described as

$$\begin{aligned} \lambda(\mathbf{X}) &= \lambda_0 + \sum_{i=1}^{N} \lambda_i(X_i) + \sum_{\substack{i_1, i_2 = 1 \\ i_1 < i_2}}^{N} \lambda_{i_1 i_2}(X_{i_1}, X_{i_2}) \\ &\quad + \cdots + \sum_{\substack{i_1, \ldots, i_S = 1 \\ i_1 < \cdots < i_S}}^{N} \lambda_{i_1 \cdots i_S}(X_{i_1}, \ldots, X_{i_S}) \\ &\quad + \cdots + \lambda_{12\cdots N}(X_1, \ldots, X_N). \end{aligned} \tag{2.8}$$

This decomposition is a finite hierarchical expansion of an output function in terms of its input random variables with increasing dimension. Here λ_0 is a constant, $\lambda_i(X_i) : \mathbb{R} \mapsto \mathbb{R}$ is a univariate component function representing individual contribution to $\lambda(\mathbf{X})$ by the input variable X_i acting alone, $\lambda_{i_1 i_2}(X_{i_1}, X_{i_2}) : \mathbb{R}^2 \mapsto \mathbb{R}$ is a bivariate

component function representing combined influence on $\lambda(\mathbf{X})$ of two input variables X_{i_1} and X_{i_2}, and $\lambda_{i_1 \cdots i_S}(X_{i_1}, \ldots, X_{i_S}) : \mathbb{R}^S \mapsto \mathbb{R}$ is an S-variate component function describing cooperative effects on $\lambda(\mathbf{X})$ of S input variables $X_{i_1}, \ldots, X_{i_S}$, and so on. The last term $\lambda_{12\cdots N}(X_1, \ldots, X_N)$ represents the residual cooperative effect of all the N input variables acting together on the multivariate function $\lambda(\mathbf{X})$. There exist two prominent variants of dimensional decomposition, described as follows.

2.3.3.1 Referential dimensional decomposition

Based on the dimensional decomposition of $\lambda(\boldsymbol{x})$ in Equation (2.8), Rahman [40] defined univariate and bivariate approximations of $\lambda(\boldsymbol{x})$, respectively, as

$$\hat{\lambda}_1(\boldsymbol{x}) := \sum_{i=1}^{N} \underbrace{\lambda(c_1, \ldots, c_{i-1}, x_i, c_{i+1}, \ldots, c_N)}_{=\lambda_i(x_i)} - \underbrace{(N-1)\lambda(\boldsymbol{c})}_{=\lambda_0}, \tag{2.9}$$

and

$$\begin{aligned} \hat{\lambda}_2(\boldsymbol{x}) \;:=\; & \sum_{\substack{i_1, i_2 = 1 \\ i_1 < i_2}}^{N} \underbrace{\lambda(c_1, \ldots, c_{i_1-1}, x_{i_1}, c_{i_1+1}, \ldots, c_{i_2-1}, x_{i_2}, c_{i_2+1}, \ldots, c_N)}_{=\lambda_{i_1 i_2}(x_{i_1}, x_{i_2})} \\ & + \sum_{i=1}^{N} \underbrace{-(N-2)\lambda(c_1, \ldots, c_{i-1}, x_i, c_{i+1}, \ldots, c_N)}_{=\lambda_i(x_i)} \\ & + \underbrace{\frac{(N-1)(N-2)}{2}\lambda(\boldsymbol{c})}_{=\lambda_0}, \end{aligned} \tag{2.10}$$

where $\boldsymbol{c} = \{c_1, \ldots, c_N\}^T$ is a reference point in the input domain, $\lambda(\boldsymbol{c}) := \lambda(c_1, \ldots, c_N)$. The constant, univariate, and bivariate component functions λ_0, $\lambda_i(x_i)$, and $\lambda_{i_1 i_2}(x_{i_1}, x_{i_2})$, respectively, of the dimension decomposition in Equation (2.8) are indicated through the underbraces in Equations (2.9) and (2.10). Further, a generalized

S-variate referential dimensional decomposition (RDD), for any integer $1 \leq S \leq N$, is given by

$$\begin{aligned}\hat{\lambda}_S(\boldsymbol{x}) \;:=\; & \sum_{i=0}^{S}(-1)^i \binom{N-S+i-1}{i} \\ & \times \sum_{\substack{k_1,\ldots,k_{S-i}=1 \\ k_1<\cdots<k_{S-i}}}^{N} \lambda\left(c_1,\ldots,c_{k_1-1},x_{k_1},c_{k_1+1},\ldots,x_{k_{S-i}},\ldots,c_N\right). \end{aligned} \tag{2.11}$$

When $S = 1$ and 2, Equation (2.11) degenerates to univariate (Equation (2.9)) and bivariate (Equation (2.10)) approximations, respectively.

When $S = N$, $\hat{\lambda}_S(\boldsymbol{x})$ converges to the exact function $\lambda(\boldsymbol{x})$. In other words, Equation (2.11) generates a hierarchical and convergent sequence of approximations of $\lambda(\boldsymbol{x})$. By replacing the eigenvalue by its S-variate RDD, the l^{th} moment of eigenvalue $\lambda^l(\boldsymbol{X})$ is approximated as

$$\begin{aligned} m_l \;\cong\; & \mathbb{E}\left[\hat{\lambda}_S^l(\boldsymbol{X})\right] \\ =\; & \sum_{i=0}^{S}(-1)^i \binom{N-S+i-1}{i} \\ & \times\mathbb{E}\left[\sum_{\substack{k_1,\ldots,k_{S-i}=1 \\ k_1<\cdots<k_{S-i}}}^{N} \lambda^l\left(c_1,\ldots,c_{k_1-1},X_{k_1},c_{k_1+1},\ldots,c_{k_{S-i}-1},X_{k_{S-i}},c_{k_{S-i}+1},\ldots,c_N\right)\right]. \end{aligned} \tag{2.12}$$

As in an S-variate decomposition given by Equation (2.8), the expectation $\mathbb{E}\left[\hat{\lambda}_S^l(\boldsymbol{X})\right]$ for $S = 1, 2, \ldots, N$ also represents a hierarchical sequence of approximations of the l^{th} moment of an eigenvalue. The advantage of using Equation (2.12) over Equation (2.8) lies in evaluating only up to S-dimensional deterministic integrations, compared

to the full N-dimensional required in Equation (2.8). For independent random vector $\boldsymbol{X}$, the S-variate approximation of moments is evaluated using standard numerical quadratures, leading to

$$\begin{aligned} m_l &= \mathbb{E}\left[\hat{\lambda}_S^l(\boldsymbol{X})\right] \cong \sum_{i=0}^{S}(-1)^i \begin{pmatrix} N-S+i-1 \\ i \end{pmatrix} \\ &\times \sum_{\substack{k_1,\ldots,k_{S-i}=1 \\ k_1<\cdots<k_{S-i}}}^{N} \sum_{j_{S-i}=1}^{n} \cdots \sum_{j_1=1}^{n} w_{k_1}^{(j_1)} \cdots w_{k_{S-i}}^{(j_{S-i})} \\ &\times \lambda^l\left(c_1,\ldots,c_{k_1-1},x_{k_1}^{(j_1)},c_{k_1+1},\ldots,c_{k_{S-i}-1},x_{k_{S-i}}^{(j_{S-i})},c_{k_{S-i}+1},\ldots,c_N\right), \end{aligned} \tag{2.13}$$

where $x_i^{(j)}$ is the j^{th} integration point of the i^{th} variable, $w_i^{(j)}$ is the associated weight, and n is the order of integration.

In order to approximate other probabilistic characteristics like the probability density functions of eigenvalues, or the correlation coefficients between two eigenvalues, Lagrange interpolation is used in evaluating the component functions and creating the RDD expansion. Consider the univariate component function $\lambda(c_1,\ldots,c_{i-1},x_i,c_{i+1},\ldots,c_N)$ in Equations (2.9) and (2.10). If for sample points $x_i = x_i^{(j)};\ j=1,\ldots,n$, n distinct eigenvalues $\lambda\left(c_1,\ldots,c_{i-1},x_i^{(j)},c_{i+1},\ldots,c_N\right)$ are given, the eigenvalue for an arbitrary x_i can be obtained by the Lagrange interpolation

$$\lambda(c_1,\ldots,c_{i-1},x_i,c_{i+1},\ldots,c_N) = \sum_{j=1}^{n}\phi_j(x_i)\,\lambda\left(c_1,\ldots,c_{i-1},x_i^{(j)},c_{i+1},\ldots,c_N\right), \tag{2.14}$$

where

$$\phi_j(x_i) = \frac{\prod_{k=1,k\neq j}^{n}\left(x_i - x_i^{(k)}\right)}{\prod_{k=1,k\neq j}^{n}\left(x_i^{(j)} - x_i^{(k)}\right)} \tag{2.15}$$

is the shape function. The same idea can be applied to obtain higher-variate compo-

nent functions. The generalized S-variate approximation is given as

$$\begin{aligned}\hat{\lambda}_S(\boldsymbol{x}) &= \sum_{i=0}^{S}(-1)^i\begin{pmatrix} N-S+i-1 \\ i \end{pmatrix} \\ &\times \sum_{\substack{k_1,\ldots,k_{S-i}=1 \\ k_1<\cdots<k_{S-i}}}^{N}\ \sum_{j_{S-i}=1}^{n}\cdots\sum_{j_1=1}^{n}\phi_{j_1}(X_{k_1})\cdots\phi_{j_{S-i}}\left(X_{k_{S-i}}\right) \\ &\times\lambda\left(c_1,\ldots,c_{k_1-1},x_{k_1}^{(j_1)},c_{k_1+1},\ldots,c_{k_{S-i}-1},x_{k_{S-i}}^{(j_{S-i})},c_{k_{S-i}+1},\ldots,c_N\right). \quad (2.16)\end{aligned}$$

Once the Lagrange shape function $\phi_j(x_i)$ and the deterministic coefficients $\lambda(\boldsymbol{c})$ to $\lambda\left(c_1,\ldots,c_{k_1-1},x_{k_1}^{(j_1)},c_{k_1+1},\ldots,c_{k_{S-i}-1},x_{k_{S-i}}^{(j_{S-i})},c_{k_{S-i}+1},\ldots,c_N\right)$ are generated, Equation (2.16) provides explicit approximation of random eigenvalues $\left\{\lambda^{(i)}(\boldsymbol{X})\right\}$, $i=1,\ldots,L$ in terms of random input $\boldsymbol{X}$. Any probabilistic characteristics of eigenvalues can be easily evaluated by performing Monte Carlo simulation on Equation (2.16). Since Equation (2.16) does not require solving additional matrix equations, the embedded Monte Carlo simulation can be efficiently performed for any sample size.

2.3.3.2 Polynomial dimensional decomposition

Rahman [87] introduced a novel PDD method for solving stochastic problems encountered in engineering and science disciplines. The method is based on the dimensional decomposition in Equation (2.8) where the component functions are Fourier-polynomial expansions in terms of orthornormal polynomial bases consistent with the probability measure of input.

Let $\mathcal{L}_2(\Omega_i,\mathcal{F}_i,P_i)$ be a Hilbert space that is equipped with a set of complete orthonormal bases $\{\psi_{ij}(x_i);\ j=0,1,\cdots\}$, which is consistent with the probability measure of X_i. For example, classical orthonormal polynomials, including Hermite,

Legendre, and Jacobi polynomials, can be used when X_i follows Gaussian, uniform, and Beta probability distributions, respectively [88]. For an arbitrary measure, approximate methods based on the Stieltjes procedure can be employed to obtain the associated orthonormal polynomials [42,88]. If $\mathbb{E}$ is the expectation operator with respect to the probability measure of $\boldsymbol{X}$, then two important properties of orthonormal polynomials are as follows [42,89].

Property 2.1: *The orthonormal polynomial basis functions have a unit mean for* $j = 0$ *and zero means for all* $j \geq 1$*, i.e.,*

$$\mathbb{E}[\psi_{ij}(X_i)] := \int_{\mathbb{R}} \psi_{ij}(x_i) f_i(x_i) dx_i = \begin{cases} 1 & \text{if } j = 0, \\ 0 & \text{if } j \geq 1. \end{cases} \tag{2.17}$$

Property 2.2: *Any two orthonormal polynomial basis functions* $\psi_{ij_1}(X_i)$ *and* $\psi_{ij_2}(X_i)$*, where* $j_1, j_2 = 0, 1, 2, \cdots$*, are uncorrelated, and each has unit variance, i.e.,*

$$\mathbb{E}[\psi_{ij_1}(X_i)\psi_{ij_2}(X_i)] := \int_{\mathbb{R}} \psi_{ij_1}(x_i)\psi_{ij_2}(x_i) f_i(x_i) dx_i = \begin{cases} 1 & \text{if } j_1 = j_2, \\ 0 & \text{if } j_1 \neq j_2. \end{cases} \tag{2.18}$$

Using Fourier-polynomial expansions of all component functions of $\lambda(\boldsymbol{X})$ in Equation (2.8) and invoking Properties 2.1 and 2.2, the PDD of a random eigenvalue $\lambda(\boldsymbol{X})$ represents a finite, hierarchical expansion [42,90]

$$\begin{aligned} \lambda_{PDD}(\boldsymbol{X}) \;:=\; & \lambda_0 + \sum_{i=1}^{N} \underbrace{\sum_{j=1}^{\infty} C_{ij}\psi_{ij}(X_i)}_{=\lambda_i(x_i)} \\ & + \sum_{i_1=1}^{N-1} \sum_{i_2=i_1+1}^{N} \underbrace{\sum_{j_2=1}^{\infty}\sum_{j_1=1}^{\infty} C_{i_1 i_2 j_1 j_2}\psi_{i_1 j_1}(X_{i_1})\psi_{i_2 j_2}(X_{i_2})}_{=\lambda_{i_1 i_2}(x_{i_1}, x_{i_2})} \\ & + \cdots + \underbrace{\sum_{j_N=1}^{\infty} \cdots \sum_{j_1=1}^{\infty} C_{i_1 \cdots i_N j_1 \cdots j_N} \prod_{q=1}^{N} \psi_{i_q j_q}(X_{i_q})}_{=\lambda_{12\cdots N}(X_1, \ldots, X_N)} \end{aligned} \tag{2.19}$$

in terms of random orthonormal polynomials $\psi_{ij}(X_i)$, $i = 1, \cdots, N$; $j = 1, \cdots, \infty$ of input variables $X_1, \cdots, X_N$ with increasing dimensions, where

$$\lambda_0 := \int_{\mathbb{R}^N} \lambda(\boldsymbol{x}) f_{\boldsymbol{X}}(\boldsymbol{x}) d\boldsymbol{x}, \tag{2.20}$$

and

$$C_{i_1 \cdots i_s j_1 \cdots j_s} := \int_{\mathbb{R}^N} \lambda(\boldsymbol{x}) \prod_{q=1}^{s} \psi_{i_q j_q}(x_{i_q}) f_{\boldsymbol{X}}(\boldsymbol{x}) d\boldsymbol{x}, \tag{2.21}$$

for $s = 1, \cdots, N$, $1 \leq i_1 < \cdots < i_s \leq N$, $j_1, \cdots, j_s = 1, \cdots, \infty$, are the associated expansion coefficients, which require calculating various high-dimensional integrals when N is large. In Equation (2.19), the term $\sum_{j_s=1}^{\infty} \cdots \sum_{j_1=1}^{\infty} C_{i_1 \cdots i_s j_1 \cdots j_s} \prod_{q=1}^{s} \psi_{i_q j_q}(X_{i_q})$ represents the s-variate component function, quantifying the cooperative effect of s input variables $X_{i_1}, \cdots, X_{i_S}$ on λ.

When the right side of Equation (2.19) is truncated by retaining at most S-variate interactive effects of input variables and at most mth-order orthonormal polynomials, the result is an S-variate, mth-order PDD approximation

$$\begin{aligned} \tilde{\lambda}_{S,m}(\boldsymbol{X}) \;=\; & \lambda_0 + \sum_{i=1}^{N} \sum_{j=1}^{m} C_{ij} \psi_{ij}(X_i) \\ & + \sum_{i_1=1}^{N-1} \sum_{i_2=i_1+1}^{N} \sum_{j_2=1}^{m} \sum_{j_1=1}^{m} C_{i_1 i_2 j_1 j_2} \psi_{i_1 j_1}(X_{i_1}) \psi_{i_2 j_2}(X_{i_2}) \\ & \vdots \\ & + \sum_{i_1=1}^{N-S+1} \cdots \sum_{i_S=i_{S-1}+1}^{N} \sum_{j_S=1}^{m} \cdots \sum_{j_1=1}^{m} C_{i_1 \cdots i_S j_1 \cdots j_S} \prod_{q=1}^{S} \psi_{i_q j_q}(X_{i_q}) \end{aligned} \tag{2.22}$$

of $\lambda(\boldsymbol{X})$. Once the coefficients are calculated, any probabilistic characteristics of eigenvalues can be evaluated by performing Monte Carlo simulation on Equation (2.22). In his work [87], Rahman employs the dimension-reduction scheme [85] for

calculating the coefficients. This scheme is discussed in Chapter 3. Similar to RDD, Equation (2.22) does not require solving additional matrix equations; the embedded Monte Carlo simulation can be efficiently performed for any sample size. However, unlike RDD, this decomposition method does not require a reference point and sample points around the reference point to approximate the component functions.

2.3.4 Polynomial chaos expansion method

The PCE of a random eigenvalue $\lambda(\boldsymbol{X})$, a function of a finite number of random variables $X_1, \cdots, X_N$, has a representation [44, 46, 91]

$$\begin{aligned} \lambda_{PCE}(\boldsymbol{X}) \;:=\; & a_0\Gamma_0 + \sum_{i=1}^{N} a_i\Gamma_1(X_i) + \sum_{i_1=1}^{N}\sum_{i_2=i_1}^{N} a_{i_1 i_2}\Gamma_2(X_{i_1}, X_{i_2}) \\ & + \cdots + \sum_{i_1=1}^{N}\cdots\sum_{i_p=i_{p-1}}^{N} a_{i_1\cdots i_p}\Gamma_p(X_{i_1}, \cdots, X_{i_p}) + \cdots \end{aligned} \tag{2.23}$$

in terms of random multidimensional polynomial chaoses, $\Gamma_p(X_{i_1}, \cdots, X_{i_p})$, $p = 0, \cdots, \infty$, $1 \le i_1 \le \cdots \le i_p \le N$, of input variables $X_{i_1}, \cdots, X_{i_p}$ with increasing orders, where

$$a_0 := \int_{\mathbb{R}^N} \lambda(\boldsymbol{x})\Gamma_0 f_{\boldsymbol{X}}(\boldsymbol{x})d\boldsymbol{x}, \tag{2.24}$$

and

$$a_{i_1\cdots i_p} := \int_{\mathbb{R}^N} \lambda(\boldsymbol{x})\Gamma_p(X_{i_1}, \cdots, X_{i_p}) f_{\boldsymbol{X}}(\boldsymbol{x})d\boldsymbol{x}, \tag{2.25}$$

for $p = 1, \cdots, \infty$, $1 \le i_1 \le \cdots \le i_p \le N$, are the corresponding expansion coefficients that also require evaluating high-dimensional integrals. When the right side of Equation (2.23) is truncated by retaining at most pth-order polynomial chaoses, the

result is pth-order PCE approximation

$$\begin{aligned}\bar{\lambda}_p(\boldsymbol{X}) \;:=\; & a_0\Gamma_0 + \sum_{i=1}^{N} a_i\Gamma_1(X_i) + \sum_{i_1=1}^{N}\sum_{i_2=i_1}^{N} a_{i_1 i_2}\Gamma_2(X_{i_1}, X_{i_2}) \\ & + \sum_{i_1=1}^{N}\sum_{i_2=i_1}^{N}\sum_{i_3=i_2}^{N} a_{i_1 i_2 i_3}\Gamma_3(X_{i_1}, X_{i_2}, X_{i_3}) \\ & \vdots \\ & + \sum_{i_1=1}^{N}\cdots\sum_{i_p=i_{p-1}}^{N} a_{i_1\cdots i_p}\Gamma_p(X_{i_1}, \cdots, X_{i_p})\end{aligned} \tag{2.26}$$

of $\lambda(\boldsymbol{X})$. Ghanem [46] has constructed the polynomial chaoses $\Gamma_p(X_{i_1}, \cdots, X_{i_p})$, $p = 0, \cdots, \infty$, $1 \le i_1 \le \cdots \le i_p \le N$, starting with the zeroth order polynomial Γ_0 as a constant and chosen to be $\Gamma_0 = 1$, and proceeded through a sequence of orthogonalization procedures with respect to Gaussian probability measure. Recently, Ghosh [92] developed a new efficient method for estimating the coefficients of the PCE for solving REPs. Ghosh further developed an enriched version of PCE that can be used to approximate non-smooth functions efficiently [93].

2.3.5 Simulation and sampling methods

Finally, simulation and sampling methods, such as crude Monte Carlo simulation [94], quasi-Monte Carlo simulation [95–97], importance sampling [98, 99], directional simulation [100,101], and others [18,102–104], are well known in the probability and statistics literature. They can be applied, at least in theory, to solve any REP described in Table 2.1. For example, the solution of an REP by crude Monte Carlo simulation comprises the following steps:

1. generate samples $\boldsymbol{A}_j(\boldsymbol{x}^{(k)})$; $j = 1, \ldots, J$, $k = 1, \ldots, N_S$ from N_S input samples $\boldsymbol{x}^{(k)}$; $k = 1, \ldots, N_S$;

2. solve the corresponding characteristic and governing equations,

$$\det\left[f\left(\lambda(\boldsymbol{x}^{(k)}); \boldsymbol{A}_1(\boldsymbol{x}^{(k)}), \cdots, \boldsymbol{A}_J(\boldsymbol{x}^{(k)})\right)\right] = 0, \tag{2.27}$$

and

$$f\left(\lambda(\boldsymbol{x}^{(k)}); \boldsymbol{A}_1(\boldsymbol{x}^{(k)}), \cdots, \boldsymbol{A}_J(\boldsymbol{x}^{(k)})\right) \boldsymbol{\phi}^{(i)}(\boldsymbol{x}^{(k)}) = \boldsymbol{0}, \tag{2.28}$$

to find samples of the eigenpairs $\left\{\lambda_i^{(k)}, \boldsymbol{\phi}_i^{(k)}\right\}$; $i = 1, \ldots, L$; $k = 1, \ldots, N_S$; and

3. develop statistics of $\{\Lambda_i, \boldsymbol{\Phi}_i\}$; $i = 1, \ldots, L$ from $\left\{\lambda_i^{(k)}, \boldsymbol{\phi}_i^{(k)}\right\}$; $i = 1, \ldots, L$; $k = 1, \ldots, N_S$.

The simulation can also provide full probabilistic description of the eigenvalues and eigenvectors, but it is computationally inefficient when the coefficient matrices $\boldsymbol{A}_j(\boldsymbol{X})$; $j = 1, \ldots, J$, are large because it requires solving the matrix equations for every set of realizations of $\boldsymbol{A}_j(\boldsymbol{X})$; $j = 1, \ldots, J$. Consequently, the simulation methods are useful only when alternative methods are inapplicable or inaccurate, and have been traditionally employed as a yardstick for evaluating approximate methods.

2.4 Numerical Algorithms for Eigenvalue Analysis

A special case of REPs listed in Table 2.1 is a linear problem of the type $\boldsymbol{A}\boldsymbol{\phi} = \lambda\boldsymbol{\phi}$. Analytical solution of such a problem using a characteristic polynomial is not feasible for systems with more than two or three degrees of freedom. Particularly large-scale complex engineering systems require highly efficient numerical algorithms for extracting eigenvalues and eigenvectors. This research work involves solution of REPs of varied sizes. Three numerical algorithms: the LR-QR algorithm [105–107], the Lanczos transformation [108, 109], and automatic multi-level substructuring

(AMS) [109–112] are employed for solution of matrix eigenvalue equations. The LR-QR algorithm was used for relatively small systems, of up to seven degrees of freedom. The Lanczos transformation and AMS algorithm were employed for eigenvalue and eigenvector extraction of large systems involving finite element models. These three methods are briefly discussed in this section.

2.4.1 LR-QR algorithm

The LR-QR algorithm is one of the most preferred methods for computing the eigenvalues of matrices of size $L \leq 25$. Before the LR-QR algorithm can be implemented to compute eigenvalues, the matrix is first balanced. The process of producing a matrix that is diagonally similar to a given matrix and that reduces the matrix norm is called balancing the matrix. Having a low matrix norm is desirable, as the errors in calculating the eigenvalues of a matrix are proportional to the Frobenius norm of the matrix. Gauss similarity transformations with partial pivoting is used to reduce this balanced matrix to a real upper Hessenberg matrix. A matrix $\boldsymbol{H}$ is an upper Hessenberg matrix if its elements below the lower off-diagonal are zero, i.e., $H_{ij} = 0$, $i > j + 1$. The LR-QR algorithm is then used to compute the eigenvalues of the Hessenberg matrix.

The LR-QR algorithm is based on the LR transformation proposed by Rutishauser [113]. The LR transformation is based on repeated LU factorization of a matrix $\boldsymbol{A}$ such that

$$\boldsymbol{A}_k = \boldsymbol{L}\boldsymbol{R} \tag{2.29}$$

for any step k of the iterative transformation. Here, $\boldsymbol{L}$ is a lower triangular matrix, and $\boldsymbol{R}$ is an upper triangular matrix. The step is completed by remultiplying the factors in reverse order, i.e.,

$$\boldsymbol{A}_{k+1} = \boldsymbol{R}\boldsymbol{L}. \tag{2.30}$$

From $\boldsymbol{R} = \boldsymbol{L}^{-1}\boldsymbol{A}_k$, the $(k+1)^{\text{th}}$ iteration of matrix $\boldsymbol{A}$ is

$$\boldsymbol{A}_{k+1} = \boldsymbol{L}^{-1}\boldsymbol{A}_k\boldsymbol{L}. \tag{2.31}$$

As transformation proceeds, the transformed matrix $\boldsymbol{A}_k$ tends to an upper triangular matrix whose eigenvalues are equal to the diagonal terms. Wilkinson [114] showed that the stability of triangular decomposition in the LR algorithm cannot be guaranteed unconditionally, since as the diagonal elements tend to approach the eigenvalues the sub-diagonal elements tend to approach zero. These limitations of the LR algorithm led to the replacement of elementary transformation by the elementary unitary transformation. Francis [106, 107] and Kublanovskaya [115] proposed that $\boldsymbol{L}$ be replaced by a unitary matrix $\boldsymbol{Q}$. This replacement gives the QR algorithm, now known as the LR-QR algorithm.

2.4.2 Lanczos method

The Lanczos method is particularly useful in situations when a few of the largest or the smallest eigenvalues of a matrix are desired. For instance, for determining the first J number of natural frequencies of vibration of a structure, only its smallest J eigenvalues are required to be extracted. This method involves partial tridiagonalization of the matrix. The algorithm transforms the matrix $\boldsymbol{A}$ into a tridi-

agonal matrix $\boldsymbol{T} = \boldsymbol{V}^T \boldsymbol{A} \boldsymbol{V}$ similar to $\boldsymbol{A}$, where $\boldsymbol{V}$ is a block of Lanczos vectors with J number of columns, and J is equal to the number of eigenvalues desired. The number of rows of $\boldsymbol{V}$ is the number of variables in the FE model, or the size of the matrix $\boldsymbol{A}$. The tridiagonal matrix $\boldsymbol{T}$ of size J is then used to solve the reduced eigenvalue problem $\boldsymbol{T}\boldsymbol{\Phi} = \boldsymbol{\Phi}\boldsymbol{\lambda}$, where $\boldsymbol{\Phi}$ is the matrix containing the eigenvectors, and $\boldsymbol{\lambda}$ is the vector containing the eigenvalues of the reduced eigenproblem.

In this work, the Lanczos method was used through the Abaqus [109] finite element computer software. The Lanczos procedure in Abaqus consists of a set of Lanczos runs, in each of which a set of iterations is performed. Each Lanczos run applies the transformation $\boldsymbol{M}\left(\boldsymbol{K} - \sigma \boldsymbol{M}\right)^{-1} \boldsymbol{M}\boldsymbol{\phi} = \lambda \boldsymbol{M}\boldsymbol{\phi}$ on the mass matrix $\boldsymbol{M}$ and the stiffness matrix $\boldsymbol{K}$, where σ is the shift, λ is the eigenvalue, and $\boldsymbol{\phi}$ is the eigenvector. This transformation allows rapid convergence to the desired eigenvalues. In general, only tens of eigenvalues closest to the shift value are computed in a single Lanczos run. The possibility of computing many eigenmodes by carrying out several runs with different shift values is an important feature of the Lanczos eigensolver. Within each run, a sequence of Krylov subspaces is created. A j^{th}-order Krylov subspace $\mathcal{K}_j$ is defined as $\mathcal{K}_j\left(\boldsymbol{A}, \boldsymbol{v}\right) = \text{span}\left\{\boldsymbol{v}, \boldsymbol{A}\boldsymbol{v}, \boldsymbol{A}^2\boldsymbol{v}, \ldots, \boldsymbol{A}^{j-1}\boldsymbol{v}\right\}$ for an $L \times L$ matrix $\boldsymbol{A}$ and an L-dimensional vector $\boldsymbol{v}$. The best possible approximation of the eigenvectors on each subspace is computed in a series of iterations. In each Lanczos iteration, the dimension of the subspace grows, allowing better approximation of the desired eigenvectors. The basic Lanczos process with no shifting is unable to determine repeated eigenvalues. The shifting strategy detects missing modes and

enforces computation of all the modes during the subsequent Lanczos runs. However, this strategy is expensive if the multiplicity of certain eigenvalues is high. Therefore, a blocked version of the Lanczos algorithm is implemented in Abaqus. This technique starts with a block of orthogonal vectors and increases the dimension of the Krylov subspaces by the block size at each Lanczos step. This approach allows automatic computation of all multiple eigenvalues if the largest multiplicity does not exceed the block size.

2.4.3 Automatic multi-level substructuring method

The Lanczos method has a very significant limitation in that it involves the solution of a set of linear equations in every iteration. Dynamic analysis of structures involves developing finite element discretization with even millions of degrees of freedom. Modal superposition is the method of choice for dynamic analysis of such large systems. Modal superposition requires a very large number (1000s) of eigenvalues and eigenvectors to be extracted. The Lanczos method proves to be prohibitively inefficient for solving problems of such large scale. Bennighof *et al.* [110–112] introduced the efficient AMS method for eigenvalue analysis of large engineering systems involving FE model with even millions of degrees of freedom. In the AMS method, the FE model is transformed so that the response is represented in terms of substructure modes. In the first step of this method, the model is partitioned automatically into substructures on a number of levels based on the sparsity structure of the system matrices. The substructures on the lowest level consist of a small number of

finite elements. These *child* substructures are assembled together to form *parents*, which are assembled together to form *grandparents*, and so on, until the model of the complete structure has been assembled. The partial eigensolutions are economical because substructure eigenvalue problems are very small.

2.5 Needs for Fundamental Research

Based on the literature review of existing works on REPs, four research directions are proposed, as follows.

2.5.1 A rigorous comparison of PDD and PCE methods

Recent developments on solving REPs include the stochastic expansion methods, notably, the PCE and PDD methods, both employing Fourier expansions in terms of orthogonal polynomials for approximating eigensolutions. These methods also provide the probability distributions of eigensolutions, although the concomitant approximations are guaranteed to converge only in the mean-square sense, provided that the eigensolutions are square-integrable functions of the random input with respect to its probability measure. However, due to the contrasting dimensional structures of PDD and PCE, the convergence properties of their truncations are not the same and may differ significantly, depending on the eigensolution and dimension of the problem. Therefore, uncovering their mathematical properties, which have ramifications in stochastic computing, including solving REPs, is a major motivation for this current work. Is PDD superior to PCE or *vice versa*? It is also desirable to compare the errors from the PDD and PCE approximations and thereby establish

appropriate criteria for grading these two methods.

2.5.2 Multiplicative PDD

The existing PDD method for solving REPs is predicated on the additive nature of a function (eigenvalue or eigenvector). This is pertinent as long as the dimensional hierarchy of a stochastic response (eigensolution) is also additive. In which case, a truncation of existing PDD, referred to as the additive PDD (A-PDD), preserving at most S-variate component functions, generates stochastic solutions with Sth-order polynomial computational complexity. However, the dimensional hierarchy of a stochastic response, in general, is not known *a priori*. Therefore, indiscriminately using A-PDD for general stochastic analysis is not desirable. When a response is dominantly of multiplicative nature, the A-PDD approximation for a chosen truncation parameter S may not predict sufficiently accurate probabilistic characteristics of a complex system. Therefore, alternative decompositions suitable for multiplicative-type response functions and measure-consistent orthogonal polynomials should be explored. For such a decomposition, it is unknown which truncation parameter S should be selected when compared with that for the additive decomposition. Is it possible to solve a stochastic problem by selecting a smaller value of S for the alternative decomposition than for the additive decomposition? If yes, then a significant, positive impact on uncertainty quantification of high-dimensional complex systems, including REPs, is anticipated.

2.5.3 Hybrid PDD

While the multiplicative PDD, discussed in the preceding section, may eliminate the shortcomings of the additive PDD, further complications may arise when a dynamic system exhibits an eigensolution that is dominantly neither additive nor multiplicative. In which case, a hybrid approach coupling both additive and multiplicative decompositions in the spirit of PDD should be developed by selecting any hybridity parameters involved optimally. These enhancements should be pursued without incurring significant additional cost, if any. In addition, theoretical error analyses of both the multiplicative PDD and hybrid PDD methods should be conducted to evaluate their improvements over the additive PDD approximation.

2.5.4 Adaptive-sparse PDD

The existing approach for creating a PDD approximation involves arbitrarily setting the truncation parameter S for the degree of interaction between input variables, and the truncation parameter m for the order of orthogonal polynomials, followed by calculation of the PDD coefficients for this truncation. Such an approach may not be the most efficient, as there may exist some coefficients that are not making significant contributions to the approximation and thus need not be calculated at all. Thus an adaptive approach of creating the PDD approximation is desired that preferably does not pre-select the truncation parameters S and m, but is based on identifying and employing only those PDD coefficients that make a significant contribution to the approximation.

CHAPTER 3
A RIGOROUS COMPARISON OF PDD AND PCE

3.1 Introduction

This chapter presents a rigorous comparison of the PDD and PCE methods for calculating the statistical moments and tail probability distributions of random eigenvalues commonly encountered in dynamics of mechanical systems. The PDD and PCE methods are discussed in detail in Section 2.2. In the current chapter, Section 3.2 provides a brief exposition of PDD and PCE, including establishing the relationship between the two expansions. Section 3.3 discusses PDD and PCE approximations resulting from series truncations, where an alternative form of the PCE approximation has been derived, leading to approximate probabilistic solutions from both methods in terms of the PDD expansion coefficients. Section 3.3 also presents an error analysis due to PDD and PCE approximations. Section 3.4 describes the dimension-reduction integration for estimating the PDD expansion coefficients, including the computational efforts required. Five numerical examples illustrate the accuracy, convergence, and computational efficiency of the PDD and PCE methods in Section 3.5. Finally, conclusions are drawn in Section 3.6.

3.2 Relationship between PDD and PCE

The PDD of a random eigenvalue $\lambda(\boldsymbol{X})$ represents a finite, hierarchical expansion [42, 90]

$$\begin{aligned}
\lambda_{PDD}(\boldsymbol{X}) \;:=\; & \lambda_0 + \sum_{i=1}^{N}\sum_{j=1}^{\infty} C_{ij}\psi_{ij}(X_i) \\
& + \sum_{i_1=1}^{N-1}\sum_{i_2=i_1+1}^{N}\sum_{j_2=1}^{\infty}\sum_{j_1=1}^{\infty} C_{i_1 i_2 j_1 j_2}\psi_{i_1 j_1}(X_{i_1})\psi_{i_2 j_2}(X_{i_2}) \\
& + \sum_{i_1=1}^{N-2}\sum_{i_2=i_1+1}^{N-1}\sum_{i_3=i_2+1}^{N}\sum_{j_3=1}^{\infty}\sum_{j_2=1}^{\infty}\sum_{j_1=1}^{\infty} C_{i_1 i_2 i_3 j_1 j_2 j_3} \\
& \times \psi_{i_1 j_1}(X_{i_1})\psi_{i_2 j_2}(X_{i_2})\psi_{i_3 j_3}(X_{i_3}) \\
& + \cdots + \sum_{i_1=1}^{1}\cdots\sum_{i_N=i_{N-1}+1}^{N}\sum_{j_N=1}^{\infty}\cdots\sum_{j_1=1}^{\infty} C_{i_1\cdots i_N j_1\cdots j_N}\prod_{q=1}^{N}\psi_{i_q j_q}(X_{i_q}) \\
= \;& \lambda_0 + \sum_{s=1}^{N}\Bigg[\underbrace{\sum_{i_1=1}^{N-s+1}\cdots\sum_{i_s=i_{s-1}+1}^{N}}_{s\text{ sums}}\;\underbrace{\sum_{j_1=1}^{\infty}\cdots\sum_{j_s=1}^{\infty}}_{s\text{ sums}} C_{i_1\cdots i_s j_1\cdots j_s}\prod_{q=1}^{s}\psi_{i_q j_q}(X_{i_q})\Bigg]
\end{aligned} \tag{3.1}$$

in terms of random orthonormal polynomials $\psi_{ij}(X_i)$, $i = 1, \cdots, N$; $j = 1, \cdots, \infty$ of input variables $X_1, \cdots, X_N$ with increasing dimensions, where

$$\lambda_0 := \int_{\mathbb{R}^N} \lambda(\boldsymbol{x}) f_{\boldsymbol{X}}(\boldsymbol{x}) d\boldsymbol{x} \tag{3.2}$$

and

$$C_{i_1\cdots i_s j_1\cdots j_s} := \int_{\mathbb{R}^N} \lambda(\boldsymbol{x}) \prod_{q=1}^{s}\psi_{i_q j_q}(x_{i_q}) f_{\boldsymbol{X}}(\boldsymbol{x}) d\boldsymbol{x}, \tag{3.3}$$

for $s = 1, \cdots, N$, $1 \le i_1 < \cdots < i_s \le N$, $j_1, \cdots, j_s = 1, \cdots, \infty$ are the associated expansion coefficients. The PCE of a random eigenvalue $\lambda(\boldsymbol{X})$, a function of a finite

number of random variables $X_1, \cdots, X_N$, has a representation [44, 46, 91]

$$\begin{aligned}\lambda_{PCE}(\boldsymbol{X}) \;:=\; & a_0\Gamma_0 + \sum_{i=1}^{N} a_i\Gamma_1(X_i) + \sum_{i_1=1}^{N}\sum_{i_2=i_1}^{N} a_{i_1 i_2}\Gamma_2(X_{i_1}, X_{i_2}) \\ & + \sum_{i_1=1}^{N}\sum_{i_2=i_1}^{N}\sum_{i_3=i_2}^{N} a_{i_1 i_2 i_3}\Gamma_3(X_{i_1}, X_{i_2}, X_{i_3}) \\ & + \cdots + \sum_{i_1=1}^{N}\cdots\sum_{i_p=i_{p-1}}^{N} a_{i_1\cdots i_p}\Gamma_p(X_{i_1}, \cdots, X_{i_p}) + \cdots\end{aligned} \tag{3.4}$$

in terms of random polynomial chaoses, $\Gamma_p(X_{i_1}, \cdots, X_{i_p})$, $p = 0, \cdots, \infty$, $1 \le i_1 \le \cdots \le i_p \le N$, of input variables $X_{i_1}, \cdots, X_{i_p}$ with increasing orders, where

$$a_0 := \int_{\mathbb{R}^N} \lambda(\boldsymbol{x})\Gamma_0 f_{\boldsymbol{X}}(\boldsymbol{x})d\boldsymbol{x} \tag{3.5}$$

and

$$a_{i_1\cdots i_p} := \int_{\mathbb{R}^N} \lambda(\boldsymbol{x})\Gamma_p(X_{i_1}, \cdots, X_{i_p}) f_{\boldsymbol{X}}(\boldsymbol{x})d\boldsymbol{x}, \tag{3.6}$$

for $p = 1, \cdots, \infty$, $1 \le i_1 \le \cdots \le i_p \le N$, are the corresponding expansion coefficients.

Using the orthonormality property of the polynomials $\psi_{ij}(X_i), i = 1, \cdots, N; j = 1, \cdots, \infty$ of input variables $X_1, \cdots, X_N$ (Properties 2.1 and 2.2), it is elementary to show that the second-moment properties of any square integrable function $\lambda(\boldsymbol{X})$, its PDD $\lambda_{PDD}(\boldsymbol{X})$, and its PCE $\lambda_{PCE}(\boldsymbol{X})$ are identical. In other words, $\lambda(\boldsymbol{X})$, $\lambda_{PDD}(\boldsymbol{X})$, and $\lambda_{PCE}(\boldsymbol{X})$ are equivalent in the mean-square sense. Indeed, there exists a striking theorem, as follows.

Theorem 3.1: *If $\lambda_{PDD}(\boldsymbol{X})$ and $\lambda_{PCE}(\boldsymbol{X})$ are two infinite series defined in Equations* (3.1) *and* (3.4)*, respectively, then one series can be rearranged to derive the other series, for instance, $\lambda_{PCE}(\boldsymbol{X}) = \lambda_{PDD}(\boldsymbol{X})$.*

Proof. The polynomial chaoses $\Gamma_p(X_{i_1}, \cdots, X_{i_p})$, $p = 0, \cdots, \infty$, $1 \le i_1 \le \cdots \le i_p \le$

N in Equation (3.4) can be more explicitly written as

$$\begin{aligned}
\Gamma_0 &= 1 \\
\Gamma_1(X_i) &= \psi_{i1}(X_i) \\
\Gamma_2(X_{i_1}, X_{i_2}) &= \psi_{i_1 2}(X_{i_1})\delta_{i_1 i_2} - \psi_{i_1 1}(X_{i_1})\psi_{i_2 1}(X_{i_2})(\delta_{i_1 i_2} - 1) \\
\Gamma_3(X_{i_1}, X_{i_2}, X_{i_3}) &= \psi_{i_1 3}(X_{i_1})\delta_{i_1 i_2}\delta_{i_1 i_3}\delta_{i_2 i_3} \\
&\quad -\psi_{i_1 1}(X_{i_1})\psi_{i_2 2}(X_{i_2})\delta_{i_2 i_3}(\delta_{i_1 i_2} - 1) \\
&\quad -\psi_{i_2 2}(X_{i_2})\psi_{i_3 1}(X_{i_3})\delta_{i_1 i_2}(\delta_{i_2 i_3} - 1) \\
&\quad -\psi_{i_1 1}(X_{i_1})\psi_{i_2 1}(X_{i_2})\psi_{i_3 1}(X_{i_3}) \\
&\quad \times(\delta_{i_1 i_2}\delta_{i_1 i_3}\delta_{i_2 i_3} - 1)(\delta_{i_1 i_2} - 1)(\delta_{i_2 i_3} - 1) \\
\cdots &= \cdots,
\end{aligned} \tag{3.7}$$

which represents various combinations of tensor products of sets of univariate orthonormal polynomials with $\delta_{i_k i_l}$, $k, l = 1, \cdots, p$, denoting various Kronecker deltas, *i.e.*, $\delta_{i_k i_l} = 1$ when $i_k = i_l$ and *zero* otherwise. Inserting Equation (3.7) into Equations (3.5) and (3.6) with Equations (3.2) and (3.3) in mind, the PCE coefficients,

$$\begin{aligned}
a_0 &= \lambda_0 \\
a_i &= C_{i1} \\
a_{i_1 i_2} &= C_{i_1 2}\delta_{i_1 i_2} - C_{i_1 i_2 11}(\delta_{i_1 i_2} - 1) \\
a_{i_1 i_2 i_3} &= C_{i_1 3}\delta_{i_1 i_2}\delta_{i_1 i_3}\delta_{i_2 i_3} - C_{i_1 i_2 12}\delta_{i_2 i_3}(\delta_{i_1 i_2} - 1) \\
&\quad -C_{i_2 i_3 21}\delta_{i_1 i_2}(\delta_{i_2 i_3} - 1) \\
&\quad -C_{i_1 i_2 i_3 111}(\delta_{i_1 i_2}\delta_{i_1 i_3}\delta_{i_2 i_3} - 1)(\delta_{i_1 i_2} - 1)(\delta_{i_2 i_3} - 1) \\
\cdots &= \cdots,
\end{aligned} \tag{3.8}$$

provide explicit connections to the PDD coefficients. Using the polynomial chaoses and PCE coefficients from Equation (3.7) and Equation (3.8), respectively, and after

some simplifications, the zero- to higher-order PCE terms become

$$\begin{aligned}
a_0\Gamma_0 &= \lambda_0 \\
\sum_{i=1}^{N} a_i\Gamma_1(X_i) &= \sum_{i=1}^{N} C_{i1}\psi_{i1}(X_i) \\
\sum_{i_1=1}^{N}\sum_{i_2=i_1}^{N} a_{i_1i_2}\Gamma_2(X_{i_1},X_{i_2}) &= \sum_{i=1}^{N} C_{i2}\psi_{i2}(X_i) \\
&\quad + \sum_{i_1,i_2=1;i_1<i_2}^{N} C_{i_1i_211}\psi_{i_11}(X_{i_1})\psi_{i_21}(X_{i_2}) \\
\sum_{i_1=1}^{N}\sum_{i_2=i_1}^{N}\sum_{i_3=i_2}^{N} a_{i_1i_2i_3}\Gamma_3(X_{i_1},X_{i_2},X_{i_3}) &= \sum_{i=1}^{N} C_{i3}\psi_{i3}(X_i) \\
&\quad + \sum_{i_1,i_2=1;i_1<i_2}^{N} C_{i_1i_212}\psi_{i_11}(X_{i_1})\psi_{i_22}(X_{i_2}) \\
&\quad + \sum_{i_1,i_2=1;i_1<i_2}^{N} C_{i_2i_321}\psi_{i_12}(X_{i_1})\psi_{i_21}(X_{i_2}) \\
&\quad + \sum_{i_1,i_2,i_3=1;i_1<i_2<i_3}^{N} C_{i_1i_2i_3111} \\
&\quad \times\psi_{i_11}(X_{i_1})\psi_{i_21}(X_{i_2})\psi_{i_31}(X_{i_3}) \\
\cdots &= \cdots,
\end{aligned} \tag{3.9}$$

revealing constituents comprising constant, univariate functions, bivariate functions, and so on. Collecting all univariate terms, all bivariate terms, *etc.*, from each appro-

priate line of Equation (3.9) leads to

$$
\begin{aligned}
\lambda_{PCE}(\boldsymbol{X}) &= \lim_{p\to\infty}\Bigg[\lambda_0 + \sum_{i=1}^{N}\sum_{j=1}^{p} C_{ij}\psi_{ij}(X_i) \\
&\quad + \sum_{i_1=1}^{N-1}\sum_{i_2=i_1+1}^{N} \underbrace{\sum_{j_2=1}^{p-1}\sum_{j_1=1}^{p-1}}_{j_1+j_2\le p} C_{i_1 i_2 j_1 j_2}\psi_{i_1 j_1}(X_{i_1})\psi_{i_2 j_2}(X_{i_2}) \\
&\quad + \sum_{i_1=1}^{N-2}\sum_{i_2=i_1+1}^{N-1}\sum_{i_3=i_2+1}^{N} \underbrace{\sum_{j_3=1}^{p-2}\sum_{j_2=1}^{p-2}\sum_{j_1=1}^{p-2}}_{j_1+j_2+j_3\le p} C_{i_1 i_2 i_3 j_1 j_2 j_3} \\
&\quad \times \psi_{i_1 j_1}(X_{i_1})\psi_{i_2 j_2}(X_{i_2})\psi_{i_3 j_3}(X_{i_3}) \\
&\quad + \cdots + \sum_{i_1=1}^{1}\cdots\sum_{i_N=i_{N-1}+1}^{N} \underbrace{\sum_{j_N=1}^{p-N+1}\cdots\sum_{j_1=1}^{p-N+1}}_{j_1+\cdots+j_N\le p} C_{i_1\cdots i_N j_1\cdots j_N}\prod_{q=1}^{N}\psi_{i_q j_q}(X_{i_q})\Bigg] \\
&= \lambda_0 + \sum_{i=1}^{N}\sum_{j=1}^{\infty} C_{ij}\psi_{ij}(X_i) \\
&\quad + \sum_{i_1=1}^{N-1}\sum_{i_2=i_1+1}^{N}\sum_{j_2=1}^{\infty}\sum_{j_1=1}^{\infty} C_{i_1 i_2 j_1 j_2}\psi_{i_1 j_1}(X_{i_1})\psi_{i_2 j_2}(X_{i_2}) \\
&\quad + \sum_{i_1=1}^{N-2}\sum_{i_2=i_1+1}^{N-1}\sum_{i_3=i_2+1}^{N}\sum_{j_3=1}^{\infty}\sum_{j_2=1}^{\infty}\sum_{j_1=1}^{\infty} C_{i_1 i_2 i_3 j_1 j_2 j_3} \\
&\quad \times \psi_{i_1 j_1}(X_{i_1})\psi_{i_2 j_2}(X_{i_2})\psi_{i_3 j_3}(X_{i_3}) \\
&\quad + \cdots + \sum_{i_1=1}^{1}\cdots\sum_{i_N=i_{N-1}+1}^{N}\sum_{j_N=1}^{\infty}\cdots\sum_{j_1=1}^{\infty} C_{i_1\cdots i_N j_1\cdots j_N}\prod_{q=1}^{N}\psi_{i_q j_q}(X_{i_q}) \\
&= \lambda_0 + \sum_{s=1}^{N}\Bigg[\underbrace{\sum_{i_1=1}^{N-s+1}\cdots\sum_{i_s=i_{s-1}+1}^{N}}_{s \text{ sums}} \underbrace{\sum_{j_1=1}^{\infty}\cdots\sum_{j_s=1}^{\infty}}_{s \text{ sums}} C_{i_1\cdots i_s j_1\cdots j_s}\prod_{q=1}^{s}\psi_{i_q j_q}(X_{i_q})\Bigg] \\
&=: \lambda_{PDD}(\boldsymbol{X}),
\end{aligned}
\tag{3.10}
$$

which proves the theorem for any square integrable function $\lambda : \mathbb{R}^N \to \mathbb{R}$, $1 \le N < \infty$, and probability distribution of $\boldsymbol{X}$. $\square$

3.3 Series Truncations and Approximate Solutions

Although Equations (3.1) and (3.4) provide an exact PDD and an exact PCE representation, respectively, they contain an infinite number of coefficients, emanating from infinite numbers of orthonormal polynomials. In practice, the number of coefficients must be finite, say, by retaining at most mth-order polynomials in each variable. Due to the contrasting dimensional structures of PDD and PCE, the convergence properties of their truncations are not the same and may differ significantly, depending on the eigensolution and dimension of the problem. This section presents the PDD and PCE approximation and an error analysis due to the approximations.

3.3.1 PDD approximation

The function λ can be approximated by a sum of at most S-variate component functions, where $1 \leq S \leq N$ is a truncation parameter, resulting in the S-variate, mth-order PDD approximation

$$\tilde{\lambda}_{S,m}(\boldsymbol{X}) = \lambda_0 + \sum_{s=1}^{S} \Bigg[\underbrace{\sum_{i_1=1}^{N-s+1} \cdots \sum_{i_s=i_{s-1}+1}^{N}}_{s \text{ sums}} \quad \underbrace{\sum_{j_1=1}^{m} \cdots \sum_{j_s=1}^{m}}_{s \text{ sums}} C_{i_1 \cdots i_s j_1 \cdots j_s} \prod_{q=1}^{s} \psi_{i_q j_q}(X_{i_q}) \Bigg], \tag{3.11}$$

containing

$$Q_{S,m} = \sum_{k=0}^{S} \binom{N}{S-k} m^{S-k} \tag{3.12}$$

number of PDD coefficients and corresponding orthonormal polynomials. The PDD approximation in Equation (3.11) includes cooperative effects of at most S input variables $X_{i_1}, \cdots, X_{i_S}$, $1 \leq i_1 \leq \cdots \leq i_S \leq N$, on λ. For instance, by selecting $S = 1$ and

2, the functions $\tilde{\lambda}_{1,m}(\boldsymbol{X})$ and $\tilde{\lambda}_{2,m}(\boldsymbol{X})$, provide univariate and bivariate mth-order approximations, respectively, contain contributions from all input variables, and should not be viewed as first- and second-order approximations; they also do not limit the nonlinearity of $\lambda(\boldsymbol{X})$. Depending on how the component functions are constructed, arbitrarily high-order univariate and bivariate terms of $\lambda(\boldsymbol{X})$ could be lurking inside $\tilde{\lambda}_{1,m}(\boldsymbol{X})$ and $\tilde{\lambda}_{2,m}(\boldsymbol{X})$. The fundamental conjecture underlying this decomposition is that the component functions arising in the function decomposition will exhibit insignificant S-variate effects cooperatively when $S \to N$, leading to useful lower-variate approximations of $\lambda(\boldsymbol{X})$. When $S \to N$ and $m \to \infty$, $\tilde{\lambda}_{S,m}(\boldsymbol{X})$ converges to $\lambda(\boldsymbol{X})$ in the mean-square sense, *i.e.*, Equation (3.11) generates a hierarchical and convergent sequence of approximations of $\lambda(\boldsymbol{X})$.

Applying the expectation operator on Equation (3.11) and noting Property 1, the mean $\mathbb{E}\left[\tilde{\lambda}_{S,m}(\boldsymbol{X})\right] = \lambda_0$ of the S-variate, mth-order approximation of the eigenvalue matches the exact mean of the eigenvalue in Equation (3.2), regardless of S or m. Applying the expectation operator again, this time on $\left[\tilde{\lambda}_{S,m}(\boldsymbol{X}) - \lambda_0\right]^2$, results in the approximate variance

$$\begin{aligned}\mathbb{E}\left[\tilde{\lambda}_{S,m}(\boldsymbol{X}) - \lambda_0\right]^2 \;=\; \sum_{s=1}^{S}\sum_{t=1}^{S}\Bigg(& \underbrace{\sum_{i_1=1}^{N-s+1}\cdots\sum_{i_s=i_{s-1}+1}^{N}\sum_{j_1=1}^{m}\cdots\sum_{j_s=1}^{m}}_{2s \text{ sums}} \\ & \times \underbrace{\sum_{k_1=1}^{N-t+1}\cdots\sum_{k_t=k_{t-1}+1}^{N}\sum_{l_1=1}^{m}\cdots\sum_{l_t=1}^{m}}_{2t \text{ sums}} C_{i_1\cdots i_s j_1\cdots j_s} \\ & \times C_{k_1\cdots k_t l_1\cdots l_t}\mathbb{E}\left[\prod_{q=1}^{s}\psi_{i_q j_q}(X_{i_q})\prod_{q=1}^{t}\psi_{k_q l_q}(X_{k_q})\right]\Bigg)\end{aligned} \tag{3.13}$$

of the eigenvalue, which depends on S and m. The number of summations inside

the parenthesis of the right side of Equation (3.13) is $2(s+t)$, where s and t are the indices of the two outer summations. By virtue of Property 2 and independent coordinates of $\boldsymbol{X}$,

$$\mathbb{E}\left[\prod_{q=1}^{s}\psi_{i_q j_q}(X_{i_q})\prod_{q=1}^{t}\psi_{k_q l_q}(X_{k_q})\right]=\prod_{q=1}^{s}\mathbb{E}\left[\psi^2_{i_q j_q}(X_{i_q})\right]=1 \tag{3.14}$$

for $s=t$, $i_q=k_q, j_q=l_q$ and *zero* otherwise, leading to

$$\mathbb{E}\left[\tilde{\lambda}_{S,m}(\boldsymbol{X})-\lambda_0\right]^2=\sum_{s=1}^{S}\left(\underbrace{\sum_{i_1=1}^{N-s+1}\cdots\sum_{i_s=i_{s-1}+1}^{N}}_{s\text{ sums}}\ \underbrace{\sum_{j_1=1}^{m}\cdots\sum_{j_s=1}^{m}}_{s\text{ sums}}C^2_{i_1\cdots i_s j_1\cdots j_s}\right) \tag{3.15}$$

as the sum of squares of the expansion coefficients from the S-variate, mth-order PDD approximation of $\lambda(\boldsymbol{X})$. Clearly, the approximate variance in Equation (3.15) approaches the exact variance

$$\begin{aligned}\mathbb{E}\left[\lambda(\boldsymbol{X})-\lambda_0\right]^2 &= \mathbb{E}\left[\lambda_{PDD}(\boldsymbol{X})-\lambda_0\right]^2\\ &= \sum_{s=1}^{N}\left(\underbrace{\sum_{i_1=1}^{N-s+1}\cdots\sum_{i_s=i_{s-1}+1}^{N}}_{s\text{ sums}}\ \underbrace{\sum_{j_1=1}^{\infty}\cdots\sum_{j_s=1}^{\infty}}_{s\text{ sums}}C^2_{i_1\cdots i_s j_1\cdots j_s}\right)\end{aligned} \tag{3.16}$$

of the eigenvalue when $S\to N$ and $m\to\infty$. The mean-square convergence of $\tilde{\lambda}_{S,m}$ is guaranteed as λ, and its component functions are all members of the associated Hilbert spaces.

Remark 3.1: The expansion order m, which is a positive integer, should be interpreted as the largest exponent of a single variable from the monomials (terms) of the PDD approximation. Based on the traditional definition, the total order of the multivariate polynomial in the right side of Equation (3.11) is Sm, although all monomials with total degrees equal to or less than Sm are not present.

3.3.2 PCE approximation

The pth-order PCE approximation

$$\begin{aligned}\bar{\lambda}_p(\boldsymbol{X}) \;:=\; & a_0\Gamma_0 + \sum_{i=1}^{N} a_i\Gamma_1(X_i) + \sum_{i_1=1}^{N}\sum_{i_2=i_1}^{N} a_{i_1i_2}\Gamma_2(X_{i_1},X_{i_2}) \\ & + \sum_{i_1=1}^{N}\sum_{i_2=i_1}^{N}\sum_{i_3=i_2}^{N} a_{i_1i_2i_3}\Gamma_3(X_{i_1},X_{i_2},X_{i_3}) \\ & + \cdots + \sum_{i_1=1}^{N}\cdots\sum_{i_p=i_{p-1}}^{N} a_{i_1\cdots i_p}\Gamma_p(X_{i_1},\cdots,X_{i_p}),\end{aligned} \tag{3.17}$$

obtained directly by truncating the right side of Equation (3.4), requires $(N+p)!/(N!p!)$ number of the PCE coefficients. However, since PDD and PCE are related, the terms of Equation (3.17) can be rearranged following similar derivations in proving Theorem 3.1, resulting in

$$\begin{aligned}\bar{\lambda}_p(\boldsymbol{X}) \;=\; & \lambda_0 + \sum_{i=1}^{N}\sum_{j=1}^{p} C_{ij}\psi_{ij}(X_i) \\ & + \sum_{i_1=1}^{N-1}\sum_{i_2=i_1+1}^{N}\underbrace{\sum_{j_2=1}^{p-1}\sum_{j_1=1}^{p-1}}_{j_1+j_2\le p} C_{i_1i_2j_1j_2}\psi_{i_1j_1}(X_{i_1})\psi_{i_2j_2}(X_{i_2}) \\ & + \sum_{i_1=1}^{N-2}\sum_{i_2=i_1+1}^{N-1}\sum_{i_3=i_2+1}^{N}\underbrace{\sum_{j_3=1}^{p-2}\sum_{j_2=1}^{p-2}\sum_{j_1=1}^{p-2}}_{j_1+j_2+j_3\le p} C_{i_1i_2i_3j_1j_2j_3} \\ & \times\psi_{i_1j_1}(X_{i_1})\psi_{i_2j_2}(X_{i_2})\psi_{i_3j_3}(X_{i_3}) \\ & + \cdots + \sum_{i_1=1}^{N-s+1}\cdots\sum_{i_s=i_{s-1}+1}^{N}\underbrace{\sum_{j_N=1}^{p-N+1}\cdots\sum_{j_1=1}^{p-N+1}}_{j_1+\cdots+j_N\le p} C_{i_1\cdots i_Nj_1\cdots j_N}\prod_{q=1}^{N}\psi_{i_qj_q}(X_{i_q})\end{aligned} \tag{3.18}$$

with the generic $(s+1)$th term, $s = 1, \cdots, p$, shown or its abbreviated form

$$\bar{\lambda}_p(\boldsymbol{X}) = \lambda_0 + \sum_{s=1}^{N} \Bigg[\underbrace{\sum_{i_1=1}^{N-s+1} \cdots \sum_{i_s=i_{s-1}+1}^{N}}_{s \text{ sums}} \underbrace{\sum_{j_1=1}^{p-s+1} \cdots \sum_{j_s=1}^{p-s+1}}_{s \text{ sums}; j_1+\cdots+j_s \leq p} C_{i_1 \cdots i_s j_1 \cdots j_s} \prod_{q=1}^{s} \psi_{i_q j_q}(X_{i_q}) \Bigg], \tag{3.19}$$

involving solely

$$Q_p = \sum_{k=0}^{N} \binom{N}{N-k} \binom{p}{N-k} \tag{3.20}$$

number of PDD coefficients and corresponding orthonormal polynomials, where $\binom{p}{N-k}$ should be interpreted as *zero* when $p < N-k$. It is elementary to show that Q_p matches $(N+p)!/(N!p!)$, the original number of PCE coefficients from Equation (3.17). The advantage of Equation (3.19) over Equation (3.17) is that the PDD coefficients, once determined, can be reused for the PCE approximation, thereby sidestepping calculations of the PCE coefficients.

Applying the expectation operator on Equation (3.19) and noting Property 1, the mean $\mathbb{E}\left[\bar{\lambda}_p(\boldsymbol{X})\right] = \lambda_0$ of the pth-order PCE approximation of the eigenvalue also matches the exact mean of the eigenvalue for any expansion order. Applying the expectation operator on $\left[\bar{\lambda}_p(\boldsymbol{X}) - \lambda_0\right]^2$ and following similar arguments as before, the variance of the pth-order PCE approximation of the eigenvalue is

$$\mathbb{E}\left[\bar{\lambda}_p(\boldsymbol{X}) - \lambda_0\right]^2 = \sum_{s=1}^{N} \Bigg(\underbrace{\sum_{i_1=1}^{N-s+1} \cdots \sum_{i_s=i_{s-1}+1}^{N}}_{s \text{ sums}} \underbrace{\sum_{j_1=1}^{p-s+1} \cdots \sum_{j_s=1}^{p-s+1}}_{s \text{ sums}; j_1+\cdots+j_s \leq p} C^2_{i_1 \cdots i_s j_1 \cdots j_s} \Bigg), \tag{3.21}$$

another sum of squares of the PDD expansion coefficients such that $j_1 + \cdots + j_s \leq p$, which also converges to $\mathbb{E}\left[\lambda(\boldsymbol{X}) - \lambda_0\right]^2$ as $p \to \infty$.

Remark 3.2: Two important observations can be made when comparing the PDD

and PCE approximations expressed by Equations (3.11) and (3.17), respectively. First, the terms in the PCE approximation are organized with respect to the order of polynomials. In contrast, the PDD approximation is structured with respect to the degree of cooperativity between a finite number of random variables. Therefore, significant differences may exist regarding the accuracy, efficiency, and convergence properties of their truncated sum or series. Second, if an eigenvalue response is highly nonlinear, but contains rapidly diminishing cooperative effects of multiple random variables, the PDD approximation is expected to be more effective than the PCE approximation. This is because the lower-variate (univariate, bivariate, *etc.*) terms of the PDD approximation can be just as nonlinear by selecting appropriate values of m in Equation (3.11). In contrast, many more terms and expansion coefficients are required to be included in the PCE approximation to capture such high nonlinearity.

Remark 3.3: Depending on the problem size (N) and truncation parameters (S, m, p), there exist a few special cases where the PDD and PCE approximations coincide: (1) when $N = 1$, the univariate, mth-order PDD and mth-order PCE approximations are the same, *i.e.*, $\tilde{\lambda}_{1,m}(X) = \bar{\lambda}_m(X)$ for any $1 \leq m < \infty$; (2) for any arbitrary value of N, the univariate, first-order PDD, and first-order PCE approximations are the same, *i.e.*, $\tilde{\lambda}_{1,1}(\boldsymbol{X}) = \bar{\lambda}_1(\boldsymbol{X})$.

Remark 3.4: The PDD and PCE approximations, regardless of the truncation parameters, predict the exact mean of an eigenvalue. However, the calculated variances of an eigenvalue from Equations (3.15) and (3.21) for $S < N$, $m < \infty$, and $p < \infty$ are neither the same nor exact in general. Therefore, an error analysis, at least per-

taining to the second-moment properties of eigensolutions, is required for comparing the PDD and PCE approximations.

3.3.3 Error analysis

Define two errors,

$$\begin{aligned} e_{S,m} &:= \mathbb{E}\left[\lambda(\boldsymbol{X}) - \tilde{\lambda}_{S,m}(\boldsymbol{X})\right]^2 \\ &= \mathbb{E}\left[\lambda_{PDD}(\boldsymbol{X}) - \tilde{\lambda}_{S,m}(\boldsymbol{X})\right]^2 = \int_{\mathbb{R}^N}\left[\lambda_{PDD}(\boldsymbol{x}) - \tilde{\lambda}_{S,m}(\boldsymbol{x})\right]^2 f_{\boldsymbol{X}}(\boldsymbol{x})d\boldsymbol{x} \end{aligned} \tag{3.22}$$

and

$$\begin{aligned} e_p &:= \mathbb{E}\left[\lambda(\boldsymbol{X}) - \bar{\lambda}_p(\boldsymbol{X})\right]^2 \\ &= \mathbb{E}\left[\lambda_{PDD}(\boldsymbol{X}) - \bar{\lambda}_p(\boldsymbol{X})\right]^2 = \int_{\mathbb{R}^N}\left[\lambda_{PDD}(\boldsymbol{x}) - \bar{\lambda}_p(\boldsymbol{x})\right]^2 f_{\boldsymbol{X}}(\boldsymbol{x})d\boldsymbol{x}, \end{aligned} \tag{3.23}$$

owing to S-variate, mth-order PDD approximation $\tilde{\lambda}_{S,m}(\boldsymbol{X})$ and pth-order PCE approximation $\bar{\lambda}_p(\boldsymbol{X})$, respectively, of $\lambda(\boldsymbol{X})$. Replacing λ_{PDD}, $\tilde{\lambda}_{S,m}$, and $\bar{\lambda}_p$ in Equations (3.22) and (3.23) with the right sides of Equations (3.1), (3.11), and (3.19), respectively, and invoking Properties 1 and 2 yields the PDD error

$$\begin{aligned} e_{S,m} = &\sum_{s=1}^{S}\left(\underbrace{\sum_{i_1=1}^{N-s+1}\cdots\sum_{i_s=i_{s-1}+1}^{N}}_{s\text{ sums}}\ \underbrace{\sum_{j_1=m+1}^{\infty}\cdots\sum_{j_s=m+1}^{\infty}}_{s\text{ sums}} C^2_{i_1\cdots i_s j_1\cdots j_s}\right) \\ &+\sum_{s=S+1}^{N}\left(\underbrace{\sum_{i_1=1}^{N-s+1}\cdots\sum_{i_s=i_{s-1}+1}^{N}}_{s\text{ sums}}\ \underbrace{\sum_{j_1=1}^{\infty}\cdots\sum_{j_s=1}^{\infty}}_{s\text{ sums}} C^2_{i_1\cdots i_s j_1\cdots j_s}\right) \end{aligned} \tag{3.24}$$

and the PCE error

$$e_p = \sum_{s=1}^{N}\left(\underbrace{\sum_{i_1=1}^{N-s+1}\cdots\sum_{i_s=i_{s-1}+1}^{N}}_{s\text{ sums}}\ \underbrace{\sum_{j_1=1}^{\infty}\cdots\sum_{j_s=1}^{\infty}}_{s\text{ sums};j_1+\cdots+j_s>p} C^2_{i_1\cdots i_s j_1\cdots j_s}\right), \tag{3.25}$$

both consisting of the eliminated PDD coefficients as a result of truncations. In Equation (3.24), the first term of the PDD error is due to the truncations of polynomial expansion orders involving main and cooperative effects of at most S variables, whereas the second term of the PDD error is contributed by ignoring the cooperative effects of larger than S variables. In contrast, the PCE error in Equation (3.25) derives from the truncations of polynomial expansion orders involving all main and cooperative effects. By selecting $1 \leq S \leq N$, $1 \leq m < \infty$, and $1 \leq p < \infty$, the errors can be determined for any PDD and PCE approximations, provided that all coefficients required by Equations (3.24) and (3.25) can be calculated.

For a general REP, comparing the PDD and PCE errors theoretically based on Equations (3.24) and (3.25) is not simple, as it depends on which expansion coefficients decay and how they decay with respect to the truncation parameters S, m, and p. However, for a class of problems where the cooperative effects of S input variables on an eigenvalue get progressively weaker as $S \to N$, the PDD and PCE errors for identical expansion orders can be weighed against each other. For this special case, $m = p$, assume that $C_{i_1 \cdots i_s j_1 \cdots j_s} = 0$, where $s = S+1, \cdots, N$, $1 \leq i_1 < \cdots < i_s \leq N$, $j_1, \cdots j_s = 1, \cdots, \infty$, for both the PDD and PCE approximations. Then, the second

term on the right side of Equation (3.24) vanishes, resulting in the PDD error

$$\begin{aligned} e_{S,m} &= \sum_{s=1}^{S}\left(\underbrace{\sum_{i_1=1}^{N-s+1}\cdots\sum_{i_s=i_{s-1}+1}^{N}}_{s \text{ sums}} \underbrace{\sum_{j_1=m+1}^{\infty}\cdots\sum_{j_s=m+1}^{\infty}}_{s \text{ sums}} C^2_{i_1\cdots i_s j_1\cdots j_s}\right) \\ &= \sum_{s=1}^{S}\left(\underbrace{\sum_{i_1=1}^{N-s+1}\cdots\sum_{i_s=i_{s-1}+1}^{N}}_{s \text{ sums}} \underbrace{\sum_{j_1=1}^{\infty}\cdots\sum_{j_s=1}^{\infty}}_{s \text{ sums}} C^2_{i_1\cdots i_s j_1\cdots j_s}\right) \\ &\quad -\sum_{s=1}^{S}\left(\underbrace{\sum_{i_1=1}^{N-s+1}\cdots\sum_{i_s=i_{s-1}+1}^{N}}_{s \text{ sums}} \underbrace{\sum_{j_1=1}^{m}\cdots\sum_{j_s=1}^{m}}_{s \text{ sums}} C^2_{i_1\cdots i_s j_1\cdots j_s}\right), \end{aligned} \tag{3.26}$$

while the PCE error can be split into

$$\begin{aligned} e_m &= \sum_{s=1}^{S}\left(\underbrace{\sum_{i_1=1}^{N-s+1}\cdots\sum_{i_s=i_{s-1}+1}^{N}}_{s \text{ sums}} \underbrace{\sum_{j_1=1}^{\infty}\cdots\sum_{j_s=1}^{\infty}}_{s \text{ sums}} C^2_{i_1\cdots i_s j_1\cdots j_s}\right) \\ &\quad -\sum_{s=1}^{S}\left(\underbrace{\sum_{i_1=1}^{N-s+1}\cdots\sum_{i_s=i_{s-1}+1}^{N}}_{s \text{ sums}} \underbrace{\sum_{j_1=1}^{m-s+1}\cdots\sum_{j_s=1}^{m-s+1}}_{s \text{ sums};j_1+\cdots+j_s\le m} C^2_{i_1\cdots i_s j_1\cdots j_s}\right) \\ &\ge \sum_{s=1}^{S}\left(\underbrace{\sum_{i_1=1}^{N-s+1}\cdots\sum_{i_s=i_{s-1}+1}^{N}}_{s \text{ sums}} \underbrace{\sum_{j_1=1}^{\infty}\cdots\sum_{j_s=1}^{\infty}}_{s \text{ sums}} C^2_{i_1\cdots i_s j_1\cdots j_s}\right) \\ &\quad -\sum_{s=1}^{S}\left(\underbrace{\sum_{i_1=1}^{N-s+1}\cdots\sum_{i_s=i_{s-1}+1}^{N}}_{s \text{ sums}} \underbrace{\sum_{j_1=1}^{m}\cdots\sum_{j_s=1}^{m}}_{s \text{ sums}} C^2_{i_1\cdots i_s j_1\cdots j_s}\right) \\ &= e_{S,m}, \end{aligned} \tag{3.27}$$

demonstrating larger error from the PCE approximation than from the PDD approximation. In the limit, when $S = N$, similar derivations show $e_m \ge e_{N,m}$, regardless of the values of the expansions coefficients. In other words, the N-variate, mth-order PDD approximation cannot be worse than the mth-order PCE approximation. When $S < N$ and $C_{i_1\cdots i_s j_1\cdots j_s}$, $s = S+1, \cdots, N$, $1 \le i_1 < \cdots < i_s \le N$, $j_1, \cdots j_s = 1, \cdots, \infty$,

are not negligible and arbitrary, numerical convergence analysis is required for comparing these two errors.

Remark 3.5: The stochastic and error analyses aimed at higher-order moments or probability distribution of λ can be envisioned, but no closed-form solutions or simple expressions are possible. However, if λ is sufficiently smooth with respect to $\boldsymbol{X}$ − a condition fulfilled by many realistic eigenvalue problems − then Monte Carlo simulation of both the PDD and PCE approximations can be efficiently conducted for estimating the tail probabilistic characteristics of eigensolutions as well.

3.4 Expansion Coefficients

The determination of the expansion coefficients required by the PDD or PCE approximation involves various N-dimensional integrals over $\mathbb{R}^N$ and is computationally prohibitive to evaluate when N is arbitrarily large. Instead, a dimension-reduction integration, presented as follows, was applied to estimate the coefficients efficiently [87].

3.4.1 Dimension-reduction integration

Let $\boldsymbol{c} = \{c_1, \cdots, c_N\}^T$ be a reference point of input $\boldsymbol{X}$ and $\lambda(c_1, \cdots, c_{i_1-1}, X_{i_1}, c_{i_1+1}, \cdots, c_{i_{R-k}-1}, X_{i_{R-k}}, c_{i_{R-k}+1}, \cdots, c_N)$ represent an $(R-k)^{\text{th}}$ dimensional component function of $\lambda(\boldsymbol{X})$, where $1 \leq R < N$ is an integer, $k = 0, \cdots, R$, and $1 \leq i_1 < \cdots < i_{R-k} \leq N$. For example, when $R = 1$, the zero-dimensional component function, which is a constant, is $\lambda(\boldsymbol{c})$ and the one-dimensional component functions are $\lambda(X_1, c_2, \cdots, c_N)$, $\lambda(c_1, X_2, \cdots, c_N)$, $\cdots$, $\lambda(c_1, c_2, \cdots, X_N)$. Using Xu

and Rahman's multivariate function theorem [85], it can be shown that the R-variate approximation of $\lambda(\boldsymbol{X})$, defined by

$$\hat{\lambda}_R(\boldsymbol{X}) \;:=\; \sum_{k=0}^{R}(-1)^k \begin{pmatrix} N-R+k-1 \\ k \end{pmatrix} \times \underbrace{\sum_{i_1=1}^{N-R+k+1} \cdots \sum_{i_{R-k}=i_{R-k-1}+1}^{N}}_{(R-k)\text{ sums}} y(c_1, \cdots, c_{i_1-1}, X_{i_1}, c_{i_1+1}, \cdots, c_{i_{R-k}-1}, X_{i_{R-k}}, c_{i_{R-k}+1}, \cdots, c_N), \tag{3.28}$$

consists of all terms of the Taylor series of $\lambda(\boldsymbol{X})$ that have less than or equal to R variables. The expanded form of Equation (3.28), when compared with the Taylor expansion of $\lambda(\boldsymbol{X})$, indicates that the residual error in $\hat{\lambda}_R(\boldsymbol{X})$ includes terms of dimensions $R+1$ and higher. All higher-order R- and lower-variate terms of $\lambda(\boldsymbol{X})$ are included in Equation (3.28), which should therefore generally provide a higher-order approximation of a multivariate function than equations derived from first- or second-order Taylor expansions. Therefore, for $R < N$, an N-dimensional integral can be efficiently estimated by at most R-dimensional integrations, if the contributions from terms of dimensions $R+1$ and higher are negligible.

Substituting $\lambda(\boldsymbol{x})$ in Equations (3.2) and (3.3) by $\hat{\lambda}_R(\boldsymbol{x})$, the coefficients can be estimated from

$$\begin{aligned} \lambda_0 \;\cong\; & \sum_{k=0}^{R}(-1)^k \begin{pmatrix} N-R+k-1 \\ k \end{pmatrix} \underbrace{\sum_{i_1=1}^{N-R+k+1} \cdots \sum_{i_{R-k}=i_{R-k-1}+1}^{N}}_{(R-k)\text{ sums}} \times \\ & \int_{R-k}^{\mathbb{R}^{R-k}} \lambda(c_1, \cdots, c_{i_1-1}, x_{i_1}, c_{i_1+1}, \cdots, c_{i_{R-k}-1}, x_{i_{R-k}}, c_{i_{R-k}+1}, \cdots, c_N) \times \\ & \prod_{q=1} f_{k_q}(x_{k_q}) dx_{k_q} \end{aligned} \tag{3.29}$$

and

$$C_{i_1\cdots i_s j_1\cdots j_s} \cong \sum_{k=0}^{R}(-1)^k \begin{pmatrix} N-R+k-1 \\ k \end{pmatrix} \underbrace{\sum_{i_1=1}^{N-R+k+1} \cdots \sum_{i_{R-k}=i_{R-k-1}+1}^{N}}_{(R-k)\text{ sums}} \times$$
$$\int_{\mathbb{R}^{R-k}} \lambda(c_1, \cdots, c_{i_1-1}, x_{i_1}, c_{i_1+1}, \cdots, c_{i_{R-k}-1}, x_{i_{R-k}}, c_{i_{R-k}+1}, \cdots, c_N) \times$$
$$\prod_{p=1}^{s} \psi_{i_p j_p}(x_{i_p}) \prod_{q=1}^{R-k} f_{k_q}(x_{k_q}) dx_{k_q}, \tag{3.30}$$

which require evaluating at most R-dimensional integrals. Equations (3.29) and (3.30), which facilitate calculation of coefficients approaching their exact values as $R \to N$, are more efficient than performing one N-dimensional integration, as in Equations (3.2) and (3.3), particularly when $R \ll N$. Hence, the computational effort in calculating the coefficients is significantly lowered using the dimension-reduction integration. When $R = 1$, 2, or 3, Equations (3.29) and (3.30) involve one-, at most two-, and at most three-dimensional integrations, respectively. Nonetheless, numerical integration is still required for a general function λ. The integration points and associated weights depend on the probability distribution of X_i. They are readily available as Gauss-Hermite, Gauss-Legendre, and Gauss-Jacobi quadrature rules when a random variable follows Gaussian, uniform, and Beta distributions, respectively [88]. In performing the dimension-reduction integration, the value of R should be selected in such a way that it is either equal to or greater than the value of s. Then the expansion coefficient $C_{i_1\cdots i_s j_1\cdots j_s}$ will have a non-trivial solution [87].

3.4.2 Computational efforts

The S-variate, mth-order PDD approximation requires evaluations of $Q_{S,m} = \sum_{k=0}^{k=S} \binom{N}{S-k} m^{S-k}$ number of PDD coefficients: λ_0 and $C_{i_1 \cdots i_s j_1 \cdots j_s}$, $s = 1, \cdots, S$, $1 \leq i_1 < \cdots < i_s \leq N$, $j_1, \cdots, j_s = 1, \cdots, m$. If these coefficients are estimated by dimension-reduction integration with $R = S < N$ and, therefore, involve at most S-dimensional tensor product of an n-point univariate quadrature rule depending on m in Equations (3.29) and (3.30), then the following deterministic responses (eigenvalue or function evaluations) are required: $\lambda(\boldsymbol{c})$, $\lambda(c_1, \cdots, c_{i_1-1}, x_{i_1}^{(k_1)}, c_{i_1+1}, \cdots, c_{i_s-1}, x_{i_s}^{(k_s)}, c_{i_s+1}, \cdots, c_N)$ for $k_1, \cdots, k_s = 1, \cdots, n(m)$, where the superscripts on variables indicate corresponding integration points. Therefore, the total cost for the S-variate, mth-order PDD approximation entails a maximum of $\sum_{k=0}^{k=S} \binom{N}{S-k} n^{S-k}(m)$ eigenvalue evaluations. If the integration points include a common point in each coordinate − a special case of symmetric input probability density functions and odd values of n (see Examples 2-5) − the number of eigenvalue evaluations reduces to $\sum_{k=0}^{k=S} \binom{N}{S-k} (n(m)-1)^{S-k}$. In other words, the computational complexity of the PDD approximation is Sth-order polynomial with respect to the number of random variables or integration points.

In contrast, the pth-order PCE approximation requires evaluations of $Q_p = \sum_{k=0}^{N} \binom{N}{N-k} \binom{p}{N-k}$ number of PDD coefficients λ_0 and $C_{i_1 \cdots i_s j_1 \cdots j_s}$, $s = 1, \cdots, N$, $1 \leq i_1 < \cdots < i_s \leq N$, $j_1 + \cdots + j_s \leq p$, which can again be estimated by dimension-reduction integration by selecting $R = p < N$, and therefore involving at most p-dimensional tensor product of an n-point univariate quadrature rule, where

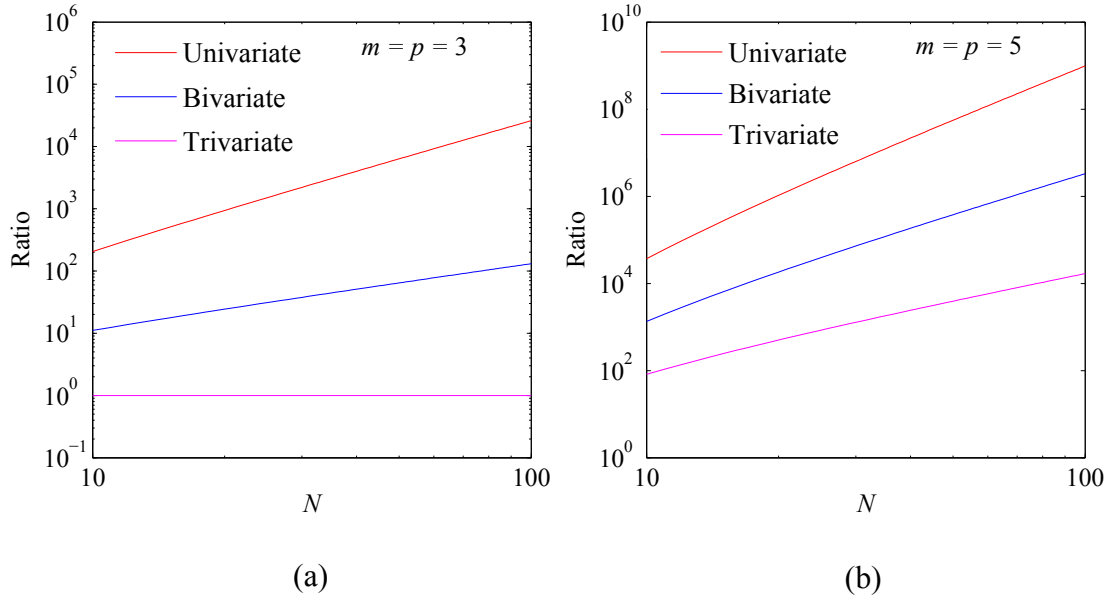

Figure 3.1: Ratio of eigenvalue evaluations by the PCE and PDD approximations for two identical polynomial expansion orders; (a) $m = p = 3$; (b) $m = p = 5$. Note: a ratio greater than one indicates higher computational cost of the PCE approximation than the PDD approximation

n depends on p. As a result, the total cost for the pth-order PCE approximation consists of a maximum of $\sum_{k=0}^{k=p} \binom{N}{p-k} n^{p-k}(p)$ eigenvalue evaluations in general, or $\sum_{k=0}^{k=p} \binom{N}{p-k} (n(p)-1)^{p-k}$ eigenvalue evaluations for a particular case discussed earlier. In either case, the computational complexity of the PCE approximation is a pth-order polynomial with respect to the number of random variables or integration points.

Figures 3.1(a) and 3.1(b) present plots of the ratio of numbers of eigenvalue evaluations by the PCE and PDD approximations, $\sum_{k=0}^{k=p} \binom{N}{p-k} \times n^{p-k}(p) / \sum_{k=0}^{k=S} \binom{N}{S-k} \times n^{S-k}(m)$, as a function of the dimension N for two cases of identical expansion orders $m = p = 3$ and $m = p = 5$, respectively, where $n = m + 1 = p + 1$. The plots in each figure were developed separately for $S = 1$ (univariate), $S = 2$

(bivariate), and $S = 3$ (trivariate) PDD approximations. From the results of Figures 3.1(a) and 3.1(b), regardless of the plot, the ratios are mostly larger than one, indicating greater computational need by the PCE approximation than by the PDD approximation. When $S \ll N$ and $m = p \gg 1$, the PCE approximation is expected to be significantly more expensive than the PDD approximation.

Remark 3.6: When $S = N$ in PDD or $p \geq N$ in PCE, Equations (3.28)-(3.30) are irrelevant, eliminating the possibility of any dimension reduction. However, these special cases, evoking merely academic interest, are rarely observed for practical applications with moderate to large numbers of random variables. Nonetheless, the expansion coefficients for these cases can be calculated using the full N-dimensional tensor product of the univariate quadrature formulae, consequently demanding n^N eigenvalue evaluations, where n depends on m or p, for both the PDD and PCE approximations.

3.5 Numerical Examples

Five numerical examples involving two well-known mathematical functions and three eigenvalue problems are presented to illustrate the performance of the PDD and PCE approximations for calculating the statistical moments of output functions or eigenvalues, including tail probability distributions of natural frequencies. In Examples 1 and 2, the classical Legendre polynomials and associated Gauss-Legendre quadrature formulae were employed to evaluate the expansion coefficients. However, in Examples 3-5, all original random variables were transformed into standard Gaus-

sian random variables, employing Hermite orthonormal polynomials as bases and the Gauss-Hermite quadrature rule for calculating the expansion coefficients. The expansion coefficients in Example 1 were calculated by full N-dimensional integrations. However, in Examples 2 through 5, the coefficients were estimated by dimension-reduction integration when $S = p < N$, so that an S-variate, mth-order PDD or pth-order PCE approximation requires at most S- or p-dimensional numerical integration. For the third and fourth examples, the eigenvalues were calculated by a hybrid double-shifted LR-QR algorithm [105]. A Lanczos algorithm embedded in the commercial code Abaqus (Version 6.9) [108] was employed for the fifth example. In Examples 3 and 4, the sample sizes for crude Monte Carlo simulation and the embedded Monte Carlo simulation of the PDD and PCE methods are both 10^6. The respective sample sizes are $50,000$ and 10^6 in Example 5. The expansion orders m and p vary depending on the example, but in all cases the number of integration points $n = m + 1$ or $n = p + 1$.

3.5.1 Polynomial function

Consider the polynomial function

$$\lambda(\boldsymbol{X}) = \frac{1}{2^N} \prod_{i=1}^{N} (3X_i^2 + 1) \tag{3.31}$$

studied by Sudret [116], where X_i, $i = 1, \cdots .N$, are independent and identical random variables, each following standard uniform distribution over [0,1]. From elementary calculations, the exact mean $\mathbb{E}[\lambda(\boldsymbol{X})] = 1$ and the exact variance $\sigma^2 = (6/5)^N - 1$.

The second-moment analysis in this example was conducted for two problem

sizes (dimensions): (1) $N = 3$; and (2) $N = 5$. For $N = 3$, Equation (3.31) represents a sixth-order, trivariate, polynomial function, which is a product of three quadratic polynomials in each variable. Therefore, a trivariate, second-order PDD approximation ($S = 3$, $m = 2$) with second-order Legendre polynomials (interval $= [-1, +1]$) in Equation (3.11) should exactly reproduce λ. Since X_1, X_2, and X_3 are independent, the highest order of integrands for calculating the expansion coefficients is four. A three-point Gauss-Legendre quadrature should then provide the exact values of all coefficients. Therefore, if the expansion coefficients are calculated using $m \geq 2$ in Equation (3.11), and Equations (3.2) and (3.3) are numerically integrated with $n \geq m + 1$, then the only source of error in a truncated PDD is the selection of S.

For $N = 3$, Table 3.1 presents the relative errors, defined as the ratio of the absolute difference between the exact and approximate variances of $\lambda(\boldsymbol{X})$ to the exact variance of $\lambda(\boldsymbol{X})$, from the univariate ($S = 1$), bivariate ($S = 2$), and trivariate ($S = 3$) PDD approximations. They were calculated for m varying from one to six, involving eight to 343 function evaluations, respectively, when estimating the expansion coefficients by full N-dimensional integrations. The errors from all three PDD approximations drop as m increases, but they level off quickly at their respective limits for the univariate and bivariate PDD approximations. When $m = 2$, the error due to the trivariate PDD approximation is *zero* as the PDD approximation coincides with $\lambda(\boldsymbol{X})$ in Equation (3.31), as expected. For comparison, the same problem was solved using the PCE approximation with p varying from one to six and correspondingly requiring eight to 343 function evaluations. The relative errors

by the PCE approximation enumerated in Table 3.1 also converge to *zero*, but at an expansion order $p = 6$, which is three times larger than the order of univariate polynomials required by the PDD method. At exactness, the PDD method is more efficient than the PCE method by a factor of $343/27 \cong 13$.

Table 3.1: Relative errors in calculating the variance of the polynomial function for $N = 3$ by the PDD and PCE approximations (Example 1)

	PDD[a]				
m or p	$S = 1$ $(\times 10^{-1})$	$S = 2$ $(\times 10^{-2})$	$S = 3$ $(\times 10^{-2})$	PCE[a]	No. of function evaluations[b]
1	2.273	8.246	7.341	2.273×10^{-1}	8
2	1.758	1.099	0	3.095×10^{-2}	27
3	1.758	1.099	–[c]	2.578×10^{-3}	64
4	1.758	1.099	–[c]	1.234×10^{-4}	125
5	1.758	1.099	–[c]	2.683×10^{-6}	216
6	1.758	1.099	–[c]	0	343

[a] The variances from trivariate PDD for $m = 2$ and PCE for $p = 6$ coincide with the exact solution: $\sigma^2 = (6/5)^N - 1$, where $N = 3$.

[b] The number of function evaluations by all three PDD and PCE methods employing a full N-dimensional numerical integration and n-point univariate Gauss-Legendre rule is n^N, where $N = 3$, $n = m + 1$, and $1 \leq m \leq 6$.

[c] Not required.

The function in Equation (3.31) was also studied for a slightly larger dimension: $N = 5$. The associated errors of the pentavariate ($S = 5$) PDD approximation and PCE approximation with several polynomial expansion orders are displayed in Table 3.2. Again, both the PDD and PCE methods produce zero errors, but, at the cost of second- and 10th-order expansions, respectively. As a result, the factor of efficiency

Table 3.2: Relative errors in calculating the variance of the polynomial function for $N = 5$ by the PDD and PCE approximations (Example 1)

m or p	Pentavariate PDD ($S = 5$)[a]	PCE[a]	No. of function evaluations[b]
1	8.528×10^{-1}	3.700×10^{-1}	32
2	0	9.189×10^{-2}	243
3	–[c]	1.610×10^{-2}	1024
4	–[c]	2.042×10^{-3}	3125
5	–[c]	1.882×10^{-4}	7776
6	–[c]	1.240×10^{-5}	16,807
7	–[c]	5.590×10^{-7}	32,768
8	–[c]	1.558×10^{-8}	59,049
9	–[c]	2.050×10^{-10}	100,000
10	–[c]	0	161,051

[a] The variances from trivariate PDD for $m = 2$ and PCE for $p = 10$ coincide with the exact solution: $\sigma^2 = (16/15)^N - 1$, where $N = 5$.

[b] The number of function evaluations by all three PDD and PCE methods employing a full N-dimensional numerical integration and n-point univariate Gauss-Legendre rule is n^N, where $N = 5$, $n = m + 1$, and $1 \leq m \leq 10$.

[c] Not required.

of the PDD method jumps to $161051/243 \cong 663$, even for such a small increase in the dimension. The higher efficiency of the PDD approximation for both problem sizes is attributed to its dimensional hierarchy, favorably exploiting the structure of λ.

3.5.2 Non-polynomial function

The second example involves second-moment analysis of the Ishigami and Homma function [117]

$$\lambda(\boldsymbol{X}) = \sin X_1 + a \sin^2 X_2 + b X_3^4 \sin X_1, \tag{3.32}$$

where X_i, $i = 1, 2, 3$, are three independent and identically distributed uniform random variables on $[-\pi, +\pi]$, and a and b are real-valued deterministic parameters. This function also permits the exact solution of the variance: $\sigma^2 = a^2/8 + b\pi^4/5 + b^2\pi^8/18 + 1/2$. Note that λ is a non-polynomial function; therefore, neither the PDD nor the PCE approximation will provide the exact solution, but their respective errors can be reduced to an arbitrarily low value by increasing the polynomial expansion orders successively. In this example, the following deterministic parameters were selected: $a = 7$, $b = 0.1$.

Since the right side of Equation (3.32) includes the cooperative effects of at most two variables, the bivariate PDD approximation is adequate for convergence analysis. In this example, the PDD expansion coefficients of the bivariate approximation were estimated using the Legendre polynomials (interval $= [-1, +1]$) of a specified order m and dimension-reduction integration (Gauss-Legendre quadrature rule) with $R = S = 2$, and $n = m + 1$. Several even orders, $m = 2, 4, 6, 8, 10, 12, 14, 16, 18$, were chosen in such a way that n remained an odd integer. In so doing, the corresponding number of function evaluations by the PDD method for a given m is $3m^2 + 3m + 1$. For the PCE approximation, the PDD expansion coefficients for a specified order $2 \leq p \leq 18$ and $n = p + 1$ were calculated by dimension-reduction integration when $p < 3$ involving $\sum_{k=0}^{k=p} \binom{3}{p-k} (n-1)^{p-k}$ function evaluations for even p and full three-dimensional integration when $p \geq 3$ involving n^3 function evaluations.

Figure 3.2 shows how the relative errors in the variances of $\lambda(\boldsymbol{X})$ from the bivariate PDD and PCE approximations vary with respect to the number (L) of

function evaluations. The data points of these plots were generated by calculating the approximate variances for the selected values of m or p and counting the corresponding number of function evaluations. Ignoring the first three data points in Figure 3.2, the errors of the PDD and PCE solutions decay proportionally to $L^{-17.5}$ and $L^{-12.1}$, respectively. Clearly, their convergence rates − the absolute values of the slopes of the trend lines in the log-log plots − are much higher than unity. The sampling-based methods, crude Monte Carlo and quasi-Monte Carlo, which have theoretical convergence rates in the range of 0.5 to 1, are no match for the PDD and PCE methods, which are endowed with significantly higher convergence rates, mostly due to the smoothness of λ. Furthermore, the PDD approximation converges markedly faster than the PCE approximation. Although a similar observation was made in Example 1, the validity of this trend depends on the function examined.

3.5.3 Two-degree-of-freedom, undamped, spring-mass system

Consider a two-degree-of-freedom, undamped, spring-mass system, shown in Figure 3.3, with random or deterministic mass and random stiffness matrices

$$\boldsymbol{M} = \begin{bmatrix} M_1(\boldsymbol{X}) & 0 \\ 0 & M_2(\boldsymbol{X}) \end{bmatrix} \text{ and } \boldsymbol{K}(\boldsymbol{X}) = \begin{bmatrix} K_1(\boldsymbol{X}) + K_3(\boldsymbol{X}) & -K_3(\boldsymbol{X}) \\ -K_3(\boldsymbol{X}) & K_2(\boldsymbol{X}) + K_3(\boldsymbol{X}) \end{bmatrix}, \tag{3.33}$$

respectively, where $K_1(\boldsymbol{X}) = 1000X_1$ N/m, $K_2(\boldsymbol{X}) = 1100X_2$ N/m, $K_3(\boldsymbol{X}) = 100X_3$ N/m, $M_1(\boldsymbol{X}) = X_4$ kg, and $M_2(\boldsymbol{X}) = 1.5X_5$ kg. The input $\boldsymbol{X} = \{X_1, X_2, X_3, X_4, X_5\}^T \in \mathbb{R}^5$ is an independent lognormal random vector with the mean vector $\boldsymbol{\mu_X} = \boldsymbol{1} \in \mathbb{R}^5$ and covariance matrix $\boldsymbol{\Sigma_X} = \text{diag}(v_1^2, v_2^2, v_3^2, v_4^2, v_5^2) \in \mathbb{R}^{5\times5}$, where v_i represents the

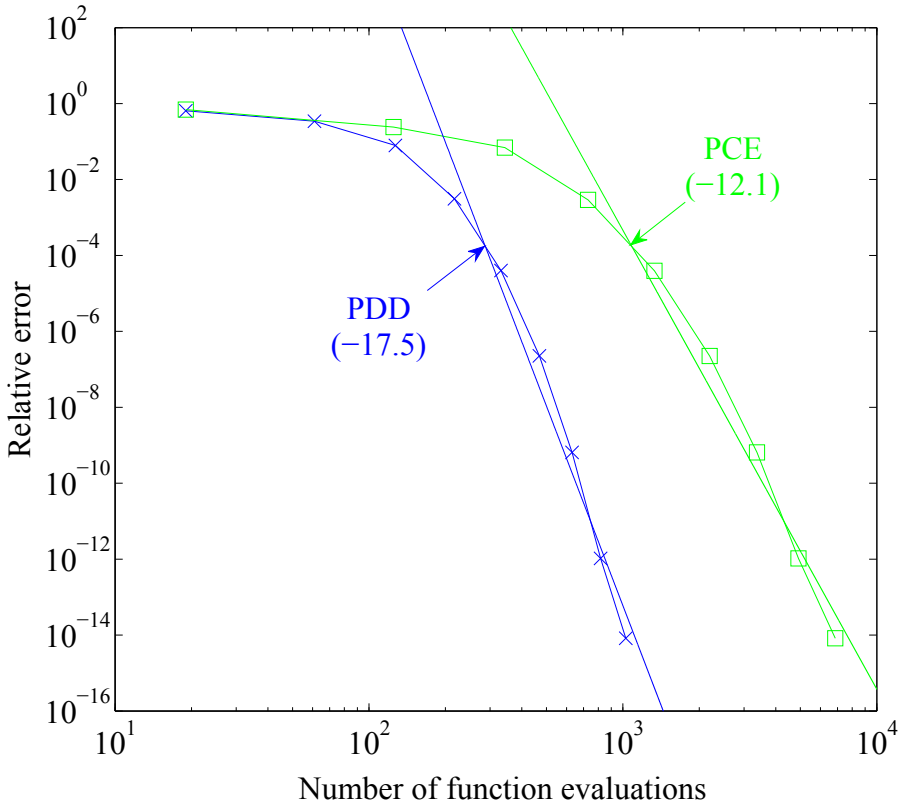

Figure 3.2: Relative errors in calculating the variance of the the Ishigami and Homma function by the PDD and PCE approximations (Example 2). Note: The parenthetical values denote slopes of the trend lines

coefficient of variation of X_i. Two cases of the problem size based on the coefficients of variations were examined: (1) $N = 2$ with $v_1 = v_2 = 0.25$, $v_3 = v_4 = v_5 = 0$; and (2) $N = 5$ with $v_1 = v_2 = 0.25$, $v_3 = v_4 = v_5 = 0.125$. The first case comprises uncertain stiffness properties of the first two springs only, whereas the second case includes uncertainties in all mass and stiffness properties. In both cases, there exist two real-valued random eigenvalues, $\lambda_1(\boldsymbol{X})$ and $\lambda_2(\boldsymbol{X})$, which are sorted into an ascending order.

Since the eigenvalues are in general non-polynomial functions of input, a con-

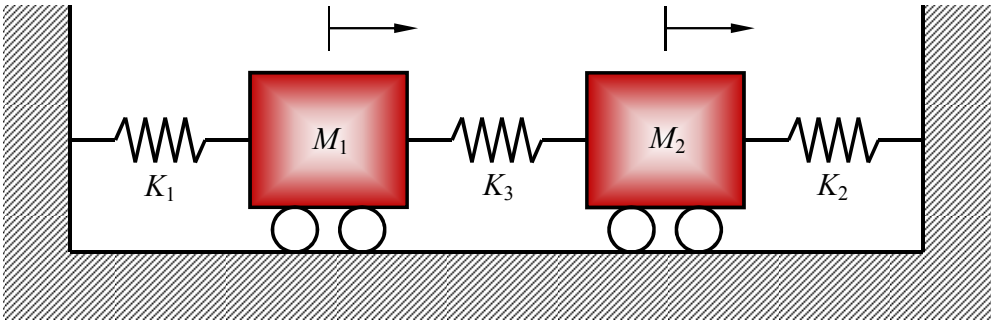

Figure 3.3: A two-degree-of-freedom, undamped, spring-mass system

vergence study with respect to the truncation parameters of PDD and PCE is required to calculate the probabilistic characteristics of eigensolutions accurately. Figures 3.4(a) and 3.4(b) depict how the normalized errors of the second-moment properties, $e_{S,m}/\mathbb{E}\left[\lambda(\boldsymbol{X}) - \lambda_0\right]^2$ and $e_p/\mathbb{E}\left[\lambda(\boldsymbol{X}) - \lambda_0\right]^2$, of the the first and second eigenvalues, respectively, decay with respect to m or p for $N = 2$. The normalized errors were calculated using Equations (3.16), (3.24), and (3.25) and employing the value of 80, a sufficiently large integer, for replacing the infinite limits of the summations. For any identical expansion orders ($m = p$), the bivariate PDD approximation ($S = N = 2$) yields smaller errors than the PCE approximation, consistent with the theoretical finding described in section 4.3. As soon as m or p becomes larger than three, the difference in the errors by the PDD and PCE approximations grows by more than an order of magnitude.

For a case of larger dimension ($N = 5$), calculating the normalized errors in the same way described above requires an enormous number of PDD coefficients. In addition, the determination of these coefficients is computationally taxing, if not

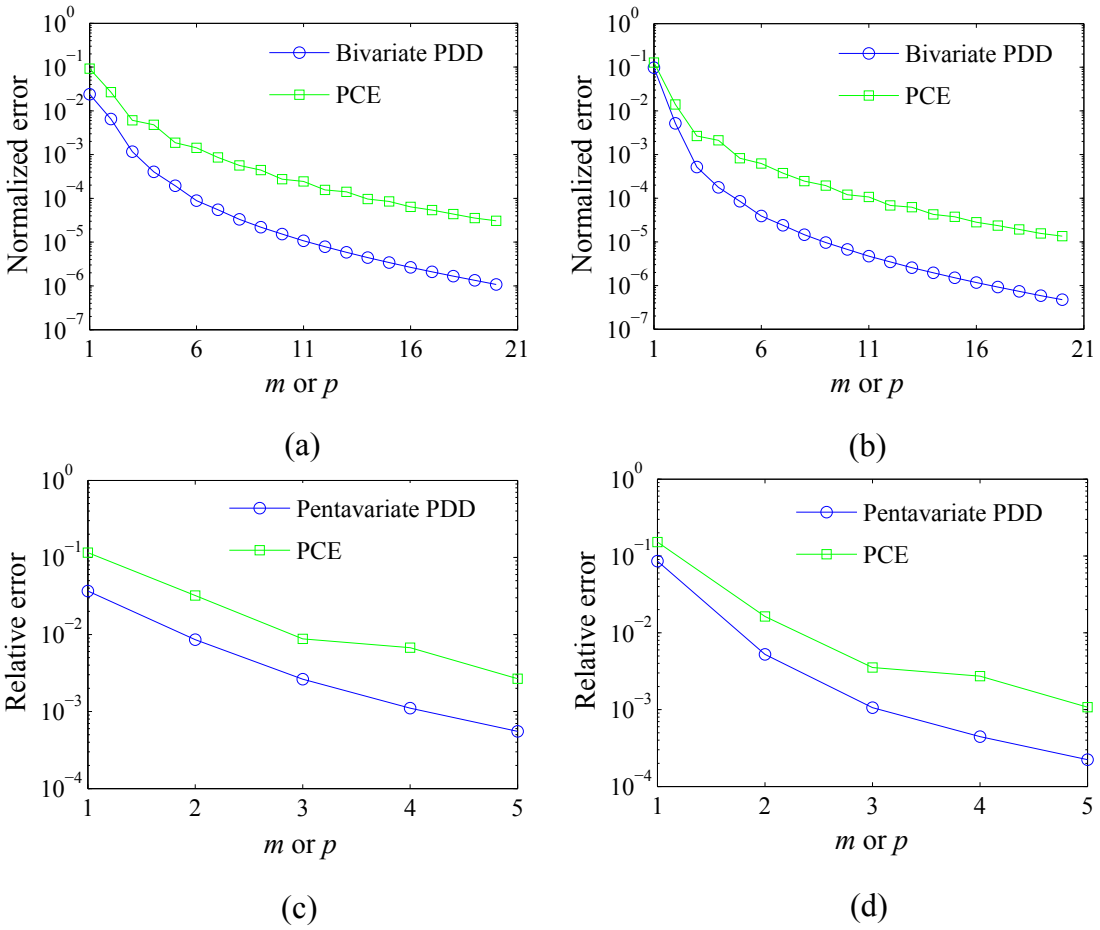

Figure 3.4: Errors in calculating the variances of eigenvalues of the two-degree-of-freedom oscillator by the PDD and PCE approximations (Example 3): (a) first eigenvalue ($N = 2$); (b) second eigenvalue ($N = 2$); (c) first eigenvalue ($N = 5$); (d) second eigenvalue ($N = 5$)

prohibitive, considering infinite limits in Equations (3.16), (3.24), and (3.25). To circumvent this problem, another relative error, defined as the ratio of the absolute difference between the numerically integrated and approximate variances of $\lambda(\boldsymbol{X})$ to the numerically integrated variance of $\lambda(\boldsymbol{X})$, employing the pentavariate ($S = 5$) PDD (Equation (3.15)) or PCE (Equation (3.21)) approximation, was evaluated. The variance estimated by numerical integration involved a full five-dimensional tensor

product of a 25-point univariate quadrature rule, where the number of integration points was ascertained adaptively. The plots of the relative error versus m or p in Figure 3.4(c) and 3.4(d) for the first and second eigenvalues, respectively, display a trend similar to that observed when $N = 2$, verifying once again that the errors from the PDD approximation are always smaller than those from the PCE approximation. In other words, the PDD method is expected to predict more accurate second-moment properties of random eigensolutions than the PCE method for, at least, the simple dynamic systems examined in this work.

3.5.4 Free-standing beam

The fourth example involves free vibration of a tall, free-standing beam shown in Figure 3.5(a) [41]. Figure 3.5(b) represents a lumped-parameter model of the beam, which comprises seven rigid, massless links hinged together. The mass of the beam is represented by seven random point masses located at the center of each link. No damping was assumed, except at the bottom joint, where the random, rotational, viscous damping coefficient due to the foundation pad is C. The random rotational stiffness at the bottom of the beam, controlled by the lower half of the bottom link and the flexibility of the foundation pad, is K. The independent random variables M, C, and K are lognormally distributed with respective means of 3000 kg, 2×10^7 N-m-s/rad, and 2×10^9 N-m/rad and have a 20 percent coefficient of variation. The flexural rigidity of the beam is represented by six rotational springs between links with stiffnesses $k(x) = k(x_i),\ i = 1, \cdots, 6$, where $x_i = il\ i = 1, \cdots, 6$,

and $l = 6$ m. The spatially varying spring stiffness $k(x) = c_\alpha \exp[\alpha(x)]$ is an independent, homogeneous, lognormal random field with mean $\mu_k = 2 \times 10^9$ N-m/rad and coefficient of variation $v_k = 0.2$, where $c_\alpha = \mu_k/\sqrt{1+v_k^2}$ and $\alpha(x)$ is a *zero*-mean, homogeneous, Gaussian random field with variance $\sigma_\alpha^2 = \ln(1+v_k^2)$ and covariance function $\Gamma_\alpha(u) := \mathbb{E}[\alpha(x)\alpha(x+u)] = \sigma_\alpha^2 \exp(-|u|/l)$. A discretization of $\alpha(x)$ yields the *zero*-mean Gaussian random vector $\boldsymbol{\alpha} = \{\alpha_1, \cdots, \alpha_6\}^T := \{\alpha(l), \cdots, \alpha(6l)\}^T \in \mathbb{R}^6$ with covariance matrix $\boldsymbol{\Sigma}_{\boldsymbol{\alpha}} := [\mathbb{E}(\alpha_u \alpha_v)],\ u, v = 1, \cdots, 6$, where $\mathbb{E}(\alpha_u \alpha_v) = \mathbb{E}(\alpha(ul)\alpha(vl)) = \Gamma_\alpha((u-v)l)$, providing complete statistical characterization of spring stiffnesses $k_i = c_\alpha \exp(\alpha_i)$. Therefore, the input random vector $\boldsymbol{X} = \{M, C, K, \alpha_1, \cdots, \alpha_6\}^T \in \mathbb{R}^9$ includes nine random variables in this example. Further details of the dynamic system, including mass, damping, and stiffness matrices, are available in a prior work of Rahman [41].

Due to non-proportional damping, the discrete beam model yields 14 complex eigenvalues $\lambda_i(\boldsymbol{X}) = \lambda_{R,i}(\boldsymbol{X}) \pm \sqrt{-1}\lambda_{I,i}(\boldsymbol{X}),\ i = 1, \cdots, 7$ in conjugate pairs, where the real parts $\lambda_{R,i}(\boldsymbol{X})$ and imaginary parts $\lambda_{I,i}(\boldsymbol{X})$ are both stochastic. Using the PDD method, Figure 3.6 presents the marginal probability distributions $F_{I,i}(\lambda_{I,i})$ and the complementary probabilities $1 - F_{I,i}(\lambda_{I,i})$, $i = 1, \cdots, 7$ of all seven imaginary parts, which also represent the natural frequencies of the beam. The distributions $F_{I,i}(\lambda_{I,i})$ and $1 - F_{I,i}(\lambda_{I,i})$ at low probabilities describe tail characteristics of λ_i at the left and right ends, respectively. Each subfigure of Figure 3.6 contains four plots: one obtained from crude Monte Carlo simulation and the remaining three generated from the univariate ($S = 1$), bivariate ($S = 2$), and trivariate ($S = 3$) PDD approxima-

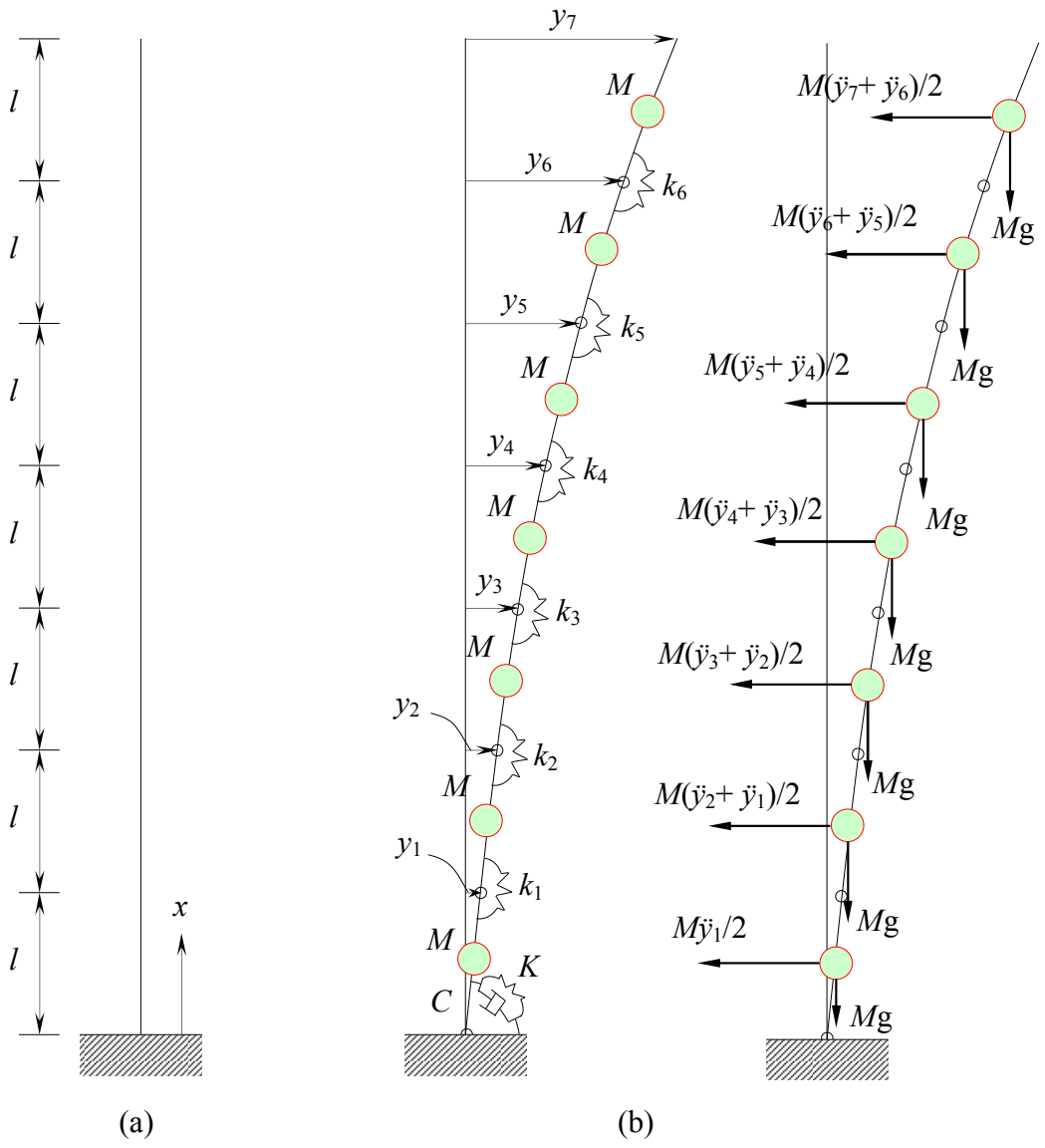

Figure 3.5: A free-standing beam: (a) continuous representation; (b) seven-degree-of-freedom discrete model

tions, employing $m = 3$, $n = 4$. In contrast, Figure 3.7 displays the same probability distributions of all seven imaginary parts of the eigenvalues calculated using the PCE method. Each subfigure of Figure 3.7 also contains four plots: one obtained from crude Monte Carlo simulation and the remaining three derived from the first-order ($p = 1$), second-order ($p = 2$), and third-order ($p = 3$) PCE approximations, employing $n = p + 1$. From Figure 3.6 or 3.7, the tail probability distributions at both ends converge rapidly with respect to S or p, regardless of the oscillatory mode. Therefore, both the PDD and PCE methods can be applied to solve this REP accurately.

To determine the computational efficiency of the PDD and PCE methods, Figures 3.8(a) and 3.8(b) portray enlarged views of the tail probability distributions of the first and seventh natural frequencies, respectively, of the beam calculated by all three variants of the PDD or PCE methods, including crude Monte Carlo simulation. Compared with crude Monte Carlo simulation, the bivariate, third-order PDD approximation; trivariate, third-order PDD approximation; and third-order PCE approximation provide excellent estimates of the tail distributions. The results further indicate that the bivariate, third-order PDD and third-order PCE approximations, both in consilience with the Monte Carlo solution, demand 613 and 5989 eigenvalue evaluations. Therefore, the PDD approximation is about $5989/613 \cong 10$ times more economical than the PCE approximation.

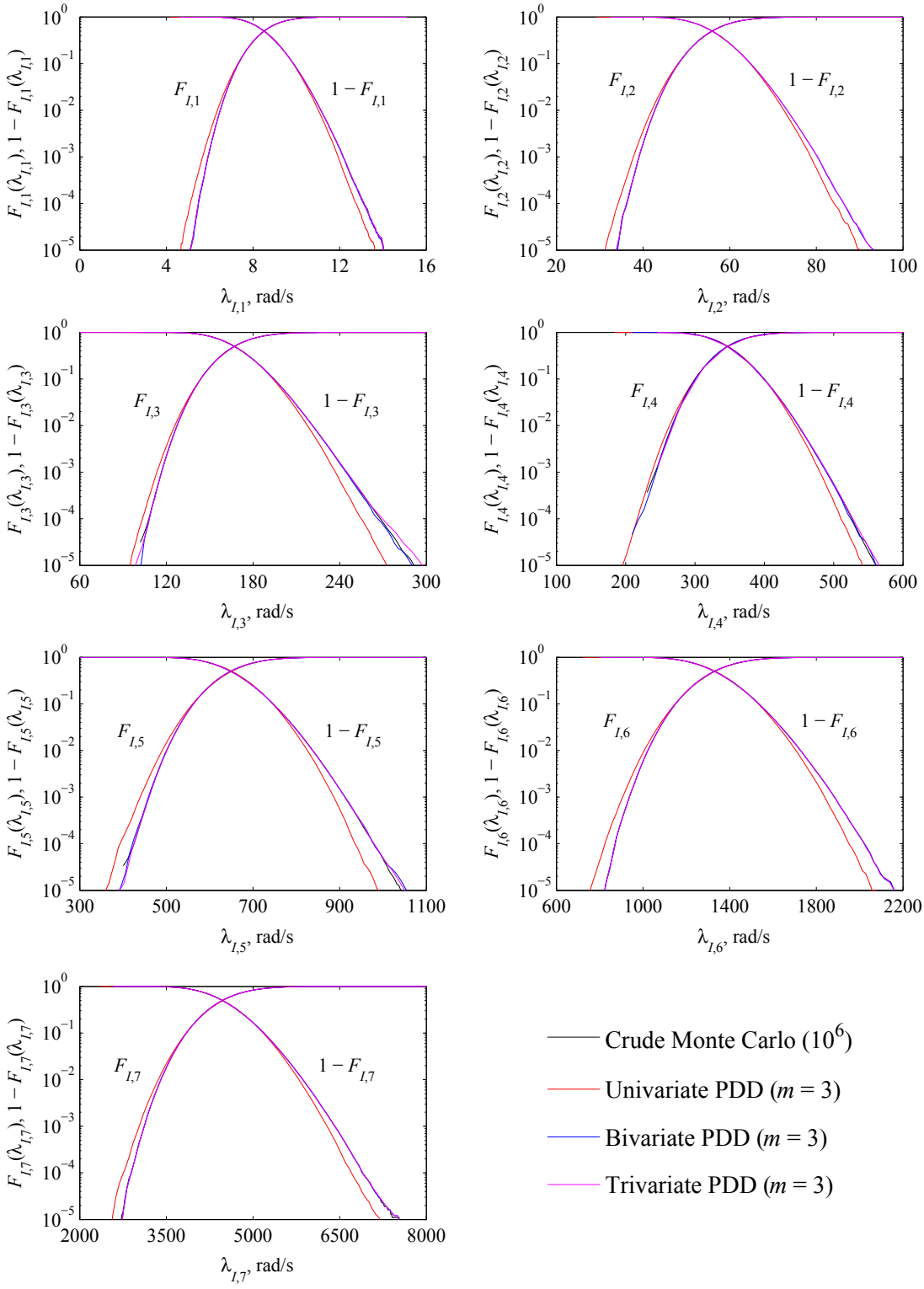

Figure 3.6: Tail probability distributions of the imaginary parts of eigenvalues of the free-standing beam by the PDD and crude Monte Carlo methods (Example 4)

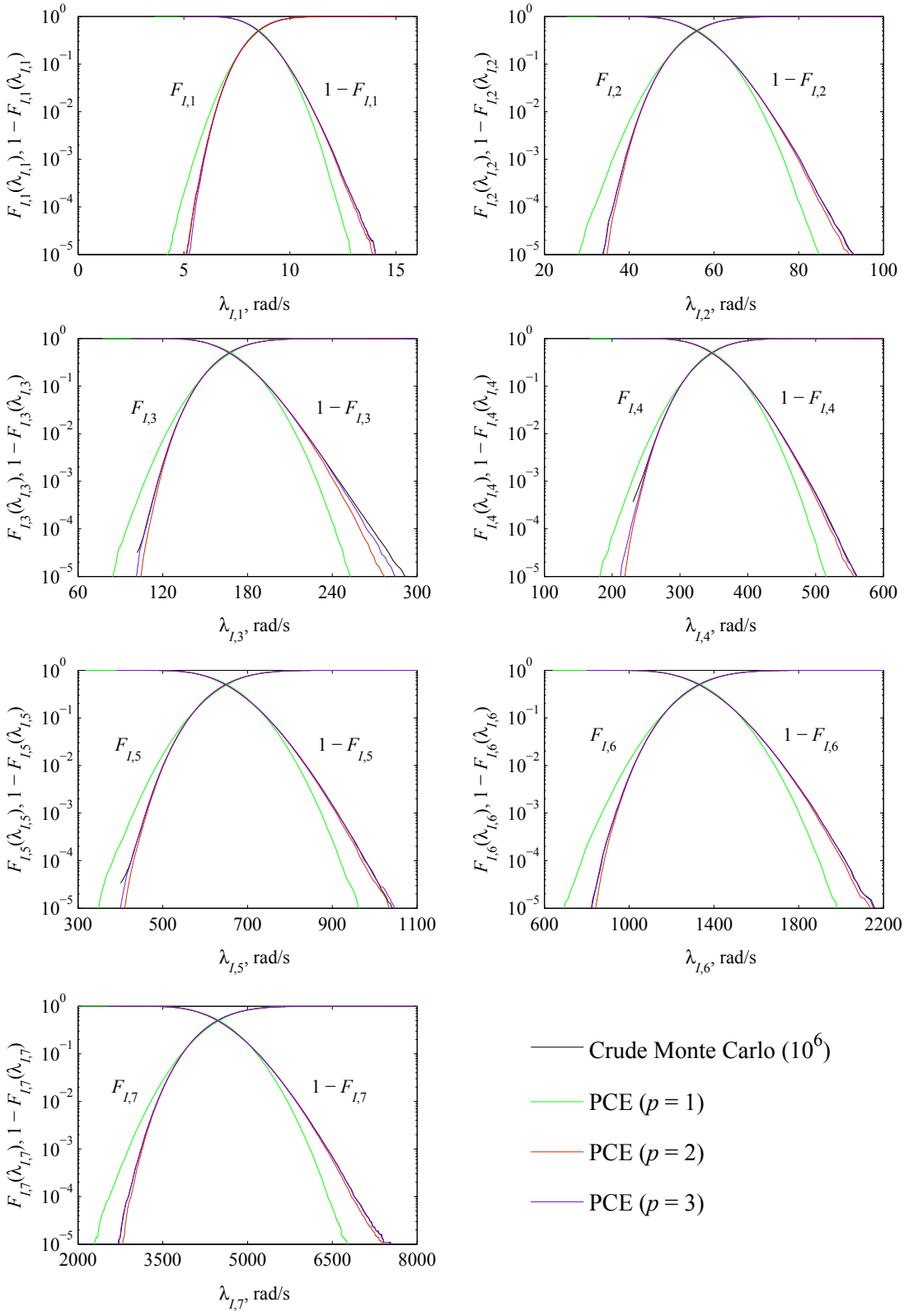

Figure 3.7: Tail probability distributions of the imaginary parts of eigenvalues of the free-standing beam by the PCE and crude Monte Carlo methods (Example 4)

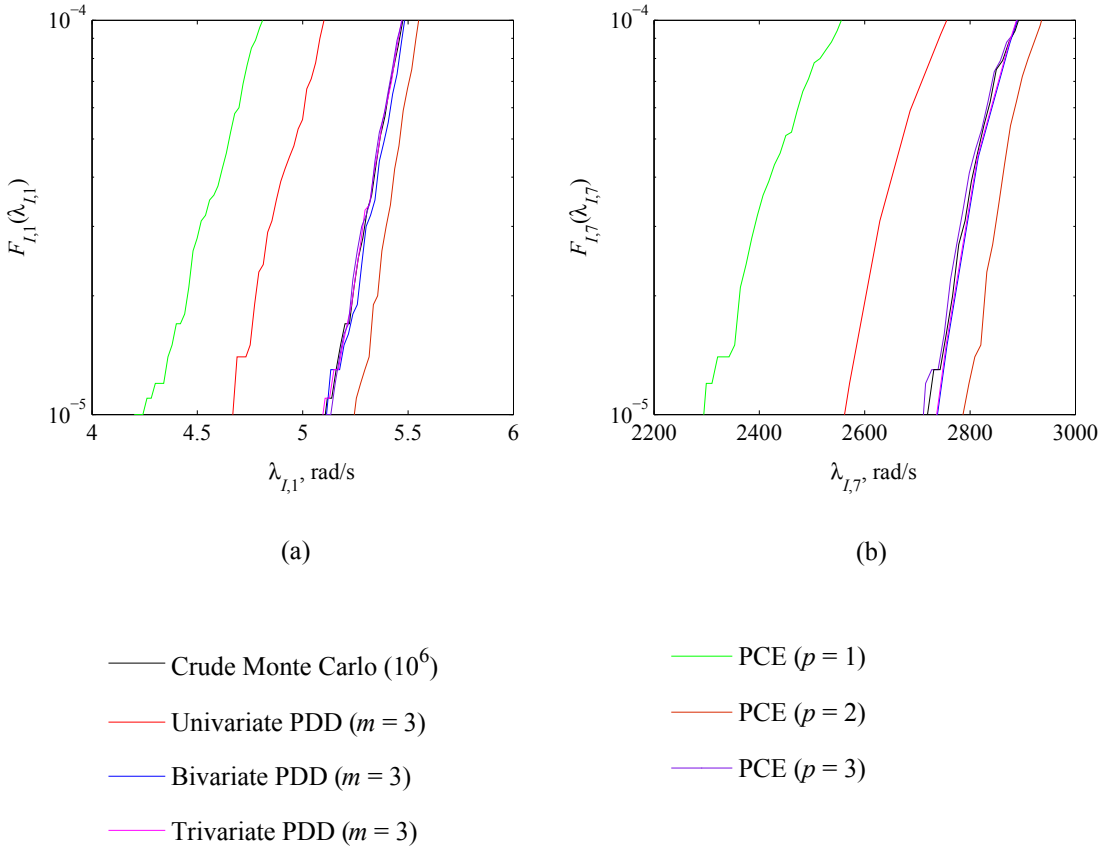

Figure 3.8: Comparisons of tail probability distributions of the imaginary parts of eigenvalues of the free-standing beam by the PDD, PCE, and crude Monte Carlo methods (Example 4); (a) $\lambda_{I,1}$; (b) $\lambda_{I,7}$

3.5.5 Piezoelectric transducer

The final example entails eigenspectrum analysis of a piezoelectric transducer commonly used for converting electrical pulses to mechanical vibrations, and *vice versa*. Figure 3.9(a) shows a 25 mm diameter cylinder made of a piezoelectric ceramic PZT4 (lead zirconate titanate) with brass end caps. The thicknesses of the transducer

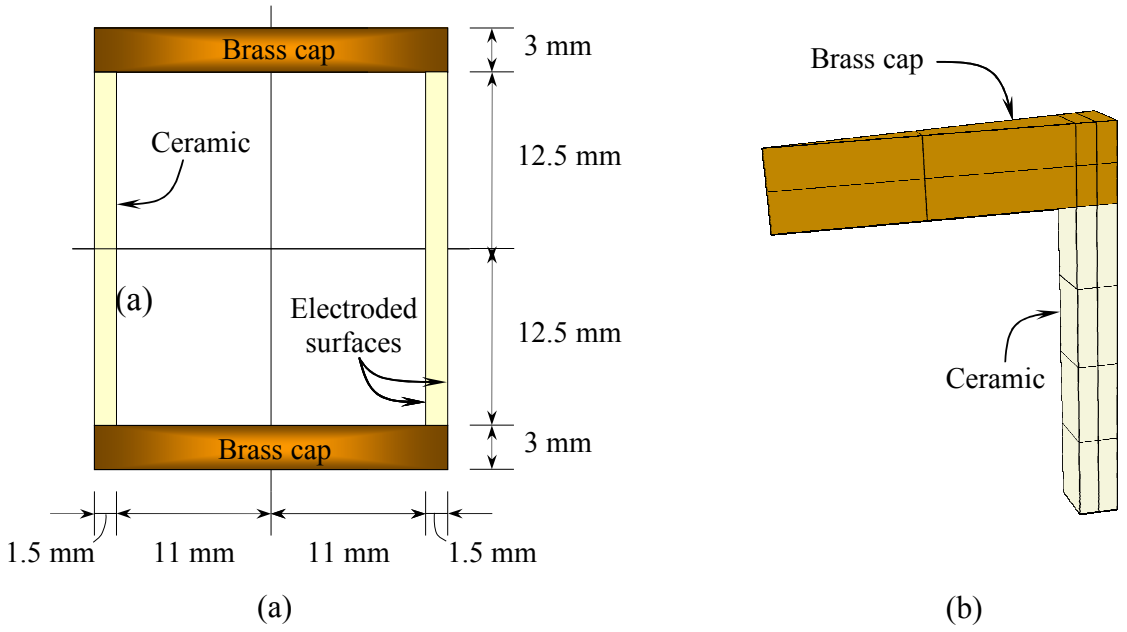

Figure 3.9: A piezoelectric transducer: (a) geometry; (b) finite-element discrete model

and end caps are 1.5 mm and 3 mm, respectively. The cylinder, 25 mm long, was electroded on both the inner and outer surfaces. The random variables include: (1) ten non-zero constants defining elasticity, piezoelectric stress coefficients, and dielectric properties of PZT4; (2) elastic modulus and Poisson's ratio of brass; and (3) mass densities of brass and PZT4 [90]. The statistical properties of all 14 random

variables are listed in Table 3.3. The random variables are independent and follow lognormal distributions. Due to axisymmetry, a 20-noded finite-element model of a slice of the transducer, shown in Figure 3.9(b), was created. The model was considered to be open-circuited. All natural frequencies calculated correspond to antiresonant frequencies. The governing equations of a piezoelectric analysis are described in Appendix A.

Table 3.3: Statistical properties of the random input for the piezoelectric cylinder

Random variable	Property[(a)]	Mean	Coefficient of variation
X_1, GPa	D_{1111}	115.4	0.15
X_2, GPa	D_{1122}, D_{1133}	74.28	0.15
X_3, GPa	D_{2222}, D_{3333}	139	0.15
X_4, GPa	D_{2233}	77.84	0.15
X_5, GPa	$D_{1212}, D_{2323}, D_{1313}$	25.64	0.15
X_6, Coulomb/m^2	e_{111}	15.08	0.1
X_7, Coulomb/m^2	e_{122}, e_{133}	-5.207	0.1
X_8, Coulomb/m^2	e_{212}, e_{313}	12.71	0.1
X_9, nF/m	D_{11}	5.872	0.1
X_{10}, nF/m	D_{22}, D_{33}	6.752	0.1
X_{11}, GPa	E_b	104	0.15
X_{12}	ν_b	0.37	0.05
X_{13}, g/m^3	ρ_b	8500	0.15
X_{14}, g/m^3	ρ_c	7500	0.15

[(a)] D_{ijkl} are elastic moduli of ceramic; e_{ijk} are piezoelectric stress coefficients of ceramic; D_{ij} are dielectric constants of ceramic; E_b, ν_b, ρ_b are elastic modulus, Poisson's ratio, and mass density of brass; ρ_c is mass density of ceramic.

Figure 3.10 presents the marginal probability distributions of the first six natural frequencies, $\Omega_i,\ i = 1, \cdots, 6$, of the transducer by the bivariate ($S = 2$), third-

order ($m = 3$) PDD and third-order ($p = 3$) PCE methods, respectively. These probabilistic characteristics, obtained by setting $n = m + 1 = p + 1 = 4$, are judged to be converged responses, as their changes due to further increases in m and p are negligibly small. Therefore, the PDD and PCE methods require 1513 and 24,809 Abaqus-aided finite element analysis, respectively − a significant mismatch in computational efforts − in generating all six probability distributions. Due to expensive FEA, crude Monte Carlo simulation was conducted only up to 50,000 realizations, producing only rough estimates of the distributions. Given the low sample size, the distributions from crude Monte Carlo simulation, also plotted in Figure 3.10, are not expected to provide very accurate tail characteristics. Nonetheless, the overall shapes of all six probability distributions generated by both expansion methods match these Monte Carlo results quite well. However, a comparison of their computational efforts once again finds the PDD method wringing more computational savings than the PCE method by an order of magnitude in solving this practical eigenvalue problem.

3.6 Conclusions

Two stochastic expansion methods originating from PDD and PCE were investigated for solving REPs commonly encountered in stochastic dynamic systems. Both methods comprise a broad range of orthonormal polynomial bases consistent with the probability measure of the random input and an innovative dimension-reduction integration for calculating the expansion coefficients. A new theorem, proven herein, demonstrates that the infinite series from PCE can be reshuffled to derive the infinite

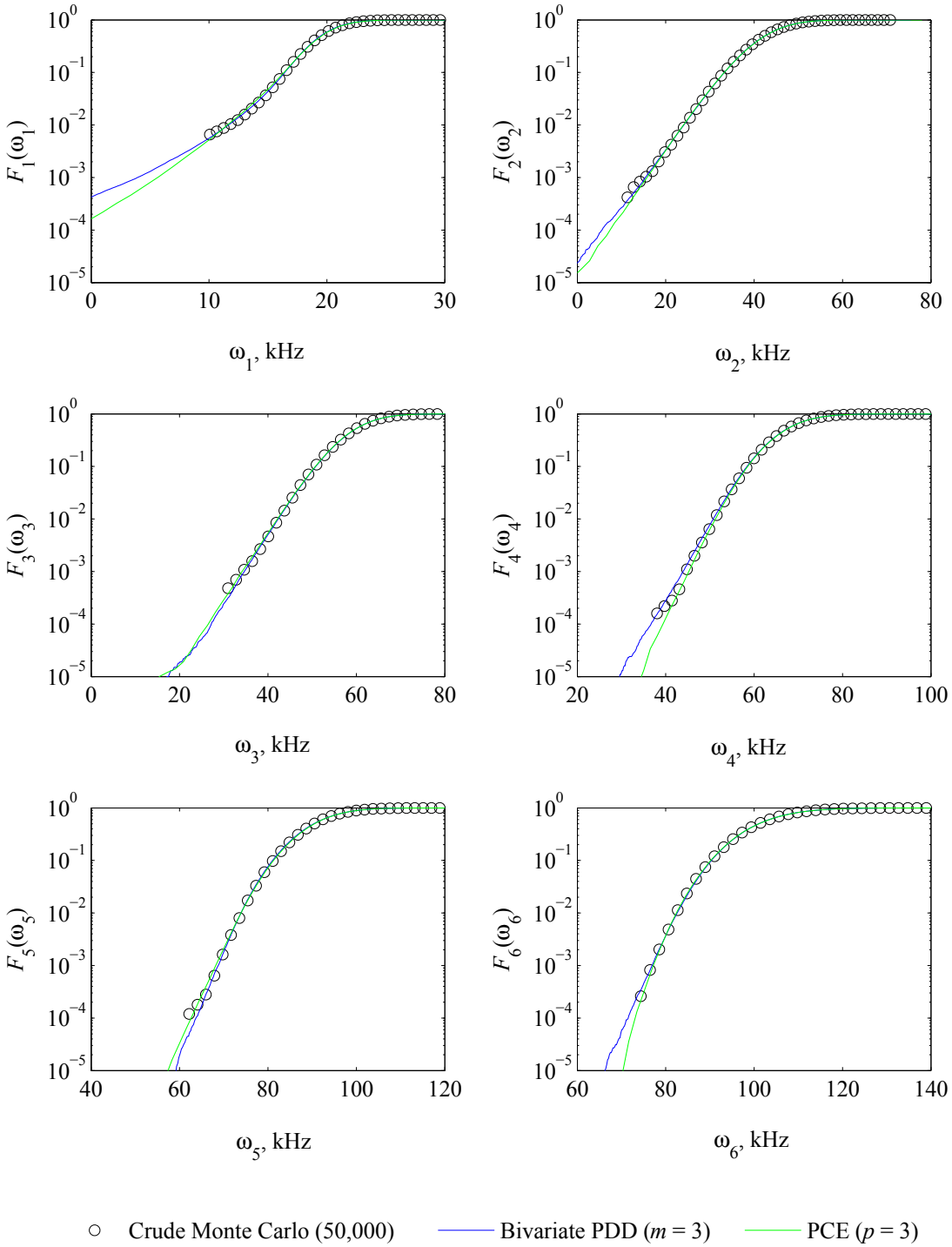

Figure 3.10: Marginal probability distributions of the first six natural frequencies of the piezoelectric transducer by the PDD, PCE, and crude Monte Carlo methods (Example 5)

series from PDD and *vice versa*. However, compared with PCE, which contains terms arranged with respect to the order of polynomials, PDD is structured with respect to the degree of cooperativity between a finite number of random variables. Therefore, significant differences exist regarding the accuracy, efficiency, and convergence properties of their truncated series.

An alternative form of the PCE approximation expressed in terms of the PDD expansion coefficients was developed. As a result, the probabilistic eigensolutions from both the PDD and PCE methods can be obtained from the same PDD coefficients, leading to closed-form expressions of the second-moment properties of eigenvalues and respective errors. For a class of REPs, where the cooperative effects of input variables on an eigenvalue get progressively weaker or vanish altogether, the error perpetrated by the PCE approximation is larger than that committed by the PDD approximation, when the expansions orders are equal. Given the same expansion orders, the PDD approximation including main and cooperative effects of all input variables cannot be worse than the PCE approximation, although the inclusion of all cooperative effects undermines the salient features of PDD.

The PDD and PCE methods were employed to calculate the second-moment properties and tail probability distributions in five numerical problems, where the output functions are either mathematical functions involving smooth polynomials or non-polynomials or real- or complex-valued eigensolutions from dynamic systems, some requiring finite element analysis (FEA). The second-moment errors from the mathematical functions indicate rapid convergence of the PDD and PCE solutions,

easily outperforming the sampling-based methods. Moreover, for the functions examined, the convergence rates of the PDD method are noticeably higher than those of the PCE approximation. The same trend was observed when calculating the variance of a two-degree-of-freedom linear oscillator regardless of the number of random variables. A comparison of the numbers of eigenvalue evaluations (numbers of FEA), required for estimating with the same accuracy the frequency distributions of a free-standing beam and a piezoelectric transducer, finds the PDD approximation to be more economical than the PCE approximation by an order of magnitude or more. The computational efficiency of the PDD method is attributed to its dimensional hierarchy, favorably exploiting the hidden dimensional structures of stochastic responses, including random eigensolutions, examined in this work.

CHAPTER 4
MULTIPLICATIVE POLYNOMIAL DIMENSIONAL DECOMPOSITION

4.1 Introduction

The central theme of this chapter is multiplicative PDD methods for solving high-dimensional stochastic problems. When a stochastic response is dominantly of multiplicative nature, the standard PDD approximation, predicated on additive function decomposition, may not provide sufficiently accurate estimates of the probabilistic characteristics of a complex system. To circumvent this problem, two multiplicative versions of PDD, referred to as factorized PDD (F-PDD) and logarithmic PDD (L-PDD), were developed to examine if they provide improved stochastic solutions. Both versions involve a hierarchical, multiplicative decomposition of a multivariate function in terms of variables with increasing dimensions, a broad range of orthonormal polynomial bases consistent with the input probability measure for Fourier-polynomial expansions of component functions, and a dimension-reduction integration or sampling technique for estimating the expansion coefficients.

The ANOVA dimensional decomposition (ADD) of a multivariate function is discussed in Section 4.2. Section 4.3 briefly explains how ADD leads up to A-PDD approximation, an existing stochastic method. A multiplicative dimensional decomposition, including a proof of existence and uniqueness, is presented in Section 4.4. In addition, the section reveals the relationship or similarity among A-PDD, F-PDD, and L-PDD, establishing how the latter two methods can exploit a hidden multiplica-

tive structure, if it exists, of a stochastic response. The calculation of the expansion coefficients by dimension-reduction integration and sampling techniques are described in Section 4.5. Section 4.6 presents three numerical examples involving mathematical functions or random eigenvalue problems, contrasting the accuracy, convergence properties, and computational efforts of the proposed and existing methods. A large-scale stochastic-dynamics problem, solved using the new PDD methods, is reported in Section 4.7. Finally, conclusions are drawn in Section 4.8.

This chapter introduces a compact notation for describing various dimensional decompositions, including ADD, A-PDD, F-PDD, and L-PDD. They lead to succinct expressions of stochastic solutions.

4.2 ANOVA Dimensional Decomposition

Let $\mathbb{N}$, $\mathbb{N}_0$, $\mathbb{R}$, and $\mathbb{R}_0^+$ represent the sets of positive integer (natural), non-negative integer, real, and non-negative real numbers, respectively. For $k \in \mathbb{N}$, denote by $\mathbb{R}^k$ the k-dimensional Euclidean space, by $\mathbb{N}_0^k$ the k-dimensional multi-index space, and by $\mathbb{R}^{k\times k}$ the set of $k \times k$ real-valued matrices. These standard notations will be used throughout the thesis.

Let $(\Omega, \mathcal{F}, P)$ be a complete probability space, where Ω is a sample space, $\mathcal{F}$ is a σ-field on Ω, and $P : \mathcal{F} \to [0, 1]$ is a probability measure. With $\mathcal{B}^N$ representing the Borel σ-field on $\mathbb{R}^N$, $N \in \mathbb{N}$, consider an $\mathbb{R}^N$-valued random vector $\mathbf{X} := (X_1, \cdots, X_N) : (\Omega, \mathcal{F}) \to (\mathbb{R}^N, \mathcal{B}^N)$, which describes the statistical uncertainties in all system and input parameters of a high-dimensional stochastic problem.

The probability law of $\mathbf{X}$ is completely defined by its joint probability density function $f_{\mathbf{X}} : \mathbb{R}^N \to \mathbb{R}_0^+$. Assuming independent coordinates of $\mathbf{X}$, its joint probability density $f_{\mathbf{X}}(\mathbf{x}) = \Pi_{i=1}^{i=N} f_i(x_i)$ is expressed by a product of marginal probability density functions f_i of X_i, $i = 1, \cdots, N$, defined on the probability triple $(\Omega_i, \mathcal{F}_i, P_i)$ with a bounded or an unbounded support on $\mathbb{R}$. For a given $u \subseteq \{1, \cdots, N\}$, $f_{\mathbf{X}_{-u}}(\mathbf{x}_{-u}) := \prod_{i=1, i\notin u}^{N} f_i(x_i)$ defines the marginal density function of $\mathbf{X}_{-u} := \mathbf{X}_{\{1,\cdots,N\}\setminus u}$.

Let $y(\mathbf{X}) := y(X_1, \cdots, X_N)$, a real-valued, measurable transformation on $(\Omega, \mathcal{F})$, define a high-dimensional stochastic response of interest and $\mathcal{L}_2(\Omega, \mathcal{F}, P)$ a Hilbert space of square-integrable functions y with respect to the induced generic measure $f_{\mathbf{X}}(\mathbf{x})d\mathbf{x}$ supported on $\mathbb{R}^N$. The ADD, expressed by the recursive form [79, 118, 119]

$$y(\mathbf{X}) = \sum_{u\subseteq\{1,\cdots,N\}} y_u(\mathbf{X}_u), \tag{4.1}$$

$$y_\emptyset = \int_{\mathbb{R}^N} y(\mathbf{x}) f_{\mathbf{X}}(\mathbf{x}) d\mathbf{x}, \tag{4.2}$$

$$y_u(\mathbf{X}_u) = \int_{\mathbb{R}^{N-|u|}} y(\mathbf{X}_u, \mathbf{x}_{-u}) f_{\mathbf{X}_{-u}}(\mathbf{x}_{-u}) d\mathbf{x}_{-u} - \sum_{v\subset u} y_v(\mathbf{X}_v), \tag{4.3}$$

is a finite, hierarchical expansion in terms of its input variables with increasing dimensions, where $u \subseteq \{1, \cdots, N\}$ is a subset with the complementary set $-u = \{1, \cdots, N\}\setminus u$ and cardinality $0 \leq |u| \leq N$, and y_u is a $|u|$-variate component function describing a constant or the interactive effect of $\mathbf{X}_u = (X_{i_1}, \cdots, X_{i_{|u|}})$, $1 \leq i_1 < \cdots < i_{|u|} \leq N$, a subvector of $\mathbf{X}$, on y when $|u| = 0$ or $|u| > 0$. The summation in Equations (4.1) comprises 2^N terms, with each term depending on a group of variables indexed by a particular subset of $\{1, \cdots, N\}$, including the empty

set $\emptyset$. In Equation (4.3), $(\mathbf{X}_u, \mathbf{x}_{-u})$ denotes an N-dimensional vector whose ith component is X_i if $i \in u$ and x_i if $i \notin u$. When $u = \emptyset$, the sum in Equation (4.3) vanishes, resulting in the expression of the constant function $y_\emptyset$ in Equation (4.2). When $u = \{1, \cdots, N\}$, the integration in Equation (4.3) is on the empty set, reproducing Equation (4.1) and hence finding the last function $y_{\{1,\cdots,N\}}$. Indeed, all component functions of y can be obtained by interpreting literally Equation (4.3). On inversion, Equations (4.1)-(4.3) result in [118, 119]

$$y(\mathbf{X}) = \sum_{u \subseteq \{1,\cdots,N\}} \sum_{v \subseteq u} (-1)^{|u|-|v|} \int_{\mathbb{R}^{N-|v|}} y(\mathbf{X}_v, \mathbf{x}_{-v}) f_{\mathbf{X}_{-v}}(\mathbf{x}_{-v}) d\mathbf{x}_{-v}, \tag{4.4}$$

providing an explicit form of the same decomposition.

Remark 4.1: The ANOVA component functions y_u, $u \subseteq \{1, \cdots, N\}$, are uniquely determined from the annihilating conditions [79, 118, 119],

$$\int_{\mathbb{R}} y_u(\mathbf{x}_u) f_i(x_i) dx_i = 0 \text{ for } i \in u, \tag{4.5}$$

resulting in two remarkable properties: (1) the component functions, y_u, $\emptyset \neq u \subseteq \{1, \cdots, N\}$, have zero means; and (2) two distinct component functions y_u and y_v, where $u \subseteq \{1, \cdots, N\}$, $v \subseteq \{1, \cdots, N\}$, and $u \neq v$, are orthogonal. Further details are available elsewhere [119].

Remark 4.2: Traditionally, Equations (4.1)-(4.3) or (4.4) with X_j, $j = 1, \cdots, N$, following independent, standard uniform distributions, are identified as the ADD [79, 118]; however, recent works reveal no fundamental requirement for a specific probability measure of $\mathbf{X}$, provided that the resultant integrals in Equations (4.1)-(4.3) or (4.4) exist and are finite [87, 90, 119]. In this work, the ADD should be

interpreted with respect to an arbitrary but product type probability measure for which it is always endowed with desirable orthogonal properties.

4.3 Additive PDD

Let $\{\psi_{ij}(X_i);\ j=0,1,\cdots\}$ be a set of orthonormal polynomial basis functions in the Hilbert space $\mathcal{L}_2(\Omega_i,\mathcal{F}_i,P_i)$ that is consistent with the probability measure P_i of X_i. For a given $\emptyset\neq u=\{i_1,\cdots,i_{|u|}\}\subseteq\{1,\cdots,N\}$, $1\leq|u|\leq N$, $1\leq i_1<\cdots<i_{|u|}\leq N$, denote a product probability triple by $(\times_{p=1}^{p=|u|}\Omega_{i_p},\times_{p=1}^{p=|u|}\mathcal{F}_{i_p},\times_{p=1}^{p=|u|}P_{i_p})$, and the associated space of square integrable $|u|$-variate component functions of y by $\mathcal{L}_2(\times_{p=1}^{p=|u|}\Omega_{i_p},\times_{p=1}^{p=|u|}\mathcal{F}_{i_p},\times_{p=1}^{p=|u|}P_{i_p}):=\{y_u:\int_{\mathbb{R}^{|u|}}y_u^2(\mathbf{x}_u)f_{\mathbf{X}_u}(\mathbf{x}_u)d\mathbf{x}_u<\infty\}$, which is a Hilbert space. Since the joint density of $(X_{i_1},\cdots,X_{i_{|u|}})$ is separable (independence), i.e., $f_{\mathbf{X}_u}(\mathbf{x}_u)=\prod_{p=1}^{|u|}f_{i_p}(x_{i_p})$, the product polynomial $\psi_{u\mathbf{j}_{|u|}}(\mathbf{X}_u):=\prod_{p=1}^{|u|}\psi_{i_pj_p}(X_{i_p})$, where $\mathbf{j}_{|u|}=(j_1,\cdots,j_{|u|})\in\mathbb{N}_0^{|u|}$, a $|u|$-dimensional multi-index with ∞-norm $\left\|\mathbf{j}_{|u|}\right\|_\infty=\max(j_1,\cdots,j_{|u|})$, constitutes an orthonormal basis in $\mathcal{L}_2(\times_{p=1}^{p=|u|}\Omega_{i_p},\times_{p=1}^{p=|u|}\mathcal{F}_{i_p},\times_{p=1}^{p=|u|}P_{i_p})$. Two important properties of these product polynomials from the tensor product of Hilbert spaces are as follows.

Proposition 4.1: *The product polynomials* $\psi_{u\mathbf{j}_{|u|}}(\mathbf{X}_u)$, $\emptyset\neq u\subseteq\{1,\cdots,N\}$, $j_1,\cdots,j_{|u|}\neq 0$, *have zero means, i.e.,*

$$\mathbb{E}\left[\psi_{u\mathbf{j}_{|u|}}(\mathbf{X}_u)\right]=0. \tag{4.6}$$

Proposition 4.2: *Two distinct product polynomials* $\psi_{u\mathbf{j}_{|u|}}(\mathbf{X}_u)$ *and* $\psi_{v\mathbf{k}_{|v|}}(\mathbf{X}_v)$, *where* $\emptyset\neq u\subseteq\{1,\cdots,N\}$, $\emptyset\neq v\subseteq\{1,\cdots,N\}$, $j_1,\cdots,j_{|u|}\neq 0$, $k_1,\cdots,k_{|v|}\neq 0$, *are*

uncorrelated, and each has unit variance, i.e.,

$$\mathbb{E}\left[\psi_{u\mathbf{j}_{|u|}}(\mathbf{X}_u)\psi_{v\mathbf{k}_{|v|}}(\mathbf{X}_v)\right] = \begin{cases} 1 & \text{if } u = v; \mathbf{j}_{|u|} = \mathbf{k}_{|v|}, \\ 0 & \text{otherwise.} \end{cases} \tag{4.7}$$

Proof. The results of Propositions 4.1 and 4.2 follow by recognizing independent coordinates of $\mathbf{X}$ and using the second-moment properties of univariate orthonormal polynomials: (1) $\mathbb{E}[\psi_{ij}(X_i)] = 1$ when $j = 0$ and *zero* when $j \geq 1$; (2) $\mathbb{E}[\psi_{ij_1}(X_i)\psi_{ij_2}(X_i)] = 1$ when $j_1 = j_2$ and *zero* when $j_1 \neq j_2$ for an arbitrary random variable X_i, where $\mathbb{E}$ is the expectation operator with respect to the probability measure $f_{\mathbf{X}}(\mathbf{x})d\mathbf{x}$. □

As a result, the orthogonal polynomial expansion of a non-constant $|u|$-variate component function becomes [87, 90]

$$y_u(\mathbf{X}_u) = \sum_{\substack{\mathbf{j}_{|u|} \in \mathbb{N}_0^{|u|} \\ j_1, \cdots, j_{|u|} \neq 0}} C_{u\mathbf{j}_{|u|}} \psi_{u\mathbf{j}_{|u|}}(\mathbf{X}_u), \; \emptyset \neq u \subseteq \{1, \cdots, N\}, \tag{4.8}$$

with

$$C_{u\mathbf{j}_{|u|}} := \int_{\mathbb{R}^N} y(\mathbf{x})\psi_{u\mathbf{j}_{|u|}}(\mathbf{x}_u) f_{\mathbf{X}}(\mathbf{x}) d\mathbf{x} \tag{4.9}$$

representing the corresponding expansion coefficient. For instance, when $u = \{i\}$, $i = 1, \cdots, N$, the univariate component functions and expansion coefficients are $y_{\{i\}}(X_i) = \sum_{i=1}^{N} \sum_{j=1}^{\infty} C_{ij}\psi_{ij}(X_i)$ and $C_{ij} := C_{\{i\}(j)}$, respectively. Using Propositions 4.1 and 4.2, all component functions y_u, $\emptyset \neq u \subseteq \{1, \cdots, N\}$, are found to satisfy the annihilating conditions of the ADD. The end result of combining Equations (4.1) and (4.8) is the additive PDD [87, 90],

$$y(\mathbf{X}) = y_\emptyset + \sum_{\emptyset \neq u \subseteq \{1, \cdots, N\}} \sum_{\substack{\mathbf{j}_{|u|} \in \mathbb{N}_0^{|u|} \\ j_1, \cdots, j_{|u|} \neq 0}} C_{u\mathbf{j}_{|u|}} \psi_{u\mathbf{j}_{|u|}}(\mathbf{X}_u), \tag{4.10}$$

providing an exact, hierarchical expansion of y in terms of an infinite number of coefficients or orthonormal polynomials. In practice, the number of coefficients or polynomials must be finite, say, by retaining at most mth-order polynomials in each variable. Furthermore, in many applications, the function y can be approximated by a sum of at most S-variate component functions, where $1 \leq S \leq N$, resulting in the S-variate, mth-order A-PDD approximation

$$\tilde{y}_{S,m}(\mathbf{X}) = y_{\emptyset} + \sum_{\substack{\emptyset \neq u \subseteq \{1,\cdots,N\} \\ 1 \leq |u| \leq S}} \sum_{\substack{\mathbf{j}_{|u|} \in \mathbb{N}_0^{|u|}, \left\|\mathbf{j}_{|u|}\right\|_\infty \leq m \\ j_1,\cdots,j_{|u|} \neq 0}} C_{u\mathbf{j}_{|u|}} \psi_{u\mathbf{j}_{|u|}}(\mathbf{X}_u), \tag{4.11}$$

containing $\sum_{k=0}^{S} \binom{N}{S-k} m^{S-k}$ number of PDD coefficients and corresponding orthonormal polynomials. Due to its additive structure, the approximation in Equation (4.11) includes degrees of interaction among at most S input variables $X_{i_1}, \cdots, X_{i_S}$, $1 \leq i_1 \leq \cdots \leq i_S \leq N$. For instance, by selecting $S = 1$ and 2, the functions, $\tilde{y}_{1,m}$ and $\tilde{y}_{2,m}$, respectively, provide univariate and bivariate mth-order approximations, contain contributions from all input variables, and should not be viewed as first- and second-order approximations, nor do they limit the nonlinearity of y. Depending on how the component functions are constructed, arbitrarily high-order univariate and bivariate terms of y could be lurking inside $\tilde{y}_{1,m}$ and $\tilde{y}_{2,m}$. When $S \to N$ and $m \to \infty$, $\tilde{y}_{S,m}$ converges to y in the mean-square sense, permitting Equation (4.11) to generate a hierarchical and convergent sequence of approximations of y.

Applying the expectation operator on $\tilde{y}_{S,m}(\mathbf{X})$ and $(\tilde{y}_{S,m}(\mathbf{X}) - y_{\emptyset})^2$ and noting Propositions 4.1 and 4.2, the mean [89]

$$\mathbb{E}\left[\tilde{y}_{S,m}(\mathbf{X})\right] = y_{\emptyset} \tag{4.12}$$

of the S-variate, mth-order PDD approximation matches the exact mean $\mathbb{E}[y(\mathbf{X})]$, regardless of S or m, and the approximate variance [89]

$$\mathbb{E}\left[\left(\tilde{y}_{S,m}(\mathbf{X}) - \mathbb{E}\left[\tilde{y}_{S,m}(\mathbf{X})\right]\right)^2\right] = \sum_{\substack{\emptyset \neq u \subseteq \{1,\cdots,N\} \\ 1 \leq |u| \leq S}} \sum_{\substack{\mathbf{j}_{|u|} \in \mathbb{N}_0^{|u|}, \left\|\mathbf{j}_{|u|}\right\|_\infty \leq m \\ j_1,\cdots,j_{|u|} \neq 0}} C^2_{u\mathbf{j}_{|u|}} \tag{4.13}$$

is calculated as the sum of squares of the expansion coefficients from the S-variate, mth-order A-PDD approximation of $y(\mathbf{X})$. A recent work proved that the approximate variance in Equation (4.13) approaches the exact variance of y when $S \to N$ and $m \to \infty$ [89]. The mean-square convergence of $\tilde{y}_{S,m}$ is guaranteed as y, and its component functions are all members of the associated Hilbert spaces.

For the special case of $S = 1$, the univariate A-PDD approximation

$$\tilde{y}_{1,m}(\mathbf{X}) = y_\emptyset + \sum_{i=1}^{N}\sum_{j=1}^{m} C_{ij}\psi_{ij}(X_i) \tag{4.14}$$

of $y(\boldsymbol{X})$ yields the exact mean

$$\mathbb{E}\left[\tilde{y}_{1,m}(\mathbf{X})\right] = y_\emptyset, \tag{4.15}$$

and an approximate variance

$$\mathbb{E}\left[\left(\tilde{y}_{1,m}(\mathbf{X}) - \mathbb{E}\left[\tilde{y}_{1,m}(\mathbf{X})\right]\right)^2\right] = \sum_{i=1}^{N}\sum_{j=1}^{m} C_{ij}^2 \tag{4.16}$$

that depends on $m < \infty$.

4.4 Proposed Multiplicative PDDs

Consider a general multiplicative form,

$$y(\mathbf{X}) = \prod_{u \subseteq \{1,\cdots,N\}} \left[1 + z_u(\mathbf{X}_u)\right], \tag{4.17}$$

of the dimensional decomposition of y, where z_u, $u \subseteq \{1, \cdots, N\}$, are various component functions of input variables with increasing dimensions. Like the sum in Equation (4.1), the product in Equation (4.17) comprises 2^N terms, with each term depending on a group of variables indexed by a particular subset of $\{1, \cdots, N\}$, including the empty set $\emptyset$. Tunga and Demiralp [120] originally proposed this decomposition, calling it factorized high-dimensional model representation. However, it is not obvious if such decomposition exists uniquely for a general multivariate function y. Lemma 4.3 and Theorem 4.4 demonstrate that, indeed, it does with some restrictions.

Lemma 4.3: *The ANOVA component functions y_v, $v \subseteq \{1, \cdots, N\}$, of a square integrable function $y : \mathbb{R}^N \to \mathbb{R}$, when integrated with respect to the probability measure $f_{\mathbf{X}_{-u}}(\mathbf{x}_{-u})d\mathbf{x}_{-u} = \prod_{i=1, i\notin u}^{N} f_i(x_i)dx_i$, $u \subseteq \{1, \cdots, N\}$, satisfy*

$$\int_{\mathbb{R}^{N-|u|}} y_v(\mathbf{x}_v) f_{\mathbf{X}_{-u}}(\mathbf{x}_{-u})d\mathbf{x}_{-u} = \begin{cases} y_v(\mathbf{x}_v) & \text{if } v \subseteq u, \\ 0 & \text{if } v \nsubseteq u. \end{cases} \tag{4.18}$$

Proof. For any two subsets $v \subseteq \{1, \cdots, N\}$, $u \subseteq \{1, \cdots, N\}$, $(v \cap -u) \subseteq -u$ and $-u = (-u \setminus (v \cap -u)) \cup (v \cap -u)$. If $v \subseteq u$, then $y_v(\mathbf{x}_v)$ does not depend on $\mathbf{x}_{-u}$, resulting in

$$\int_{\mathbb{R}^{N-|u|}} y_v(\mathbf{x}_v) f_{\mathbf{X}_{-u}}(\mathbf{x}_{-u})d\mathbf{x}_{-u} = y_v(\mathbf{x}_v) \int_{\mathbb{R}^{N-|u|}} f_{\mathbf{X}_{-u}}(\mathbf{x}_{-u})d\mathbf{x}_{-u} = y_v(\mathbf{x}_v), \tag{4.19}$$

the non-trivial result of Equation (4.18). When $v \nsubseteq u$, consider an integer $k \in (v \cap -u)$, so that $k \in v$. Then,

$$\begin{aligned}\int_{\mathbb{R}^{N-|u|}} y_v(\mathbf{x}_v) f_{\mathbf{X}_{-u}}(\mathbf{x}_{-u}) d\mathbf{x}_{-u} &= \int_{\mathbb{R}^{N-|u|-|v\cap -u|}} \int_{\mathbb{R}^{|v\cap -u|}} y_v(\mathbf{x}_v) f_{\mathbf{X}_{-u}}(\mathbf{x}_{-u}) d\mathbf{x}_{v\cap -u} d\mathbf{x}_{-u\setminus(v\cap -u)} \\ &= \int_{\mathbb{R}^{N-|u|-|v\cap -u|-1}} \left(\int_{\mathbb{R}} y_v(\mathbf{x}_v) f_k(x_k) dx_k \right) \\ &\quad \times \prod_{j\in(v\cap -u), j\neq k} f_j(x_j) d\mathbf{x}_{(v\cap -u)\setminus\{k\}} d\mathbf{x}_{-u\setminus(v\cap -u)} \\ &= 0, \end{aligned} \tag{4.20}$$

where the equality to *zero* in the last line follows from using Equation (4.5). □

Theorem 4.4: *A square integrable function $y : \mathbb{R}^N \to \mathbb{R}$ for a given probability measure $f_{\mathbf{X}}(\mathbf{x})d\mathbf{x} = \Pi_{i=1}^{i=N} f_i(x_i)dx_i$ admits a unique multiplicative dimensional decomposition expressed by Equation* (4.17).

Proof. Changing the dummy index from u to v, replacing $\mathbf{X}$ with $\mathbf{x}$, and integrating both sides of Equation (4.1) with respect to the measure $f_{\mathbf{X}_{-u}}(\mathbf{x}_{-u})d\mathbf{x}_{-u}$, that is, over all variables except $\mathbf{x}_u$, yields

$$\int_{\mathbb{R}^{N-|u|}} y(\mathbf{x}) f_{\mathbf{X}_{-u}}(\mathbf{x}_{-u}) d\mathbf{x}_{-u} = \sum_{v\subseteq\{1,\cdots,N\}} \int_{\mathbb{R}^{N-|u|}} y_v(\mathbf{x}_v) f_{\mathbf{X}_{-u}}(\mathbf{x}_{-u}) d\mathbf{x}_{-u}. \tag{4.21}$$

Using Lemma 4.3, Equation (4.21) simplifies to

$$\int_{\mathbb{R}^{N-|u|}} y(\mathbf{x}) f_{\mathbf{X}_{-u}}(\mathbf{x}_{-u}) d\mathbf{x}_{-u} = \sum_{v\subseteq u} y_v(\mathbf{x}_v) = y_u(\mathbf{x}_u) + \sum_{v\subset u} y_v(\mathbf{x}_v), \tag{4.22}$$

with $\subset$ representing proper subset (strict inclusion). Therefore, for any $u \subseteq \{1, \cdots, N\}$, including $\emptyset$,

$$y_u(\mathbf{x}_u) = \int_{\mathbb{R}^{N-|u|}} y(\mathbf{x}) f_{\mathbf{X}_{-u}}(\mathbf{x}_{-u}) d\mathbf{x}_{-u} - \sum_{v\subset u} y_v(\mathbf{x}_v), \tag{4.23}$$

proving the existence and uniqueness of ANOVA component functions for a square integrable function. To do the same for the multiplicative component functions, expand the right side of Equation (4.17) to form

$$\begin{aligned} y(\mathbf{X}) = z_\emptyset + & \sum_{\substack{u\subseteq\{1,\cdots,N\}\\|u|=1}} r_u\left(z_v(\mathbf{X}_v); v\subseteq u\right) + \sum_{\substack{u\subseteq\{1,\cdots,N\}\\|u|=2}} r_u\left(z_v(\mathbf{X}_v); v\subseteq u\right) + \cdots + \\ & r_{\{1,\cdots,N\}}\left(z_v(\mathbf{X}_v); v\subseteq\{1,\cdots,N\}\right) \\ = & \sum_{u\subseteq\{1,\cdots,N\}} r_u\left(z_v(\mathbf{X}_v); v\subseteq u\right), \end{aligned} \tag{4.24}$$

where $r_u\left(z_v(\mathbf{X}_v); v\subseteq u\right)$ is a function of at most $|u|$-variate multiplicative component functions of y. For instance, when $u=\emptyset$, $u=\{i\}$, and $u=\{i_1,i_2\}$, $i,i_1,i_2=1,\cdots,N$, $i_2>i_1$, the corresponding r_u-functions are $r_\emptyset=z_\emptyset$, $r_{\{i\}}(z_\emptyset, z_{\{i\}}(X_i))$, and $r_{\{i_1,i_2\}}(z_\emptyset, z_{\{i_1\}}(X_{i_1}), z_{\{i_2\}}(X_{i_2}), z_{\{i_1,i_2\}}(X_{i_1},X_{i_2}))$, respectively. Comparing Equations (4.1) and (4.24) yields the recursive relationship,

$$r_u\left(z_v(\mathbf{X}_v); v\subseteq u\right) = y_u(\mathbf{X}_u), \tag{4.25}$$

which, on inversion, expresses z_u, $u\subseteq\{1,\cdots N\}$, in terms of the additive ANOVA component functions y_v, $v\subseteq u$. Therefore, given a probability measure of $\mathbf{X}$, the functions r_u and z_u, $u\subseteq\{1,\cdots N\}$, also exist and are unique. □

In this work, two new multiplicative PDDs, referred to as factorized PDD and logarithmic PDD, were developed in the spirit of additive PDD for tackling high-dimensional stochastic response functions endowed with multiplicative dimensional hierarchies. Both decompositions, rooted in Equation (4.17), exploit the smoothness properties of a stochastic solution, if they exist, by measure-consistent orthogonal polynomials, and are described in the following subsections.

4.4.1 Factorized PDD

The F-PDD is built on two principal steps: (1) finding the explicit relationships between the component functions of the ANOVA and the multiplicative dimensional decompositions of a multivariate function y, and (2) expanding the ANOVA component functions in terms of the measure-consistent orthonormal polynomial basis functions. Theorem 4.5 reveals the desired relationships in the first step.

Theorem 4.5: *The recursive relationships between component functions of the ANOVA and multiplicative dimensional decompositions of a square integrable function* $y : \mathbb{R}^N \to \mathbb{R}$*, represented by Equations* (4.1) *and* (4.17)*, respectively, are*

$$1 + z_u(\mathbf{X}_u) = \frac{\sum\limits_{v \subseteq u} y_v(\mathbf{X}_v)}{\prod\limits_{v \subset u} [1 + z_v(\mathbf{X}_v)]},\ u \subseteq \{1, \cdots, N\}. \tag{4.26}$$

Proof. Since Equations (4.1) and (4.17) represent the same function y,

$$\sum_{u \subseteq \{1,\cdots,N\}} y_u(\mathbf{X}_u) = \prod_{u \subseteq \{1,\cdots,N\}} [1 + z_u(\mathbf{X}_u)], \tag{4.27}$$

which, as is, is unwieldy when solving for z_u. However, from Equation (4.25), the solution z_u for $u \subseteq \{1, \cdots, N\}$ depends only on functions y_v such that $v \subseteq u$. Therefore, all remaining additive or multiplicative component functions not involved can be assigned arbitrary values. In particular, setting $y_v = z_v = 0$ for all $v \nsubseteq u$ in Equation (4.27) results in

$$\sum_{v \subseteq u} y_v(\mathbf{X}_v) = \prod_{v \subseteq u} [1 + z_v(\mathbf{X}_v)] = [1 + z_u(\mathbf{X}_u)] \prod_{v \subset u} [1 + z_v(\mathbf{X}_v)], \tag{4.28}$$

which, on inversion, yields Equation (4.26), completing the proof. □

Corollary 4.1: *Recursive evaluations of Equation* (4.26) *eliminate* $1 + z_v$*,* $v \subset u$*,*

leading to an explicit form of

$$1+z_u(\mathbf{X}_u)=\frac{\sum\limits_{w_{|u|}\subseteq u} y_{w_{|u|}}\left(\mathbf{X}_{w_{|u|}}\right)}{\prod\limits_{w_{|u|}\subset u}\frac{\sum\limits_{w_{|u|-1}\subseteq w_{|u|}} y_{w_{|u|-1}}\left(\mathbf{X}_{w_{|u|-1}}\right)}{\ddots\prod\limits_{w_{|u|-1}\subset w_{|u|}}\frac{}{\ddots\prod\limits_{w_2\subset w_3}\frac{\sum\limits_{w_1\subseteq w_2} y_{w_1}\left(\mathbf{X}_{w_1}\right)}{\prod\limits_{w_1\subset w_2}\frac{\sum\limits_{w_0\subseteq w_1} y_{w_0}\left(\mathbf{X}_{w_0}\right)}{1}}}}} \tag{4.29}$$

for any $u\subseteq\{1,\cdots,N\}$, solely in terms of the ANOVA component functions.

Corollary 4.2: *The multiplicative constant, univariate, and bivariate component functions of a square integrable function $y:\mathbb{R}^N\to\mathbb{R}$, obtained by setting $u=\emptyset$, $u=\{i\}$; $i=1,\cdots,N$, and $u=\{i_1,i_2\}$; $i_1<i_2=1,\cdots,N$, respectively, in Equation* (4.26) *or* (4.29) *are*

$$1+z_\emptyset=y_\emptyset, \tag{4.30}$$

$$1+z_{\{i\}}(X_i)=\frac{y_\emptyset+y_{\{i\}}(X_i)}{y_\emptyset}, \tag{4.31}$$

and

$$1+z_{\{i_1,i_2\}}(X_{i_1},X_{i_2})=\frac{y_\emptyset+y_{\{i_1\}}(X_{i_1})+y_{\{i_2\}}(X_{i_2})+y_{\{i_1,i_2\}}(X_{i_1},X_{i_2})}{y_\emptyset\left[\frac{y_\emptyset+y_{\{i_1\}}(X_{i_1})}{y_\emptyset}\right]\left[\frac{y_\emptyset+y_{\{i_2\}}(X_{i_2})}{y_\emptyset}\right]}. \tag{4.32}$$

Remark 4.3: Equations (4.30), (4.31), and (4.32) can also be obtained employing the identity and first- and second-degree idempotent operators [120]. However, to obtain similar expressions for trivariate and higher-variate multiplicative component

functions, an extensive amount of algebra associated with third- and higher-degree idempotent operators will be required. This is a primary reason why component functions with variables equal to three or greater have yet to be reported in the current literature. Theorem 4.5, in contrast, is simpler and, more importantly, provides a general expression − Equation (4.26) or (4.29) − that is valid for a multiplicative component function of an arbitrary number of variables.

The next step entails representing the ANOVA component functions by their Fourier-polynomial expansions, that is, applying Equation (4.8) into Equation (4.26), which results in expressing the multiplicative component functions

$$1+z_u(\mathbf{X}_u)=\frac{y_\emptyset+\displaystyle\sum_{\emptyset\neq v\subseteq u}\sum_{\substack{\mathbf{j}_{|v|}\in\mathbb{N}_0^{|v|}\\ j_1,\cdots,j_{|v|}\neq 0}} C_{v\mathbf{j}_{|v|}}\psi_{v\mathbf{j}_{|v|}}(\mathbf{X}_v)}{\displaystyle\prod_{v\subset u}[1+z_v(\mathbf{X}_v)]},\ u\subseteq\{1,\cdots,N\}, \tag{4.33}$$

in terms of orthonormal polynomials as well. Finally, combining Equations (4.17) and (4.33) creates the F-PDD of

$$y(\mathbf{X})=y_\emptyset\prod_{\emptyset\neq u\subseteq\{1,\cdots,N\}}\left[\frac{y_\emptyset+\displaystyle\sum_{\emptyset\neq v\subseteq u}\sum_{\substack{\mathbf{j}_{|v|}\in\mathbb{N}_0^{|v|}\\ j_1,\cdots,j_{|v|}\neq 0}} C_{v\mathbf{j}_{|v|}}\psi_{v\mathbf{j}_{|v|}}(\mathbf{X}_v)}{\displaystyle\prod_{v\subset u}[1+z_v(\mathbf{X}_v)]}\right], \tag{4.34}$$

also an exact representation of $y(\mathbf{X})$, where infinite orthonormal polynomials of increasing dimensions are structured with a multiplicative hierarchy, as opposed to the additive hierarchy in Equation (4.10). Consequently, an S-variate, mth-order L-PDD approximation, retaining at most S-variate component functions and mth-order or-

thogonal polynomials, becomes

$$\hat{y}_{S,m}(\mathbf{X}) = y_{\emptyset} \prod_{\substack{\emptyset \neq u \subseteq \{1,\cdots,N\} \\ 1 \leq |u| \leq S}} \left[\frac{y_{\emptyset} + \sum_{\emptyset \neq v \subseteq u} \sum_{\substack{\mathbf{j}_{|v|} \in \mathbb{N}_0^{|v|}, \left\|\mathbf{j}_{|u|}\right\|_\infty \leq m \\ j_1,\cdots,j_{|v|} \neq 0}} C_{v\mathbf{j}_{|v|}} \psi_{v\mathbf{j}_{|v|}}(\mathbf{X}_v)}{\prod_{v \subset u} [1 + z_v(\mathbf{X}_v)]} \right], \tag{4.35}$$

which converges to $y(\mathbf{X})$ in the mean-square sense when $S \to N$ and $m \to \infty$. It is worth noting that Equations (4.33)-(4.35) can also be expressed explicitly, solely in terms of orthonormal polynomials exploiting Equation (4.29). However, they are not reported here because of their more complicated form.

Although the right side of Equation (4.35) contains products of at most S univariate polynomials, no simple expressions are available for the second-moment properties of $\hat{y}_{S,m}(\mathbf{X})$ if S and m are selected arbitrarily. However, any probabilistic characteristic of $y(\mathbf{X})$ is easily estimated by the MCS of $\hat{y}_{S,m}(\mathbf{X})$ in Equation (4.35). When $S = 1$, the univariate F-PDD approximation,

$$\hat{y}_{1,m}(\mathbf{X}) = y_{\emptyset} \left[\prod_{i=1}^{N} \left\{ 1 + \frac{1}{y_{\emptyset}} \sum_{j=1}^{m} C_{ij} \psi_{ij}(X_i) \right\} \right], \tag{4.36}$$

forms a product of univariate polynomials, guiding to closed-form expressions of its second-moment properties. Indeed, it is elementary to show that Equation (4.36) results in the exact mean

$$\mathbb{E}\left[\hat{y}_{1,m}(\mathbf{X})\right] = y_{\emptyset}, \tag{4.37}$$

but an approximate variance

$$\mathbb{E}\left[\left(\hat{y}_{1,m}(\mathbf{X}) - \mathbb{E}\left[\hat{y}_{1,m}(\mathbf{X})\right]\right)^2\right] = y_{\emptyset}^2 \left[\prod_{i=1}^{N} \left(1 + \frac{1}{y_{\emptyset}^2} \sum_{j=1}^{m} C_{ij}^2 \right) - 1 \right], \tag{4.38}$$

that are valid for an arbitrary $m < \infty$.

4.4.2 Logarithmic PDD

The L-PDD is constructed by invoking the ADD of the logarithmic transformation of a stochastic response, followed by the Fourier-polynomial expansions of the ANOVA component functions in terms of the measure-consistent orthonormal polynomial basis functions.

The ADD of the logarithm of a stochastic response $w(\boldsymbol{X}) := \ln y(\boldsymbol{X})$, if it exists, is

$$w(\mathbf{X}) = \sum_{u \subseteq \{1,\cdots,N\}} w_u(\mathbf{X}_u), \tag{4.39}$$

$$w_\emptyset = \int_{\mathbb{R}^N} \ln y(\mathbf{x}) f_{\mathbf{X}}(\mathbf{x}) d\mathbf{x}, \tag{4.40}$$

$$w_u(\mathbf{X}_u) = \int_{\mathbb{R}^{N-|u|}} \ln y(\mathbf{X}_u, \mathbf{x}_{-u}) f_{\mathbf{X}_{-u}}(\mathbf{x}_{-u}) d\mathbf{x}_{-u} - \sum_{v \subset u} w_v(\mathbf{X}_v), \tag{4.41}$$

where w_u is a $|u|$-variate component function describing a constant or the interactive effect of $\mathbf{X}_u$ on w when $|u| = 0$ or $|u| > 0$. On exponentiation, Equation (4.39) reverts to

$$y(\mathbf{X}) = \prod_{u \subseteq \{1,\cdots,N\}} \exp\left[w_u(\mathbf{X}_u)\right], \tag{4.42}$$

an expansion of the original function. Compared with Equation (4.17), Equation (4.42) represents another multiplicative dimensional decomposition when $\exp\left[w_u(\mathbf{X}_u)\right] = 1 + z_u(\mathbf{X}_u)$ for all $u \subseteq \{1, \cdots, N\}$. Expanding the non-constant component functions of $w(\mathbf{X})$ in terms of measure-consistent orthonormal polynomials yields

$$w_u(\mathbf{X}_u) = \sum_{\substack{\mathbf{j}_{|u|} \in \mathbb{N}_0^{|u|} \\ j_1,\cdots,j_{|u|} \neq 0}} D_{u\mathbf{j}_{|u|}} \psi_{u\mathbf{j}_{|u|}}(\mathbf{X}_u),\ \emptyset \neq u \subseteq \{1, \cdots, N\}, \tag{4.43}$$

with

$$D_{u\boldsymbol{j}_{|u|}} := \int_{\mathbb{R}^N} \ln y(\mathbf{x}) \psi_{u\mathbf{j}_{|u|}}(\mathbf{x}_u) f_{\mathbf{X}}(\mathbf{x}) d\mathbf{x} \tag{4.44}$$

defining a distinct but similar set of expansion coefficients. Finally, combining Equations (4.42) and (4.43) leads to the L-PDD of

$$y(\mathbf{X}) = \exp(w_\emptyset) \prod_{\emptyset \neq u \subseteq \{1,\cdots,N\}} \exp\left[\sum_{\substack{\mathbf{j}_{|u|} \in \mathbb{N}_0^{|u|} \\ j_1,\cdots,j_{|u|} \neq 0}} D_{u\mathbf{j}_{|u|}} \psi_{u\mathbf{j}_{|u|}}(\mathbf{X}_u) \right], \tag{4.45}$$

which is yet another exact representation of $y(\mathbf{X})$, where infinite orthonormal polynomials of increasing dimensions are structured with a multiplicative hierarchy, as opposed to an additive hierarchy in Equation (4.10). Consequently, an S-variate, mth-order F-PDD approximation, retaining at most S-variate component functions and mth-order orthogonal polynomials, becomes

$$\bar{y}_{S,m}(\mathbf{X}) = \exp(w_\emptyset) \prod_{\substack{\emptyset \neq u \subseteq \{1,\cdots,N\} \\ 1 \leq |u| \leq S}} \exp\left[\sum_{\substack{\mathbf{j}_{|u|} \in \mathbb{N}_0^{|u|}, \left\|\mathbf{j}_{|u|}\right\|_\infty \leq m \\ j_1,\cdots,j_{|u|} \neq 0}} D_{u\mathbf{j}_{|u|}} \psi_{u\mathbf{j}_{|u|}}(\mathbf{X}_u) \right], \tag{4.46}$$

which also converges to $y(\mathbf{X})$ in the mean-square sense when $S \to N$ and $m \to \infty$.

Similar to F-PDD, no simple expressions are available for the second-moment properties of $\bar{y}_{S,m}(\mathbf{X})$ when S and m are arbitrary. However, a probabilistic characteristic of $y(\mathbf{X})$ is also easily estimated by the MCS of $\bar{y}_{S,m}(\mathbf{X})$ in Equation (4.46). When $S = 1$, the univariate L-PDD approximation with $D_{ij} := D_{\{i\}(j)}$ becomes

$$\bar{y}_{1,m}(\mathbf{X}) = \exp(w_\emptyset) \prod_{i=1}^{N} \exp\left[\sum_{j=1}^{m} D_{ij} \psi_{ij}(X_i) \right], \tag{4.47}$$

forming a product of exponential functions of univariate polynomials. In this case, the approximate mean and variance of $\bar{y}_{1,m}(\boldsymbol{X})$ are readily calculated from

$$\mathbb{E}\left[\bar{y}_{1,m}(\mathbf{X})\right] = \exp(w_\emptyset) \prod_{i=1}^{N} \mathbb{E}\left[\exp\left\{\sum_{j=1}^{m} D_{ij}\psi_{ij}(X_i)\right\}\right], \tag{4.48}$$

and

$$\begin{aligned}\mathbb{E}\left[\left(\bar{y}_{1,m}(\mathbf{X}) - \mathbb{E}\left[\bar{y}_{1,m}(\mathbf{X})\right]\right)^2\right] = \exp(2w_\emptyset) \prod_{i=1}^{N} \mathbb{E}\left[\exp\left\{2\sum_{j=1}^{m} D_{ij}\psi_{ij}(X_i)\right\}\right] \\ - \exp(w_\emptyset) \prod_{i=1}^{N} \mathbb{E}\left[\exp\left\{\sum_{j=1}^{m} D_{ij}\psi_{ij}(X_i)\right\}\right],\end{aligned} \tag{4.49}$$

respectively, that are valid for an arbitrary $m < \infty$, provided that the expectations exist and are finite. It is important to note that the expectations in Equations (4.48) and (4.49) require at most univariate integrals regardless of N or m, and involve the expansion coefficients D_{ij}, $i = 1, \cdots, N$ and $j = 1, \cdots, m$, stemming from the univariate L-PDD approximation in Equation (4.47).

Remark 4.4: The A-PDD approximation $\tilde{y}_{1,m}(\mathbf{X})$ is called univariate because Equation (4.14) comprises a sum of at most univariate component functions, describing only the main effect of $\mathbf{X}$. In contrast, the F-PDD approximation $\hat{y}_{1,m}(\mathbf{X})$ in Equation (4.36) and the L-PDD approximation $\bar{y}_{1,m}(\mathbf{X})$ in Equation (4.47) contain products of various univariate functions. Therefore, some effects of interactions between two input variables X_i and X_j, $i \neq j$, subsist in $\hat{y}_{1,m}(\mathbf{X})$ or $\bar{y}_{1,m}(\mathbf{X})$. As an example, consider a function, $y = y_\emptyset + y_{\{1\}}(X_1) + y_{\{2\}}(X_2) + y_{\{1\}}(X_1)y_{\{2\}}(X_2)/y_\emptyset$, of two variables, containing a sum and a product of its univariate ANOVA component functions. The univariate A-PDD approximation, $\tilde{y}_{1,m} = y_\emptyset + y_{\{1\}}(X_1) + y_{\{2\}}(X_2)$, captures only the main effects of X_1 and X_2, and may produce non-negligible errors if the product term

of y is significant. On the other hand, the univariate F-PDD approximation, $\hat{y}_{1,m} = (1 + z_{\emptyset})[1 + z_{\{1\}}(X_1)][1 + z_{\{2\}}(X_2)] = y_{\emptyset} + y_{\{1\}}(X_1) + y_{\{2\}}(X_2) + y_{\{1\}}(X_1)y_{\{2\}}(X_2)/y_{\emptyset}$, obtained using the relationships in Equations (4.30) and (4.31), exactly reproduces y, thereby capturing not only the main effects, but also the interactive effect of input variables. Therefore, the term "univariate" used in this thesis for the multiplicative PDD approximations should be interpreted in the context of including at most univariate component functions, not necessarily preserving only the main effects. It would be intriguing to study if a univariate approximation from a multiplicative PDD results in more accurate stochastic solutions of real-life problems than from the additive PDD.

Remark 4.5: When $y_{\emptyset}$ is *zero* or is close to *zero*, Equations (4.30)-(4.38) may fail or become ill-conditioned, raising questions about the suitability of the F-PDD approximation in such conditions. The L-PDD approximation faces a similar situation when a stochastic response is non-positive or close to *zero*, as the logarithmic transformation employed in Equations (4.39)-(4.49) is invalid or highly nonlinear. However, they do not necessarily imply that the L-PDD or F-PDD cannot be used. Indeed, all of these problems can be remedied by appropriately conditioning the stochastic response y. For instance, by adding a non-zero constant to y or multiplying y with a non-zero constant, Equations (4.30)-(4.38) for the pre-conditioned y remain valid and well-behaved. Similarly, by adding a non-negative constant to y or multiplying y with a non-zero constant, the pre-conditioned y can be made to always remain positive or well-behaved. The Application section (Section 4.7) describes how such

problems may arise in a practical situation and includes simple adjustments to work around them.

Remark 4.6: The MCS of PDD approximations, $\tilde{y}_{S,m}(\mathbf{X})$, $\hat{y}_{S,m}(\mathbf{X})$, or $\bar{y}_{S,m}(\mathbf{X})$, referred to as embedded MCS in this thesis, entail evaluations of simple analytical functions. Hence, an arbitrarily large sample size can be accommodated in an embedded MCS for estimating rare-event probabilities. In contrast, the MCS of $y(\boldsymbol{X})$, referred to as crude MCS in this thesis, requires expensive numerical calculations and can, therefore, be prohibitive when estimating such probabilities.

4.5 Calculation of Expansion Coefficients

The determination of the expansion coefficients, $y_{\emptyset}$, $C_{u\mathbf{j}_{|u|}}$, $w_{\emptyset}$, and $D_{u\mathbf{j}_{|u|}}$in Equations (4.2), (4.9), (4.40), and (4.44), respectively, involves various N-dimensional integrals over $\mathbb{R}^N$. For large N, a full numerical integration employing an N-dimensional tensor product of a univariate quadrature formula is computationally prohibitive. Instead, a dimension-reduction integration scheme and a sampling technique were applied to estimate the coefficients efficiently.

4.5.1 Dimension-reduction integration

The dimension-reduction integration, developed by Xu and Rahman [85], entails approximating a high-dimensional integral of interest by a finite sum lower-dimensional integrations. For calculating the expansion coefficients, $y_{\emptyset}$, $C_{u\mathbf{j}_{|u|}}$, $w_{\emptyset}$, and $D_{u\mathbf{j}_{|u|}}$, this is accomplished by replacing the N-variate function y or $\ln y$ in Equations (4.2), (4.9), (4.40), and (4.44) with an R-variate truncation, where $R < N$, of

its referential dimensional decomposition at a chosen reference point [86,119]. The result is a reduced integration scheme, requiring evaluations of at most R-dimensional integrals. The scheme facilitates calculation of the coefficients approaching their exact values as $R \to N$, and is significantly more efficient than performing one N-dimensional integration, particularly when $R \ll N$. Hence, the computational effort is significantly decreased using the dimension-reduction integration. When $R = 1$ or 2, the scheme involves one-, or at most, two-dimensional integrations, respectively. Nonetheless, numerical integration is still required for a general integrand. The integration points and associated weights, which depend on the probability distribution of X_i, are readily available when the basis functions are polynomials [88, 90].

The S-variate, mth-order A-PDD, F-PDD, and L-PDD approximations require evaluations of $Q_{S,m} = \sum_{k=0}^{k=S} \binom{N}{S-k} m^{S-k}$ number of expansion coefficients, including $y_\emptyset$ or $w_\emptyset$. If these coefficients are estimated by dimension-reduction integration with $R = S < N$ and, therefore, involve at most an S-dimensional tensor product of an n-point univariate quadrature rule depending on m, then the total cost for the S-variate, mth-order approximation entails a maximum of $\sum_{k=0}^{k=S} \binom{N}{S-k} n^{S-k}(m)$ function evaluations. If the integration points include a common point in each coordinate − a special case of symmetric input probability density functions and odd values of n (see Example 3) − the number of function evaluations reduces to $\sum_{k=0}^{k=S} \binom{N}{S-k} (n(m)-1)^{S-k}$. In other words, the computational complexity of the PDD approximations is an Sth-order polynomial with respect to the number of random variables or integration points.

4.5.2 Crude MCS

Sampling techniques, including crude MCS or quasi MCS, for estimating the expansion coefficients comprise two simple steps: (1) generate a point set $\mathcal{P}_L := \{\mathbf{x}^{(l)} \in \mathbb{R}^N,\ l = 1, \cdots, L\}$ of size $L \in \mathbb{N}$ consistent with the probability measure of the random input $\mathbf{X}$; (2) approximate the integrals in Equations (4.2), (4.9), (4.40), and (4.44) as the averages of y, $y\psi_{u\mathbf{j}_{|u|}}$, $\ln y$, and $\ln y\psi_{u\mathbf{j}_{|u|}}$ evaluated at all points of $\mathcal{P}_L$. In crude MCS, $\mathcal{P}_L$ contains a sequence of pseudo-random numbers, following the probability distributions of $\mathbf{X}$. In quasi MCS, $\mathcal{P}_L$ is a set of a low-discrepancy sequence. The advantage of one MCS over the other depends on the smoothness properties of the integrand and the dimension of the integral [121].

It is important to emphasize that the F-PDD and L-PDD approximations involve the same or similar expansion coefficients as those defined in the additive PDD approximation. Therefore, the computational effort of the additive PDD approximation is recycled for generating both the F-PDD and L-PDD approximations. No additional computational cost is incurred by either variant of the PDD approximation.

4.6 Numerical Examples

Three numerical examples are presented to illustrate the performance of the additive and multiplicative PDD approximations in calculating the statistical moments of random mathematical functions or random eigenvalues, including the tail probability distributions of natural frequencies. In Example 1, classical Legendre or Hermite polynomials were used to define the orthonormal polynomials, and all ex-

pansion coefficients were determined analytically. In Examples 2 and 3, all original random variables were transformed into standard Gaussian random variables, facilitating the use of Hermite orthonormal polynomials as bases and the Gauss-Hermite quadrature rule for calculating the expansion coefficients. The expansion order m varies depending on the example, but in all cases the number of integration points $n = m + 1$. In Example 2, the sample sizes for crude MCS and the embedded MCS of all three PDD methods are 10^7. The respective sample sizes are $50,000$ and 10^6 in Example 3.

4.6.1 Two mathematical functions

Consider a polynomial function and an exponential function, expressed by

$$y_1(\mathbf{X}) = \frac{1}{2^N} \prod_{i=1}^{N} \left(3X_i^2 + 1\right) \text{ and} \tag{4.50}$$

$$y_2(\mathbf{X}) = \frac{1}{(4/5)^{N/2}} \prod_{i=1}^{N} \left[\exp\left(\frac{X_i^2}{10}\right)\right], \tag{4.51}$$

respectively, where X_i, $i = 1, \cdots .N$, are independent and identical random variables. Each variable follows standard uniform distribution over [0,1] for the polynomial function and standard Gaussian distribution with *zero* mean and *unit* variance for the exponential function. From elementary calculations, the exact mean and variance of y_1 are 1 and $(6/5)^N - 1$, respectively, and of y_2 are 1 and $(16/15)^{N/2} - 1$, respectively. The purpose of this example is to compare the second-moment statistics of both functions for $N = 5$ obtained using A-PDD (Equations (4.12) and (4.13)), F-PDD (Equations (4.37) and (4.38)), and L-PDD (Equations (4.48) and (4.49)) approximations. The integrals in Equations (4.48) and (4.49) were evaluated by $m + 1$-point

Gauss-Legendre rule for y_1, but analytically for y_2.

Table 4.1 presents relative errors, defined as the ratio of the absolute difference between the exact and approximate variances of y_1 to the exact variance, committed by the additive and multiplicative PDD approximations for various combinations of the truncation parameters $1 \leq S \leq 5$ and $1 \leq m \leq 8$. The errors from A-PDD approximations drop as m increases, but they level off quickly at their respective limits for the univariate to quadrivariate A-PDD approximations. When $m = 2$, the error due to the pentavariate, second-order A-PDD approximation reaches *zero*, as the approximation coincides with y_1. The error remains *zero* for the univariate, second-order F-PDD approximation, as y_1 is a product of univariate quadratic polynomials. For the same reason, there is no need to employ higher-variate or higher-order F-PDD approximations. In contrast, the univariate L-PDD approximation also yields progressively smaller errors as m increases, but unlike in F-PDD, the error does not vanish. This is because the logarithmic transformation inducing additional nonlinearity to y_1 creates a non-polynomial that cannot be exactly reproduced by a polynomial, regardless of how large $m < \infty$ becomes. Nonetheless, the L-PDD, which also requires only univariate approximation, is more accurate than the univariate to quadrivariate A-PDD approximations when $m \geq S$. Both the F-PDD and L-PDD approximations favorably exploit the multiplicative structure of y_1, but the former approximation is superior to the latter approximation when dealing with multiplicative polynomials.

Table 4.2 displays the results from similar error analysis performed for y_2, a product of univariate functions, although not polynomials. As expected, the errors

Table 4.1: Relative errors in calculating the variance of y_1 by various PDD approximations.

	A-PDD[(a)]					F-PDD[(a)]	L-PDD
m	$S=1$ $(\times 10^{-1})$	$S=2$ $(\times 10^{-2})$	$S=3$ $(\times 10^{-3})$	$S=4$ $(\times 10^{-4})$	$S=5$ $(\times 10^{-2})$	$S=1$ $(\times 10^{-2})$	$S=1$
1	3.7	13.0	90.0	850.0	8.5	8.5	5.9×10^{-2}
2	3.3	5.9	5.6	2.2	0	0	3.7×10^{-2}
3	3.3	5.9	5.6	2.2	-[(b)]	-[(b)]	3.5×10^{-4}
4	3.3	5.9	5.6	2.2	-[(b)]	-[(b)]	8.3×10^{-7}
5	3.3	5.9	5.6	2.2	-[(b)]	-[(b)]	1.1×10^{-6}
6	3.3	5.9	5.6	2.2	-[(b)]	-[(b)]	1.6×10^{-7}
7	3.3	5.9	5.6	2.2	-[(b)]	-[(b)]	3.3×10^{-7}
8	3.3	5.9	5.6	2.2	-[(b)]	-[(b)]	3.3×10^{-7}

[(a)] The variances from the pentavariate, second-order A-PDD and univariate, second-order L-PDD approximations coincide with the exact solution: $(6/5)^N - 1$, where $N = 5$.

[(b)] Not required.

emanating from A-PDD approximations decline as S or m rises. Since the pentavariate A-PDD and the univariate F-PDD of y_2 are identical polynomials, the respective errors coincide regardless of m. Again, due to the multiplicative nature of y_2, the F-PDD approximation is more appropriate to use than the A-PDD approximation. However, neither converges to exactness, as y_2 is a non-polynomial function to begin with. In contrast, the logarithmic transformation, not beneficial to y_1, creates a polynomial image of y_2, which is, therefore, exactly reproduced by an L-PDD approximation. Indeed, the univariate, second-order L-PDD approximation yields the exact variance of y_2, turning the tables on the F-PDD approximation for tackling multiplicative non-polynomials. In summary, both functions y_1 and y_2, although simple and somewhat contrived, demonstrate a clear advantage of multiplicative PDD over

additive PDD approximations.

Table 4.2: Relative errors in calculating the variance of y_2 by various PDD approximations.

	A-PDD					F-PDD	L-PDD[a]
m	$S=1$ $(\times 10^{-1})$	$S=2$ $(\times 10^{-2})$	$S=3$ $(\times 10^{-3})$	$S=4$ $(\times 10^{-4})$	$S=5$ $(\times 10^{-5})$	$S=1$ $(\times 10^{-5})$	$S=1$
1	-[b]	-[b]	-[b]	-[b]	-[b]	-[b]	-[b]
2	1.1	5.2	51	500	5000	5000	0
3	1.1	5.2	51	500	5000	5000	-[c]
4	0.6	0.47	2.7	26	260	260	-[c]
5	0.6	0.47	2.7	26	260	260	-[c]
6	0.6	0.02	0.18	1.5	15	15	-[c]
7	0.6	0.02	0.18	1.5	15	15	-[c]
8	0.6	0.02	0.06	0.3	2.6	2.6	-[c]

[a] The variance from the univariate, second-order L-PDD approximation coincides with the exact solution: $(16/15)^{N/2}-1$, where $N=5$.

[b] 100% error.

[c] Not required.

4.6.2 Two-degree-of-freedom, undamped, spring-mass system

Consider a two-degree-of-freedom, undamped, spring-mass system, shown in Figure 4.1, with random mass and random stiffness matrices

$$\boldsymbol{M}(\mathbf{X})=\begin{bmatrix} M_1(\mathbf{X}) & 0 \\ 0 & M_2(\mathbf{X}) \end{bmatrix} \text{ and } \boldsymbol{K}(\mathbf{X})=\begin{bmatrix} K_1(\mathbf{X})+K_3(\mathbf{X}) & -K_3(\mathbf{X}) \\ -K_3(\mathbf{X}) & K_2(\mathbf{X})+K_3(\mathbf{X}) \end{bmatrix}, \tag{4.52}$$

respectively, where $K_1(\mathbf{X})=1000X_1$ N/m, $K_2(\mathbf{X})=1100X_2$ N/m, $K_3(\mathbf{X})=100X_3$ N/m, $M_1(\mathbf{X})=X_4$ kg, and $M_2(\mathbf{X})=1.5X_5$ kg. The input $\mathbf{X}=\{X_1,X_2,X_3,X_4,X_5\}^T\in\mathbb{R}^5$ is an independent lognormal random vector with its mean vector $\mu_{\mathbf{X}}=\mathbf{1}\in\mathbb{R}^5$

and covariance matrix $\mathbf{\Sigma_X} = \text{diag}(v_1^2, v_2^2, v_3^2, v_4^2, v_5^2) \in \mathbb{R}^{5\times5}$, where v_i, $i = 1, \cdots, 5$, representing the coefficients of variation of X_i, are as follows: $v_1 = v_2 = 0.25$, $v_3 = v_4 = v_5 = 0.125$. There exist two real-valued random eigenvalues, $\lambda_1(\mathbf{X})$ and $\lambda_2(\mathbf{X})$, which are sorted into an ascending order.

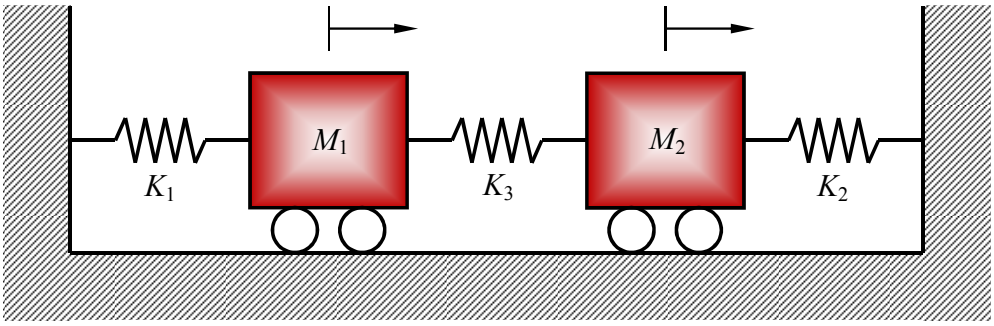

Figure 4.1: A two-degree-of-freedom, undamped, spring-mass system. (Repeat of Figure 3.3)

Since the eigenvalues are in general non-polynomial functions of input, a convergence study with respect to the truncation parameters of PDD approximations is required to calculate the probabilistic characteristics of eigensolutions accurately. The expansion coefficients were calculated by a full five-dimensional tensor product of an $m + 1$-point, univariate Gauss-Hermite quadrature formula. Figures 4.2(a) and 4.2(b) depict how the relative errors in the probabilities, $P\left[\lambda_1(\mathbf{X}) \le \lambda_{01}\right]$ and $P\left[\lambda_2(\mathbf{X}) \le \lambda_{02}\right]$, of the two random eigenvalues decay with respect to S for $m = 15$ when the thresholds $\lambda_{01} = 780$ (rad/s)^2; $\lambda_{02} = 1200$ (rad/s)^2 and $\lambda_{01} = 300$ (rad/s)^2; $\lambda_{02} = 565$ (rad/s)^2, respectively. The relative error is defined as the ratio of the ab-

solute difference in the probabilities estimated by crude MCS and embedded MCS of PDD approximations to the probability calculated by crude MCS. When $\lambda_{01} = 780$ $(\text{rad/s})^2$; $\lambda_{02} = 1200$ $(\text{rad/s})^2$, the probabilities are relatively large, for which, according to Figure 4.2(a), there is no notable difference in the errors from the A-PDD, F-PDD, and L-PDD approximations. Therefore, any of the three approximations can be a method of choice. However, when $\lambda_{01} = 300$ $(\text{rad/s})^2$; $\lambda_{02} = 565$ $(\text{rad/s})^2$, the probabilities are relatively small, in which case, the lower-variate ($S = 1$ or 2) F-PDD and L-PDD approximations, shown in Figure 4.2(b), commit smaller errors than do the corresponding A-PDD approximations. Therefore, a multiplicative PDD approximation may be preferred over an additive PDD approximation when calculating the tail distributions of a stochastic response.

4.6.3 Modal analysis of a functionally graded cantilever plate

The third example involves free vibration analysis of a $2\,\text{m} \times 1\,\text{m} \times 10\,\text{mm}$ cantilever plate, shown in Figure 4.3(a), made of a functionally graded material (FGM)[1], where silicon carbide (SiC) particles varying along the horizontal coordinate ξ are randomly dispersed in an aluminum (Al) matrix. The result is a random inhomogeneous plate, where the effective elastic modulus $E(\xi)$, effective Poisson's ratio $\nu(\xi)$, and effective mass density $\rho(\xi)$ are random fields. They depend on two principal sources of uncertainties: (1) randomness in the volume fraction of SiC particles $\phi_{\text{SiC}}(\xi)$, which

[1]Functionally graded materials are two- or multi-phase particulate composites in which material composition and microstructure vary spatially in the macroscopic length scale to meet a desired functional performance.

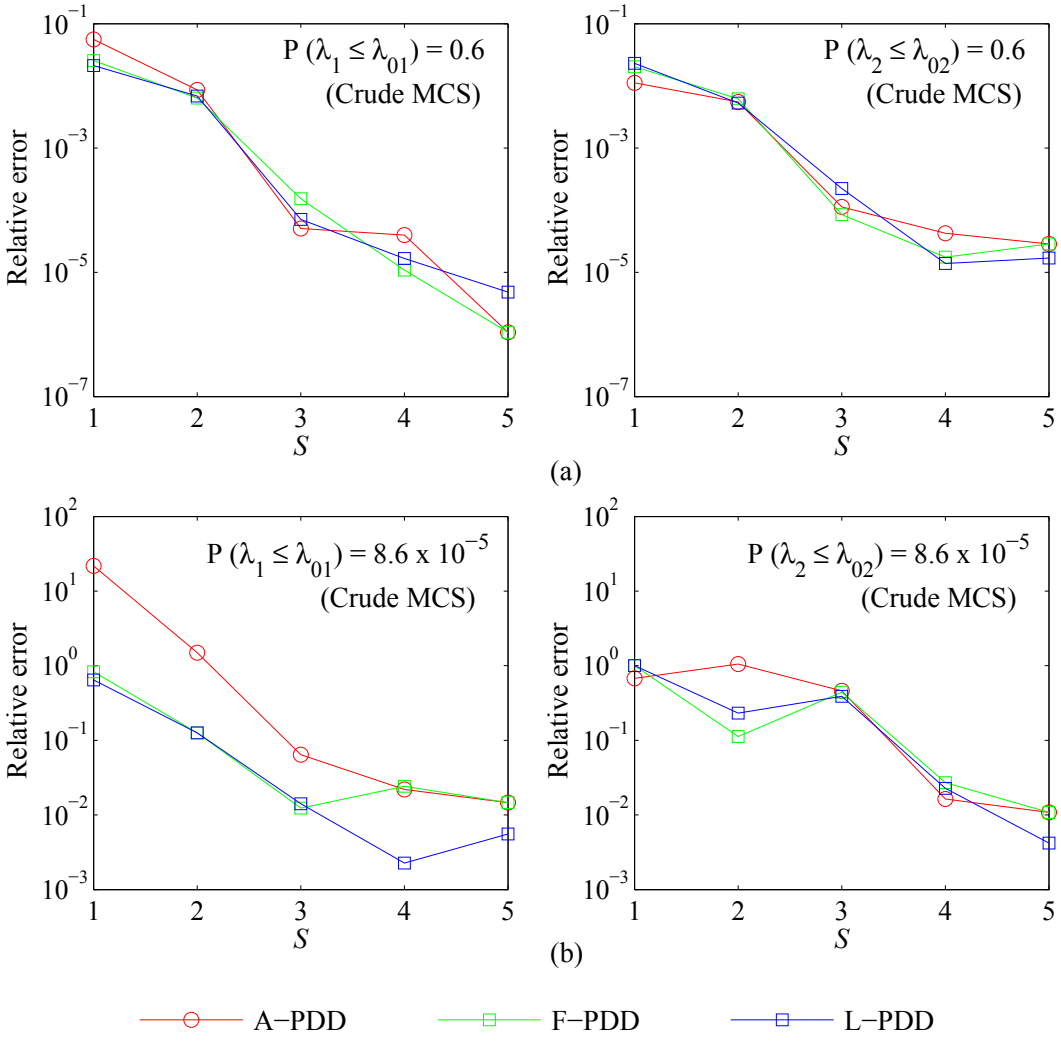

Figure 4.2: Relative errors in $P\left[\lambda_1(\mathbf{X}) \leq \lambda_{01}\right]$, $P\left[\lambda_2(\mathbf{X}) \leq \lambda_{02}\right]$ of the spring-mass system by various PDD methods: (a) $\lambda_{01} = 780$ $(\text{rad/s})^2$, $\lambda_{02} = 1200$ $(\text{rad/s})^2$; (b) $\lambda_{01} = 300$ $(\text{rad/s})^2$, $\lambda_{02} = 565$ $(\text{rad/s})^2$.

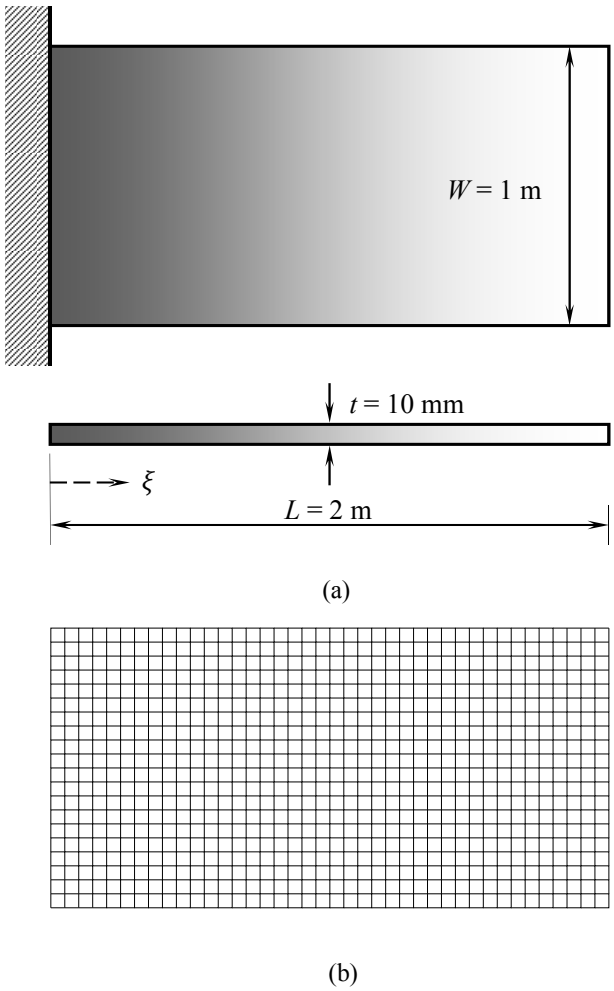

Figure 4.3: An FGM cantilever plate: (a) geometry; (b) a 20×40 FEA mesh.

varies only along ξ, and (2) randomness in constituent material properties, comprising elastic moduli E_{SiC} and E_{Al}, Poisson's ratios ν_{SiC} and ν_{Al}, and mass densities ρ_{SiC} and ρ_{Al} of SiC and Al material phases, respectively. The particle volume fraction $\phi_{\mathrm{SiC}}(\xi)$ is a one-dimensional, inhomogeneous, Beta random field with mean $\mu_{\mathrm{SiC}}(\xi) = 1 - \xi/L$, standard deviation $\sigma_{\mathrm{SiC}}(\xi) = (\xi/L)(1 - \xi/L)$, where L is the length of the plate. Assuming an appropriately bounded covariance function of $\phi_{\mathrm{SiC}}(\xi)$, the standardized volume fraction, $\tilde{\phi}_{\mathrm{SiC}}(\xi) := [\phi_{\mathrm{SiC}}(\xi) - \mu_{\mathrm{SiC}}(\xi)]/\sigma_{\mathrm{SiC}}(\xi)$, was mapped to a zero-mean, homogeneous, Gaussian image field $\alpha(\xi)$ with an exponential covariance function $\Gamma_\alpha(t) := \mathbb{E}[\alpha(\xi)\alpha(\xi + t)] = \exp(-|t|/0.125L)$ via $\tilde{\phi}_{\mathrm{SiC}}(\xi) = F^{-1}_{\mathrm{SiC}}[\Phi(\alpha(\xi))]$, where Φ is the distribution function of a standard Gaussian random variable and F_{SiC} is the marginal distribution function of $\tilde{\phi}_{\mathrm{SiC}}(\xi)$. The K-L approximation [122] was employed to discretize $\alpha(\xi)$ and hence $\phi_{\mathrm{SiC}}(\xi)$ into 28 standard Gaussian random variables. Further details of the K-L approximation are provided in Appendix B. In addition, the constituent material properties, E_{SiC}, E_{Al}, ν_{SiC}, ν_{Al}, ρ_{SiC}, ρ_{Al}, were modeled as independent lognormal random variables with their means and coefficients of variation described in Table 4.3. Therefore, a total of 34 random variables are involved in this example. Employing a rule of mixture, $E(\xi) \cong E_{\mathrm{SiC}}\phi_{\mathrm{SiC}}(\xi) + E_{\mathrm{Al}}[1 - \phi_{\mathrm{SiC}}(\xi)]$; $\nu(\xi) \cong \nu_{\mathrm{SiC}}\phi_{\mathrm{SiC}}(\xi) + \nu_{\mathrm{Al}}[1 - \phi_{\mathrm{SiC}}(\xi)]$; and $\rho(\xi) \cong \rho_{\mathrm{SiC}}\phi_{\mathrm{SiC}}(\xi) + \rho_{\mathrm{Al}}[1 - \phi_{\mathrm{SiC}}(\xi)]$. Using these spatially variant effective properties, a 20×40 mesh consisting of 800 eight-noded, second-order shell elements, shown in Figure 4.3(b), was constructed for finite-element analysis (FEA), to determine the natural frequencies of the FGM plate. No damping was included. A Lanczos algorithm [123] was employed for calculating the

eigenvalues.

Table 4.3: Statistical material properties of constituents in SiC-Al FGM.

Material properties[(a)]	Mean	Coefficient of variation, %
E_{SiC}, GPa	419.2	15
ν_{SiC}	0.19	5
ρ_{SiC}, kg/m^3	3210	15
E_{Al}, GPa	69.7	15
ν_{Al}	0.34	5
ρ_{Al}, kg/m^3	2520	15

[(a)] E_{SiC} = elastic modulus of SiC, ν_{SiC} = Poisson's ratio of SiC, ρ_{SiC} = mass density of SiC, E_{Al} = elastic modulus of Al, ν_{Al} = Poisson's ratio of Al, ρ_{Al} = mass density of Al.

The probability distributions of natural frequencies of the FGM plate were evaluated using the univariate, fourth-order A-PDD, F-PDD, and L-PDD approximations, including crude MCS. The expansion coefficients of the PDD approximations were estimated using dimension-reduction integration with $R = S = 1$ and $n = 5$. Figure 4.4 presents the marginal probability distributions $F_i(\omega_i) := P[\Omega_i \leq \omega_i]$ of the first six natural frequencies Ω_i, $i = 1, \cdots, 6$, where the PDD solutions were obtained from embedded MCS. The plots are made over a semi-logarithmic scale to delineate the distributions in the tail regions. For all six frequencies, the probability distributions obtained from the F-PDD and L-PDD approximations are much closer to the crude Monte Carlo results compared with those obtained from the A-PDD approximation. Each PDD approximation requires only 127 FEA, which is significantly lower than the 50,000 FEA employed by crude MCS, to generate the small probabilities in

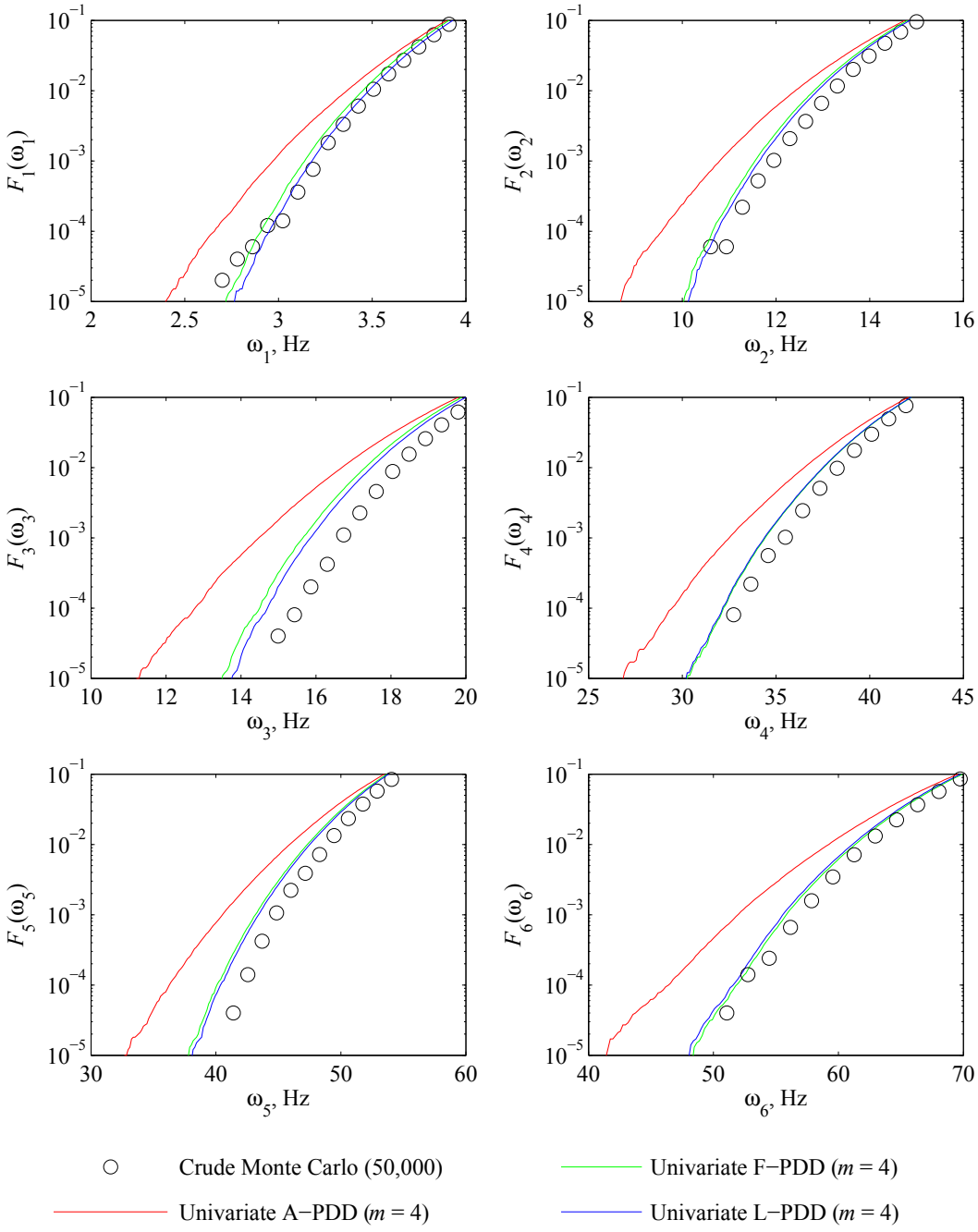

Figure 4.4: Marginal probability distributions of the first six natural frequencies of the FGM plate by various PDD approximations and crude MCS.

Figure 4.4.

Figure 4.5 displays the joint probability density function $f_{12}(\omega_1, \omega_2)$ of the first two natural frequencies Ω_1 and Ω_2 obtained by crude MCS and the univariate, fourth-order A-PDD, L-PDD, and F-PDD approximations. Although visually

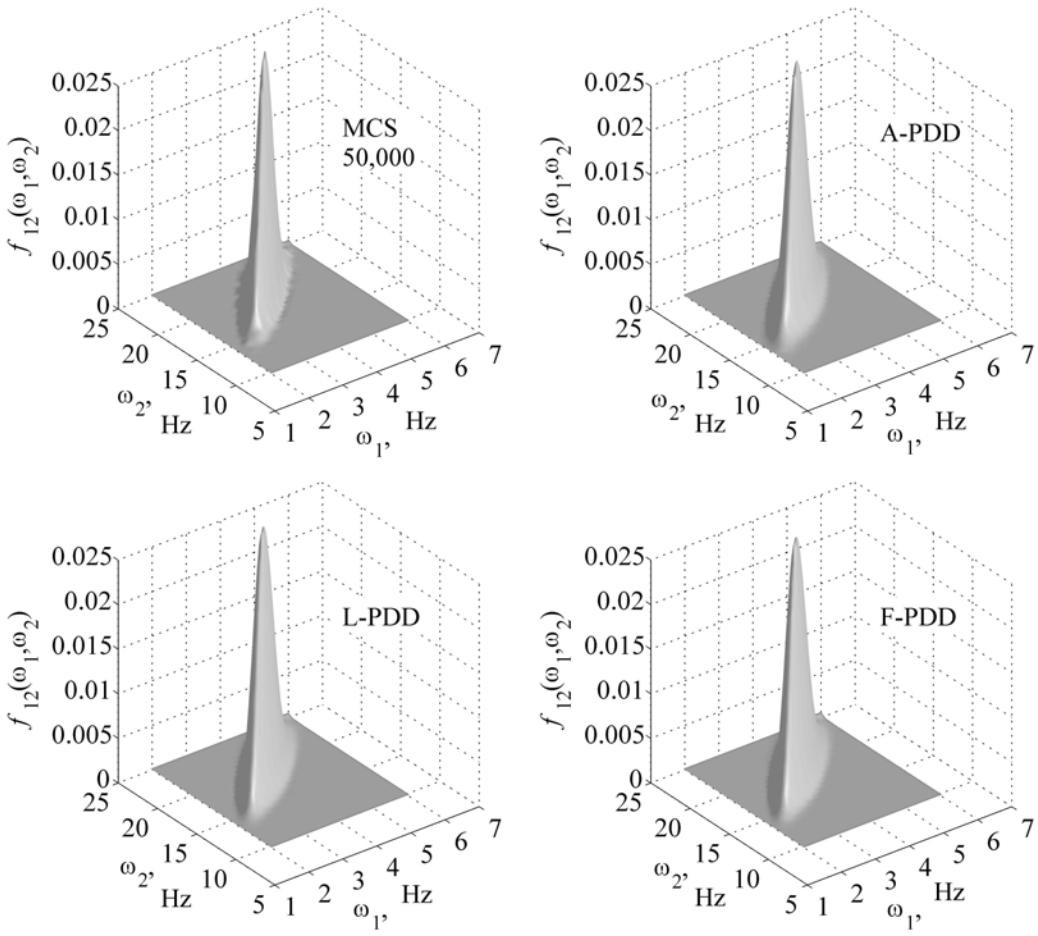

Figure 4.5: Joint probability density function of the first and second natural frequencies of the FGM plate by various PDD approximations and crude MCS.

comparing these three-dimensional plots is not simple, the joint distributions from

all three PDD approximations and the crude Monte Carlo method seem to match reasonably well. Indeed, the contours evaluated at a relatively high level, for instance $f_{12} = 0.005$, and exhibited in Figure 4.6(a), confirm a fairly good agreement among all four distributions. However, when examined at a relatively low level, for instance $f_{12} = 0.0005$, the contours in Figure 4.6(b) reveal the F-PDD or L-PDD approximation to be more accurate than the A-PDD approximation. These findings

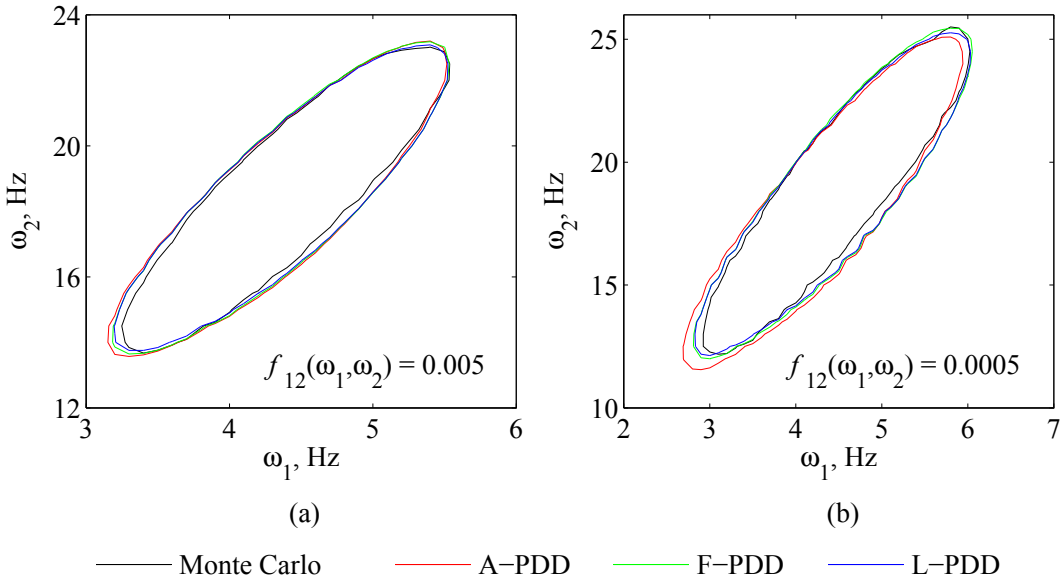

Figure 4.6: Contours of the joint density function of the first and second natural frequencies of the FGM plate by various PDD approximations and crude MCS: (a) $f_{12} = 0.005$; (b) $f_{12} = 0.0005$.

are consistent with the marginal distributions of natural frequencies discussed in the preceding section. It appears that a lower-variate multiplicative PDD approximation, in this case a univariate F-PDD or L-PDD approximation, may provide more accu-

rate probabilistic characteristics of a stochastic response than a univariate additive PDD approximation. This is because a univariate multiplicative PDD approximation subsumes some interactive effects of input variables, as alluded to in Remark 4.4.

4.7 Application: An SUV Body-in-White

This section illustrates the effectiveness of the proposed multiplicative PDD methods in solving a large-scale practical engineering problem. The application involves predicting the dynamic behavior of a sport utility vehicle (SUV) in terms of the statistical properties of mode shapes and frequency response functions. Figure 4.7(a) presents a computer-aided design (CAD) model of an SUV body-in-white (BIW), referring to the automotive design stage where a car body's sheet metal components have been welded together, before moving parts, motor, chassis sub-assemblies, and trim have been added. The BIW consists of the bare metal shell of the frame body, including fixed windshields. A finite-element mesh of the model, comprising 127,213 linear shell elements and 794,292 active degrees of freedom, is displayed in Figure 4.7(b). Portrayed in Figure 4.7(a), the CAD model contains 17 distinct materials having random properties, including 17 Young's moduli and 17 mass densities. In addition, six of these materials, which are used in ceiling, floor, hood, and side body of the vehicle, have random structural damping factors. In aggregate, there exist 40 random variables X_i, $i = 1, \cdots, 40$, as follows: X_1 to X_{17} = Young's moduli of materials 1 to 17; X_{18} to X_{34} = mass densities of materials 1 to 17; and X_{35} to X_{40} = damping factors of materials 1 to 6. Their means, $\mu_i := \mathbb{E}[X_i], i = 1, \ldots, 40$, are listed

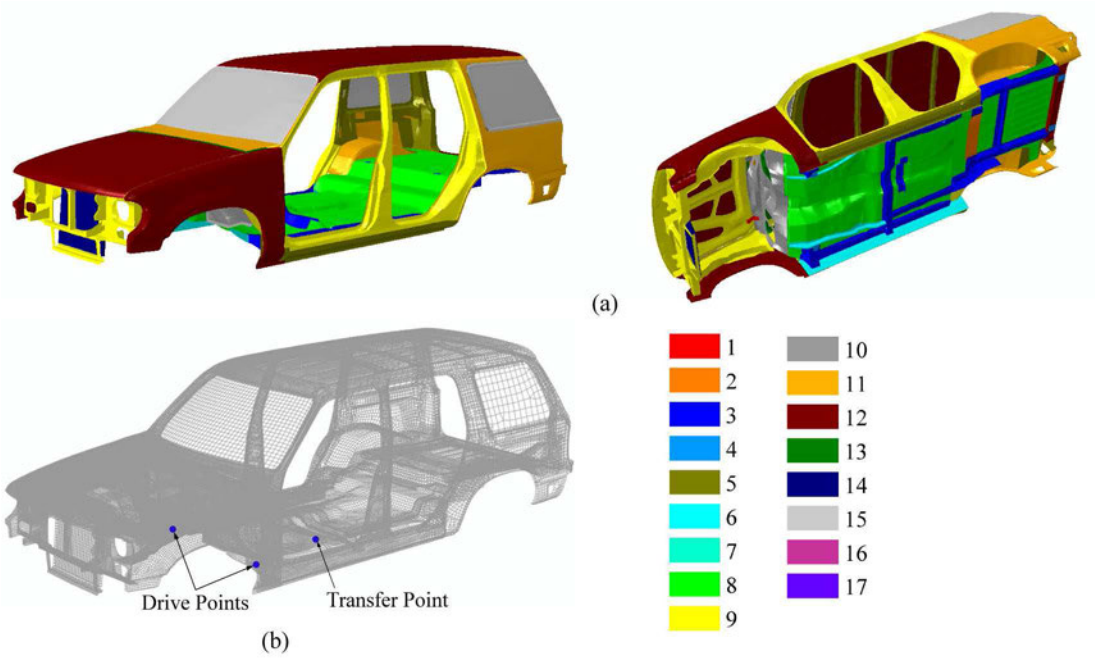

Figure 4.7: An SUV BIW: (a) a CAD model; (b) an FEA mesh.

in Table 4.4. Each variable follows an independent, truncated Gaussian distribution with lower limit $a_i = 0.55\mu_i$, upper limit $b_i = 1.45\mu_i$, and coefficient of variation v_i= 0.15. The deterministic Poisson's ratios are as follows: 0.28 for materials 1 to 13; 0.2 for materials 14 and 15; and 0.3 for materials 16 and 17.

4.7.1 Steady-state dynamic analysis

A mode-based steady-state dynamic analysis consists of two steps: an eigensolution extraction, followed by a frequency response calculation. For obtaining eigensolutions, the upper bound of the frequency extraction range was chosen as 300 Hz, and the frequency response functions were computed up to 150 Hz. The AMS method [124] embedded in Abaqus (Version 6.11) [109] was employed for extracting natural frequen-

Table 4.4: Mean values of the random input variables for an SUV BIW.

Material	Young's modulus, GPa	Mass density, kg/m^3	Damping factor, %
1	207	9500	1
2	207	9500	1
3	207	8100	1
4	207	29,260	1
5	207	29,260	1
6	207	37,120	1
7	207	9500	–[(a)]
8	207	8100	–[(a)]
9	207	8100	–[(a)]
10	207	29,260	–[(a)]
11	207	30,930	–[(a)]
12	207	37,120	–[(a)]
13	207	52,010	–[(a)]
14	69	2700	–[(a)]
15	69	2700	–[(a)]
16	20	1189	–[(a)]
17	200	1189	–[(a)]

[(a)] The damping factors for materials 7-17 are equal to zero (deterministic).

cies and mode shapes. The AMS eigensolver approximates global eigenmodes below the global cutoff frequency of 300 Hz, and the frequency response solutions below 150 Hz were calculated at 1 Hz increments. Since the BIW model is not constrained, there exist six rigid body modes.

For the steady-state dynamic analysis, the rolling motion of the vehicle was simulated by applying two harmonic loads with concentrated vertical force of unit amplitude at the nodes, called drive points, located at the two pivot points on the bottom of the vehicle floor. The frequency response functions were calculated at a node, called the transfer point, under the driver's seat. The drive and transfer points are marked in Figure 4.7(b).

Due to the uncertainty in material properties, the eigensolutions or frequency response functions are stochastic. The univariate, second-order multiplicative PDD approximations were employed to find their second-moment characteristics and various response probabilities. The associated expansion coefficients of PDD were estimated by crude MCS with 500 samples. The sample size for the embedded MCS of the PDD approximations varies from 500 to 10^6, depending on the response desired.

4.7.2 Results

4.7.2.1 Moments of mode shapes

The univariate, second-order F-PDD and L-PDD approximations were employed to calculate the second-moment statistics of each nodal displacement component of an eigenvector describing the associated mode shape of the BIW structure. All input random variables were transformed into standard Gaussian random variables, permitting the use of Hermite orthonormal polynomials as basis functions. For F-PDD, the statistics were calculated directly using Equations (4.37) and (4.38). However, for L-PDD, the statistics were estimated from the embedded MCS of Equation (4.47), sidestepping the need to evaluate the integrals in Equations (4.48) and (4.49) for each displacement component at all nodes. When a displacement y is non-positive, the mean plus ten times the standard deviation of y, estimated from crude MCS used in obtaining the coefficients, was added, resulting in a positive displacement required by L-PDD. No conditioning was needed or performed for F-PDD. These simple modifications aid in calculating the means and variances of displace-

ment components at all nodes. Based on these statistics, the $\mathcal{L}_2$-norms (square root of sum of squares) of the mean and variance of a nodal displacement were calculated. Figures 4.8(a) and 4.8(b) present contour plots of the $\mathcal{L}_2$-norms of the means and variances, respectively, of an arbitrarily selected 21st mode shape, calculated using the F-PDD and L-PDD approximations. Both approximations yield reasonably close

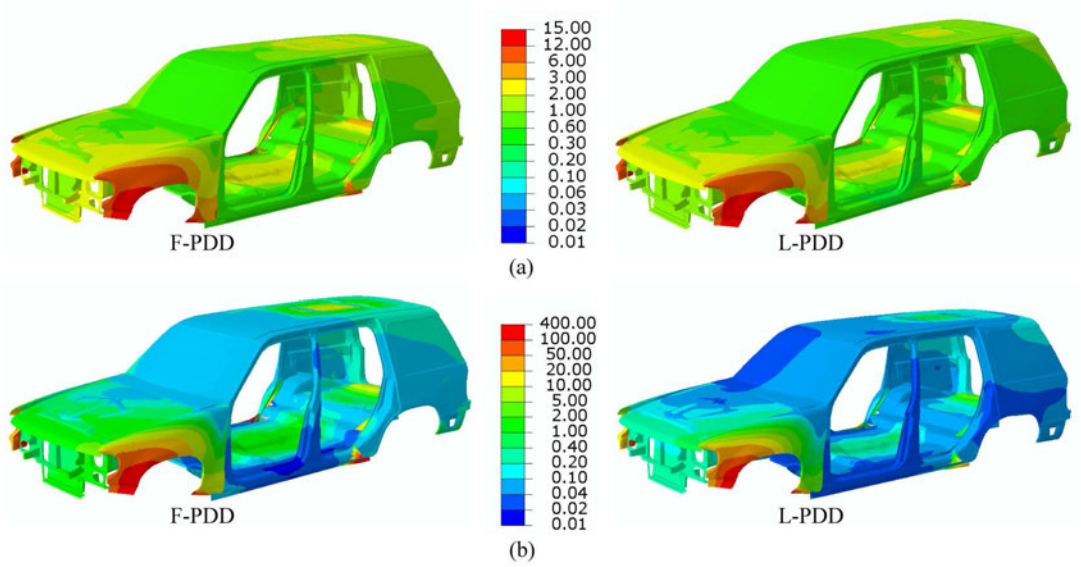

Figure 4.8: Contour plots of the $\mathcal{L}_2$-norm of 21st mode shape of an SUV BIW by two multiplicative PDD approximations: (a) mean; (b) variance.

statistical moments, including the variances of the mode shape. Similar results can be generated for other mode shapes if desired.

4.7.2.2 Percentile functions of receptance, mobility, and inertance

For mode-based steady-state dynamic analysis, three types of frequency response functions were examined: receptance, mobility, and inertance. They are ap-

proximated by

$$u_{p,d_1d_2t}(\omega) \simeq (i\omega)^p \sum_{k=1}^{K} \frac{[\phi_{k,d_1} + \phi_{k,d_2}]\,\phi_{k,t}}{[\Omega_k^2\,(1 + is_k) - \omega^2]}, \tag{4.53}$$

where $i = \sqrt{-1}$, K is the number of eigenmodes retained, ϕ_{k,d_1} and ϕ_{k,d_2} are the two drive point vertical components of the k^{th} eigenmode, $\phi_{k,t}$ is the transfer point vertical component of the k^{th} eigenmode, Ω_k is the k^{th} eigenfrequency, s_k is its corresponding structural damping factor, and ω is the excitation frequency over which the frequency response function is desired. The exponent p corresponds to the type of frequency response calculated: $p = 0$ for receptance, $p = 1$ for mobility, and $p = 2$ for inertance. All three frequency response functions are commonly used in the automotive industry to evaluate the dynamic performance of vehicle designs. For random input, it is insightful to study the probabilities of receptance and mobility for a vehicle subjected to a range of excitation frequency. When a frequency response function y was positive, but very close to zero, it was multiplied by a factor of $10^{-\log y}$, creating a well-behaved function in L-PDD. No such conditioning was required in F-PDD. Figures 4.9(a), 4.9(b), and 4.9(c) show various percentiles of real parts of receptance, mobility, and inertance under the driver's seat, respectively, obtained from the two univariate multiplicative PDD approximations. The respective results for imaginary parts are depicted in Figures 4.10(a), 4.10(b), and 4.10(c). In both sets of figures, the percentiles were calculated from 10^4 embedded MCS of each PDD approximation at an increment of 1 Hz for the excitation frequency range of 1 Hz to 150 Hz. Again, both the F-PDD and L-PDD approximations produce similar results. Therefore, either of the multiplicative PDD methods can be used for stochastic dynamic analysis.

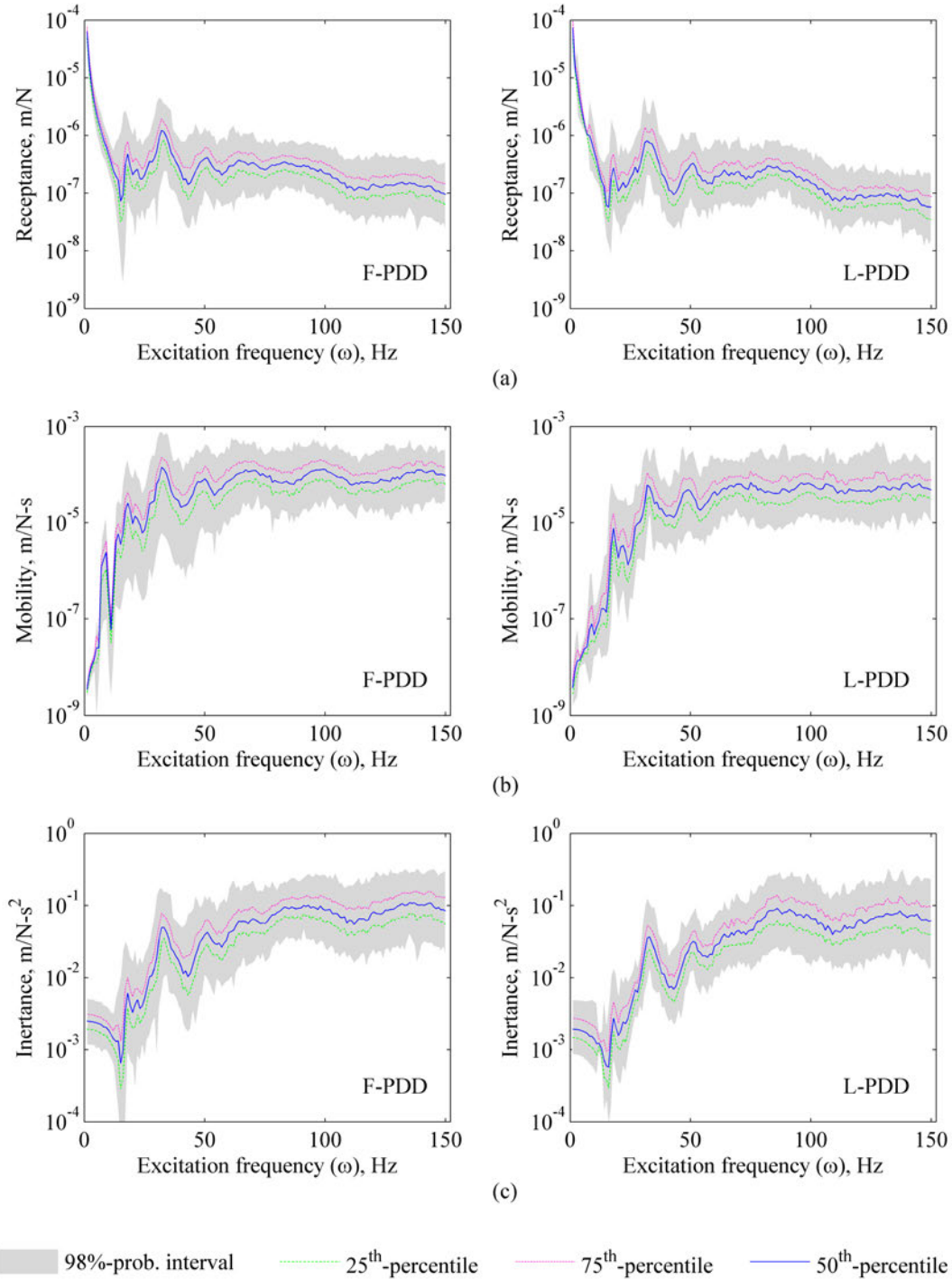

Figure 4.9: Percentiles of frequency response functions at the driver's seat of an SUV BIW by two multiplicative PDD approximations: (a) receptance; (b) mobility; (c) inertance.

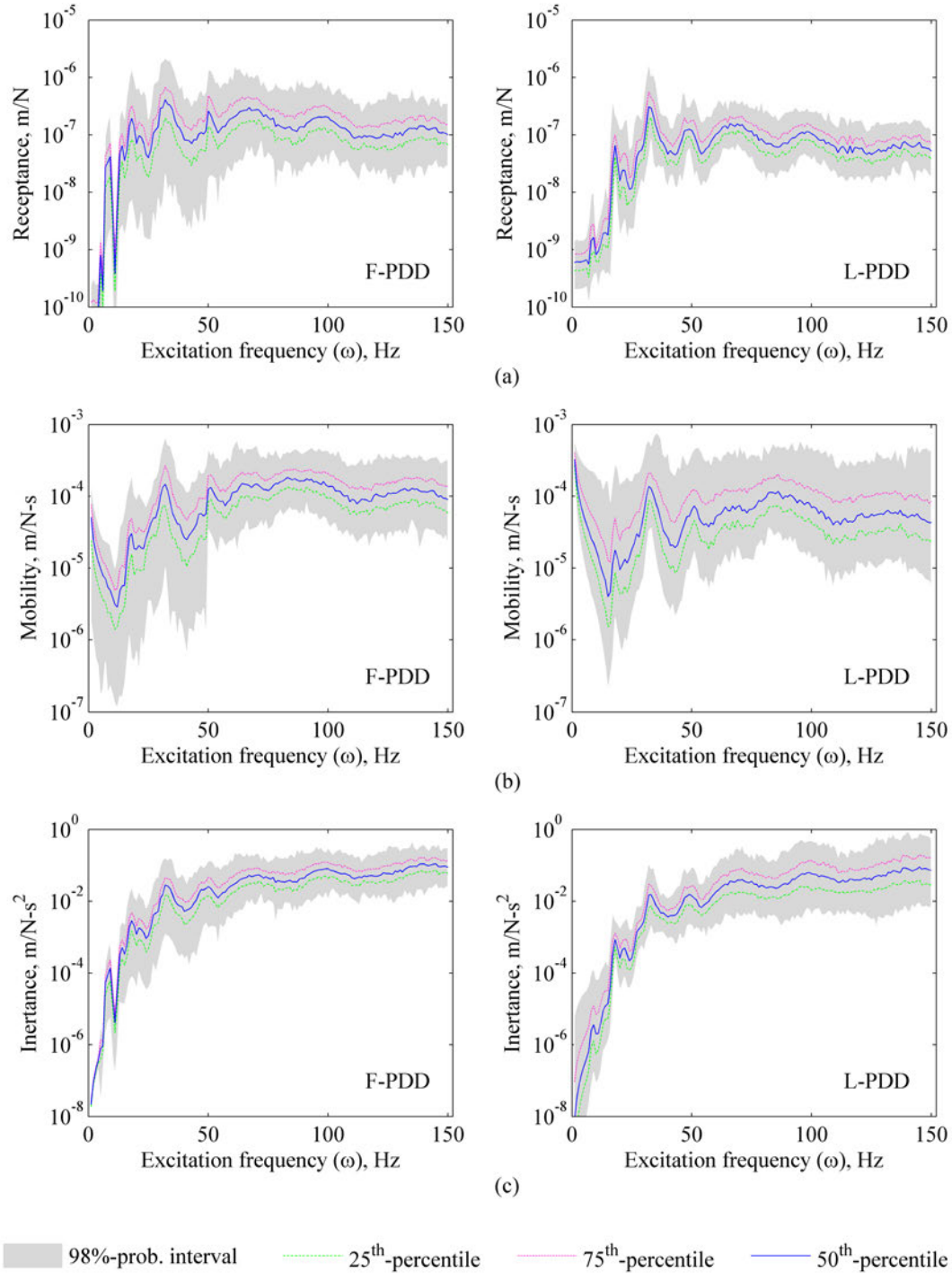

Figure 4.10: Percentiles of imaginary parts of frequency response functions at the driver's seat of an SUV BIW by two multiplicative PDD approximations: (a) receptance; (b) mobility; (c) inertance.

4.7.2.3 Acceleration probabilities

Finally, Table 4.5 presents the probabilities of a weighted root mean square (RMS) value of the vertical component of the acceleration under the driver's seat lying within the following intervals: $[0, 0.315]$ (not uncomfortable), $[0.315, 0.63]$ (a little uncomfortable), $[0.5, 1]$ (fairly uncomfortable), $[0.8, 1.6]$ (uncomfortable), $[1.25, 2.5]$ (very uncomfortable), and $[2, \infty)$ (extremely uncomfortable). These intervals, developed and calibrated by the International Standard ISO 2631 [1], define acceptable values of accelerations inside a vehicle for various levels of passenger comfort. The higher the interval endpoints, the harsher the level of passenger experience. The weighted RMS acceleration, obtained for an assumed applied load of 1000 N, was calculated from $[(1/150)\sum_{j=1}^{150}\{1000\alpha_j u_{2,d_1d_2t}(\omega_j)\}^2]^{1/2}$, where α_j and ω_j are the jth weight and excitation frequency, respectively, described in Appendix C [1].

Table 4.5: Probability of acceleration under the driver's seat of an SUV BIW.

	Interval of acceptable accelerations $(\mathrm{m/s^2})^{(a)}$					
Method	$[0, 0.315]$ $(\times 10^{-1})$	$[0.315, 0.63]$ $(\times 10^{-1})$	$[0.5, 1]$ $(\times 10^{-2})$	$[0.8, 1.6]$ $(\times 10^{-3})$	$[1.25, 2.5]$ $(\times 10^{-3})$	$[2, \infty)$ $(\times 10^{-4})$
A-PDD	7.4	2.6	0.3	0	0	0
F-PDD	6.9	2.7	3.6	3.2	0.7	4.1
L-PDD	8.4	1.1	3.4	8.8	2.1	4.3

(a) From International Standard ISO 2631 [1].

The probabilities were calculated by the univariate, second-order A-PDD, F-PDD, and L-PDD approximations and 10^6 embedded MCS. The acceleration prob-

abilities in Table 4.5 predicted by both versions of the multiplicative PDD approximations have the same order and are reasonably close to each other, considering their low values. In contrast, the additive PDD approximation either significantly underpredicts or fails altogether in calculating the probabilities for all intervals examined. Therefore, the multiplicative PDD methods provide stochastic solutions that are unattainable by the additive PDD method, at least in this problem. It is important to emphasize that the probabilistic characteristics of eigensolutions or frequency response functions reported here were generated using only 500 FEA, representing the computational effort by the multiplicative PDD methods. Obtaining percentile functions or acceleration probabilities employing 10^4 or 10^6 crude MCS would be computationally prohibitive in today's desktop computing environment, illustrating the efficacy of the PDD methods. Furthermore, the methods developed are non-intrusive and can be easily adapted to solving complex stochastic problems requiring external legacy codes.

4.8 Conclusions

Two new multiplicative variants of PDD, namely, factorized PDD and logarithmic PDD, were developed for uncertainty quantification of high-dimensional complex systems. They are based on hierarchical, multiplicative decompositions of a multivariate function in terms of lower-variate component functions, Fourier-polynomial expansions of lower-variate component functions by measure-consistent orthonormal polynomial bases, and a dimension-reduction integration or sampling technique for

estimating the expansion coefficients. Compared with the existing, additive PDD, the factorized and logarithmic PDDs exploit the multiplicative dimensional hierarchy of a stochastic response when it exists. Since both PDDs are rooted in the ADD, their existence and uniqueness are guaranteed for a square integrable function. A theorem, proven herein, reveals the relationship between all component functions of factorized PDD and ADD, so far available only for the univariate and bivariate component functions. Similar to the additive PDD, truncations of a multiplicative PDD lead to a convergent sequence of lower-dimensional estimates of the probabilistic characteristics of a general stochastic response. Using the properties of orthogonal polynomials, explicit formulae were derived for calculating the response statistics by the univariate factorized PDD and univariate logarithmic PDD approximations in terms of the expansion coefficients. Unlike the univariate additive PDD approximation, which captures only the main effects of input variables, a univariate truncation of multiplicative PDD includes some effects of interactions among input variables.

The additive and multiplicative PDD methods were employed to calculate the second-moment properties and tail probability distributions in three numerical problems, where the output functions are either simple mathematical functions or eigenvalues of dynamic systems, including natural frequencies of an FGM plate. When a function is purely multiplicative, the factorized or logarithmic PDD requires at most univariate approximation, resulting in a much faster convergence than the additive PDD approximation. However, the relative superiority of one multiplicative PDD approximation over the other depends on the nature of the function and whether a

logarithmic transformation enhances or reduces the nonlinearity of the function. A similar trend was observed when calculating small probabilities of eigenvalues of a linear oscillator, where the multiplicative PDDs commit lower errors than does the additive PDD. Given the same computational effort of univariate approximations, both variants of the multiplicative PDD yield more accurate tail probabilistic characteristics of natural frequencies of an FGM plate than the additive PDD. Finally, a successful evaluation of random eigensolutions of a SUV represents a significant advance in the ability of the new methods in solving practical engineering problems.

Neither variant of the multiplicative PDD approximation encounters additional cost to that required by the additive PDD approximation. Indeed, the computational complexities of all three variants of the PDD approximation are identical and polynomial, as opposed to exponential, with respect to the number of input variables. Therefore, a PDD approximation, whether additive or multiplicative, mitigates the curse of dimensionality to some degree.

CHAPTER 5
HYBRID POLYNOMIAL DIMENSIONAL DECOMPOSITION

5.1 Introduction

When a stochastic response is neither dominantly additive nor dominantly multiplicative in its structure, then a mixed approach comprising the best combination of additive and multiplicative PDD is required for estimating the probabilistic characteristics of the response. The major limitation of the additive PDD method is that it can not be successfully applied to responses that lack an additive structure. This limitation of additive PDD was the motivation for developing the multiplicative PDD methods earlier in this work. It can be argued that the multiplicative PDD methods also face a limitation similar to that of the additive PDD: that it cannot be successfully applied for solving responses that lack a multiplicative structure. The corresponding limitations of both additive and multiplicative PDD methods are the motivation for developing a novel hybrid PDD method. Not losing sight of the objective of developing highly efficient computational methods for solving high-dimensional REPs, a hybrid PDD method is developed that is based on a linear combination of additive PDD and a variant of multiplicative PDD: factorized PDD.

This chapter presents a new hybrid PDD method for solving high-dimensional stochastic problems. The method is presented in Section 5.2 along with the second moment properties of the resultant approximation. Section 5.3 presents the univariate hybrid PDD. The methods for calculating the hybrid model parameters are also

discussed. Section 5.4 describes the quasi MCS method for calculating the PDD expansion coefficients. Section 5.5 presents two numerical examples illustrating the accuracy, efficiency, and convergence properties of the hybrid PDD method and compares results with those obtained from additive and factorized PDD methods. In Section 5.6 a large, complex engineering problem, entailing coupled acoustic-structural analysis of a pickup truck, is solved using the hybrid PDD method. Finally, conclusions are drawn in Section 5.7.

5.2 Proposed Hybrid PDD

Two new hybrid approximations, which are based on a linear mixture of the additive PDD and factorized PDD described in Sections 4.3 and 4.4.1, respectively, are proposed.

5.2.1 Hybrid approximations

Given S-variate, mth-order additive PDD and factorized PDD approximations $\tilde{y}_{S,m}(\mathbf{X})$ and $\hat{y}_{S,m}(\mathbf{X})$, let

$$\bar{y}_{S,m}(\mathbf{X};\alpha_{S,m},\beta_{S,m},\ldots) := \begin{cases} y_{\emptyset} & \text{if } S=0, \\ h\left(\tilde{y}_{S,m}(\mathbf{X}),\hat{y}_{S,m}(\mathbf{X});\alpha_{S,m},\beta_{S,m},\ldots\right) & \text{if } 1\le S<N, \\ y(\mathbf{X}) & \text{if } S=N,\ m\to\infty, \end{cases} \tag{5.1}$$

define a general, S-variate, mth-order hybrid PDD approximation of $y(\boldsymbol{X})$, where h is a chosen linear model function such that $\mathbb{E}\left[\bar{y}_{S,m}(\mathbf{X};\alpha_{S,m},\beta_{S,m},\ldots)\right] = y_{\emptyset}$ and $\alpha_{S,m}$,

$\beta_{S,m}, \ldots$ are the associated model parameters. Define the *zero*-mean functions

$$w(\mathbf{X}) := y(\mathbf{X}) - y_{\emptyset}, \tag{5.2}$$

$$\tilde{w}_{S,m}(\mathbf{X}) := \tilde{y}_{S,m}(\mathbf{X}) - y_{\emptyset}, \tag{5.3}$$

$$\hat{w}_{S,m}(\mathbf{X}) := \hat{y}_{S,m}(\mathbf{X}) - \mathbb{E}\left[\hat{y}_{S,m}(\mathbf{X})\right], \tag{5.4}$$

and

$$\bar{w}_{S,m}(\mathbf{X}; \alpha_{S,m}, \beta_{S,m}, \ldots) := \bar{y}_{S,m}(\mathbf{X}; \alpha_{S,m}, \beta_{S,m}, \ldots) - y_{\emptyset}, \tag{5.5}$$

that will be used throughout this section. Theorem 5.1 and Corollary 5.2 describe two optimal hybrid approximations $\bar{y}_{S,m}(\mathbf{X}; \alpha_{S,m}, \beta_{S,m})$ and $\bar{y}'_{S,m}\left(\mathbf{X}; \alpha'_{S,m}, \beta'_{S,m}\right)$ for $1 \leq S < N$, $m < \infty$, both producing the exact mean $y_{\emptyset}$. The two hybrid approximations have their *zero*-mean counterparts defined as

$$\bar{w}_{S,m}(\mathbf{X}; \alpha_{S,m}, \beta_{S,m}) := \bar{y}_{S,m}(\mathbf{X}; \alpha_{S,m}, \beta_{S,m}) - y_{\emptyset} \tag{5.6}$$

and

$$\bar{w}'_{S,m}\left(\mathbf{X}; \alpha'_{S,m}\right) := \bar{y}'_{S,m}\left(\mathbf{X}; \alpha'_{S,m}\right) - y_{\emptyset}. \tag{5.7}$$

Theorem 5.1: *Given integers* $1 \leq S < N < \infty$ *and* $1 \leq m < \infty$, *let* $\tilde{w}_{S,m}(\mathbf{X})$ *and* $\hat{w}_{S,m}(\mathbf{X})$ *represent zero-mean, S-variate, mth-order additive PDD and factorized PDD approximations with variances* $\tilde{\sigma}^2_{S,m} := \mathbb{E}\left[\tilde{y}_{S,m}(\mathbf{X}) - y_{\emptyset}\right]^2 = \mathbb{E}\left[\tilde{w}^2_{S,m}(\mathbf{X})\right]$ *and* $\hat{\sigma}^2_{S,m} := \mathbb{E}\left[\hat{y}_{S,m}(\mathbf{X}) - y_{\emptyset}\right]^2 = \mathbb{E}\left[\hat{w}^2_{S,m}(\mathbf{X})\right]$, *respectively, of a real-valued, zero-mean, square-integrable function* $w(\mathbf{X})$. *Then there exists an optimal, linear, S-variate, mth-order hybrid PDD approximation*

$$\bar{w}_{S,m}(\mathbf{X}; \alpha_{S,m}, \beta_{S,m}) = \alpha_{S,m}\tilde{w}_{S,m}(\mathbf{X}) + \beta_{S,m}\hat{w}_{S,m}(\mathbf{X}) \tag{5.8}$$

of $w(\mathbf{X})$*, where*

$$\alpha_{S,m} = \frac{\hat{\sigma}^2_{S,m}\mathbb{E}\left[w(\mathbf{X})\,\tilde{w}_{S,m}(\mathbf{X})\right] - \mathbb{E}\left[\tilde{w}_{S,m}(\mathbf{X})\,\hat{w}_{S,m}(\mathbf{X})\right]\mathbb{E}\left[w(\mathbf{X})\,\hat{w}_{S,m}(\mathbf{X})\right]}{\tilde{\sigma}^2_{S,m}\hat{\sigma}^2_{S,m} - \left(\mathbb{E}\left[\tilde{w}_{S,m}(\mathbf{X})\,\hat{w}_{S,m}(\mathbf{X})\right]\right)^2}, \tag{5.9}$$

$$\beta_{S,m} = \frac{\tilde{\sigma}^2_{S,m}\mathbb{E}\left[w(\mathbf{X})\,\hat{w}_{S,m}(\mathbf{X})\right] - \mathbb{E}\left[\tilde{w}_{S,m}(\mathbf{X})\,\hat{w}_{S,m}(\mathbf{X})\right]\mathbb{E}\left[w(\mathbf{X})\,\tilde{w}_{S,m}(\mathbf{X})\right]}{\tilde{\sigma}^2_{S,m}\hat{\sigma}^2_{S,m} - \left(\mathbb{E}\left[\tilde{w}_{S,m}(\mathbf{X})\,\hat{w}_{S,m}(\mathbf{X})\right]\right)^2}. \tag{5.10}$$

Proof. For a square-integrable function $w(\mathbf{X})$, define a second-moment error

$$\bar{e}_{S,m} := \mathbb{E}\left[w(\mathbf{X}) - \bar{w}_{S,m}(\mathbf{X};\alpha_{S,m},\beta_{S,m})\right]^2 \tag{5.11}$$

committed by its S-variate, mth-order hybrid PDD approximation $\bar{w}_{S,m}(\mathbf{X};\alpha_{S,m},\beta_{S,m})$. For $\bar{e}_{S,m}$ to be minimum, set

$$\begin{aligned} \frac{\partial \bar{e}_{S,m}}{\partial \alpha_{S,m}} &= 0, \\ \frac{\partial \bar{e}_{S,m}}{\partial \beta_{S,m}} &= 0. \end{aligned} \tag{5.12}$$

Exchanging the orders of differential and expectation operators, and substituting the expression of $\bar{w}_{S,m}(\mathbf{X};\alpha_{S,m},\beta_{S,m})$ from Equation (5.8) yields

$$\begin{aligned} \alpha_{S,m}\mathbb{E}\left[\tilde{w}^2_{S,m}(\mathbf{X})\right] + \beta_{S,m}\mathbb{E}\left[\tilde{w}_{S,m}(\mathbf{X})\,\hat{w}_{S,m}(\mathbf{X})\right] &= \mathbb{E}\left[w(\mathbf{X})\,\tilde{w}_{S,m}(\mathbf{X})\right], \\ \alpha_{S,m}\mathbb{E}\left[\tilde{w}_{S,m}(\mathbf{X})\,\hat{w}_{S,m}(\mathbf{X})\right] + \beta_{S,m}\mathbb{E}\left[\hat{w}^2_{S,m}(\mathbf{X})\right] &= \mathbb{E}\left[w(\mathbf{X})\,\hat{w}_{S,m}(\mathbf{X})\right]. \end{aligned} \tag{5.13}$$

Noting $\tilde{\sigma}^2_{S,m} = \mathbb{E}\left[\tilde{w}^2_{S,m}(\mathbf{X})\right]$, and $\hat{\sigma}^2_{S,m} = \mathbb{E}\left[\hat{w}^2_{S,m}(\mathbf{X})\right]$, the solution Equations (5.13) produces the expressions of $\alpha_{S,m}$ and $\beta_{S,m}$ as in Equations (5.9) and (5.10), proving the theorem. □

Corollary 5.2: *Constraining the sum of two model parameters to be unity in Equation* (5.8) *through* (5.13) *creates another optimal, linear, S-variate hybrid approximation*

$$\bar{w}'_{S,m}\left(\mathbf{X};\alpha'_{S,m}\right) = \alpha'_{S,m}\tilde{w}_{S,m}(\mathbf{X}) + \left(1-\alpha'_{S,m}\right)\hat{w}_{S,m}(\mathbf{X}) \tag{5.14}$$

of $w(\mathbf{X})$, $1 \leq S < N < \infty$, $m < \infty$, *where the optimal model parameter*

$$\alpha'_{S,m} = \frac{\mathbb{E}\left[\left\{w(\mathbf{X}) - \hat{w}_{S,m}(\mathbf{X})\right\}\left\{\tilde{w}_{S,m}(\mathbf{X}) - \hat{w}_{S,m}(\mathbf{X})\right\}\right]}{\mathbb{E}\left[\tilde{w}_{S,m}(\mathbf{X}) - \hat{w}_{S,m}(\mathbf{X})\right]^2}. \tag{5.15}$$

Proof. For a square-integrable function $w(\mathbf{X})$, define another second-moment error

$$\bar{e}'_{S,m} := \mathbb{E}\left[w(\mathbf{X}) - \bar{w}'_{S,m}\left(\mathbf{X}; \alpha'_{S,m}\right)\right]^2 \tag{5.16}$$

owing to its S-variate, mth-order hybrid PDD approximation $\bar{w}'_{S,m}\left(\mathbf{X}; \alpha'_{S,m}\right)$. For $\bar{e}'_{S,m}$ to be minimum, set

$$\frac{\partial \bar{e}'_{S,m}}{\partial \alpha'_{S,m}} = 0. \tag{5.17}$$

Again, swapping the orders of differential and expectation operators, and substituting the expression of $\bar{w}'_{S,m}\left(\mathbf{X}; \alpha'_{S,m}\right)$ from Equation (5.14) results in the expression of $\alpha'_{S,m}$ as in Equation (5.15), proving the corollary. □

Remark 5.1: The linear hybrid PDD approximations, $\bar{w}_{S,m}(\mathbf{X}; \alpha_{S,m}, \beta_{S,m})$ and $\bar{w}'_{S,m}\left(\mathbf{X}; \alpha'_{S,m}\right)$, for a given $1 \leq S < N < \infty$, and $1 \leq m < \infty$, can exactly reproduce the original *zero*-mean function $w(\mathbf{X})$ under the following two conditions: (1) If the original function is endowed with a purely additive structure, i.e., $w(\mathbf{X}) = \tilde{w}_{S,m}(\mathbf{X})$, then Equations (5.9), (5.10), and (5.15) yield $\alpha_{S,m} = \alpha'_{S,m} = 1$, and $\beta_{S,m} = 0$, which in turn results in $\bar{w}_{S,m}(\mathbf{X}) = \bar{w}'_{S,m}(\mathbf{X}) = \tilde{w}_{S,m}(\mathbf{X}) = w(\mathbf{X})$; (2) If the original function possesses a purely multiplicative structure, i.e., $w(\mathbf{X}) = \hat{w}_{S,m}(\mathbf{X})$, then Equations (5.9), (5.10), and (5.15) produce $\alpha_{S,m} = \alpha'_{S,m} = 0$ and $\beta_{S,m} = 1$, and therefore $\bar{w}_{S,m}(\mathbf{X}) = \bar{w}'_{S,m}(\mathbf{X}) = \hat{w}_{S,m}(\mathbf{X}) = w(\mathbf{X})$.

5.2.2 Second-moment properties

Applying the expectation operator on Equations (5.8) and (5.14) yields the exact mean

$$\mathbb{E}\left[\bar{y}_{S,m}\left(\mathbf{X};\alpha_{S,m},\beta_{S,m}\right)\right]=\mathbb{E}\left[\bar{y}'_{S,m}\left(\mathbf{X};\alpha'_{S,m}\right)\right]=y_{\emptyset}, \tag{5.18}$$

by both the hybrid approximations. However, their respective variances, obtained by applying the expectation operator on $\bar{w}_{S,m}\left(\mathbf{X};\alpha_{S,m},\beta_{S,m}\right)^2$ and $\bar{w}'_{S,m}\left(\mathbf{X};\alpha'_{S,m},\beta'_{S,m}\right)^2$ respectively, vary according to

$$\begin{aligned}\bar{\sigma}^2_{S,m} &:= \mathbb{E}\left[\bar{w}^2_{S,m}\left(\mathbf{X};\alpha_{S,m},\beta_{S,m}\right)\right]\\ &= \alpha^2_{S,m}\tilde{\sigma}^2_{S,m}+\beta^2_{S,m}\hat{\sigma}^2_{S,m}+2\alpha_{S,m}\beta_{S,m}\mathbb{E}\left[\tilde{w}_{S,m}\left(\mathbf{X}\right)\hat{w}_{S,m}\left(\mathbf{X}\right)\right]\end{aligned} \tag{5.19}$$

and

$$\begin{aligned}\bar{\sigma}'^2_{S,m}:=&\mathbb{E}\left[\bar{w}'^2_{S,m}\left(\mathbf{X};\alpha'_{S,m}\right)\right]\\ =&\alpha'^2_{S,m}\tilde{\sigma}^2_{S,m}+\left(1-\alpha'_{S,m}\right)^2\hat{\sigma}^2_{S,m}+2\alpha'_{S,m}\left(1-\alpha'_{S,m}\right)\mathbb{E}\left[\tilde{w}_{S,m}\left(\mathbf{X}\right)\hat{w}_{S,m}\left(\mathbf{X}\right)\right].\end{aligned} \tag{5.20}$$

Compared with the additive and factorized PDD approximations, the hybrid PDD approximations proposed require expectation of product of $\tilde{w}_{S,m}\left(\mathbf{X}\right)$ and $\hat{w}_{S,m}\left(\mathbf{X}\right)$ to calculate the variance.

5.3 Univariate Hybrid PDD Approximation

In the root of developing the factorized PDD method lies the principal motive of achieving high accuracy in calculating probabilistic characteristics of high-dimensional random responses while keeping the computational efforts to a minimum. This objective was attained through applying univariate factorized PDD approxi-

mations in solving high-dimensional stochastic problems. The numerical examples (Section 4.6) and application (Section 4.7) in Chapter 4 illustrate remarkably higher efficiency of univariate factorized PDD methods in obtaining results comparable to the expensive higher-variate additive PDD methods. Considering the key advantage of high efficiency of a univariate additive and factorized PDD approximations, only the univariate hybrid PDD method was employed in this work. Proposition 5.3 formally describes the univariate hybrid PDD approximation.

Proposition 5.3: *A linear, univariate, mth-order hybrid PDD approximation of $w(\mathbf{X})$, obtained by setting $S = 1$ in Equations* (5.8)-(5.10)*, is*

$$\bar{w}_{1,m}(\mathbf{X}; \alpha_{1,m}, \beta_{1,m}) = \alpha_{1,m}\tilde{w}_{1,m}(\mathbf{X}) + \beta_{1,m}\hat{w}_{1,m}(\mathbf{X}) \tag{5.21}$$

where the model parameters

$$\alpha_{1,m} = \frac{\hat{\sigma}^2_{1,m} - \mathbb{E}\left[w(\mathbf{X})\,\hat{w}_{1,m}(\mathbf{X})\right]}{\hat{\sigma}^2_{1,m} - \tilde{\sigma}^2_{1,m}} \tag{5.22}$$

and

$$\beta_{1,m} = \frac{\mathbb{E}\left[w(\mathbf{X})\,\hat{w}_{1,m}(\mathbf{X})\right] - \tilde{\sigma}^2_{1,m}}{\hat{\sigma}^2_{1,m} - \tilde{\sigma}^2_{1,m}}. \tag{5.23}$$

Proof. Consider the univariate, mth-order additive and factorized PDD approximations

$$\tilde{w}_{1,m}(\mathbf{X}) = \sum_{i=1}^{N}\sum_{j=1}^{m} C_{ij}\psi_{ij}(X_i), \tag{5.24}$$

$$\hat{w}_{1,m}(\mathbf{X}) = y_\emptyset\left[\prod_{i=1}^{N}\left\{1 + \frac{1}{y_\emptyset}\sum_{j=1}^{m} C_{ij}\psi_{ij}(X_i)\right\}\right] - y_\emptyset \tag{5.25}$$

of

$$w(\mathbf{X}) = \sum_{\emptyset \neq u \subseteq \{1,\cdots,N\}}\ \sum_{\substack{\mathbf{j}_{|u|}\in\mathbb{N}_0^{|u|} \\ j_1,\cdots,j_{|u|}\neq 0}} C_{u\mathbf{j}_{|u|}}\psi_{u\mathbf{j}_{|u|}}(\mathbf{X}_u). \tag{5.26}$$

From Propositions 4.1 and 4.2,

$$\begin{aligned}\mathbb{E}\left[w\left(\mathbf{X}\right)\tilde{w}_{1,m}\left(\mathbf{X}\right)\right] &= \mathbb{E}\left[\tilde{w}_{1,m}\left(\mathbf{X}\right)\hat{w}_{1,m}\left(\mathbf{X}\right)\right] \\ &= \sum_{i=1}^{N}\sum_{j=1}^{m}C_{ij}^{2} = \tilde{\sigma}_{1,m}^{2}. \end{aligned} \tag{5.27}$$

Applying Equation (5.27) to Equations (5.9) and (5.10), the model parameters for $S = 1$ and $m < \infty$ are obtained as in Equations (5.22) and (5.23). □

Remark 5.2: The two parameters $\alpha_{1,m}$ and $\beta_{1,m}$ of the hybrid model described by Equation (5.21) add up to one. This is due to special properties of $\tilde{w}_{1,m}\left(\mathbf{X}\right)$ and $\hat{w}_{1,m}\left(\mathbf{X}\right)$ expressed in Equations (5.24) and (5.25). Therefore, the hybrid model described by Equation (5.14) at univariate truncation ($S = 1$), is redundant, as it leads to the same solution of the first model described by (5.21).

Since $\beta_{1,m} = 1 - \alpha_{1,m}$, let

$$\begin{aligned}\bar{w}_{1,m}\left(\mathbf{X};\alpha_{1,m}\right) &:= \bar{y}_{1,m}\left(\mathbf{X};\alpha_{1,m}\right) - y_{\emptyset} \\ &= \alpha_{1,m}\tilde{w}_{1,m}\left(\mathbf{X}\right) + \left(1-\alpha_{1,m}\right)\hat{w}_{1,m}\left(\mathbf{X}\right) \end{aligned} \tag{5.28}$$

denote the univariate hybrid PDD approximation of $w\left(\mathbf{X}\right)$. The mean of $\bar{w}_{1,m}\left(\mathbf{X};\alpha_{1,m}\right)$ is *zero* and, therefore, $\mathbb{E}\left[\bar{y}_{1,m}\left(\mathbf{X};\alpha_{1,m}\right)\right] = y_{\emptyset}$, matching the exact mean of $y\left(\mathbf{X}\right)$. The variance of $\bar{w}_{1,m}\left(\mathbf{X};\alpha_{1,m}\right)$ or $\bar{y}_{1,m}\left(\mathbf{X};\alpha_{1,m}\right)$ is

$$\bar{\sigma}_{1,m}^{2} := \mathbb{E}\left[\bar{w}_{1,m}^{2}\left(\mathbf{X};\alpha_{1,m}\right)\right] = \left(2\alpha_{1,m} - \alpha_{1,m}^{2}\right)\tilde{\sigma}_{1,m}^{2} + \left(1-\alpha_{1,m}\right)^{2}\hat{\sigma}_{1,m}^{2}, \tag{5.29}$$

which is a linear combination of the variances from univariate additive PDD and univariate factorized PDD approximations. The variances $\tilde{\sigma}_{1,m}^{2}$ and $\hat{\sigma}_{1,m}^{2}$, expressed by Equations (4.16) and (4.38), are obtained from the univariate PDD expansion

coefficients. However, determining the model parameter $\alpha_{1,m}$ involves evaluation of an N-dimensional integral that will incur additional computational expense in excess of the computations performed for estimating the PDD expansions coefficients. A quasi MCS was employed for estimating the model parameters, described as follows.

5.3.1 Calculation of the hybrid model parameter

The basic idea of a quasi MCS is to replace the random or pseudo-random samples in crude MCS by well-chosen deterministic samples that are highly equidistributed [125]. The qausi MCS samples are often selected from a low-discrepancy sequence [125–128] or by lattice rules [129] to minimize the integration errors. The estimation of the expectation of the multi-variate function $w(\mathbf{X})\,\hat{w}_{1,m}(\mathbf{X})$, which is a high-dimensional integral, comprises three simple steps: (1) generate a low-discrepancy point set $\mathcal{P}_L := \{\mathbf{u}^{(k)} \in [0,1]^N,\ k = 1, \cdots, L\}$ of size $L \in \mathbb{N}$; (2) map each sample from $\mathcal{P}_L$ to the sample $\mathbf{x}^{(k)} \in \mathbb{R}^N$ following the probability measure of the random input $\mathbf{X}$; and (3) approximate the expectation as $\mathbb{E}\left[w(\mathbf{X})\,\hat{w}_{1,m}(\mathbf{X})\right] \cong \frac{1}{L}\sum_{k=1}^{L}\left[w\left(\mathbf{x}^{(k)}\right)\hat{w}_{1,m}\left(\mathbf{x}^{(k)}\right)\right]$. Thus, using quasi MCS, the model parameter is given by

$$\alpha_{1,m} \cong \frac{\hat{\sigma}^2_{1,m} - \dfrac{1}{L}\displaystyle\sum_{k=1}^{L}\left[w\left(\mathbf{x}^{(k)}\right)\hat{w}_{1,m}\left(\mathbf{x}^{(k)}\right)\right]}{\hat{\sigma}^2_{1,m} - \tilde{\sigma}^2_{1,m}}, \tag{5.30}$$

where $\hat{\sigma}^2_{1,m}$, and $\tilde{\sigma}^2_{1,m}$ are obtained from Equations (4.16) and (4.38). However, when $\hat{\sigma}^2_{1,m} = \mathbb{E}\left[\hat{w}^2_{1,m}(\mathbf{X})\right]$ and $\tilde{\sigma}^2_{1,m} = \mathbb{E}\left[\tilde{w}^2_{1,m}(\mathbf{X})\right]$ are also estimated from a quasi MCS

method, then the model parameter can also be obtained from

$$\alpha_{1,m} \cong \frac{\frac{1}{L}\sum_{k=1}^{L}\left[\hat{w}_{1,m}^2\left(\mathbf{x}^{(k)}\right)\right] - \frac{1}{L}\sum_{k=1}^{L}\left[w\left(\mathbf{x}^{(k)}\right)\hat{w}_{1,m}\left(\mathbf{x}^{(k)}\right)\right]}{\frac{1}{L}\sum_{k=1}^{L}\left[\hat{w}_{1,m}^2\left(\mathbf{x}^{(k)}\right)\right] - \frac{1}{L}\sum_{k=1}^{L}\left[\tilde{w}_{1,m}^2\left(\mathbf{x}^{(k)}\right)\right]}. \tag{5.31}$$

Both Equations (5.30) and (5.31) were employed for estimating $\alpha_{1,m}$ in this work. Further details, clarifying which equation is used, are given in the numerical examples section.

5.3.2 Error analysis

Given the univariate truncation ($S = 1$), which approximation stemming additive PDD, factorized PDD, and hybrid PDD is more accurate? Lemma 5.4 and Theorem 5.5 address this question.

Lemma 5.4: Let $y(\mathbf{X})$ be a real-valued, square integrable function with $\tilde{y}_{1,m}(\mathbf{X})$ and $\hat{y}_{1,m}(\mathbf{X})$ denoting its univariate additive PDD and univariate factorized PDD approximations, respectively. Let

$$\tilde{\sigma}_{1,m}^2 = \sum_{i=1}^{N}\sum_{j=1}^{m} C_{ij}^2 \tag{5.32}$$

and

$$\hat{\sigma}_{1,m}^2 = y_{\emptyset}^2\left[\prod_{i=1}^{N}\left(1 + \frac{1}{y_{\emptyset}^2}\sum_{j=1}^{m} C_{ij}^2\right) - 1\right] \tag{5.33}$$

be the variances of $\tilde{y}_{1,m}(\mathbf{X})$ and $\hat{y}_{1,m}(\mathbf{X})$, respectively. Then

$$\hat{\sigma}_{1,m}^2 \geq \tilde{\sigma}_{1,m}^2.$$

Proof. From Equation (5.33) the variance from a univariate factorized PDD is

$$\begin{aligned}
\hat{\sigma}^2_{1,m} &= \sum_{i=1}^{N}\sum_{j=1}^{m} C_{ij}^2 + \frac{1}{y_\emptyset^2}\sum_{i_1<i_2}^{N}\sum_{j=1}^{m} C_{i_1 j}^2 \sum_{j=1}^{m} C_{i_2 j}^2 \\
&\quad + \frac{1}{y_\emptyset^3}\sum_{i_1<i_2<i_3}^{N}\sum_{j=1}^{m} C_{i_1 j}^2 \sum_{j=1}^{m} C_{i_2 j}^2 \sum_{j=1}^{m} C_{i_3 j}^2 + \cdots + \frac{1}{y_\emptyset^N}\prod_{i=1}^{N}\left(\sum_{j=1}^{m} C_{ij}^2\right) \\
&= \tilde{\sigma}^2_{1,m} + \frac{1}{y_\emptyset^2}\sum_{i_1<i_2}^{N}\sum_{j=1}^{m} C_{i_1 j}^2 \sum_{j=1}^{m} C_{i_2 j}^2 \\
&\quad + \frac{1}{y_\emptyset^3}\sum_{i_1<i_2<i_3}^{N}\sum_{j=1}^{m} C_{i_1 j}^2 \sum_{j=1}^{m} C_{i_2 j}^2 \sum_{j=1}^{m} C_{i_3 j}^2 + \cdots + \frac{1}{y_\emptyset^N}\prod_{i=1}^{N}\left(\sum_{j=1}^{m} C_{ij}^2\right) \\
&\geq \tilde{\sigma}^2_{1,m}, \qquad (5.34)
\end{aligned}$$

where the second equality uses Equation (5.32). □

Theorem 5.5: Let $y(\mathbf{X})$ be a real-valued, square integrable function with $\tilde{y}_{1,m}(\mathbf{X})$, $\hat{y}_{1,m}(\mathbf{X})$ and $\bar{y}_{1,m}(\mathbf{X})$ denoting its univariate additive PDD, univariate factorized PDD, and univariate hybrid PDD approximations, respectively, with $\tilde{\sigma}^2_{1,m}$, $\hat{\sigma}^2_{1,m}$ and $\bar{\sigma}^2_{1,m}$ as the variances obtained from respective approximations. If

$$\tilde{e}_{1,m} := \mathbb{E}\left[y(\mathbf{X}) - \tilde{y}_{1,m}(\mathbf{X})\right]^2 = \mathbb{E}\left[w(\mathbf{X}) - \tilde{w}_{1,m}(\mathbf{X})\right]^2 \qquad (5.35)$$

$$\hat{e}_{1,m} := \mathbb{E}\left[y(\mathbf{X}) - \hat{y}_{1,m}(\mathbf{X})\right]^2 = \mathbb{E}\left[w(\mathbf{X}) - \hat{w}_{1,m}(\mathbf{X})\right]^2 \qquad (5.36)$$

and

$$\bar{e}_{1,m} := \mathbb{E}\left[y(\mathbf{X}) - \bar{y}_{1,m}(\mathbf{X})\right]^2 = \mathbb{E}\left[w(\mathbf{X}) - \bar{w}_{1,m}(\mathbf{X})\right]^2 \qquad (5.37)$$

are the errors committed by univariate additive PDD, univariate factorized PDD and univariate hybrid PDD, respectively, in calculating σ^2, the variance of $y(\mathbf{X})$, then,

$$\bar{e}_{1,m} \leq \tilde{e}_{1,m}$$

and

$$\bar{e}_{1,m} \leq \hat{e}_{1,m}.$$

Proof. From Equations (5.35) and (5.37),

$$\tilde{e}_{1,m} = \sigma^2 - \tilde{\sigma}^2_{1,m} \tag{5.38}$$

and

$$\begin{aligned} \bar{e}_{1,m} &= \mathbb{E}\left[w^2(\mathbf{X})\right] + \mathbb{E}\left[\bar{w}^2(\mathbf{X})\right] - 2\mathbb{E}\left[w(\mathbf{X})\,\bar{w}_{1,m}(\mathbf{X})\right] \\ &= \sigma^2 + \bar{\sigma}^2_{1,m} - 2\mathbb{E}\left[w(\mathbf{X})\,\bar{w}_{1,m}(\mathbf{X})\right]. \end{aligned} \tag{5.39}$$

Subtracting Equation (5.38) from Equation (5.39) yields

$$\begin{aligned} \bar{e}_{1,m} - \tilde{e}_{1,m} &= \bar{\sigma}^2_{1,m} - 2\mathbb{E}\left[w(\mathbf{X})\,\bar{w}_{1,m}(\mathbf{X})\right] + \tilde{\sigma}^2_{1,m} \\ &= \left(2\alpha_{1,m} - \alpha^2_{1,m}\right)\tilde{\sigma}^2_{1,m} + \left(1-\alpha_{1,m}\right)^2\hat{\sigma}^2_{1,m} + \tilde{\sigma}^2_{1,m} \\ &\quad -2\mathbb{E}\left[w(\mathbf{X})\left\{\alpha_{1,m}\tilde{w}_{1,m}(\mathbf{X}) + \left(1-\alpha_{1,m}\right)\hat{w}_{1,m}(\mathbf{X})\right\}\right] \\ &= 2\left(1-\alpha_{1,m}\right)\left(\tilde{\sigma}^2_{1,m} - \mathbb{E}\left[w(\mathbf{X})\,\hat{w}_{1,m}(\mathbf{X})\right]\right) \\ &\quad + \left(1-\alpha_{1,m}\right)^2\left(\hat{\sigma}^2_{1,m} - \tilde{\sigma}^2_{1,m}\right) \\ &= -\left(1-\alpha_{1,m}\right)^2\left(\hat{\sigma}^2_{1,m} - \tilde{\sigma}^2_{1,m}\right) \\ &\leq 0, \end{aligned} \tag{5.40}$$

following Lemma 5.4, where the second equality uses Equations (5.29) and (5.28) and the last equality uses Equation (5.23).

Similarly, from Equation (5.36),

$$\hat{e}_{1,m} = \sigma^2 + \hat{\sigma}^2_{1,m} - 2\mathbb{E}\left[w(\mathbf{X})\,\hat{w}_{1,m}(\mathbf{X})\right]. \tag{5.41}$$

Subtracting Equation (5.41) from Equation (5.39) yields

$$\begin{aligned}
\bar{e}_{1,m} - \hat{e}_{1,m} &= \bar{\sigma}^2_{1,m} - 2\mathbb{E}\left[w\left(\mathbf{X}\right)\bar{w}_{1,m}\left(\mathbf{X}\right)\right] - \hat{\sigma}^2_{1,m} + 2\mathbb{E}\left[w\left(\mathbf{X}\right)\hat{w}_{1,m}\left(\mathbf{X}\right)\right] \\
&= \left(2\alpha_{1,m} - \alpha^2_{1,m}\right)\tilde{\sigma}^2_{1,m} + \left(1-\alpha_{1,m}\right)^2\hat{\sigma}^2_{1,m} \\
&\quad -2\mathbb{E}\left[w\left(\mathbf{X}\right)\left\{\alpha_{1,m}\tilde{w}_{1,m}\left(\mathbf{X}\right) + \left(1-\alpha_{1,m}\right)\hat{w}_{1,m}\left(\mathbf{X}\right)\right\}\right] \\
&\quad -\hat{\sigma}^2_{1,m} + 2\mathbb{E}\left[w\left(\mathbf{X}\right)\hat{w}_{1,m}\left(\mathbf{X}\right)\right] \\
&= \tilde{\sigma}^2_{1,m} - \hat{\sigma}^2_{1,m} - 2\alpha_{1,m}\left(\tilde{\sigma}^2_{1,m} - \mathbb{E}\left[w\left(\mathbf{X}\right)\hat{w}_{1,m}\left(\mathbf{X}\right)\right]\right) \\
&\quad + \left(1-\alpha_{1,m}\right)^2\left(\hat{\sigma}^2_{1,m} - \tilde{\sigma}^2_{1,m}\right) \\
&= -\alpha^2_{1,m}\left(\hat{\sigma}^2_{1,m} - \tilde{\sigma}^2_{1,m}\right) \\
&\leq 0, \qquad (5.42)
\end{aligned}$$

following Lemma 5.4, where, again, the second equality uses Equations (5.29) and (5.28) and the last equality uses Equation (5.23). □

The significance of Theorem 5.5 lies in providing analytical relations comparing the errors committed in calculating the variances by univariate additive PDD, factorized PDD and hybrid PDD approximations. It is clear from Theorem 5.5 that the error committed by univariate hybrid PDD can never be greater than the error committed by either univariate additive PDD or univariate factorized PDD.

5.4 Calculation of Expansion Coefficients by Quasi MCS

The calculation of PDD expansion coefficients involves evaluating various N-dimensional integrals. In the preceding chapters of this thesis, the expansion coefficients have been calculated using the efficient dimension reduction integration tech-

nique and the crude MCS method, discussed in Sections 4.5.1 and 4.5.2, respectively. For the high-dimensional problems handled in this chapter, the PDD coefficients were calculated using dimensional reduction integration and quasi MCS method, described as follows.

Section 5.3.1 gives a brief overview of the quasi MCS method. Employing the quasi MCS method for the estimation of the PDD expansion coefficients, which are high-dimensional integrals defined in Equations (4.2) and (4.9), again comprises three simple steps: (1) generate a low-discrepancy point set $\mathcal{P}_L := \{\mathbf{u}^{(k)} \in [0,1]^N,\ k = 1, \cdots, L\}$ of size $L \in \mathbb{N}$; (2) map each sample from $\mathcal{P}_L$ to the sample $\mathbf{x}^{(k)} \in \mathbb{R}^N$ following the probability measure of the random input $\mathbf{X}$; and (3) approximate the coefficients by

$$y_{\emptyset} \cong \frac{1}{L} \sum_{k=1}^{L} y\left(\mathbf{x}^{(k)}\right), \tag{5.43}$$

$$C_{u\mathbf{j}_{|u|}} \cong \frac{1}{L} \sum_{k=1}^{L} y\left(\mathbf{x}^{(k)}\right) \psi_{u\mathbf{j}_{|u|}}\left(\mathbf{x}_u^{(k)}\right). \tag{5.44}$$

The well-known Koksma–Hlawka inequality reveals that the error committed by a quasi MCS is bounded by the variation of the integrand in the sense of Hardy and Krause and the star-discrepancy, a measure of uniformity, of the point set $\mathcal{P}_L$ [125]. Therefore, constructing a point set with star-discrepancy as small as possible and seeking variance reduction of the integrand are vital for the success of the quasi MCS. It should be mentioned here that many authors, including Halton [126], Faure [127], Niederreiter [125], Sobol [128], and Wang [130], have extensively studied how to generate the best low-discrepancy point sets and sequences and to engender variance

reduction. For a bounded variation of the integrand, the quasi MCS has a theoretical error bound $O(L^{-1}(\log L)^N$ compared with the probabilistic error bound $O(N^{-1/2})$ of crude MCS, indicating significantly faster convergence of the quasi MCS than crude MCS.

5.5 Numerical Examples

Two numerical examples are presented to illustrate the hybrid PDD method developed in calculating the second-moment statistics and tail probability distributions of random mathematical functions and random eigensolutions of a simple stochastic dynamical system. Classical Legendre polynomials were used to define the orthonormal polynomials in Example 1, and all PDD expansion coefficients and the hybrid model parameter were determined analytically. In Example 2 all original random variables were transformed into standard Gaussian random variables, facilitating the use of classical Hermite orthonormal polynomials as bases. The expansion coefficients in Example 2 were calculated using dimensional-reduction integration ($R = 1$) involving five-point univariate Gauss-Hermite quadrature rule. The hybrid model parameter was estimated by quasi MCS using Sobol's low-discrepancy sequence of 100 and 500 points and Equation (5.30). The sample size for the embedded MCS in Example 2 is 10^6.

5.5.1 Polynomial function

Consider a polynomial function

$$y(\mathbf{X}) = \left[\frac{2}{N}\sum_{i=1}^{N} X_i\right]^q$$

where $N = 5$, X_i, $i = 1, \ldots, N$, are independent and identical random variables, each following the standard uniform distribution over $[0, 1]$, and $q \in \mathbb{N}$ is an exponent. The function $y(\mathbf{X})$ has a purely additive structure when $q = 1$, but as the value of q increases, the function $y(\mathbf{X})$ evolves from strongly additive to strongly multiplicative. The objective of this example is to compare univariate additive PDD, univariate factorized PDD, and univariate hybrid PDD approximations in calculating the variance of $y(\mathbf{X})$ for $q = 2, 3, 4, 5, 6, 7, 8$.

Since y is a multivariate polynomial of degree q, the truncation parameter m for a PDD approximation, whether additive, factorized, or hybrid, was set equal to q. Figure 5.1 shows how the hybrid model parameter $\alpha_{1,m}$ varies with respect to q, where $\tilde{\sigma}^2_{1,m}$, $\hat{\sigma}^2_{1,m}$, and the expectation in Equation (5.22) of $\alpha_{1,m}$ are calculated exactly. The parameter $\alpha_{1,m}$ is relatively close to one when $q = 2$, and decreases monotonically as q increases, indicating the diminishing additive structure of the function y. When $q = 8$, $\alpha_{1,m}$ is relatively close to zero, that is, y is dominantly multiplicative.

Figure 5.2 presents the relative errors, defined as the ratio of the absolute difference between the exact and approximate variances of $y(\mathbf{X})$ to the exact variance, committed by the univariate additive PDD, univariate factorized PDD, and univariate hybrid PDD methods. The second-moment properties of $y(\mathbf{X})$, given q, were calculated exactly. The function $y(\mathbf{X})$ is strongly additive when $q = 2$ or 3, therefore, the univariate additive PDD approximation has lower error than the factorized

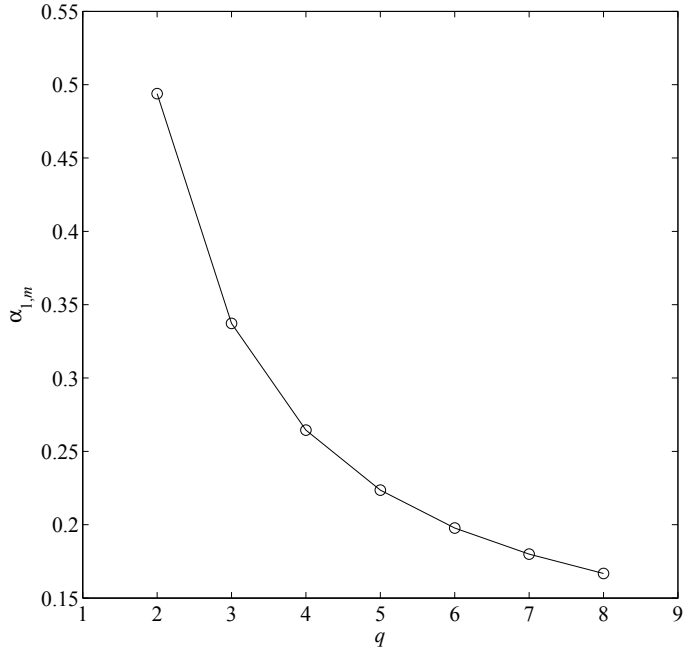

Figure 5.1: Variation of $\alpha_{1,m}$ with respect to q (Example 1).

PDD approximation. But the trend reverses for $4 \leq q \leq 8$, the range of higher values examined. This is because the function switches from dominantly additive ($q \leq 3$) to dominantly multiplicative ($q > 3$) as q increases. Nonetheless, for all the values of q considered, the univariate hybrid PDD approximation commits lower errors than either univariate additive PDD or univariate factorized PDD approximation. These results are consistent with the findings of Theorem 5.5.

5.5.2 Three-degree-of-freedom, undamped, spring-mass system

Consider a three-degree-of-freedom, undamped, spring-mass system, shown in Figure 5.3, with random mass and random stiffness matrices

$$\mathbf{M}(\mathbf{X}) = \begin{bmatrix} M_1(\mathbf{X}) & 0 & 0 \\ 0 & M_2(\mathbf{X}) & 0 \\ 0 & 0 & M_3(\mathbf{X}) \end{bmatrix} \tag{5.45}$$

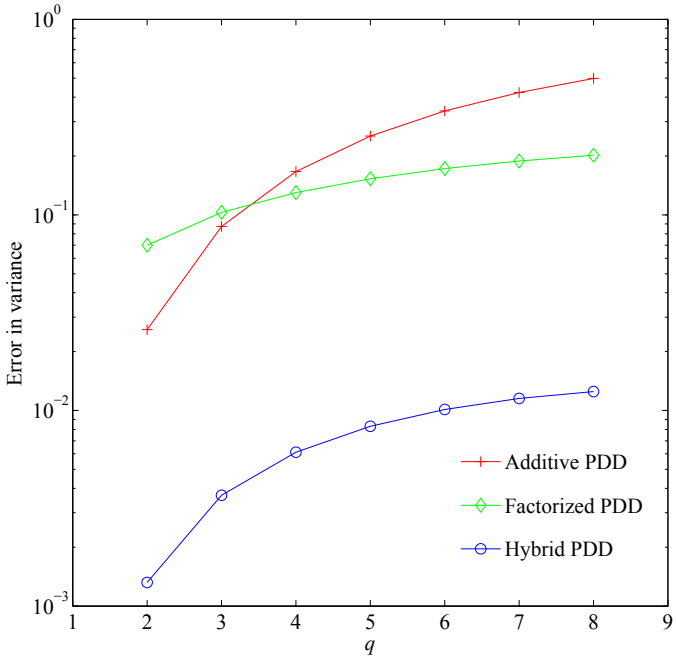

Figure 5.2: Error in variance calculation from additive PDD, factorized PDD, and hybrid PDD approximations (Example 1).

and

$$\mathbf{K}(\mathbf{X}) = \begin{bmatrix} K_{11}(\mathbf{X}) & K_{12}(\mathbf{X}) & K_{13}(\mathbf{X}) \\ & K_{22}(\mathbf{X}) & K_{23}(\mathbf{X}) \\ (\text{sym.}) & & K_{33}(\mathbf{X}) \end{bmatrix}, \tag{5.46}$$

respectively, where $K_{11}(\mathbf{X}) = K_1(\mathbf{X}) + K_4(\mathbf{X}) + K_6(\mathbf{X})$, $K_{12}(\mathbf{X}) = -K_4(\mathbf{X})$, $K_{13}(\mathbf{X}) = -K_6(\mathbf{X})$, $K_{22}(\mathbf{X}) = K_4(\mathbf{X}) + K_5(\mathbf{X}) + K_2(\mathbf{X})$, $K_{23}(\mathbf{X}) = -K_5(\mathbf{X})$, and $K_{33}(\mathbf{X}) = K_5(\mathbf{X}) + K_3(\mathbf{X}) + K_6(\mathbf{X})$; the masses $M_i(\mathbf{X}) = \mu_i X_i$; $i = 1, 2, 3$ with $\mu_i = 1.0$ kg; $i = 1, 2, 3$, and spring stiffnesses $K_i(\mathbf{X}) = \mu_{i+3} X_{i+3}$; $i = 1, \cdots, 6$ with $\mu_{i+3} = 1.0$ N/m; $i = 1, \cdots, 5$ and $\mu_9 = 3.0$ N/m. The input $\mathbf{X} = \{X_1, \cdots, X_9\}^T \in \mathbb{R}^9$ is an independent lognormal random vector with mean $\boldsymbol{\mu}_{\mathbf{X}} = \mathbf{1} \in \mathbb{R}^9$ and covariance matrix $\boldsymbol{\Sigma}_{\mathbf{X}} = \nu^2 \mathbf{I} \in \mathbb{R}^{9\times 9}$ with coefficient of variation $\nu = 0.3$.

The primary objective of this example is to demonstrate high accuracy of univariate hybrid PDD approximation in calculating cumulative distribution functions of

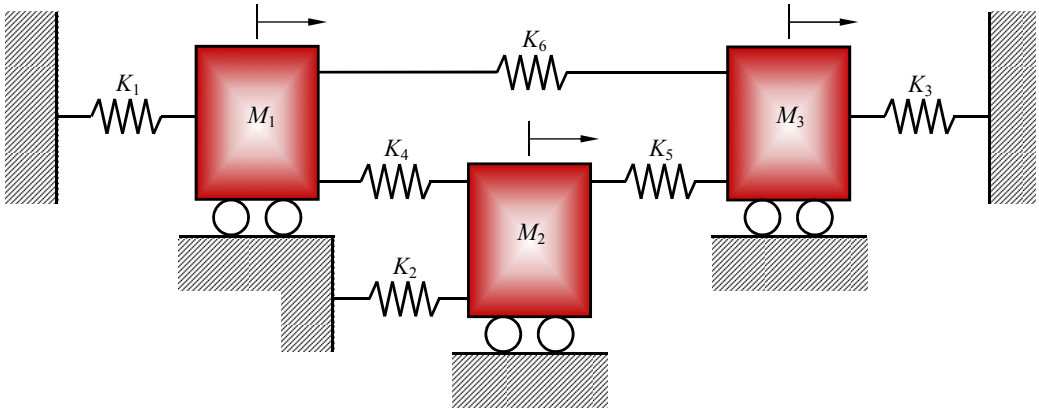

Figure 5.3: A three-degree-of-freedom, undamped, spring-mass system (Example 2).

the three eigenvalues of the three-degree-of-freedom system. The secondary, although significant, objective of this example is to show that the quasi MCS method, with a relatively small sample size for calculating the model parameter of univariate hybrid PDD approximation, is capable of delivering results comparable to those obtained from the expensive bivariate additive PDD approximation.

The probability distributions of three eigenvalues of the three-degree-of-freedom system were calculated using the benchmark solution of 10^6 crude MCS method, and five different fourth-order ($m = 4$) PDD methods: (1) univariate additive PDD, (2) bivariate additive PDD, (3) univariate factorized PDD, (4) univariate hybrid PDD with $\alpha_{1,4}$ estimated using 500 quasi MCS samples, and (5) univariate hybrid PDD with $\alpha_{1,4}$ estimated using 100 quasi MCS samples. Figure 5.4 presents the marginal probability distributions $F_i(\lambda_i) := P[\Lambda_i \leq \lambda_i]$ of three eigenvalues λ_i, $i = 1, 2, 3$, where all the PDD solutions were obtained from the embedded MCS; the parenthetical values reflect the total number of function evaluations required by the respective

methods. The plots are made over a semi-logarithmic scale to delineate the distributions in the tail regions. For all three eigenvalues, the probability distributions obtained from the univariate additive PDD method is far from the crude MCS results, divulging the clear inadequacy of the univariate additive PDD approximation in calculating tail probabilities. The univariate factorized PDD method performs relatively better than its additive counterpart, indicating dominantly multiplicative structure of the functions; however, it still leaves wide room for improvement compared with the benchmark crude MCS results. The univariate hybrid PDD method requires additional computational effort owing to quasi MCS for estimating $\alpha_{1,4}$ in Equation (5.30), but the improved results obtained clearly justify the additional cost. To put the results of the univariate hybrid PDD method in perspective, the results from bivariate ($S = 2$) additive PDD method, also obtained, show dramatic improvement over the univariate additive PDD method, as expected. However, the bivariate additive PDD method also leads to a significantly larger number of function evaluations compared with the univariate hybrid PDD with quasi MCS (100 samples). Therefore, a hybrid PDD approximation in desirable, where only univariate truncations are feasible, but not necessarily rendering adequate accuracy in stochastic solutions by either additive or factorized PDD approximation alone.

5.6 Application: A Pickup Truck

This section illustrates the effectiveness of the proposed hybrid PDD method in solving a large-scale practical engineering problem. The application involves predict-

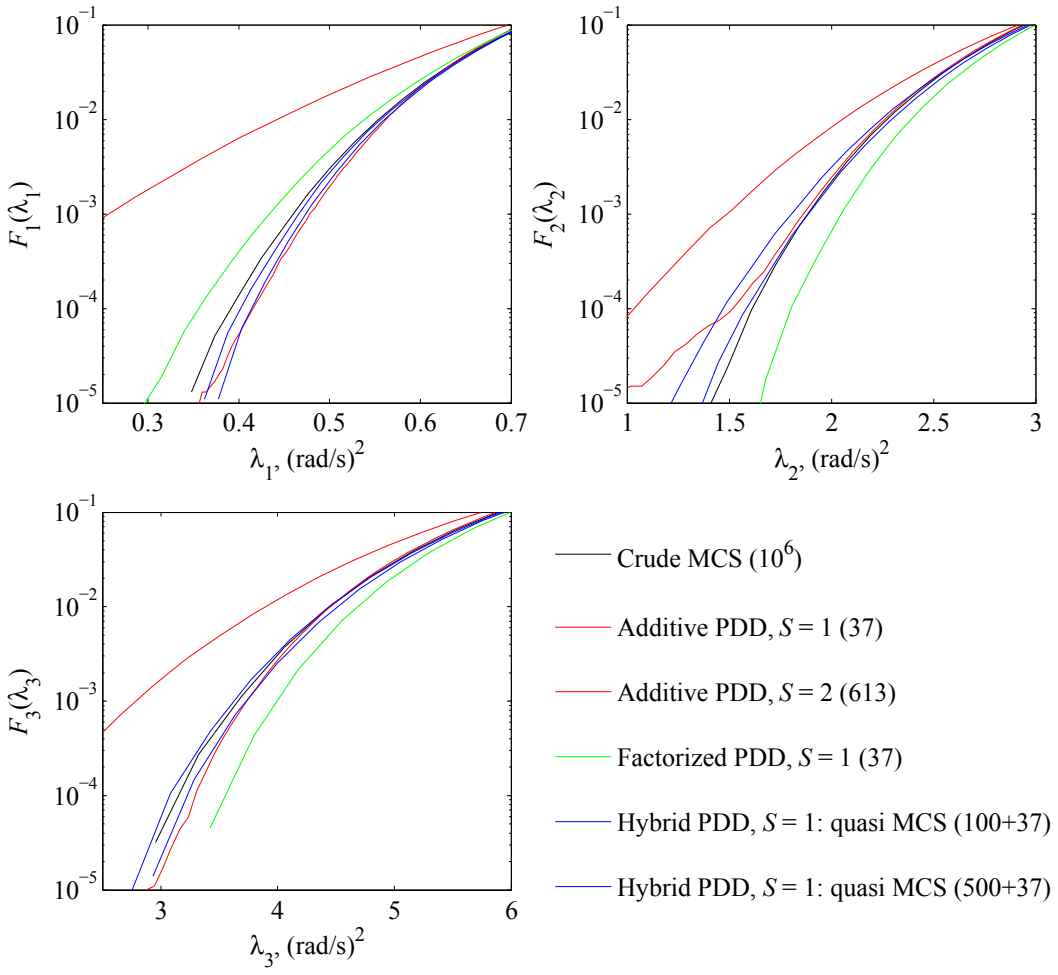

Figure 5.4: Tail probabilities of three eigenvalues of the three-degree-of-freedom, undamped, spring-mass system by various PDD approximations and crude MCS

ing probabilistic characteristics of sound pressure levels inside the cabin of a pickup truck. The acoustics, measured through sound pressure levels, inside a vehicle are widely considered a prominent parameter revealing the overall quality and build of the vehicle. In which case, a coupled acoustic-structural analysis is critically important in the automotive industry as it paves the way towards designing vehicles for ride comfort and quietness. Figure 5.5(a) presents a computer-aided design (CAD) cabin-air-chassis model of a pickup truck [131]. A finite-element mesh of the model, comprising 43,663 structural elements used to model the cabin and the chassis and 12,171 acoustic elements used to model the air interior, with a total of 207,994 degrees of freedom, is displayed in Figure 5.5(b). Figure 5.6(a) depicts the cabin model without air mesh and doors to show the space occupied by the air mesh, and Figure 5.6(b) displays the air mesh that fills the cabin interior. A tie constraint was employed to connect the air mesh to the structural parts inside the cabin surface or onto the seat surface.

Portrayed in Figure 5.5(a), the CAD model contains 24 distinct materials, with 22 structural materials and two non-structural materials, representing the air inside the cabin, and the carpet on the cabin floor. Twenty-one of the structural materials are modeled as shell elements, and the remaining material as beam elements defining the circular beam used for headrest mounting. The Young's moduli of 22 structural materials are random variables. The mass densities of the 21 materials modeled as shell elements are also random variables. Seven elastic-plastic materials forming the interior of the cabin and doors have random yield stress. Apart from the structural

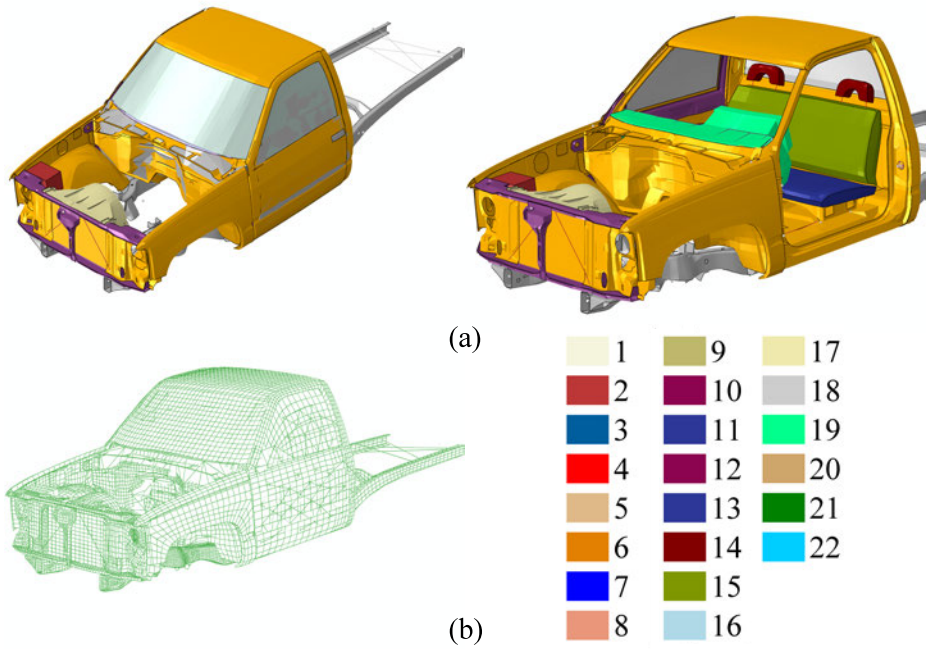

Figure 5.5: Cabin-air-chassis model of pickup truck: (a) a CAD model, (b) an FEA mesh

material properties, the bulk modulus and mass density of the air inside the cabin are also random variables. Finally, the proportionality factor between the pressure and velocity of the carpet surface in the normal direction is also a random variable. This proportionality constant defines the acoustic admittance of the carpet surface on the cabin floor. In aggregate, there exist 53 random variables $X_i = 1, \ldots, 53$, as follows: X_1 to X_{22} = Young's moduli of materials 1 to 22; X_{23} to X_{43} = mass densities of materials 1 to 21; X_{44} to X_{50} = yield stress of materials 1 to 7; X_{51} = bulk modulus of air inside the cabin; X_{52} = mass density of air inside the cabin; and X_{53} = acoustic admittance of the carpet surface on the cabin floor. All 53 random variables are independent and uniformly distributed with the coefficient of variation

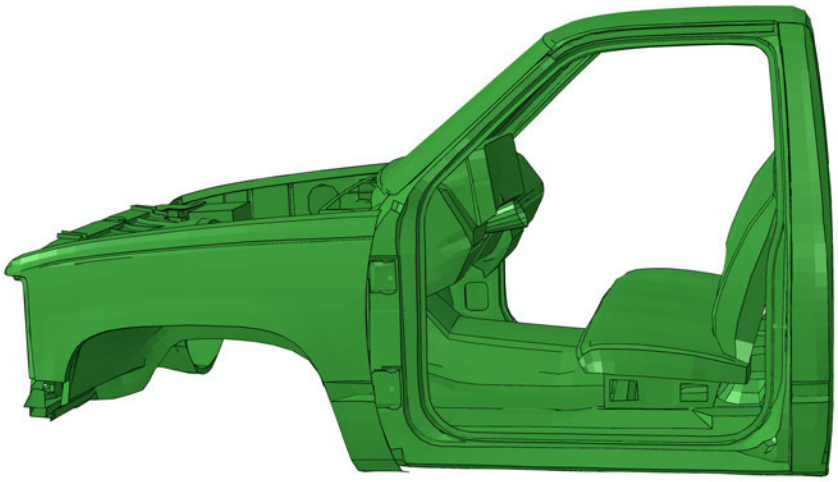

(a)

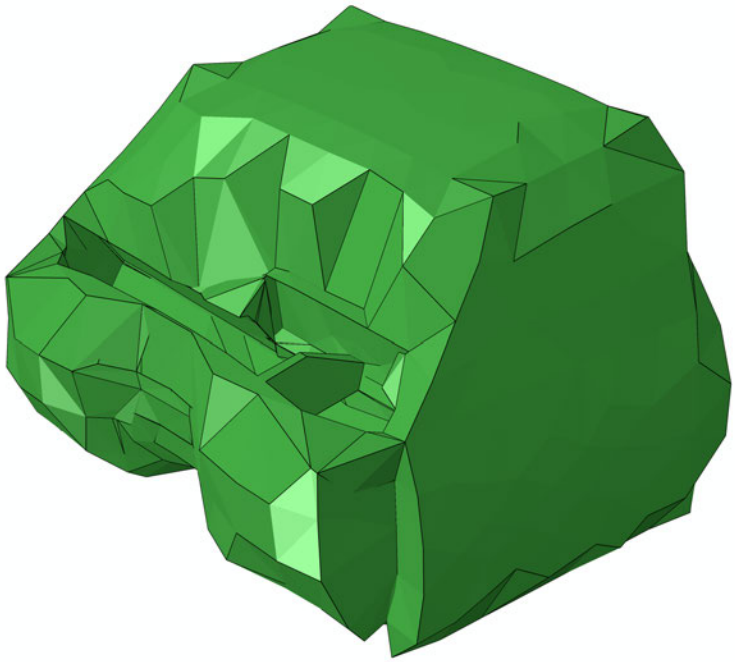

(b)

Figure 5.6: Cabin model of pickup truck with air mesh: (a) cabin model with doors removed for clearer illustration; (b) the air mesh inside the cabin

equal to 0.2. The means of random variables corresponding to the 22 structural materials, $\mu_i := \mathbb{E}[X_i]$, $i = 1, \ldots, 50$, are listed in Table 5.1. The means of the bulk modulus and mass density of air inside the cabin are $\mu_{51} = 0.139$ GPa and $\mu_{52} = 1.2 \times 10^{-12}$ kg/mm^3. The mean of the acoustic admittance of the carpet surface on the cabin floor is $\mu_{53} = 0.5 \times 10^6$ mm$^2 s$/kg. All structural materials, except materials 8, 9, and 10, have a deterministic Rayleigh stiffness proportional damping defined by the parameter $\beta_R = 0.4 \times 10^{-6}$ s. For a given value of β_R, the damping fraction ξ_i for a mode i with natural frequency ω_i is given by the formula $\xi_i = \beta_R \omega_i / 2$. The value of β_R chosen in this model is to give approximately 1 percent critical damping for the modes whose natural frequencies are in the middle of the range of excitation, i.e., at about 80 Hz at mean input. The Poisson's ratios of all structural materials are deterministic and are equal to 0.3.

5.6.1 Coupled acoustic-structural analysis

A mode-based coupled acoustic-structural analysis consists of two steps: an eigensolution extraction, followed by a steady-state dynamic analysis involving sound pressure level calculations. For obtaining eigensolutions, the first 200 eigenfrequencies were extracted. The Lanczos method (Section 2.4.2) embedded in Abaqus (Version 6.12) [131] was employed for extracting natural frequencies and mode shapes. For steady-state dynamic analysis, the airborne load originating from engine vibration was modeled as a diffuse field incident wave loading on the bulkhead below the dashboard. In the steady-state dynamic analysis, the sound pressure level at a location in the

Table 5.1: Mean values of the random input variables for structural materials in pickup truck

Material	Young's modulus GPa	Mass density kg/m^3	Yield stress GPa
1	210	7890	0.27
2	210	7890	0.27
3	210	7890	0.27
4	210	7890	0.35
5	2.8	1200	0.045
6	76	2500	0.14
7	3.4	1100	0.10
8	210	7890	-[a]
9	210	20900	-[a]
10	210	6910	-[a]
11	250	8060	-[a]
12	210	7890	-[a]
13	2.0	253	-[a]
14	2.0	169	-[a]
15	2.0	755	-[a]
16	210	2500	-[a]
17	200	7800	-[a]
18	210	1960	-[a]
19	120	3890	-[a]
20	21	1820	-[a]
21	210	7890	-[a]
22	200	-[b]	-[a]

[a] Materials 8 to 22 are not elastic-plastic and do not require yield stress to be defined.

[b] Not required.

vicinity of the driver's ear was calculated. The location of the driver's ear was defined through a node in the air mesh inside the cabin, in accordance with the specifications of location for measurement of noise inside motor vehicles defined in International Standard ISO-5128 [132]. The values of the sound pressure level were calculated at 200 evenly spaced points in the excitation frequency range of 35 Hz to 120 Hz. This

frequency range corresponds to engine-induced vibrations in the range of 2100-7200 rpm. The governing equations of a coupled acoustic-structural analysis are described in Appendix D.

Due to the uncertainty in material properties, the eigensolutions and sound pressure level values are random functions. The univariate, second-order hybrid PDD approximation was employed to determine their second-moment characteristics and various response probabilities. The associated expansion coefficients of PDD and the hybrid model parameter were estimated by quasi MCS method with 500 samples. The sample size for the embedded MCS of the PDD approximation is 5000.

5.6.2 Results

5.6.2.1 Moments of mode shapes

The univariate, second-order hybrid PDD method was employed to calculate the second-moment statistics of each nodal pressure component of an eigenvector describing the associated mode shape of the air inside the cabin. All input random variables were transformed into uniform random variables, permitting the use of Legendre orthonormal polynomials as basis functions. The second-moment statistics were calculated from Equations (5.43) and (5.29), where the hybrid model parameter was estimated from Equation (5.31). Based on these statistics, the $\mathcal{L}_2$-norms (square root of sum of squares) of the mean and variance of a nodal pressure were calculated. Figures 5.7(a) and (b) present contour plots of the $\mathcal{L}_2$-norms of the mean and variances, respectively, of an arbitrarily selected 35th mode shape, calculated using hybrid PDD

approximation. Similar results can be generated for other mode shapes if desired.

5.6.2.2 Sound pressure level: probabilistic characteristics

The sound pressure level in decibels (dB) is calculated in the vicinity of the driver's ears as $\text{SPL} = 20\log_{10}\left[p/\left(p_{ref}\sqrt{2}\right)\right]$, where p is the pressure in Pa obtained in mode-based steady-dynamic analysis, and $p_{ref} = 2 \times 10^{-5}$ Pa is the *zero* or reference sound pressure, which is considered the threshold of human hearing.

Figure 5.8 shows various percentiles of sound pressure level in the vicinity of driver's ear calculated from the univariate, second-order hybrid PDD approximation. The percentiles were calculated from 5000 embedded MCS of the hybrid PDD approximation at 200 evenly spaced points in the excitation frequency range of 35 Hz to 120 Hz. Figure 5.9 presents the probability density function of the maximum sound pressure level in the excitation frequency range of 35 Hz to 120 Hz, as calculated from 5000 embedded MCS of the hybrid PDD approximation. These results provide vital information pertaining to the acoustic performance of the vehicle operating under several random input parameters. A designer can utilize these valuable results for optimizing the vehicle design to achieve a desired acoustic performance.

5.7 Conclusion

A univariate hybrid PDD method was developed for uncertainty quantification of high-dimensional complex systems. The method is built from a linear combination of an additive and a multiplicative PDD approximation, both obtained from lower-dimensional ANOVA component functions of a general, square-integrable multivariate

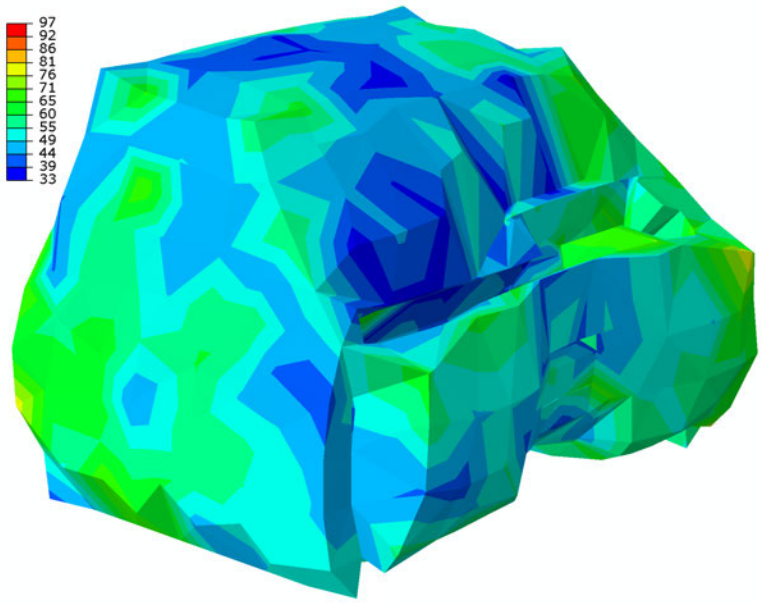

(a)

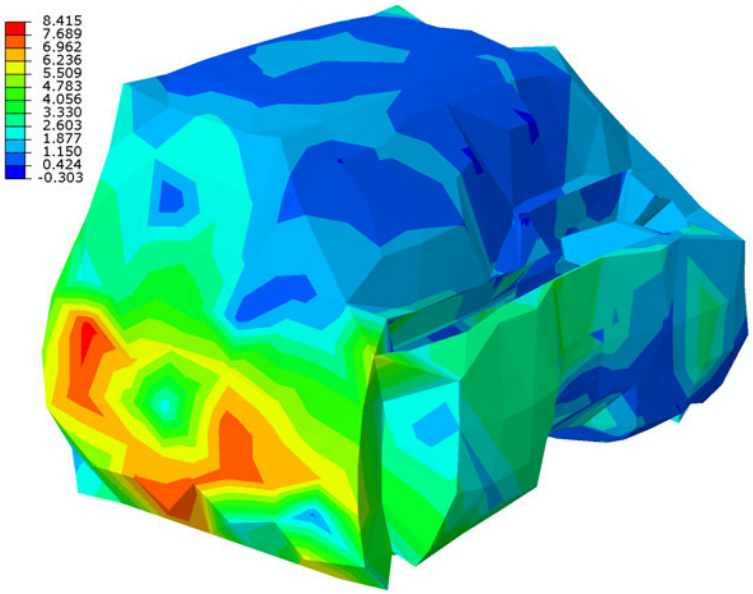

(b)

Figure 5.7: Contour plots of the $\mathcal{L}_2$-norms of 35th mode shape of air inside the cabin of a pickup truck by the hybrid PDD approximation: (a) mean, (b) variance

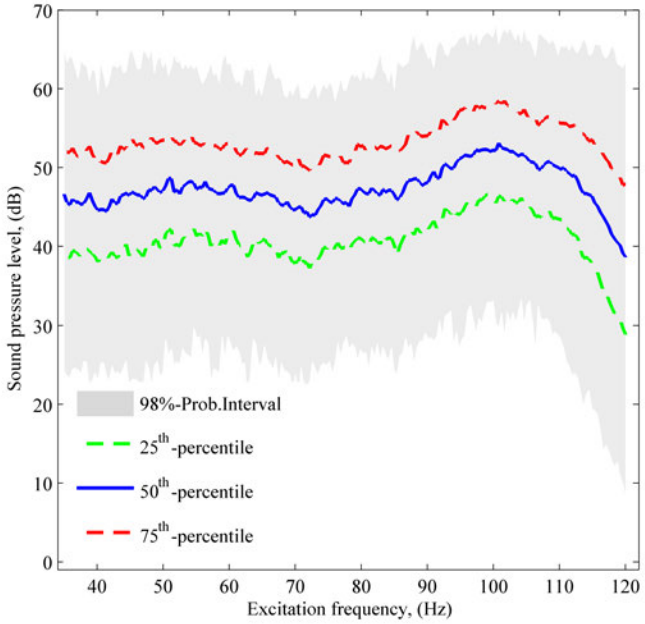

Figure 5.8: Percentiles of sound pressure levels in the vicinity of the driver's ear in a pickup truck by the hybrid PDD approximation

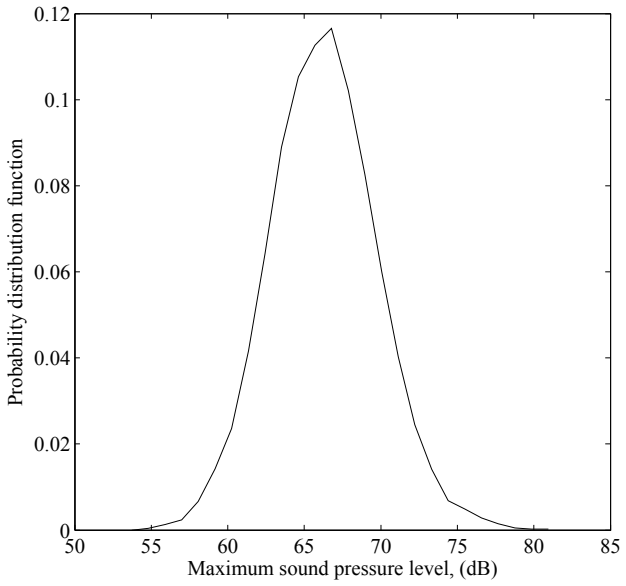

Figure 5.9: Probability density function of the maximum sound pressure level in excitation frequency range of 35 Hz to 120 Hz, estimated by the hybrid PDD approximation

function. When a stochastic response is not endowed with a specific dimensional hierarchy, the hybrid PDD approximation, optimally blending the additive PDD and multiplicative PDD approximations, is the best choice. A theorem and a corollary proven herein give analytical expressions for the model parameters that form the linear combinations of additive PDD and multiplicative PDD approximations, resulting in the hybrid PDD method. Using properties of orthonormal polynomials, explicit formulae were derived for calculating the response statistics by the univariate hybrid PDD approximation.

The new hybrid PDD method along with univariate additive PDD and multiplicative PDD approximations were employed to calculate the second-moment properties and tail probability distribution in two numerical problems, where the output functions are either simple mathematical functions or eigenvalues of a simple linear oscillator. For a function with a mixed additive and multiplicative structure, the univariate hybrid PDD approximation commits remarkably lower errors in calculating the variance compared with both univariate additive and multiplicative PDD approximations. The univariate hybrid PDD approximation is also more accurate than either the univariate additive or multiplicative PDD methods, and is more efficient than the bivariate additive PDD method in determining the tail probabilistic characteristics of eigenvalues of the dynamic system examined. Finally, a successful evaluation of random eigensolutions of a pickup truck, subjected to 53 input random variables, involving coupled acoustic-structure analysis demonstrates the ability of the new method in solving large-scale practical engineering problems.

CHAPTER 6
ADAPTIVE-SPARSE POLYNOMIAL DIMENSIONAL DECOMPOSITION

6.1 Introduction

For practical applications, the PDD must be truncated with respect to S and m, defining the largest degree of interactions among input variables and the largest order of orthogonal polynomials retained in the concomitant approximations. These truncation parameters depend on the dimensional structure and nonlinearity of a stochastic response. The higher the values of S and m, the higher the accuracy, but also the computational cost that is endowed with an Sth- or mth-order polynomial computational complexity. However, the dimensional hierarchy or nonlinearity, in general, is not known *a priori*. Therefore, indiscriminately assigning the truncation parameters is not desirable, nor is it possible to do so when a stochastic solution is obtained via complex numerical algorithms. In which case, one must perform these truncations automatically by progressively drawing in higher-variate or higher-order contributions as appropriate. Furthermore, all S-variate components functions of PDD may not contribute equally or even appreciably to be considered in the resulting approximation. Hence, a sparse approximation, expelling component functions with negligible contributions, should be considered as well. Indeed, addressing some of these concerns have led to adaptive versions of the cut-high-dimensional model representation (cut-HDMR) [133] and the anchored decomposition [134], employed in conjunction with the sparse-grid collocation methods, for solving stochastic problems

in fluid dynamics. It is important to clarify that the cut-HDMR and anchored decompositions are the same as the RDD [119, 135, 136], which was initially presented as "dimension-reduction" [85] or "decomposition" [86] methods by Xu and Rahman for statistical moment and reliability analyses, respectively. Therefore, both adaptive methods essentially employ RDD for multivariate function approximations, where the mean values of random input are treated as the reference or anchor point − a premise originally proposed by Xu and Rahman [86]. The developments of these adaptive methods were motivated by the fact that an RDD approximation requires only function evaluations, as opposed to high-dimensional integrals required for an ADD approximation. However, recent error analysis [119] reveals the sub-optimality of RDD approximations, meaning that an RDD approximation, regardless of how the reference point is chosen, cannot be better than an ADD approximation for identical degrees of interaction. The analysis also finds ADD approximations to be exceedingly more precise than RDD approximations at higher-variate truncations. In addition, the criteria implemented in existing adaptive methods are predicated on retaining higher-variate component functions by examining the second-moment properties of only univariate component functions, where the largest degree of interaction and polynomial order in the approximation are still left to the user's discretion, instead of being determined automatically based on the problem being solved. Therefore, more intelligently derived adaptive-sparse approximations and decompositions rooted in ADD or PDD should be explored by developing relevant criteria and acceptable error thresholds. These enhancements, some of which are indispensable, should be pursued

without sustaining significant additional cost.

This chapter presents two new adaptive-sparse versions of the PDD method for solving high-dimensional stochastic problems commonly encountered in computational science and engineering. The methods are based on (1) variance-based global sensitivity analysis for defining pruning criteria for retaining PDD component functions; (2) a unified computational algorithm for retaining PDD component functions and determining the largest orders of their orthogonal polynomial expansions; (3) two distinct ranking schemes for grading PDD component functions; and (4) a full- or sparse-grid dimension-reduction integration and quasi MCS for estimating the expansion coefficients. Section 6.2 briefly describes the existing dimensional decompositions, including PDD and its S-variate, mth-order approximation, to be contrasted with the proposed methods. Two adaptive-sparse PDD methods are formally presented in Section 6.3, along with a computational algorithm and a flowchart for numerical implementation of the method. Two different approaches for calculating the PDD coefficients, one emanating from dimension-reduction integration and the other employing quasi MCS, are explained in Section 6.4. Section 6.5 presents three numerical examples for probing the accuracy, efficiency, and convergence properties of the proposed methods, including a comparison with the existing PDD methods. Section 6.6 reports a large-scale stochastic dynamics problem solved using a proposed adaptive-sparse method. Finally, conclusions are drawn in Section 6.7.

6.2 Truncated Dimensional Decompositions

The three dimensional decompositions - ADD (Section 4.2), RDD (Section 2.3.3.1), and PDD (Section 2.3.3.2) - are grounded on a fundamental conjecture known to be true in many real-world applications: given a high-dimensional function y, its $|u|$-variate component functions decay rapidly with respect to $|u|$, leading to accurate lower-variate approximations of y. Indeed, given the integers $0 \leq S < N$, $1 \leq m < \infty$ for all $1 \leq |u| \leq S$, the truncated dimensional decompositions

$$\tilde{y}_S(\mathbf{X}) = \sum_{\substack{u \subseteq \{1,\cdots,N\} \\ 0 \leq |u| \leq S}} y_u(\mathbf{X}_u), \tag{6.1}$$

$$\hat{y}_S(\mathbf{X};\mathbf{c}) = \sum_{\substack{u \subseteq \{1,\cdots,N\} \\ 0 \leq |u| \leq S}} w_u(\mathbf{X}_u;\mathbf{c}), \tag{6.2}$$

and

$$\tilde{y}_{S,m}(\mathbf{X}) = y_\emptyset + \sum_{\substack{\emptyset \neq u \subseteq \{1,\cdots,N\} \\ 1 \leq |u| \leq S}} \sum_{\substack{\mathbf{j}_{|u|} \in \mathbb{N}_0^{|u|}, \left\|\mathbf{j}_{|u|}\right\|_\infty \leq m \\ j_1,\cdots,j_{|u|} \neq 0}} C_{u\mathbf{j}_{|u|}} \psi_{u\mathbf{j}_{|u|}}(\mathbf{X}_u), \tag{6.3}$$

respectively, describe S-variate ADD, RDD, and PDD, approximations, which for $S > 0$ include interactive effects of at most S input variables $X_{i_1}, \cdots, X_{i_S}$, $1 \leq i_1 < \cdots < i_S \leq N$, on y. It is elementary to show that when $S \to N$ and/or $m \to \infty$, $\tilde{y}_S$, $\hat{y}_S$, and $\tilde{y}_{S,m}$ converge to y in the mean-square sense, generating a hierarchical and convergent sequence of approximation of y from each decomposition.

6.2.1 ADD and RDD Errors

For ADD or RDD to be useful, what are the approximation errors committed by $\tilde{y}_S(\mathbf{X})$ and $\hat{y}_S(\mathbf{X};\mathbf{c})$ in Equations (6.1) and (6.2)? More importantly, for a given $0 \leq S < N$, which approximation between ADD and RDD is better? A recently

obtained theoretical result provides the answer.

Theorem 6.1: *Let* $\mathbf{c} = (c_1, \cdots, c_N) \in \mathbb{R}^N$ *be a random vector with the joint probability density function of the form* $f_{\mathbf{X}}(\mathbf{c}) = \prod_{j=1}^{j=N} f_j(c_j)$*, where* f_j *is the marginal probability density function of its* j*th coordinate of* $\mathbf{X} = (X_1, \cdots, X_N)$*. Define two second-moment errors*

$$e_{S,A} := \mathbb{E}\left[(y(\mathbf{X}) - \tilde{y}_S(\mathbf{X}))^2\right] := \int_{\mathbb{R}^N} \left[y(\mathbf{x}) - \tilde{y}_S(\mathbf{x})\right]^2 f_{\mathbf{X}}(\mathbf{x}) d\mathbf{x}, \tag{6.4}$$

and

$$e_{S,R}(\mathbf{c}) := \mathbb{E}\left[(y(\mathbf{X}) - \hat{y}_S(\mathbf{X};\mathbf{c}))^2\right] := \int_{\mathbb{R}^N} \left[y(\mathbf{x}) - \hat{y}_S(\mathbf{x};\mathbf{c})\right]^2 f_{\mathbf{X}}(\mathbf{x}) d\mathbf{x}, \tag{6.5}$$

committed by the S*-variate ADD and RDD approximations, respectively, of* $y(\mathbf{X})$*. Then the lower and upper bounds of the expected error* $\mathbb{E}[e_{S,R}] := \int_{\mathbb{R}^N} e_{S,R}(\mathbf{c}) f_{\mathbf{X}}(\mathbf{c}) d\mathbf{c}$ *from the* S*-variate RDD approximation, expressed in terms of the error* $e_{S,A}$ *from the* S*-variate ADD approximation, are*

$$2^{S+1} e_{S,A} \leq \mathbb{E}[e_{S,R}] \leq \left[1 + \sum_{k=0}^{S} \binom{N-S+k-1}{k}^2 \binom{N}{S-k}\right] e_{S,A}. \tag{6.6}$$

where $0 \leq S < N$*,* $S + 1 \leq N < \infty$*.*

Proof. See Theorem 4.12 and Corollary 4.13 presented by Rahman [119].

Remark 6.1: Theorem 6.1 reveals that the expected error from the univariate ($S = 1$) RDD approximation is at least four times larger than the error from the univariate ADD approximation. In contrast, the expected error from the bivariate ($S = 2$) RDD approximation can be eight or more times larger than the error from

the bivariate ADD approximation. Given an arbitrary truncation, an ADD approximation is superior to an RDD approximation. In addition, RDD approximations may perpetrate very large errors at upper bounds when there exist a large number of variables and appropriate conditions. Therefore, existing adaptive methods [133,134] anchored in RDD approximations should be used with a caveat. Furthermore, using PDD for adaptivity is advocated, but doing so engenders its own computational challenges, to be explained in the forthcoming sections.

6.2.2 Statistical moments of PDD

The S-variate, mth-order PDD approximation $\tilde{y}_{S,m}(\mathbf{X})$ in Equation (6.3) includes degrees of interaction among at most S input variables $X_{i_1}, \cdots, X_{i_S}$, $1 \leq i_1 \leq \cdots \leq i_S \leq N$. For instance, by selecting $S = 1$ and 2, the functions $\tilde{y}_{1,m}$ and $\tilde{y}_{2,m}$, respectively, provide univariate and bivariate mth-order PDD approximations, contain contributions from all input variables, and should not be viewed as first- and second-order approximations, nor do they limit the nonlinearity of y. Depending on how the component functions are constructed, arbitrarily high-order univariate and bivariate terms of y could be lurking inside $\tilde{y}_{1,m}$ and $\tilde{y}_{2,m}$. A recent work by Rahman reveals that the measure-consistent PDD leads to faster convergence of stochastic solutions, when compared with the classical ADD employing uniform probability measure [90].

Applying the expectation operator on $\tilde{y}_{S,m}(\mathbf{X})$ and $(\tilde{y}_{S,m}(\mathbf{X}) - y_\emptyset)^2$ and noting Propositions 4.1 and 4.2, the mean [135]

$$\mathbb{E}\left[\tilde{y}_{S,m}(\mathbf{X})\right] = y_\emptyset \tag{6.7}$$

of the S-variate, mth-order PDD approximation matches the exact mean $\mathbb{E}[y(\mathbf{X})]$, regardless of S or m, and the approximate variance [89]

$$\sigma_{S,m}^2 := \mathbb{E}\left[\left(\tilde{y}_{S,m}(\mathbf{X}) - \mathbb{E}\left[\tilde{y}_{S,m}(\mathbf{X})\right]\right)^2\right] = \sum_{\substack{\emptyset \neq u \subseteq \{1,\cdots,N\} \\ 1 \leq |u| \leq S}} \sum_{\substack{\mathbf{j}_{|u|} \in \mathbb{N}_0^{|u|}, \left\|\mathbf{j}_{|u|}\right\|_\infty \leq m \\ j_1,\cdots,j_{|u|} \neq 0}} C_{u\mathbf{j}_{|u|}}^2 \tag{6.8}$$

is calculated as the sum of squares of the expansion coefficients from the S-variate, mth-order PDD approximation of $y(\mathbf{X})$. Clearly, the approximate variance approaches the exact variance [89]

$$\sigma^2 := \mathbb{E}\left[\left(y(\mathbf{X}) - \mathbb{E}\left[y(\mathbf{X})\right]\right)^2\right] = \sum_{\emptyset \neq u \subseteq \{1,\cdots,N\}} \sum_{\substack{\mathbf{j}_{|u|} \in \mathbb{N}_0^{|u|} \\ j_1,\cdots,j_{|u|} \neq 0}} C_{u\mathbf{j}_{|u|}}^2 \tag{6.9}$$

of y when $S \to N$ and $m \to \infty$ for all $1 \leq |u| \leq S$. The mean-square convergence of $\tilde{y}_{S,m}$ is guaranteed as y, and its component functions are all members of the associated Hilbert spaces.

The S-variate, mth-order PDD approximation $\tilde{y}_{S,m}(\mathbf{X})$ in Equation (6.3) contains

$$\tilde{K}_{S,m} = 1 + \sum_{\substack{\emptyset \neq u \subseteq \{1,\cdots,N\} \\ 1 \leq |u| \leq S}} \sum_{\substack{\mathbf{j}_{|u|} \in \mathbb{N}_0^{|u|}, \left\|\mathbf{j}_{|u|}\right\|_\infty \leq m \\ j_1,\cdots,j_{|u|} \neq 0}} 1 = \sum_{k=0}^{S} \binom{N}{k} m^k \tag{6.10}$$

number of PDD coefficients and corresponding orthonormal polynomials. Therefore, the computational complexity of a truncated PDD is polynomial, as opposed to exponential, thereby alleviating the curse of dimensionality to some extent.

Remark 6.2: Constructing a PDD approximation by pre-selecting S and/or m, unless they are quite small, is computationally intensive, if not impossible, for high-dimensional uncertainty quantification. In other words, the existing PDD is neither

scalable nor adaptable, which is crucial for solving industrial-scale stochastic problems. A requisite theoretical basis and innovative numerical algorithms for overcoming these limitations are presented in Section 6.3.

Remark 6.3: The PDD approximation and its second-moment analysis require the expansion coefficients $C_{u\mathbf{j}_{|u|}}$, which, according to their definition in Equation (4.9), involve various N-dimensional integrals over $\mathbb{R}^N$. For large N, a full numerical integration employing an N-dimensional tensor product of a univariate quadrature formula is computationally prohibitive. This is one drawback of ADD and PDD, since their component functions entail calculating high-dimensional integrals. Therefore, novel dimension-reduction integration schemes or sampling techniques, to be described in Section 6.4, are needed to estimate the coefficients efficiently.

6.3 Proposed Adaptive-Sparse PDD Methods

6.3.1 Global sensitivity indices

The global sensitivity analysis quantifies how an output function of interest is influenced by individual or subsets of input variables, illuminating the dimensional structure lurking behind a complex response. Indeed, these sensitivity indices have been used to rank variables, fix unessential variables, and reduce dimensions of large-scale problems [137, 138]. These indices, developed in conjunction with PDD, are exploited for adaptive-sparse PDD approximations as follows.

The global sensitivity index of $y(\mathbf{X})$ for a subset $\mathbf{X}_u$, $\emptyset \neq u \subseteq \{1, \cdots, N\}$, of

input variables $\mathbf{X}$, denoted by G_u, is defined as the non-negative ratio [137, 138]

$$G_u := \frac{\mathbb{E}\left[y_u^2(\mathbf{X})\right]}{\sigma^2},\ 0 < \sigma^2 < \infty, \tag{6.11}$$

representing the fraction of the variance of $y(\mathbf{X})$ contributed by the ADD component function y_u. Since $\emptyset \neq u \subseteq \{1, \cdots, N\}$, there exist $2^N - 1$ such indices, adding up to $\sum_{u \subseteq \{1,\cdots,N\}} G_u = 1$. Applying the Fourier-polynomial approximation of $y_u(\mathbf{X})$, that is, Equation (4.8), and noting Propositions 4.1 and 4.2, the component variance

$$\mathbb{E}\left[y_u^2(\mathbf{X}_u)\right] = \sum_{\substack{\mathbf{j}_{|u|} \in \mathbb{N}_0^{|u|} \\ j_1, \cdots, j_{|u|} \neq 0}} C_{u\mathbf{j}_{|u|}}^2 \tag{6.12}$$

of y_u is the sum of squares of its PDD expansion coefficients. When the right side of Equation (6.12) is truncated at $\left\|\mathbf{j}_{|u|}\right\|_\infty = m_u$, where $m_u \in \mathbb{N}$, and then used to replace the numerator of Equation (6.11), the result is an m_uth-order approximation

$$\tilde{G}_{u,m_u} := \frac{1}{\sigma^2} \sum_{\substack{\mathbf{j}_{|u|} \in \mathbb{N}_0^{|u|}, \left\|\mathbf{j}_{|u|}\right\|_\infty \leq m_u \\ j_1, \cdots, j_{|u|} \neq 0}} C_{u\mathbf{j}_{|u|}}^2, \tag{6.13}$$

which approaches G_u as $m_u \to \infty$. Given $2 \leq m_u < \infty$, consider two approximate global sensitivity indices $\tilde{G}_{u,m_u-1}$ and $\tilde{G}_{u,m_u}$for $\mathbf{X}_u$ such that $\tilde{G}_{u,m_u-1} \neq 0$. Then the normalized index, defined by

$$\Delta\tilde{G}_{u,m_u} := \frac{\tilde{G}_{u,m_u} - \tilde{G}_{u,m_u-1}}{\tilde{G}_{u,m_u-1}},\ \tilde{G}_{u,m_u-1} \neq 0, \tag{6.14}$$

represents the relative change in the approximate global sensitivity index when the largest polynomial order increases from $m_u - 1$ to m_u. The sensitivity indices $\tilde{G}_{u,m_u}$ and $\Delta\tilde{G}_{u,m_u}$ provide an effective means to truncate the PDD in Equation (4.10) both adaptively and sparsely.

6.3.2 The fully adaptive-sparse PDD method

Let $\epsilon_1 \geq 0$ and $\epsilon_2 \geq 0$ denote two non-negative error tolerances that specify the minimum values of $\tilde{G}_{u,m_u}$ and $\Delta\tilde{G}_{u,m_u}$, respectively. Then a fully adaptive-sparse PDD approximation

$$\bar{y}(\mathbf{X}) := y_{\emptyset} + \sum_{\emptyset \neq u \subseteq \{1,\cdots,N\}} \sum_{m_u=1}^{\infty} \sum_{\substack{\left\|\mathbf{j}_{|u|}\right\|_{\infty} = m_u,\, j_1,\cdots,j_{|u|} \neq 0 \\ \tilde{G}_{u,m_u} > \epsilon_1, \Delta\tilde{G}_{u,m_u} > \epsilon_2}} C_{u\mathbf{j}_{|u|}} \psi_{u\mathbf{j}_{|u|}}(\mathbf{X}_u) \tag{6.15}$$

of $y(\mathbf{X})$ is formed by the subset of PDD component functions, satisfying two inclusion criteria: (1) $\tilde{G}_{u,m_u} > \epsilon_1$, and (2) $\Delta\tilde{G}_{u,m_u} > \epsilon_2$ for all $1 \leq |u| \leq N$ and $1 \leq m_u < \infty$. The first criterion requires the contribution of an m_u-th order polynomial approximation of $y_u(\mathbf{X})$ towards the variance of $y(\mathbf{X})$ to exceed ϵ_1 in order to be accommodated within the resultant truncation. The second criterion identifies the augmentation in the variance contribution from $y_u(\mathbf{X})$ evoked by a single increment in the polynomial order m_u and determines if it surpasses ϵ_2. In other words, these two criteria ascertain which interactive effects between two input random variables are retained and dictate the largest order of polynomials in a component function, formulating a fully adaptive-sparse PDD approximation.

When compared with the PDD in Equation (4.10), the adaptive-sparse PDD approximation in Equation (6.15) filters out the relatively insignificant component functions with a scant compromise on the accuracy of the resulting approximation. Furthermore, there is no need to pre-select the truncation parameters of the existing PDD approximation. The level of accuracy achieved by the fully adaptive-sparse PDD is meticulously controlled through the tolerances ϵ_1 and ϵ_2. The lower the tolerance

values, the higher the accuracy of the approximation. Proposition 6.3 shows that the mean-squared error in the fully adaptive-sparse PDD approximation disappears when the tolerances vanish.

Proposition 6.3: *If* $\epsilon_1 \to 0$ *and* $\epsilon_2 \to 0$*, then* $\bar{y}(\mathbf{X}) \to y(\mathbf{X})$ *in the mean-square sense.*

Proof. From Equation (6.15),

$$\begin{aligned}\lim_{\epsilon_1\to 0,\epsilon_2\to 0}\bar{y}(\mathbf{X}) &= y_{\emptyset} + \sum_{\emptyset\neq u\subseteq\{1,\cdots,N\}}\sum_{m_u=1}^{\infty}\sum_{\substack{\|\mathbf{j}_{|u|}\|_\infty=m_u\\ j_1,\cdots,j_{|u|}\neq 0}} C_{u\mathbf{j}_{|u|}}\psi_{u\mathbf{j}_{|u|}}(\mathbf{X}_u)\\ &= y_{\emptyset} + \sum_{\emptyset\neq u\subseteq\{1,\cdots,N\}}\sum_{\substack{\mathbf{j}_{|u|}\in\mathbb{N}_0^{|u|}\\ j_1,\cdots,j_{|u|}\neq 0}} C_{u\mathbf{j}_{|u|}}\psi_{u\mathbf{j}_{|u|}}(\mathbf{X}_u)\\ &= y(\mathbf{X}),\end{aligned} \tag{6.16}$$

where the last line follows from Equation (4.10). □

6.3.3 A partially adaptive-sparse PDD method

Based on the past experience, an S-variate PDD approximation, where $S \ll N$, is adequate, when solving real-world engineering problems, with the computational cost varying polynomially (S-order) with respect to the number of variables [87, 90]. As an example, consider the selection of $S = 2$ for solving a stochastic problem in 100 dimensions by a bivariate PDD approximation, comprising $100 \times 99/2 = 4950$ bivariate component functions. If all such component functions are included, then the computational effort for even a full bivariate PDD approximation may exceed the computational budget allocated to solving this problem. But many of these component functions contribute little to the probabilistic characteristics sought and can be safely ignored. Similar conditions may prevail for higher-variate component functions.

Henceforth, define an S-variate, partially adaptive-sparse PDD approximation

$$\bar{y}_S(\mathbf{X}) := y_\emptyset + \sum_{\substack{\emptyset \neq u \subseteq \{1,\cdots,N\} \\ 1 \leq |u| \leq S}} \sum_{m_u=1}^{\infty} \sum_{\substack{\left\|\mathbf{j}_{|u|}\right\|_\infty = m_u,\, j_1,\cdots,j_{|u|} \neq 0 \\ \tilde{G}_{u,m_u} > \epsilon_1, \Delta\tilde{G}_{u,m_u} > \epsilon_2}} C_{u\mathbf{j}_{|u|}} \psi_{u\mathbf{j}_{|u|}}(\mathbf{X}_u) \tag{6.17}$$

of $y(\mathbf{X})$, which is attained by subsuming at most S-variate component functions, but fulfilling two relaxed inclusion criteria: (1) $\tilde{G}_{u,m_u} > \epsilon_1$ for $1 \leq |u| \leq S \leq N$, and (2) $\Delta\tilde{G}_{u,m_u} > \epsilon_2$ for $1 \leq |u| \leq S \leq N$. Again, the same two criteria are used for the degree of interaction and the order of orthogonal polynomials, but the truncations are restricted to at most S-variate component functions of y.

An S-variate, partially adaptive-sparse PDD approximation behaves differently from the S-variate, mth-order PDD approximation. While the latter approximation includes a sum containing at most S-variate component functions, the former approximation may or may not include all such component functions, depending on the tolerance ϵ_1. For $\epsilon_1 > 0$, an S-variate, partially adaptive-sparse PDD will again trim the component functions with meager contributions. However, unlike $\bar{y}$ converging to y, $\bar{y}_S$ converges to the S-variate, mth-order PDD approximation $\tilde{y}_{S,m}$ (see Proposition 6.4), when $\epsilon_1 \to 0$, $\epsilon_2 \to 0$, $m \to \infty$, and $S < N$. If $S = N$, then both partially and fully adaptive-sparse PDD approximations coincide for identical tolerances.

Proposition 6.4: *If $\epsilon_1 \to 0$ and $\epsilon_2 \to 0$, then $\bar{y}_S(\mathbf{X}) \to \tilde{y}_{S,m}(\mathbf{X})$ as $m \to \infty$ in the mean-square sense.*

Proof. From Equation (6.17),

$$\begin{aligned}
\lim_{\epsilon_1\to 0,\epsilon_2\to 0}\bar{y}_S(\mathbf{X}) &= y_\emptyset + \sum_{\substack{\emptyset\neq u\subseteq\{1,\cdots,N\}\\ 1\leq|u|\leq S}}\sum_{m_u=1}^{\infty}\sum_{\substack{\left\|\mathbf{j}_{|u|}\right\|_\infty=m_u\\ j_1,\cdots,j_{|u|}\neq 0}} C_{u\mathbf{j}_{|u|}}\psi_{u\mathbf{j}_{|u|}}(\mathbf{X}_u)\\
&= y_\emptyset + \sum_{\substack{\emptyset\neq u\subseteq\{1,\cdots,N\}\\ 1\leq|u|\leq S}}\sum_{\substack{\mathbf{j}_{|u|}\in\mathbb{N}_0^{|u|}\\ j_1,\cdots,j_{|u|}\neq 0}} C_{u\mathbf{j}_{|u|}}\psi_{u\mathbf{j}_{|u|}}(\mathbf{X}_u)\\
&= \lim_{m\to\infty}\left[y_\emptyset + \sum_{\substack{\emptyset\neq u\subseteq\{1,\cdots,N\}\\ 1\leq|u|\leq S}}\sum_{\substack{\mathbf{j}_{|u|}\in\mathbb{N}_0^{|u|},\left\|\mathbf{j}_{|u|}\right\|_\infty\leq m\\ j_1,\cdots,j_{|u|}\neq 0}} C_{u\mathbf{j}_{|u|}}\psi_{u\mathbf{j}_{|u|}}(\mathbf{X}_u)\right]\\
&= \lim_{m\to\infty}\tilde{y}_{S,m}(\mathbf{X}),
\end{aligned} \tag{6.18}$$

where the last line follows from Equation (6.3). □

6.3.4 Stochastic Solutions

6.3.4.1 Second-moment properties

Applying the expectation operator on $\bar{y}(\mathbf{X})$ and $\bar{y}_S(\mathbf{X})$ and recognizing Proposition 4.1, the means

$$\mathbb{E}\left[\bar{y}(\mathbf{X})\right] = \mathbb{E}\left[\bar{y}_S(\mathbf{X})\right] = y_\emptyset \tag{6.19}$$

of fully and partially adaptive-sparse PDD approximations both also agree with the exact mean $\mathbb{E}\left[y(\mathbf{X})\right] = y_\emptyset$ for any ϵ_1, ϵ_2, and S. However, the respective variances, obtained by applying the expectation operator on $(\bar{y}(\mathbf{X})-y_\emptyset)^2$ and $(\bar{y}_S(\mathbf{X})-y_\emptyset)^2$ and noting Propositions 4.1 and 4.2, vary according to

$$\bar{\sigma}^2 := \mathbb{E}\left[\left(\bar{y}(\mathbf{X}) - \mathbb{E}\left[\bar{y}(\mathbf{X})\right]\right)^2\right] = \sum_{\emptyset\neq u\subseteq\{1,\cdots,N\}}\sum_{m_u=1}^{\infty}\sum_{\substack{\left\|\mathbf{j}_{|u|}\right\|_\infty=m_u,\, j_1,\cdots,j_{|u|}\neq 0\\ \tilde{G}_{u,m_u}>\epsilon_1,\Delta\tilde{G}_{u,m_u}>\epsilon_2}} C^2_{u\mathbf{j}_{|u|}} \tag{6.20}$$

and

$$\bar{\sigma}_S^2 := \mathbb{E}\left[\left(\bar{y}_S(\mathbf{X}) - \mathbb{E}\left[\bar{y}_S(\mathbf{X})\right]\right)^2\right] = \sum_{\substack{\emptyset \neq u \subseteq \{1,\cdots,N\} \\ 1 \leq |u| \leq S}} \sum_{m_u=1}^{\infty} \sum_{\substack{\left\|\mathbf{j}_{|u|}\right\|_\infty = m_u, j_1, \cdots, j_{|u|} \neq 0 \\ \tilde{G}_{u,m_u} > \epsilon_1, \Delta\tilde{G}_{u,m_u} > \epsilon_2}} C^2_{u\mathbf{j}_{|u|}}, \tag{6.21}$$

where the squares of the expansion coefficients are summed following the same two pruning criteria discussed in the preceding subsections. Equations (6.19)-(6.21) provide closed-form expressions of the approximate second-moment properties of any square-integrable function y in terms of the PDD expansion coefficients.

When $\epsilon_1 = \epsilon_2 = 0$, the right sides of Equation (6.20) and (6.9) coincide, whereas the right side of (6.21) approaches that of (6.8) for $m_u \to \infty$. As a consequence, the variance from the fully adaptive-sparse PDD approximation $\bar{y}(\mathbf{X})$ converges to the exact variance of $y(\mathbf{X})$ as $\epsilon_1 \to 0$ and $\epsilon_2 \to 0$. In contrast, the variance from the S-variate, partially adaptive-sparse PDD approximation $\bar{y}_S(\mathbf{X})$ does not follow suit, as it converges to the variance of the S-variate, mth-order PDD approximation $\tilde{y}_{S,m}(\mathbf{X})$ as $\epsilon_1 \to 0$ and $\epsilon_2 \to 0$, provided that $m \to \infty$. Therefore, the fully adaptive-sparse PDD approximation is more rigorous than a partially adaptive-sparse PDD approximation, but the latter can be more useful than the former when solving practical engineering problems and will be demonstrated in the Numerical Examples and Application sections.

6.3.4.2 Probability distribution

Although the PDD approximations are mean-square convergent, Equations (6.15) and (6.17) can also be used to estimate higher-order moments and probabil-

ity distributions, including rare-event probabilities, of sufficiently smooth stochastic responses. In this work, the probability distribution of $y(\mathbf{X})$ was approximated by performing Monte Carlo simulation of $\bar{y}(\mathbf{X})$ and/or $\bar{y}_S(\mathbf{X})$. This simulation of the PDD approximation should not be confused with *crude* Monte Carlo simulation. The crude Monte Carlo method, which commonly requires numerical calculations of y for input samples, can be expensive or even prohibitive, particularly when the sample size needs to be very large for estimating small failure probabilities. In contrast, the Monte Carlo simulation embedded in a PDD approximation requires evaluations of simple analytical functions. Therefore, an arbitrarily large sample size can be accommodated in the PDD approximation.

It is also possible to estimate the probability distribution of $y(\mathbf{X})$ from the knowledge of the cumulant generating function of a PDD approximation, provided that it exists, and then exploit the saddle point approximation for obtaining an exponential family of approximate distributions. Readers interested in this alternative approach are referred to the recent work on stochastic sensitivity analysis by Xuchun and Rahman [139].

6.3.5 Numerical Implementation

The application of fully and partially adaptive-sparse PDD approximations described by Equations (6.15) and (6.17) requires selecting PDD component functions $y_u(\mathbf{X}_u)$, $\emptyset \neq u \subseteq \{1, \cdots, N\}$ and assigning the largest orders of their orthogonal polynomial expansions $1 \leq m_u < \infty$ efficiently such that $\tilde{G}_{u,m_u} > \epsilon_1$ and $\Delta\tilde{G}_{u,m_u} > \epsilon_2$.

This section presents a unified computational algorithm and an associated flowchart developed to accomplish numerical implementation of the two proposed methods.

6.3.5.1 A unified algorithm

The iterative process for constructing an adaptive-sparse PDD approximation, whether full or partial, comprises two main stages: (1) continue incrementing the polynomial order m_u for a chosen component function $y_u(\mathbf{X}_u)$ unless the criterion $\Delta\tilde{G}_{u,m_u} > \epsilon_2$ fails; and (2) continue selecting the component functions $y_u(\mathbf{X}_u)$, $\emptyset \neq u \subseteq \{1, \cdots, N\}$, unless the criterion $\tilde{G}_{u,m_u} > \epsilon_1$ fails. These two stages are first executed over all univariate PDD component functions $y_u(\mathbf{X}_u)$, $|u| = 1$, before progressing to all bivariate component functions $y_u(\mathbf{X}_u)$, $|u| = 2$, and so on, until $|u| = N$ for the fully adaptive-sparse PDD approximation or until $|u| = S$ for a partially adaptive-sparse PDD approximation, where S is specified by the user. The implementation details of the iterative process are described in Algorithm 6.1 and through the flowchart in Figure 6.1.

The first stage of the algorithm presented is predicated on accurate calculations of the sensitivity indices $\tilde{G}_{u,m_u}$ and $\Delta\tilde{G}_{u,m_u}$, which require the variance σ^2 of $y(\mathbf{X})$ as noted by Equations (6.13) and (6.14). Since there exist an infinite number of expansion coefficients emanating from all PDD component functions, calculating the variance exactly from Equation (6.9) is impossible. To overcome this quandary, it is proposed to estimate the variance by utilizing all PDD expansion coefficients available at a juncture of the iterative process. For instance, let $v \in V$ be an element of the

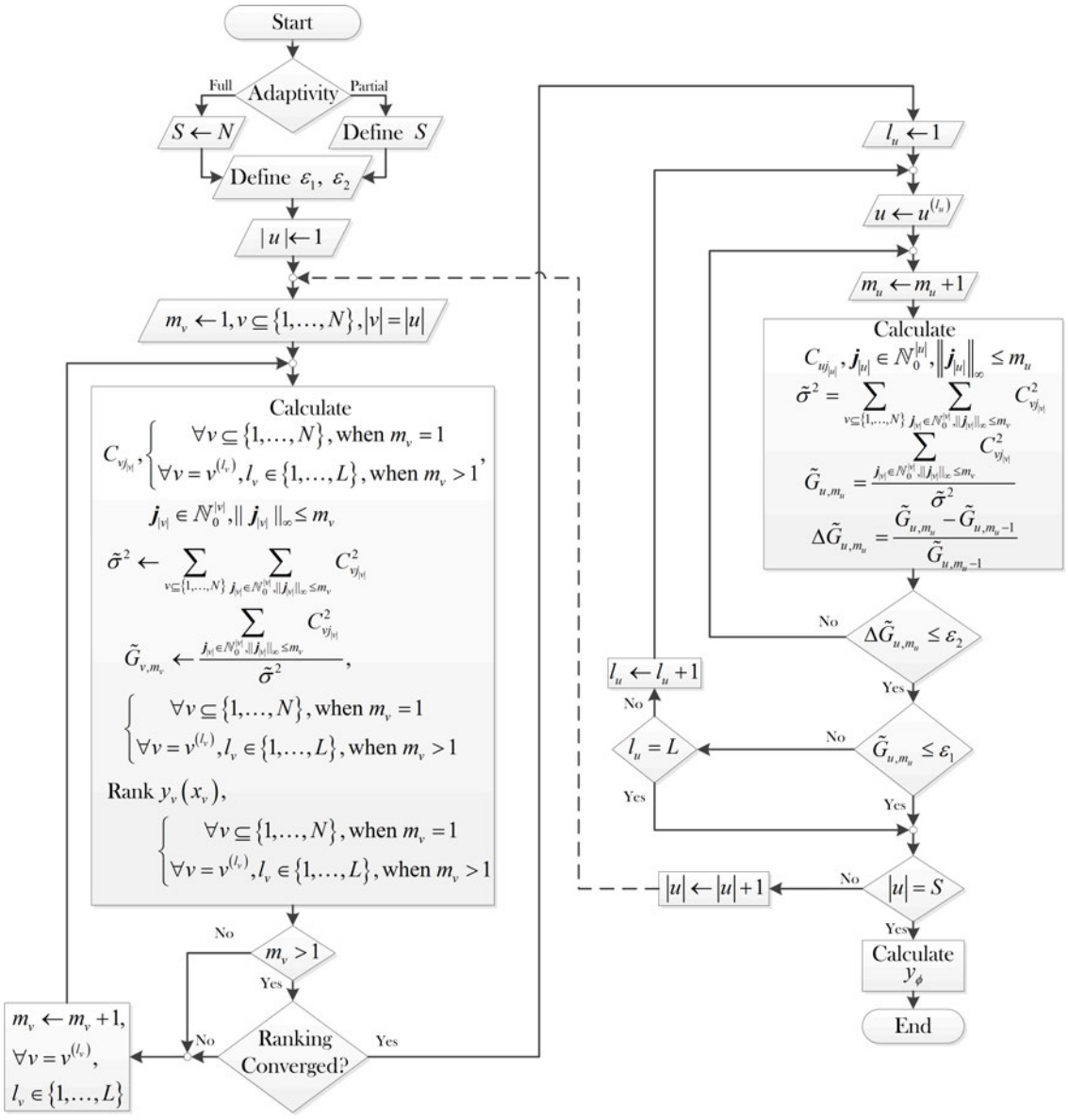

Figure 6.1: A flowchart for constructing an adaptive-sparse polynomial dimensional decomposition.

index set $V \subseteq \{1, \cdots, N\}$, which comprises the subsets of $\{1, \cdots, N\}$ selected so far at a given step of the iterative process. Then the approximate variance

$$\tilde{\sigma}_V^2 = \sum_{\emptyset \neq v \in V \subseteq \{1,\cdots,N\}} \sum_{\substack{\mathbf{j}_{|v|} \in \mathbb{N}_0^{|v|}, \left\|\mathbf{j}_{|v|}\right\|_\infty \leq m_v \\ j_1, \cdots, j_{|v|} \neq 0}} C_{v\mathbf{j}_{|v|}}^2 \tag{6.22}$$

replacing the exact variance σ^2 in Equations (6.13) and (6.14) facilitates an effective iterative scheme for estimating $\tilde{G}_{u,m_u}$ and $\Delta\tilde{G}_{u,m_u}$ as well. Equation (6.22) was implemented in the proposed algorithm, as explained in Algorithm 6.1 and Figure 6.1.

The second stage of the algorithm requires an efficient procedure for selecting appropriate PDD component functions that are retained in an adaptive-sparse PDD approximation. For a given $1 \leq |u| \leq N$, let $y_u(\mathbf{X}_u)$, $\emptyset \neq u \subseteq \{1, \cdots, N\}$ denote all $|u|$-variate non-constant PDD component functions of y. It is elementary to count the number of these component functions to be $L_{|u|} = \binom{N}{|u|}$. Depending on the tolerance criteria specified, some or none of these component functions may contribute towards the resultant PDD approximation. Since the component functions are not necessarily hierarchically arranged, determining their relative significance to PDD approximation is not straightforward. Therefore, additional efforts to rank the component functions are needed, keeping in mind that the same efforts may be recycled for the PDD approximation. For this purpose, two distinct ranking schemes are proposed: (1) a full ranking scheme, and (2) a reduced ranking scheme, both exploiting the global sensitivity index G_u as a measure of the significance of $y_u(\mathbf{X}_u)$. However, since G_u is estimated by its m_uth-order polynomial approximation $\tilde{G}_{u,m_u}$, any ranking system

Algorithm 6.1 Numerical implementation of fully and partially adaptive-sparse PDD approximations

Define S ▷ [$S \leftarrow N$ for Fully adaptive]
Define $\epsilon_1, \epsilon_2, \epsilon_3$
for $|u| \leftarrow 1$ to S **do**
$|v| \leftarrow |u|, v \subseteq \{1, \cdots, N\}$
$m_v \leftarrow 0$
  repeat ▷ [continue incrementing the polynomial order m_v unless the ranking of component functions $y_v(\boldsymbol{x}_v)$ converges]
  $m_v \leftarrow m_v + 1$ ▷ [start with the polynomial order $m_v = 1$]
  calculate $C_{vj_v}, \mathbf{j}_{|v|} \in \mathbb{N}_0^{|v|}, \left\|\mathbf{j}_{|v|}\right\|_\infty \leq m_v$ ▷ [from Equation (4.9)]
  calculate $\tilde{\sigma}_V^2 \leftarrow \sum_{\emptyset \neq v \in V \subseteq \{1,\cdots,N\}} \sum_{\mathbf{j}_{|v|} \in \mathbb{N}_0^{|v|}, \left\|\mathbf{j}_{|v|}\right\|_\infty \leq m_v} C^2_{v\mathbf{j}_{|v|}}$ ▷ [from Equation (6.22)]
  calculate $\tilde{G}_{v,m_v} \leftarrow \left(\sum_{\mathbf{j}_{|v|} \in \mathbb{N}_0^{|v|}, \left\|\mathbf{j}_{|v|}\right\|_\infty \leq m_v} C^2_{v\mathbf{j}_{|v|}}\right) / \tilde{\sigma}_V^2$ ▷ [from Equation (6.13)]
  rank $y_v(\boldsymbol{x}_v)$: $y_{v^{(1)}}(\boldsymbol{x}_{v^{(1)}})$ to $y_{v^{(N)}}(\boldsymbol{x}_{v^{(N)}})$ ▷ [from Algorithm 6.2]
  Get L ▷ [from Algorithm 6.2]
  $N_{m_u} \leftarrow 0$
    for $i \leftarrow 1$ to L **do** ▷ [comparing rankings from m_u with those from $(m_u - 1)$ to check for convergence]
    $R_{m_u}(i) \leftarrow i$
      if $R_{m_u-1}(i) = R_{m_u}(i)$ **then** $N_{m_u} \leftarrow N_{m_u} + 1$
      end if
    end for
  until $N_m / L \geq \epsilon_3$ ▷ [ranking converge]
  for $l_u \leftarrow 1$ to L **do** ▷ [start the adaptivity algorithm with the highest ranking $|u|-$variate component function]
  $u \leftarrow u^{(l_u)}$
    repeat ▷ [continue incrementing the polynomial order m_u unless the adaptivity condition $\triangle\tilde{G}_{u,m_u} > \epsilon_2$ fails]
    $m_u \leftarrow m_u + 1$
    calculate $C_{uj_u}, \mathbf{j}_{|u|} \in \mathbb{N}_0^{|u|}, \left\|\mathbf{j}_{|u|}\right\|_\infty \leq m_u$ ▷ [from Equation (4.9)]
    calculate $\tilde{\sigma}_V^2 \leftarrow \sum_{\emptyset \neq v \in V \subseteq \{1,\cdots,N\}} \sum_{\mathbf{j}_{|v|} \in \mathbb{N}_0^{|v|}, \left\|\mathbf{j}_{|v|}\right\|_\infty \leq m_v} C^2_{v\mathbf{j}_{|v|}}$ ▷ [from Equation (6.22)]
    calculate $\tilde{G}_{u,m_u} \leftarrow \left(\sum_{\mathbf{j}_{|v|} \in \mathbb{N}_0^{|v|}, \left\|\mathbf{j}_{|v|}\right\|_\infty \leq m_v} C^2_{v\mathbf{j}_{|v|}}\right) / \tilde{\sigma}_V^2$ ▷ [from Equation (6.13)]
    calculate $\triangle\tilde{G}_{u,m_u} \leftarrow \left(\tilde{G}_{u,m_u} - \tilde{G}_{u,m_u-1}\right) / \tilde{G}_{u,m_u-1}$ ▷ [from Equation (6.14)]
    until $\triangle\tilde{G}_{u,m_u} \leq \epsilon_2$
    if $\tilde{G}_{u,m_u} \leq \epsilon_1$ **then** exit
    end if ▷ [exit the adaptivity algorithm]
  end for
end for
calculate $y_\emptyset$ ▷ [from Equation (4.2)]

based on $\tilde{G}_{u,m_u}$, where m_u is finite, may be in a flux and should hence be carefully interpreted. This implies that a ranking scheme resulting from $\tilde{G}_{u,m_u}$, whether full or reduced, must be iterated for increasing values of m_u until the ranking scheme converges according to a specified criterion. In the full ranking scheme, all $|u|$-variate component functions are re-ranked from scratch for each increment of m_u until a converged ranking scheme emerges. Consequently, the full ranking scheme affords any component function to contribute to the resultant PDD approximation, provided that the criterion $\tilde{G}_{u,m_u} > \epsilon_1$ is satisfied only at convergence. In contrast, a subset of $|u|$-variate component functions, determined from the previous ranking results and truncations set by the tolerance criterion, are re-ranked for each increment of m_u in the reduced ranking scheme until convergence is achieved. Therefore, for a component function from the reduced ranking scheme to contribute to the resultant PDD approximation, the criterion $\tilde{G}_{u,m_u} > \epsilon_1$ must be satisfied at all ranking iterations including the converged one. Therefore, the full ranking scheme is both meticulous and exhaustive, but it may rapidly become inefficient or impractical when applied to high-dimensional stochastic responses. The reduced ranking scheme, obtained less

Algorithm 6.2 Ranking of PDD component functions

sort $y_{v^{(l)}}(\boldsymbol{x}_{v^{(l)}})$: $l = 1, \ldots, L$; $l = 1$ for largest $\tilde{G}_{v,m_v}$ ▷ [$L = N$ for full ranking, or when $m_v = 1$]

Truncation for reduced ranking:

$l \leftarrow 1$

while $\tilde{G}_{v^{(l)},m_{v^{(l)}}} > \epsilon_1$ **do** ▷ [truncating the ranking when adaptivity condition $\tilde{G}_{v^{(l)},m_{v^{(l)}}} > \epsilon_1$ fails]

$L \leftarrow l$

$l \leftarrow l + 1$

end while

rigorously than the former, is highly efficient and is ideal for solving industrial-scale high-dimensional problems. A ranking system obtained at $m_u = m$, $2 \leq m < \infty$, for all $|u|$-variate component functions is considered to be converged if the ranking discrepancy ratio, defined as the ratio of the number of ranked positions changed when m_u increases from $m-1$ to m to the number of component functions ranked at $m_u = m-1$, does not exceed the ranking tolerance $0 \leq \epsilon_3 \leq 1$. The number of component functions ranked in the full ranking scheme is $L_{|u|}$, the total number of $|u|$-variate component functions, and is the same for any m_u or function y. In contrast, the number of component functions ranked in the reduced ranking scheme, which is equal to or less than $L_{|u|}$, depends on m_u, y, and ϵ_1. Both ranking schemes are described in Algorithm 6.2.

6.3.5.2 Computational effort

For uncertainty quantification, the computational effort is commonly determined by the total number of original function evaluations. Consequently, the efforts required by the proposed methods are proportional to the total numbers of the PDD expansion coefficients retained in the concomitant approximations and depend on the numerical techniques used to calculate the coefficients. The numerical evaluation of the expansion coefficients are discussed in Section 6.4.

The numbers of coefficients by the fully and partially adaptive-sparse PDD

methods are

$$\begin{aligned} \bar{K} &= 1 + \sum_{\emptyset \neq u \subseteq \{1,\cdots,N\}} \sum_{m_u=1}^{\infty} \sum_{\substack{\left\|\mathbf{j}_{|u|}\right\|_\infty = m_u,\, j_1,\cdots,j_{|u|} \neq 0 \\ \tilde{G}_{u,m_u} > \epsilon_1, \Delta\tilde{G}_{u,m_u} > \epsilon_2}} 1 \\ &= 1 + \sum_{\emptyset \neq u \subseteq \{1,\cdots,N\}} \sum_{m_u=1}^{\infty} \sum_{\tilde{G}_{u,m_u} > \epsilon_1, \Delta\tilde{G}_{u,m_u} > \epsilon_2} \left[m_u^{|u|} - (m_u - 1)^{|u|} \right] \end{aligned} \tag{6.23}$$

and

$$\begin{aligned} \bar{K}_S &= 1 + \sum_{\substack{\emptyset \neq u \subseteq \{1,\cdots,N\} \\ 1 \leq |u| \leq S}} \sum_{m_u=1}^{\infty} \sum_{\substack{\left\|\mathbf{j}_{|u|}\right\|_\infty = m_u,\, j_1,\cdots,j_{|u|} \neq 0 \\ \tilde{G}_{u,m_u} > \epsilon_1, \Delta\tilde{G}_{u,m_u} > \epsilon_2}} 1 \\ &= 1 + \sum_{\substack{\emptyset \neq u \subseteq \{1,\cdots,N\} \\ 1 \leq |u| \leq S}} \sum_{m_u=1}^{\infty} \sum_{\tilde{G}_{u,m_u} > \epsilon_1, \Delta\tilde{G}_{u,m_u} > \epsilon_2} \left[m_u^{|u|} - (m_u - 1)^{|u|} \right], \end{aligned} \tag{6.24}$$

respectively. It is elementary to show that $\bar{K}_S \leq \bar{K}$ when $S \leq N$ for identical tolerances, as expected, with equality when $S = N$. Therefore, a partially adaptive-sparse PDD method in general is more economical than the fully adaptive-sparse PDD method.

What can be inferred from the numbers of coefficients required by a partially adaptive-sparse PDD method and the existing truncated PDD method? The following two results, Proposition 6.5 and 6.6, provide some insights when the tolerances vanish and when the largest orders of polynomials are identical.

Proposition 6.5: *If* $\epsilon_1 \to 0$*, and* $\epsilon_2 \to 0$*, then* $\bar{K}_S \to \tilde{K}_{S,m}$ *as* $m \to \infty$*.*

Proof. From Equation (6.24),

$$\begin{aligned}
\lim_{\epsilon_1\to 0,\epsilon_2\to 0}\bar{K}_S &= 1+\sum_{\substack{\emptyset\neq u\subseteq\{1,\cdots,N\}\\ 1\leq|u|\leq S}}\sum_{m_u=1}^{\infty}\sum_{\substack{\left\|\mathbf{j}_{|u|}\right\|_\infty=m_u\\ j_1,\cdots,j_{|u|}\neq 0}}1\\
&= 1+\sum_{\substack{\emptyset\neq u\subseteq\{1,\cdots,N\}\\ 1\leq|u|\leq S}}\sum_{\substack{\mathbf{j}_{|u|}\in\mathbb{N}_0^{|u|}\\ j_1,\cdots,j_{|u|}\neq 0}}1\\
&= \lim_{m\to\infty}\left[1+\sum_{\substack{\emptyset\neq u\subseteq\{1,\cdots,N\}\\ 1\leq|u|\leq S}}\sum_{\substack{\mathbf{j}_{|u|}\in\mathbb{N}_0^{|u|},\left\|\mathbf{j}_{|u|}\right\|_\infty\leq m\\ j_1,\cdots,j_{|u|}\neq 0}}1\right]\\
&= \lim_{m\to\infty}\left[\sum_{k=0}^{S}\binom{N}{k}m^k\right]\\
&= \lim_{m\to\infty}\tilde{K}_{S,m},
\end{aligned}\tag{6.25}$$

where the last line follows from Equation (6.10). □

Proposition 6.6: *If*

$$m=\max_{\substack{\emptyset\neq u\subseteq\{1,\cdots,N\},1\leq|u|\leq S\\ \tilde{G}_{u,m_u}>\epsilon_1,\Delta\tilde{G}_{u,m_u}>\epsilon_2}}m_u<\infty\tag{6.26}$$

is the largest order of polynomial expansion for any component function $y_u(\mathbf{X}_u)$, $\emptyset\neq u\subseteq\{1,\cdots,N\}$, $1\leq|u|\leq S$, *such that* $\tilde{G}_{u,m_u}>\epsilon_1, \Delta\tilde{G}_{u,m_u}>\epsilon_2$, *then* $\bar{K}_S\leq\tilde{K}_{S,m}$.

Proof. From Equation (6.24),

$$\begin{aligned}
\bar{K}_S &= 1+\sum_{\substack{\emptyset\neq u\subseteq\{1,\cdots,N\}\\ 1\leq|u|\leq S}}\sum_{m_u=1}^{\infty}\sum_{\substack{\left\|\mathbf{j}_{|u|}\right\|_\infty=m_u,\,j_1,\cdots,j_{|u|}\neq 0\\ \tilde{G}_{u,m_u}>\epsilon_1,\Delta\tilde{G}_{u,m_u}>\epsilon_2}}1\\
&\leq 1+\sum_{\substack{\emptyset\neq u\subseteq\{1,\cdots,N\}\\ 1\leq|u|\leq S}}\sum_{\substack{\mathbf{j}_{|u|}\in\mathbb{N}_0^{|u|},\left\|\mathbf{j}_{|u|}\right\|_\infty\leq m\\ j_1,\cdots,j_{|u|}\neq 0}}1\\
&= \sum_{k=0}^{S}\binom{N}{k}m^k\\
&= \tilde{K}_{S,m},
\end{aligned}\tag{6.27}$$

where the last line follows from Equation (6.10). □

According to Proposition 6.6, the partially adaptive-sparse PDD approximation for non-trivial tolerances should be computationally more efficient than the truncated PDD approximation. This issue will be further explored in the Numerical Examples section.

6.4 Calculation of Expansion Coefficients

The determination of the expansion coefficients $y_\emptyset$ and $C_{u\mathbf{j}_{|u|}}$ in Equations (4.2) and (4.9) involves various N-dimensional integrals over $\mathbb{R}^N$. For large N, a full numerical integration employing an N-dimensional tensor product of a univariate quadrature formula is computationally prohibitive and is, therefore, ruled out. In this work, the expansion coefficients are estimated using the quasi MCS method (Section 5.3) and the Dimension-Reduction Integration (Section 3.4.1) in conjunction with the full-grid integration and with the sparse-grid integration. Following subsections describe employing the Dimension-Reduction Integration with the full-grid integration and the sparse-grid integration, followed by a comparison of computational effort required by the two techniques.

The dimension-reduction integration, developed by Xu and Rahman [85], entails approximating a high-dimensional integral of interest by a finite sum of lower-dimensional integrations. For calculating the expansion coefficients $y_\emptyset$ and $C_{u\mathbf{j}_{|u|}}$, this is accomplished by replacing the N-variate function y in Equations (4.2) and (4.9) with an R-variate RDD approximation at a chosen reference point, where $R \leq N$ [85, 86]. The result is a reduced integration scheme, requiring evaluations

of at most R-dimensional integrals.

Given a reference point $\mathbf{c} = (c_1, \cdots, c_N) \in \mathbb{R}^N$ and RDD component functions $w_\emptyset$ and $w_u(\mathbf{X}_u; \mathbf{c})$, let $\hat{y}_R(\mathbf{X}; \mathbf{c})$ denote an R-variate RDD approximation of $y(\mathbf{X})$. Replacing $y(\mathbf{x})$ with $\hat{y}_R(\mathbf{x}; \mathbf{c})$ in Equation (6.2), the coefficients $y_\emptyset$ and $C_{u\mathbf{j}_{|u|}}$ are estimated from [85]

$$y_\emptyset \cong \sum_{i=0}^{R} (-1)^i \binom{N-R+i-1}{i} \sum_{\substack{v \subseteq \{1,\cdots,N\} \\ |v|=R-i}} \int_{\mathbb{R}^{|v|}} y(\mathbf{x}_v, \mathbf{c}_{-v}) f_{\mathbf{X}_v}(\mathbf{x}_v) d\mathbf{x}_v \tag{6.28}$$

and

$$C_{u\mathbf{j}_{|u|}} \cong \sum_{i=0}^{R} (-1)^i \binom{N-R+i-1}{i} \sum_{\substack{v \subseteq \{1,\cdots,N\} \\ |v|=R-i, u \subseteq v}} \int_{\mathbb{R}^{|v|}} y(\mathbf{x}_v, \mathbf{c}_{-v}) \psi_{u\mathbf{j}_{|u|}}(\mathbf{x}_u) f_{\mathbf{X}_v}(\mathbf{x}_v) d\mathbf{x}_v \tag{6.29}$$

respectively, requiring evaluation of at most R-dimensional integrals. The reduced integration facilitates calculation of the coefficients approaching their exact values as $R \to N$, and is significantly more efficient than performing one N-dimensional integration, particularly when $R \ll N$. Hence, the computational effort is significantly decreased using the dimension-reduction integration. For instance, when $R = 1$ or 2, Equations (6.28) and (6.29) involve one-, or at most, two-dimensional integrations, respectively. Nonetheless, numerical integrations are still required for performing various $|v|$-dimensional integrals over $\mathbb{R}^{|v|}$, where $0 \leq |v| \leq R|$. When $R > 1$, the multivariate integrations can be conducted using full or sparse grids, as follows.

6.4.1 Full-grid integration

The full-grid dimension-reduction integration entails constructing a tensor product of underlying univariate quadrature rules. For a given $v \subseteq \{1, \cdots, N\}$, $1 < |v| \leq R$, let $v = \{i_1, \cdots i_{|v|}\}$, where $1 \leq i_1 < \cdots < i_{|v|} \leq N$. Denote by $\{x_{i_p}^{(1)}, \cdots, x_{i_p}^{(n_v)}\} \subset \mathbb{R}$ a set of integration points of x_{i_p} and by $\{w_{i_p}^{(1)}, \cdots, w_{i_p}^{(n_v)}\}$ the associated weights generated from a chosen univariate quadrature rule and a positive integer $n_v \in \mathbb{N}$. Denote by $P^{(n_v)} = \times_{p=1}^{p=|v|}\{x_{i_p}^{(1)}, \cdots, x_{i_p}^{(n_v)}\}$ a rectangular grid consisting of all integration points generated by the variables indexed by the elements of v. Then the coefficients using dimension-reduction numerical integration with a full-grid are approximated by

$$y_{\emptyset} \cong \sum_{i=0}^{R}(-1)^i \binom{N-R+i-1}{i} \sum_{\substack{v\subseteq\{1,\cdots,N\}\\|v|=R-i}} \sum_{\mathbf{k}_{|v|}\in P^{(n_v)}} w^{(\mathbf{k}_{|v|})} y(\mathbf{x}_v^{(\mathbf{k}_{|v|})}, \mathbf{c}_{-v}) \tag{6.30}$$

$$\begin{aligned} C_{u\mathbf{j}_{|u|}} \cong & \sum_{i=0}^{R}(-1)^i \binom{N-R+i-1}{i} \\ & \sum_{\substack{v\subseteq\{1,\cdots,N\}\\|v|=R-i, u\subseteq v}} \sum_{\mathbf{k}_{|v|}\in P^{(n_v)}} w^{(\mathbf{k}_{|v|})} y(\mathbf{x}_v^{(\mathbf{k}_{|v|})}, \mathbf{c}_{-v}) \psi_{u\mathbf{j}_{|u|}}(\mathbf{x}_u^{(\mathbf{k}_{|u|})}) \end{aligned} \tag{6.31}$$

where $\mathbf{x}_v^{(\mathbf{k}_{|v|})} = \{x_{i_1}^{(k_1)}, \cdots, x_{i_{|v|}}^{(k_{|v|})}\}$ and $w^{(\mathbf{k}_{|v|})} = \prod_{p=1}^{p=|v|} w_{i_p}^{(k_p)}$ is the product of integration weights generated by the variables indexed by the elements of v. For independent coordinates of $\mathbf{X}$, as assumed here, a univariate Gauss quadrature rule is commonly used, where the integration points and associated weights depend on the probability distribution of X_i. They are readily available, for example, as the Gauss-Hermite or Gauss-Legendre quadrature rule, when X_i follows Gaussian or uniform distribution [88]. For an arbitrary probability distribution of X_i, the Stieltjes procedure [88]

can be employed to generate the measure-consistent Gauss quadrature formulae [90]. An n_v-point Gauss quadrature rule exactly integrates a polynomial of total degree at most $2n_v - 1$.

The calculation of $y_\emptyset$ and $C_{u\mathbf{j}_{|u|}}$ from Equations (6.30) and (6.31) involves at most R-dimensional tensor products of an n_v-point univariate quadrature rule, requiring the following deterministic responses or function evaluations: $y(\mathbf{c})$, $y(\mathbf{x}_v^{(\mathbf{j}_{|v|})}, \mathbf{c}_{-v})$ for $i = 0, \cdots, R$, $v \subseteq \{1, \cdots, N\}$, $|v| = R - i$, and $\mathbf{j}_{|v|} \in P^{(n_v)}$. Accordingly, the total cost for estimating the PDD expansion coefficients entails

$$L_{FG} = \sum_{i=0}^{R} \sum_{\substack{v \subseteq \{1,\cdots,N\} \\ |v| = R-i}} n_v^{|v|} \tag{6.32}$$

function evaluations, encountering a computational complexity that is Rth-order polynomial − for instance, linear or quadratic when $R = 1$ or 2 − with respect to the number of random variables or integration points. For $R < N$, the technique alleviates the curse of dimensionality to an extent determined by R.

6.4.2 Sparse-grid integration

Although, the full-grid dimension-reduction integration has been successfully applied to the calculation of the PDD expansion coefficients in the past [87,89,90,135], it faces a major drawback when the polynomial order m_u for a PDD component function y_u needs to be modulated for adaptivity. As the value of m_u is incremented by one, a completely new set of integration points is generated by the univariate Gauss quadrature rule, rendering all expensive function evaluations on prior integration points as useless. Therefore, a nested Gauss quadrature rule, such as the

fully symmetric interpolatory rule, that is capable of exploiting dimension-reduction integration is proposed.

6.4.2.1 Fully symmetric interpolatory rule

The fully symmetric interpolatory (FSI) rules developed by Genz and his associates [140,141], is a sparse-grid integration technique for performing high-dimensional numerical integration. Applying this rule to the $|v|$-dimensional integrations in Equations (6.28) and (6.29), the PDD expansion coefficients are approximated by

$$\begin{aligned} y_{\emptyset} \cong \sum_{i=0}^{R} (-1)^i \binom{N-R+i-1}{i} \sum_{\substack{v \subseteq \{1,\cdots,N\} \\ |v|=R-i}} \sum_{\mathbf{p}_{|v|} \in P^{(\tilde{n}_v,|v|)}} w_{\mathbf{p}_{|v|}} \\ \sum_{\mathbf{q}_{|\mathbf{v}|} \in \Pi_{\mathbf{p}_{|v|}}} \sum_{\mathbf{t}_{|v|}} y\left(t_{i_1}\alpha_{q_{i_1}}, \cdots, t_{i_{|v|}}\alpha_{q_{i_{|v|}}}, \mathbf{c}_{-v}\right), \end{aligned} \tag{6.33}$$

$$\begin{aligned} C_{u\mathbf{j}_{|u|}} \cong \sum_{i=0}^{R} (-1)^i \binom{N-R+i-1}{i} \sum_{\substack{v \subseteq \{1,\cdots,N\} \\ |v|=R-i, u \subseteq v}} \sum_{\mathbf{p}_{|v|} \in P^{(\tilde{n}_v,|v|)}} w_{\mathbf{p}_{|v|}} \\ \sum_{\mathbf{q}_{|\mathbf{v}|} \in \Pi_{\mathbf{p}_{|v|}}} \sum_{\mathbf{t}_{|v|}} y\left(t_{i_1}\alpha_{q_{i_1}}, \cdots, t_{i_{|v|}}\alpha_{q_{i_{|v|}}}, \mathbf{c}_{-v}\right) \psi_{u\mathbf{j}_{|u|}}\left(t_{i_1}\alpha_{q_{i_1}}, \cdots, t_{i_{|u|}}\alpha_{q_{i_{|u|}}}\right), \end{aligned} \tag{6.34}$$

where $v = \{i_1, \cdots i_{|v|}\}$, $\mathbf{t}_{|v|} = (t_{i_1}, \cdots, t_{i_{|v|}})$, $\mathbf{p}_{|v|} = (p_{i_1}, \cdots, p_{i_{|v|}})$,

$$P^{(\tilde{n}_v,|v|)} = \{\mathbf{p}_{|v|} : \tilde{n}_v \geq p_{i_1} \geq \cdots \geq p_{i_{|v|}} \geq 0, \left\|\mathbf{p}_{|v|}\right\| \leq \tilde{n}_v\} \tag{6.35}$$

where $\left\|\mathbf{p}_{|v|}\right\| = \sum_{r=1}^{|v|} p_{i_r}$ is the set of all distinct $|v|$-partitions of the integers $0, 1, \cdots, \tilde{n}_v$, and $\Pi_{\mathbf{p}_{|v|}}$ is the set of all permutations of $\mathbf{p}_{|v|}$. The innermost sum over $\mathbf{t}_{|v|}$ is taken over all of the sign combinations that occur when $t_{i_r} = \pm 1$ for those values of i_r with

generators $\alpha_{q_{i_r}} \neq 0$ [141]. The weight

$$w_{\mathbf{p}_{|\mathbf{v}|}} = 2^{-K} \sum_{\|\mathbf{k}_{|\mathbf{v}|}\| \leqslant \tilde{n}_v - \|\mathbf{p}_{|v|}\|} \prod_{r=1}^{|v|} \frac{a_{k_{i_r}+p_{i_r}}}{k_{i_r}+p_{i_r}} \prod_{j=0, j\neq p_{i_r}} \left(\alpha_{p_{i_r}}^2 - \alpha_j^2\right)}, \tag{6.36}$$

where K is the number of nonzero components in $\mathbf{p}_{|v|}$ and a_i is a constant that depends on the probability measure of X_i, for instance,

$$a_i = \frac{1}{\sqrt{2\pi}} \int_{\mathbb{R}} \exp\left(-\frac{\xi^2}{2}\right) \prod_{j=0}^{i-1} \left(\xi^2 - \alpha_j^2\right) d\xi \tag{6.37}$$

for $i > 0$ and $a_0 = 1$ when X_i follows the standard Gaussian distribution [141]. An $\tilde{n}_v$-parameter FSI rule exactly integrates a polynomial of degree at most $2\tilde{n}_v + 1$.

6.4.2.2 Extended fully symmetric interpolatory rule

The number of function evaluations by the original FSI rule [140] increases rapidly as $|v|$ and $\tilde{n}_v$ increase. To enhance the efficiency, Genz and Keister [141] proposed an extended FSI rule in which the function evaluations are significantly reduced if the generator set is chosen such that some of the weights $w_{\mathbf{p}_{|\mathbf{v}|}}$ are zero. The pivotal step in constructing such an FSI rule is to extend a $(2\beta+1)$-point Gauss-Hermite quadrature rule by adding 2γ points or generators $\pm\alpha_{\beta+1}, \pm\alpha_{\beta+2}, \ldots, \pm\alpha_{\beta+\gamma}$ with the objective of maximizing the degree of polynomial exactness of the extended rule, where $\beta \in \mathbb{N}$ and $\gamma \in \mathbb{N}$. Genz and Keister [141] presented a special case of initiating the FSI rule from the univariate Gauss-Hermite rule over the interval $(-\infty, \infty)$. The additional generators in this case are determined as roots of the monic polynomial $\zeta^{2\gamma} + t_{\gamma-1}\zeta^{2\gamma-1} + \cdots + t_0$, where the coefficients $t_{\gamma-1}, \cdots, t_0$ are

obtained by invoking the condition

$$\frac{1}{\sqrt{2\pi}} \int_{\mathbb{R}} \exp\left(-\frac{\xi^2}{2}\right) \prod_{j=0}^{\beta} \xi^{2b} \left(\xi^2 - \alpha_j^2\right) d\xi = 0, \tag{6.38}$$

where $\gamma > \beta$. A new set of generators is propagated based on the prior rule and, therefore, as the polynomial degree of exactness of the rule increases, all the previous points and the expensive function evaluations over those points are preserved. A remarkable feature of the extended FSI rule is that the choice of generators is such that some of the weights $w_{\mathbf{p}_{|\mathbf{v}|}} = 0$ in each step of the extension [141], thus eliminating the need for function evaluations at the integration points corresponding to zero weights, making the extended FSI rule significantly more efficient than its earlier version.

6.4.3 Integration points

The number of integration points determines the computational expense incurred in calculating the PDD expansion coefficients. Therefore, it is instructive to compare the numbers of integration points required by full- or sparse-grid dimension-reduction integrations. To do so, consider the efforts in performing a $|v|$-dimensional integration in Equation (6.28) or (6.29) over the interval $(-\infty, \infty)$ by three different numerical techniques: (1) the full-grid integration technique; (2) the sparse-grid integration technique using the extended FSI rule; and (3) the sparse-grid integration technique using Smolyak's algorithm [142]. The Smolyak's algorithm is included because it is commonly used as a preferred sparse-grid numerical technique for approximating high-dimensional integrals. Define an integer $l \in \mathbb{N}$ such that all three techniques can exactly integrate a polynomial function of total degree $2l - 1$. For

instance, when $l = 3$, all three techniques exactly integrate a quintic polynomial. Figure 6.2 presents a comparison of the total numbers of integration points in a two-dimensional grid, that is, when $|v| = 2$, for l ranging from one through five by the three distinct multivariate integration techniques. Each plot illustrates two numbers: the first number indicates the number of integration points required at the given value of l; the second number, inside the parenthesis, indicates the total number of cumulative integration points added up to the value of l. It is imperative to add the integration points from all the previous values of l as it reflects the total number of function evaluations required in an adaptive algorithm. For the full-grid integration, the two numbers are different for all $l > 1$, indicating a lack of nesting of the integration points. Whereas in the sparse-grid with extended FSI rule, the two numbers are equal for all l, reflecting the fully nested integration points in this rule. As l increments, a completely new set of points is introduced in the full-grid integration, rendering the prior points useless. However, for fairness in comparison, it is necessary to consider all points from prior values of l as the expensive function evaluations have already been performed. Therefore, Figure 6.2 captures the cumulative numbers of integration points as l increases steadily. For values of l up to two, all three techniques require the same number of integration points. However, differences in the numbers of points start to appear in favor of the extended FSI rule when l exceeds two, making it the clear favorite among all three techniques for high-order numerical integration. The Smolyak's algorithm, which is not nested, is the least efficient of the three techniques. The extended FSI rule, in contrast, is fully nested, establishing a

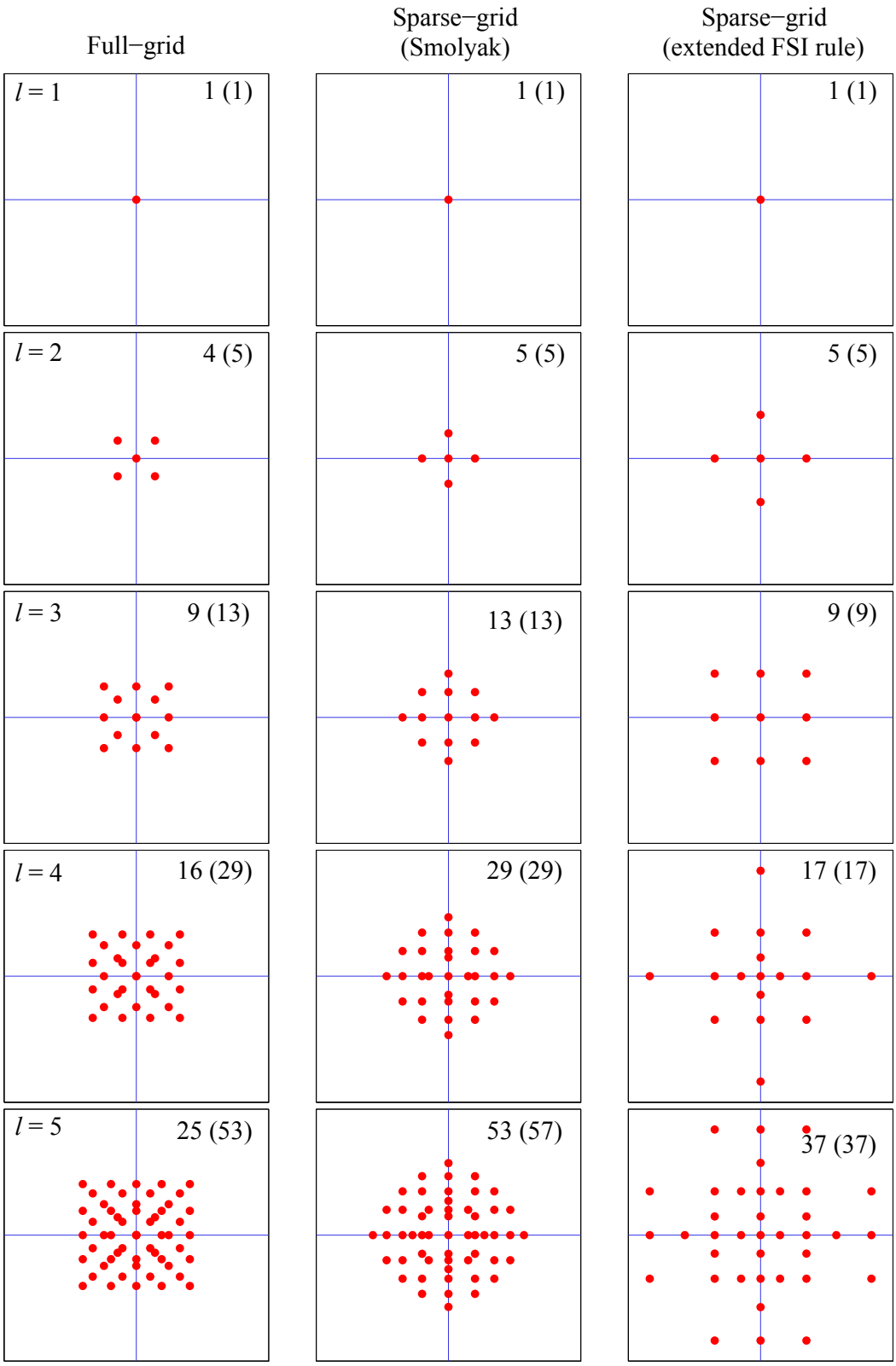

Figure 6.2: Gauss-Hermite integration points in a two-dimensional grid by the full-grid technique, sparse-grid with the extended FSI rule, and sparse-grid with Smolyak's algorithm for various levels. Each grid is plotted over a square axis from -5 to 5.

principal advantage over Smolyak's algorithm for adaptive numerical integration.

Table 6.1 lists the number of integration points required at the integration rule corresponding to a given value of l, for $2 \leq |v| \leq 10$ and $2 \leq l \leq 5$. It is important to note that the number of integration points listed is not cumulative. It appears that for higher-dimensional integrations, that is, for $|v| > 2$, the extended FSI rule is markedly more efficient than full-grid or other sparse-grid techniques even for the non-cumulative points. The efficiency of extended FSI rule is more pronounced for cumulative number of integration points. For further details, the reader is referred to the work of Genz and Keister [141], who examined the extended FSI rule for dimensions up to 20.

Table 6.1: Number of integration points in various $|v|$-dimensional integration techniques, each technique exactly integrates polynomials of total order $2l - 1$.

	$\|v\|$								
l	2	3	4	5	6	7	8	9	10
	(a) Full-grid								
2	4	8	16	32	64	128	256	512	1024
3	9	27	81	243	729	2187	6561	19683	59049
4	16	64	256	1024	4096	16384	65536	262144	1048576
5	25	125	625	3125	15625	78125	390625	1953125	9765625
	(b) Sparse-grid (Smolyak)								
2	5	7	9	11	13	15	17	19	21
3	13	25	41	61	85	113	145	181	221
4	29	69	137	241	389	589	849	1177	1581
5	53	165	385	781	1433	2437	3905	5965	8761
	(c) Sparse-grid (extended FSI rule)								
2	5	7	9	11	13	15	17	19	21
3	9	19	33	51	73	99	129	163	201
4	17	39	81	151	257	407	609	871	1201
5	37	93	201	401	749	1317	2193	3481	5301

6.5 Numerical Examples

Three numerical examples are put forward to illustrate the adaptive-sparse PDD methods developed in calculating various probabilistic characteristics of random mathematical functions and random eigensolutions of stochastic dynamical systems. Classical Legendre polynomials were used to define the orthonormal polynomials in Example 1, and all expansion coefficients were determined analytically. In Examples 2 and 3, all original random variables were transformed into standard Gaussian random variables, facilitating the use of classical Hermite orthonormal polynomials as bases. Since Example 2 consists of only nine input random variables, the expansion coefficients were estimated using a nine-dimensional tensor product of the five-point univariate Gauss-Hermite quadrature rule. The expansion coefficients in Example 3 were approximated by both the full-grid dimension-reduction integration and sparse-grid dimension-reduction integration with a fully symmetric interpolatory rule. The sample size for crude MCS in Example 2 is 10^6. In Example 3, the sample size for crude MCS is $50,000$, and for the embedded MCS, whether the truncated or adaptive-sparse PDD method, the sample size is 10^6.

6.5.1 Polynomial function

Consider a polynomial function

$$y(\mathbf{X}) = \frac{\prod_{i=1}^{N}\left(\frac{3}{i}X_i^5 + 1\right)}{\mathbb{E}\left[\prod_{i=1}^{N}\left(\frac{3}{i}X_i^5 + 1\right)\right]} \tag{6.39}$$

where X_i, $i = 1, \cdots, N$, are independent and identical random variables, each following the standard uniform distribution over $[0, 1]$. Since the coefficient of X_i^5 is inversely proportional to i, the first and last random variables have the largest and least influence on y. From elementary calculations, the exact mean and variance of y are 1 and

$$\frac{\prod_{i=1}^{N}\left(\frac{9}{11i^2}+\frac{1}{i}+1\right)}{\left\{\mathbb{E}\left[\prod_{i=1}^{N}\left(\frac{9}{11i^2}+\frac{1}{i}+1\right)\right]\right\}^2}$$

respectively. All PDD expansion coefficients were calculated analytically. Therefore, the ranking of component functions was performed once and for all, avoiding any role of the ranking scheme in this particular example. The numerical results that follow in the remainder of this subsection were obtained for $N = 5$.

Figure 6.3 shows how the relative errors, defined as the ratio of the absolute difference between the exact (Equation (6.9)) and approximate (Equation (6.8)) variances of y to the exact variance, committed by S-variate, m-th order PDD approximations, vary with increasing polynomial order m. The five plots of univariate ($S = 1$) to pentavariate ($S = 5$) PDD approximations clearly show that the error drops monotonically with respect to m regardless of S. When m reaches five, the pentavariate PDD approximation does not perpetrate any error, producing the exact variance of y as expected. In contrast, the relative errors in variance caused by fully adaptive-sparse PDD approximations (Equation (6.20)), also illustrated in Figure 6.3 for specified tolerances ranging from 10^{-9} to 10^{-3}, do not rely on S or m, as the degrees of interaction and polynomial orders are adaptively modulated in the con-

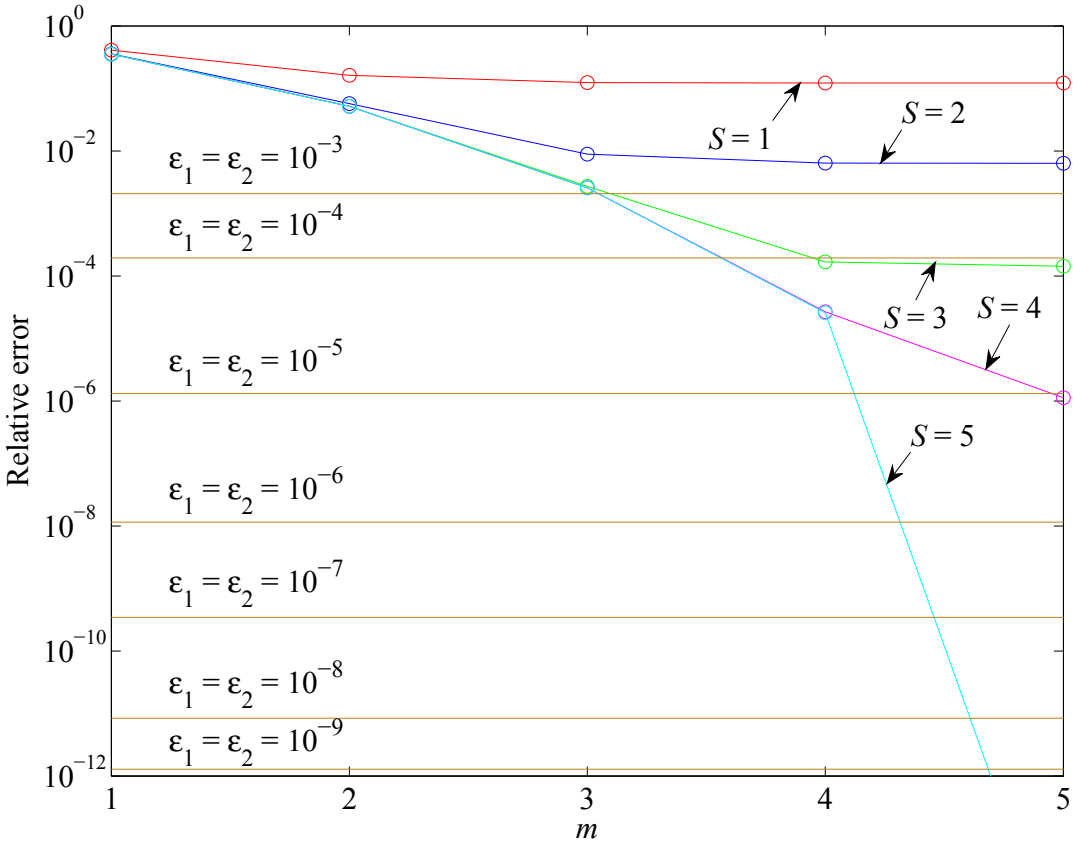

Figure 6.3: Relative error in calculating the variance of a mathematical function by fully adaptive-sparse and truncated PDD methods (Example 1).

comitant approximations. The adaptive-sparse PDD approximations with tolerances equal to 10^{-3} and 10^{-4} yield relative errors in variance marginally higher than the tolerance values; however, the relative errors achieved are invariably smaller than all respective values of the subsequent tolerances, demonstrating a one-to-one relationship between the tolerance and relative error attained in calculating the variance. While a traditional truncated PDD approximation provides options to increase the values of S and/or m for reducing the relative error, the user remains blinded to the outcome of such an action. The adaptive-sparse PDD method, in the form of tolerances, provides a direct key to regulate the accuracy of the resultant approximation.

Figure 6.4 displays the increase in the number of PDD expansion coefficients required by truncated (Equation (6.10)) and fully adaptive-sparse (Equation (6.23)) PDD methods in order to achieve a user-specified relative error in variance ranging from 10^{-1} to 10^{-12}. The relative error decreases from left to right along the horizontal axis of the plot. The plot of the truncated PDD approximation is generated by trial-and-error, increasing the value of either S or m until the desired relative error is achieved and then counting the total number of coefficients required to attain that relative error. For obtaining the plot of the adaptive-sparse PDD approximation, the tolerance values were reduced monotonically, and the corresponding total number of coefficients was noted for each value of relative error. Ignoring the two lowest relative errors, the comparison of the plots from these two methods clearly demonstrates how the adaptive-sparse PDD method requires fewer expansion coefficients than the truncated PDD method to achieve the desired level of relative error. While the

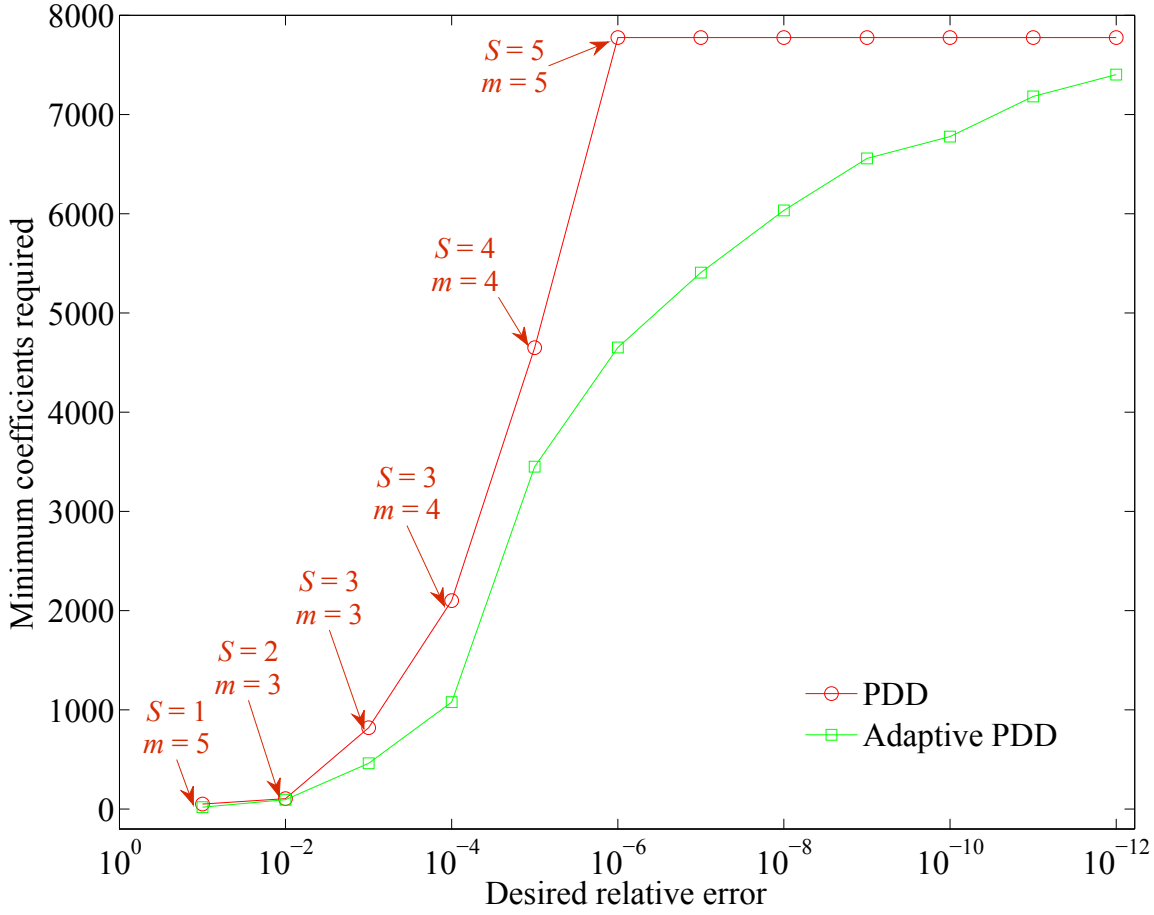

Figure 6.4: Minimum number of coefficients required to achieve a desired relative error in the variance of a mathematical function by fully adaptive-sparse and truncated PDD methods (Example 1).

adaptive-sparse PDD method intelligently calculates only those coefficients that are making significant contribution to the variance, the truncated PDD method ends up calculating more coefficients than required. Therefore, the adaptive-sparse PDD approximation represents a more scientific and efficient method than the truncated PDD methods.

6.5.2 Three-degree-of-freedom, undamped, spring-mass system

Consider a three-degree-of-freedom, undamped, spring-mass system, shown in Figure 6.5, with random mass and random stiffness matrices

$$\mathbf{M}(\mathbf{X}) = \begin{bmatrix} M_1(\mathbf{X}) & 0 & 0 \\ 0 & M_2(\mathbf{X}) & 0 \\ 0 & 0 & M_3(\mathbf{X}) \end{bmatrix} \tag{6.40}$$

and

$$\mathbf{K}(\mathbf{X}) = \begin{bmatrix} K_{11}(\mathbf{X}) & K_{12}(\mathbf{X}) & K_{13}(\mathbf{X}) \\ & K_{22}(\mathbf{X}) & K_{23}(\mathbf{X}) \\ \text{(sym.)} & & K_{33}(\mathbf{X}) \end{bmatrix}, \tag{6.41}$$

respectively, where $K_{11}(\mathbf{X}) = K_1(\mathbf{X}) + K_4(\mathbf{X}) + K_6(\mathbf{X})$, $K_{12}(\mathbf{X}) = -K_4(\mathbf{X})$, $K_{13}(\mathbf{X}) = -K_6(\mathbf{X})$, $K_{22}(\mathbf{X}) = K_4(\mathbf{X}) + K_5(\mathbf{X}) + K_2(\mathbf{X})$, $K_{23}(\mathbf{X}) = -K_5(\mathbf{X})$, and $K_{33}(\mathbf{X}) = K_5(\mathbf{X}) + K_3(\mathbf{X}) + K_6(\mathbf{X})$; the masses $M_i(\mathbf{X}) = \mu_i X_i$; $i = 1, 2, 3$ with $\mu_i = 1.0$ kg; $i = 1, 2, 3$, and spring stiffnesses $K_i(\mathbf{X}) = \mu_{i+3} X_{i+3}$; $i = 1, \cdots, 6$ with $\mu_{i+3} = 1.0$ N/m; $i = 1, \cdots, 5$ and $\mu_9 = 3.0$ N/m. The input $\mathbf{X} = \{X_1, \cdots, X_9\}^T \in \mathbb{R}^9$ is an independent lognormal random vector with mean $\boldsymbol{\mu}_{\mathbf{X}} = \mathbf{1} \in \mathbb{R}^9$ and covariance matrix $\boldsymbol{\Sigma}_{\mathbf{X}} = \nu^2 \mathbf{I} \in \mathbb{R}^{9\times 9}$ with coefficient of variation $\nu = 0.3$.

Three partially adaptive-sparse PDD methods with $S = 1$, 2, and 3 were applied to calculate the variances (Equation (6.21)) of the three random eigenvalues of the dynamic system. The tolerance values are as follows: $\epsilon_1 = \epsilon_2 = 10^{-6}$ and $\epsilon_3 = 0.7$.

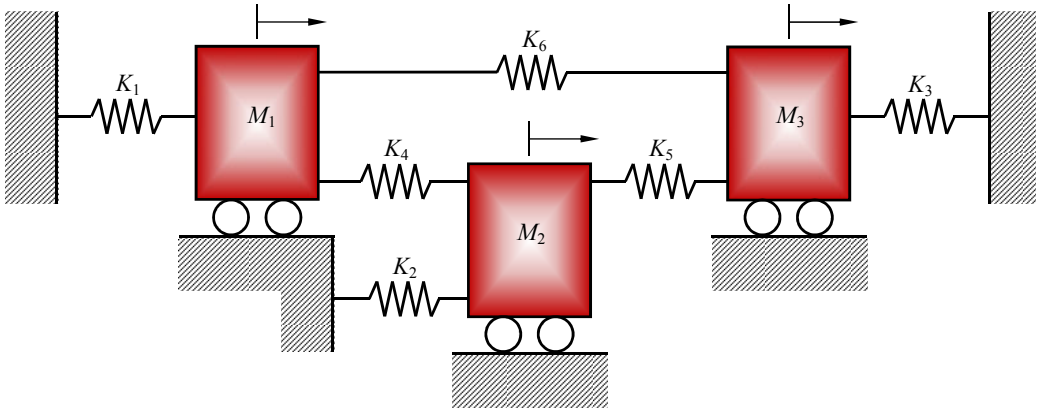

Figure 6.5: A three-degree-of-freedom undamped, spring-mass system (Example 2). (Repeat of Figure 5.3)

Table 6.2 presents the variances of eigenvalues from various partially adaptive-sparse PDD methods calculated according to Algorithms 6.1 and 6.2. The results of both full and reduced ranking systems are tabulated. Also included in Table 6.2 are the variance calculations from crude MCS. The variances obtained using the univariate ($S = 1$) partially adaptive-sparse PDD approximation are relatively far from the benchmark results of crude MCS since the univariate approximation is unable to capture any interactive effects of the input variables. However, the bivariate ($S = 2$) and trivariate ($S = 3$) partially adaptive-sparse PDD approximations achieve very high accuracy in calculating the variances of all three random eigenvalues. Remarkably, the reduced ranking scheme delivers the same level of accuracy, at least up to three decimal places shown, of the full ranking scheme in calculating the variances.

In order to study the efficiency of the reduced ranking scheme vis-a-vis the full ranking scheme in a trivariate partially adaptive-sparse PDD approximation, the corresponding total numbers of coefficients (Equation (6.24)) required were compared,

Table 6.2: Variances of three eigenvalues of a three-degree-of-freedom linear oscillator by three partially adaptive-sparse PDD methods and crude MCS

	$S=1$		$S=2$		$S=3$		MCS
λ	Full ranking	Reduced ranking	Full ranking	Reduced ranking	Full ranking	Reduced ranking	10^6
1	0.057	0.057	0.060	0.060	0.060	0.060	0.060
2	1.152	1.152	1.204	1.204	1.215	1.215	1.219
3	7.289	7.289	7.576	7.576	7.585	7.585	7.585

along with the total number of coefficients (Equation (6.10)) required in a trivariate, fifth-order truncated PDD approximation, in Figure 6.6. While the partially adaptive-sparse PDD method with either ranking scheme requires fewer coefficients than does the truncated PDD method, it is the reduced ranking scheme that is the clear winner in efficiency with the least number of coefficients. The largest reduction in the number of coefficients achieved by the reduced ranking system is approximately sixty-eight percent when calculating the variance of the third eigenvalue. These results are in agreement with Proposition 6.6.

6.5.3 Modal analysis of a functionally graded cantilever plate

The third example involves free vibration analysis of a $2\,\mathrm{m} \times 1\,\mathrm{m} \times 10\,\mathrm{mm}$ cantilever plate, shown in Figure 6.7(a), made of a functionally graded material (FGM)[1], where silicon carbide (SiC) particles varying along the horizontal coordinate ξ are randomly dispersed in an aluminum (Al) matrix [143]. The result is a random inhomogeneous plate, where the effective elastic modulus $E(\xi)$, effective Poisson's ratio

[1]Functionally graded materials are two- or multi-phase particulate composites in which material composition and microstructure vary spatially in the macroscopic length scale to meet a desired functional performance.

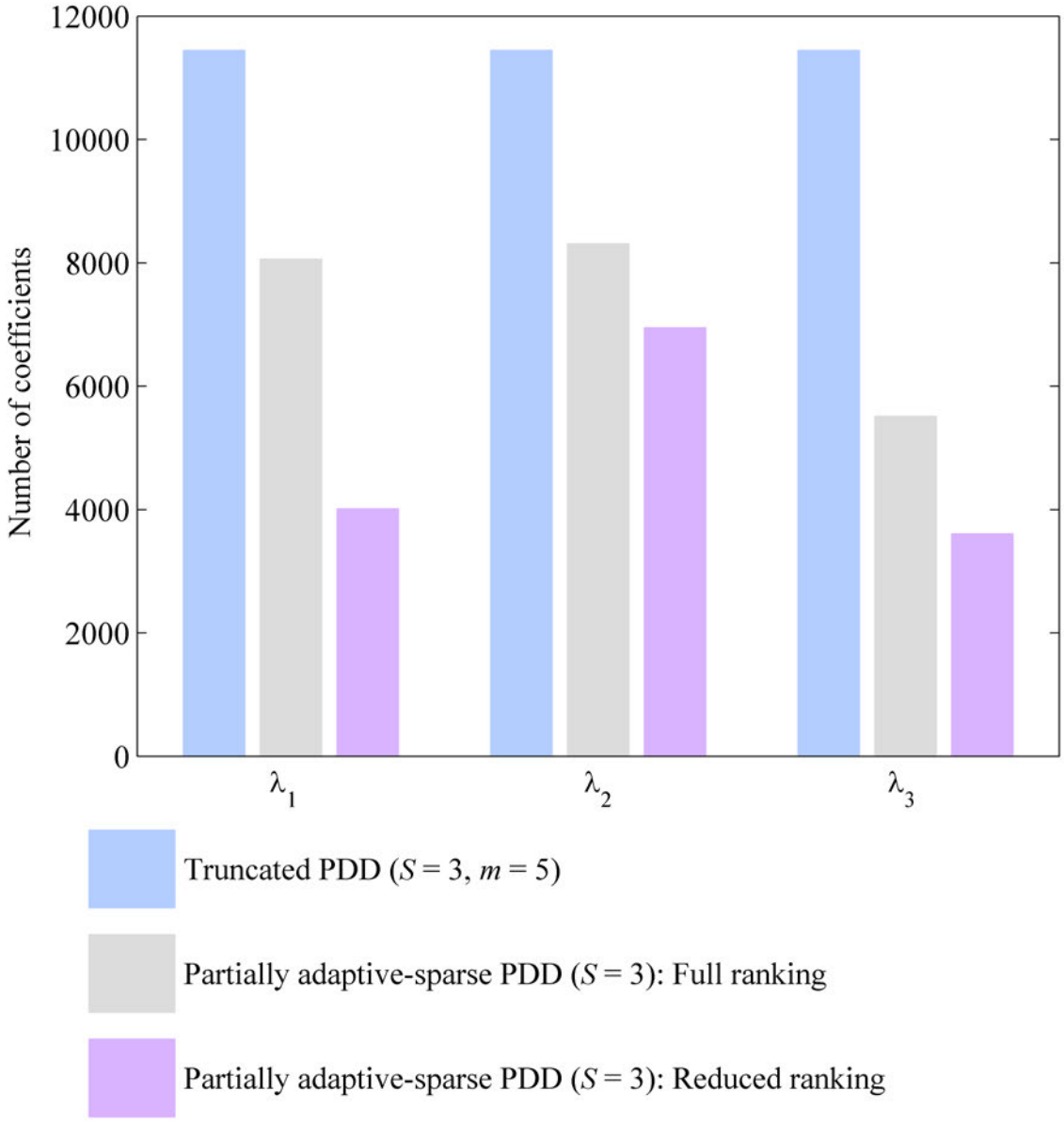

Figure 6.6: Number of coefficients required for calculating the variance of a three-degree-of-freedom linear oscillator by trivariate partially adaptive-sparse PDD approximations using full and reduced ranking schemes.

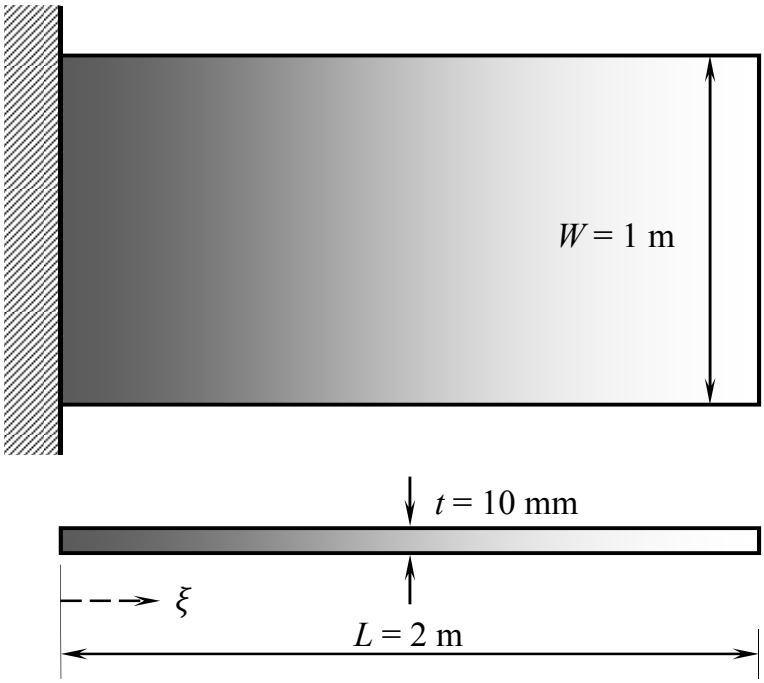

(a)

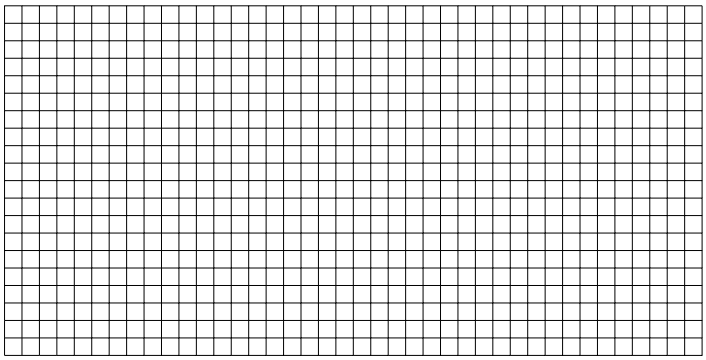

(b)

Figure 6.7: An FGM cantilever plate: (a) geometry; (b) a 20×40 FEA mesh. (Repeat of Figure 4.3)

$\nu(\xi)$, and effective mass density $\rho(\xi)$ are random fields. They depend on two principal sources of uncertainties: (1) randomness in the volume fraction of SiC particles $\phi_{\mathrm{SiC}}(\xi)$, which varies only along ξ, and (2) randomness in constituent material properties, comprising elastic moduli E_{SiC} and E_{Al}, Poisson's ratios ν_{SiC} and ν_{Al}, and mass densities ρ_{SiC} and ρ_{Al} of SiC and Al material phases, respectively. The particle volume fraction $\phi_{\mathrm{SiC}}(\xi)$ is a one-dimensional, inhomogeneous, Beta random field with mean $\mu_{\mathrm{SiC}}(\xi) = 1 - \xi/L$, and standard deviation $\sigma_{\mathrm{SiC}}(\xi) = (\xi/L)(1 - \xi/L)$, where L is the length of the plate. Assuming an appropriately bounded covariance function of $\phi_{\mathrm{SiC}}(\xi)$, the standardized volume fraction, $\tilde{\phi}_{\mathrm{SiC}}(\xi) := [\phi_{\mathrm{SiC}}(\xi) - \mu_{\mathrm{SiC}}(\xi)]/\sigma_{\mathrm{SiC}}(\xi)$, was mapped to a zero-mean, homogeneous, Gaussian image field $\alpha(\xi)$ with an exponential covariance function $\Gamma_\alpha(t) := \mathbb{E}[\alpha(\xi)\alpha(\xi + t)] = \exp(-|t|/0.125L)$ via $\tilde{\phi}_{\mathrm{SiC}}(\xi) = F^{-1}_{\mathrm{SiC}}[\Phi(\alpha(\xi))]$, where Φ is the distribution function of a standard Gaussian random variable and F_{SiC} is the marginal distribution function of $\tilde{\phi}_{\mathrm{SiC}}(\xi)$. The Karhunen-Loève approximation [122] was employed to discretize $\alpha(\xi)$ and hence $\phi_{\mathrm{SiC}}(\xi)$ into 28 standard Gaussian random variables. In addition, the constituent material properties, E_{SiC}, E_{Al}, ν_{SiC}, ν_{Al}, ρ_{SiC}, and ρ_{Al}, were modeled as independent lognormal random variables with their means and coefficients of variation described in Table 6.3. Therefore, a total of 34 random variables are involved in this example. Employing a rule of mixture, $E(\xi) \cong E_{\mathrm{SiC}}\phi_{\mathrm{SiC}}(\xi) + E_{\mathrm{Al}}[1 - \phi_{\mathrm{SiC}}(\xi)]$, $\nu(\xi) \cong \nu_{\mathrm{SiC}}\phi_{\mathrm{SiC}}(\xi) + \nu_{\mathrm{Al}}[1 - \phi_{\mathrm{SiC}}(\xi)]$, and $\rho(\xi) \cong \rho_{\mathrm{SiC}}\phi_{\mathrm{SiC}}(\xi) + \rho_{\mathrm{Al}}[1 - \phi_{\mathrm{SiC}}(\xi)]$. Using these spatially variant effective properties, a 20×40 mesh consisting of 800 eight-noded, second-order shell elements, shown in Figure 6.7(b), was constructed for finite-

element analysis (FEA), to determine the natural frequencies of the FGM plate. No damping was included. A Lanczos algorithm [123] was employed for calculating the eigenvalues.

Table 6.3: Statistical material properties of constituents in SiC-Al FGM.

Material properties[(a)]	Mean	Coefficient of variation, %
E_{SiC}, GPa	419.2	15
ν_{SiC}	0.19	5
ρ_{SiC}, kg/m^3	3210	15
E_{Al}, GPa	69.7	15
ν_{Al}	0.34	5
ρ_{Al}, kg/m^3	2520	15

[(a)] E_{SiC} = elastic modulus of SiC, ν_{SiC} = Poisson's ratio of SiC, ρ_{SiC} = mass density of SiC, E_{Al} = elastic modulus of Al, ν_{Al} = Poisson's ratio of Al, ρ_{Al} = mass density of Al.

The probability distributions of the first six natural frequencies of the functionally graded material plate were evaluated using four different PDD methods: (1) the bivariate partially adaptive-sparse PDD method with full-grid dimension-reduction integration; (2) the bivariate partially adaptive-sparse PDD method with sparse-grid dimension-reduction integration with a fully symmetric interpolatory rule; (3) the univariate, fifth-order PDD method; and (4) the bivariate, fifth-order PDD method; and the crude MCS. The tolerances used for adaptive and ranking algorithms are $\epsilon_1 = \epsilon_2 = 10^{-6}$ and $\epsilon_3 = 0.9$. Figure 6.8 presents the marginal probability distributions $F_i(\omega_i) := P[\Omega_i \leq \omega_i]$ of the first six natural frequencies Ω_i, $i = 1, \cdots, 6$, where all the PDD solutions were obtained from embedded MCS. The plots are made over

a semi-logarithmic scale to delineate the distributions in the tail regions. For all six frequencies, the probability distributions obtained from a bivariate partially adaptive-sparse PDD method, whether using either full-grid or sparse-grid, and the bivariate fifth-order PDD method are much closer to the crude Monte Carlo results compared with those obtained from the univariate, fifth-order PDD method. While all PDD approximations require fewer function evaluations than the crude MCS, both variants of the partially adaptive-sparse PDD approximations remit exceptionally high efficiency by a average factor of six when compared with the bivariate fifth-order PDD approximation. However, the advantage of the sparse-grid integration over the full-grid integration employed in the adaptive-sparse approximation is modest in terms of computational efficiency.

The efficient reduced ranking algorithm was employed in this example. When the bivariate component functions were ranked for $m_u = 1$, the coefficient calculation for both full-grid and sparse-grid involved function evaluation at the point $(0, 0)$ as shown for $l = 1$ in Figure 6.2. The function evaluations at this point return only the functions already evaluated at the point $(\boldsymbol{c})$, i.e., response at mean $y(\boldsymbol{c})$, thus the bivariate component functions could not be ranked for $m_u = 1$. When the polynomial order was incremented to $m_u = 2$, the full-grid for $l = 2$ comprises of four non-zero integration points, resulting in non-trivial bivariate function evaluations at those points. However, the sparse-grid consists of four new points lying on the axes, failing to capture the interaction effect of two variables. This results in bivariate function evaluations that are not useful in creating a ranking. Thus, for $m_u = 2$, full-grid

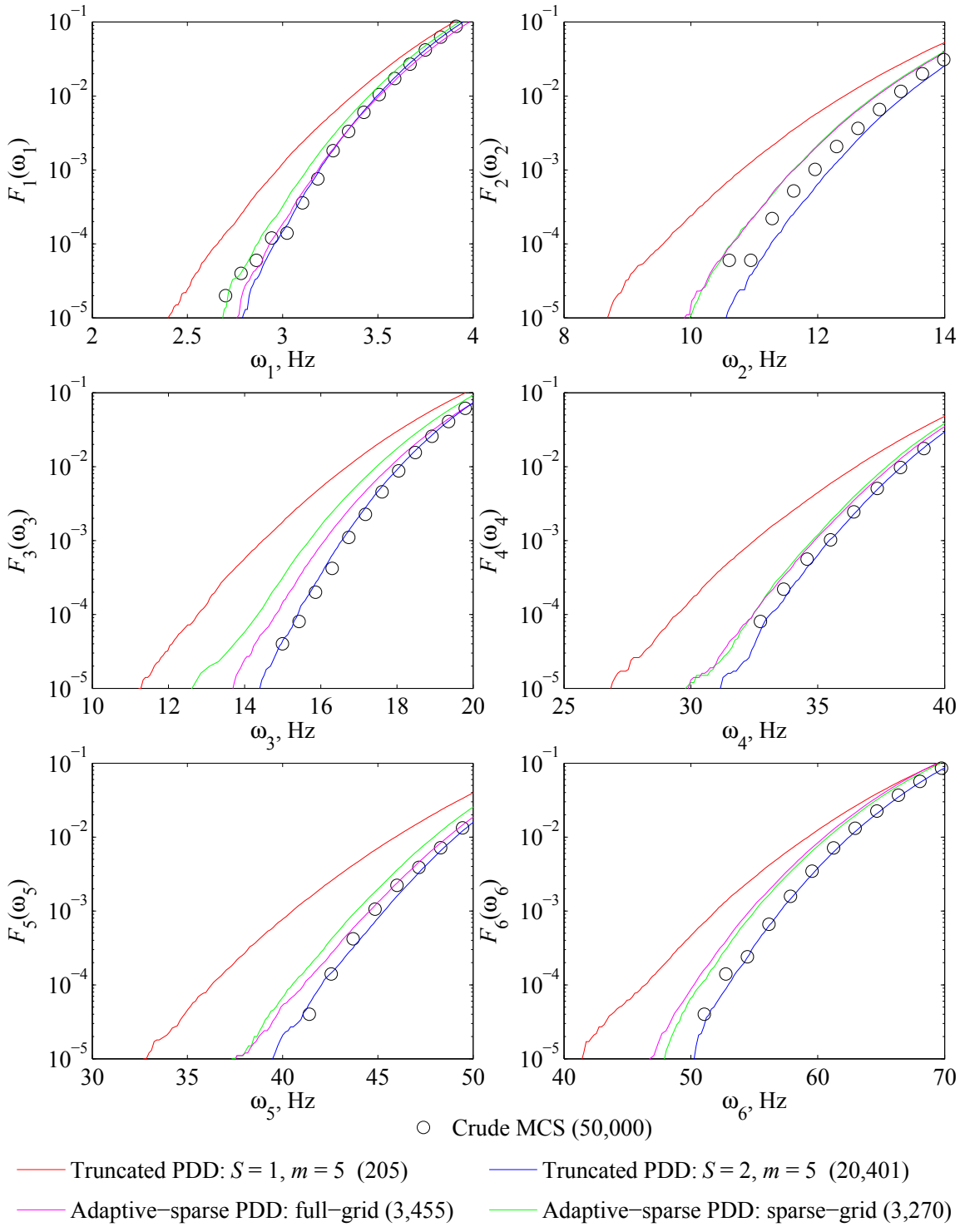

Figure 6.8: Marginal probability distributions of the first six natural frequencies of an FGM plate by various PDD approximations and crude MCS

involves ranking all the $28 \times 27/2 = 378$ bivariate component functions, with $378 \times 4 = 1512$ new function evaluations, while the sparse-grid was still lacking any ranking. Moving to $m_u = 3$, full-grid can afford to exploit the efficient reduced-ranking by truncating the ranking from $m_u = 2$ and calculating coefficients only for fewer than 378 component functions. However, the sparse-grid is forced to evaluate all 378 component functions for $m_u = 3$, resulting in $378 \times 4 = 1512$ function evaluations at four new integration points, depriving this efficient technique of any initial advantage. The modest advantage in computational efficiency that the sparse-grid eventually achieves was obtained only after ranking at $m_u = 4$ and onwards.

Figure 6.9 displays the joint probability density function $f_{12}(\omega_1, \omega_2)$ of the first two natural frequencies Ω_1 and Ω_2 obtained by the two variants of the bivariate partially adaptive-sparse PDD method, the bivariate, fifth-order PDD method, and crude MCS. Although visually comparing these three-dimensional plots is not simple, the joint distributions from all PDD approximations and the crude Monte Carlo method seem to match reasonably well. The contours of these three-dimensional plots were studied at two notably different levels: $f_{12} = 0.005$ (high level) and $f_{12} = 0.0005$ (low level), as depicted in Figures 6.10(a) and 6.10(b), respectively. For both levels examined, a good agreement exists among the contours from all four distributions. These results are consistent with the marginal distributions of the natural frequencies discussed in the preceding paragraph.

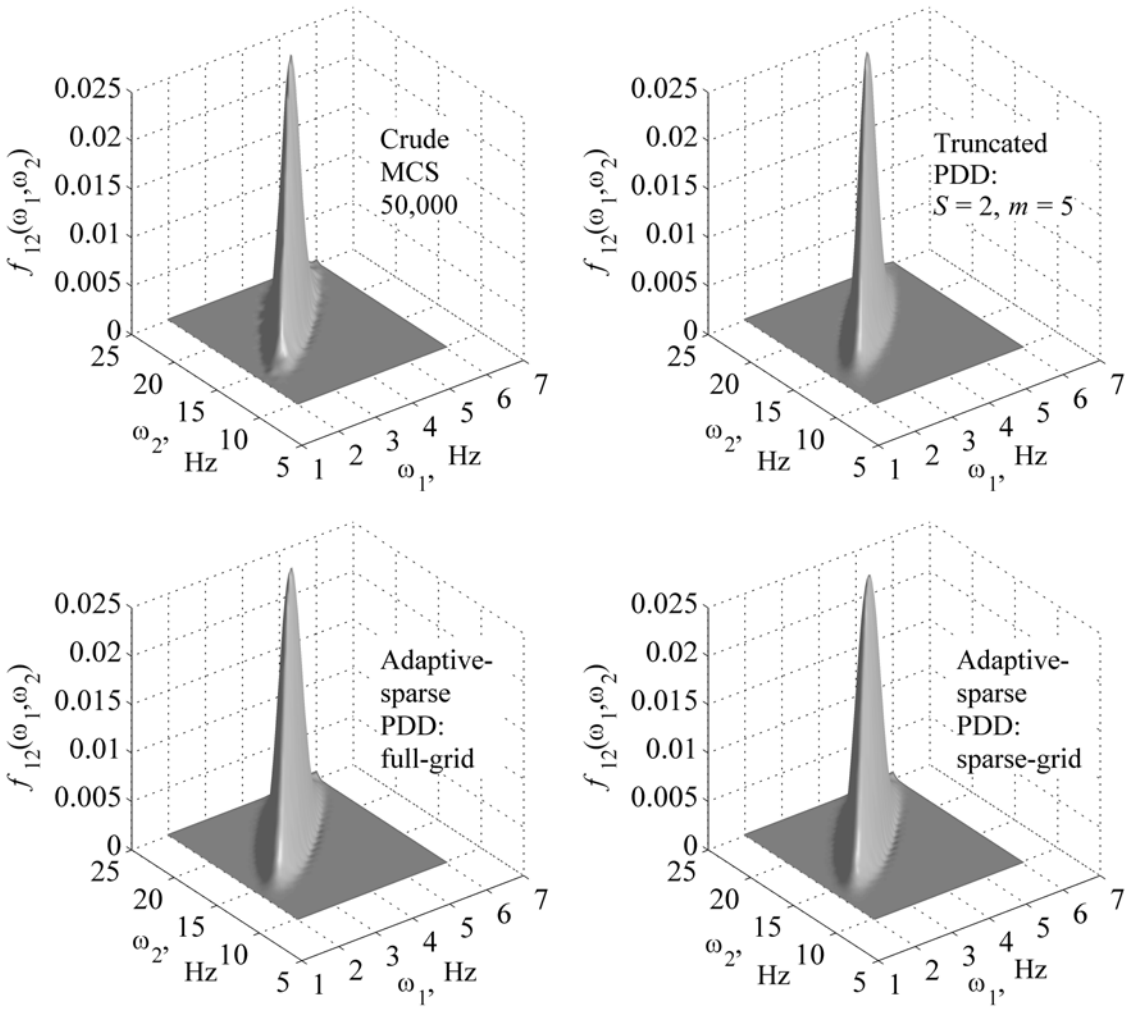

Figure 6.9: Joint probability density function of the first and second natural frequencies of the FGM plate by various PDD approximations and crude MCS

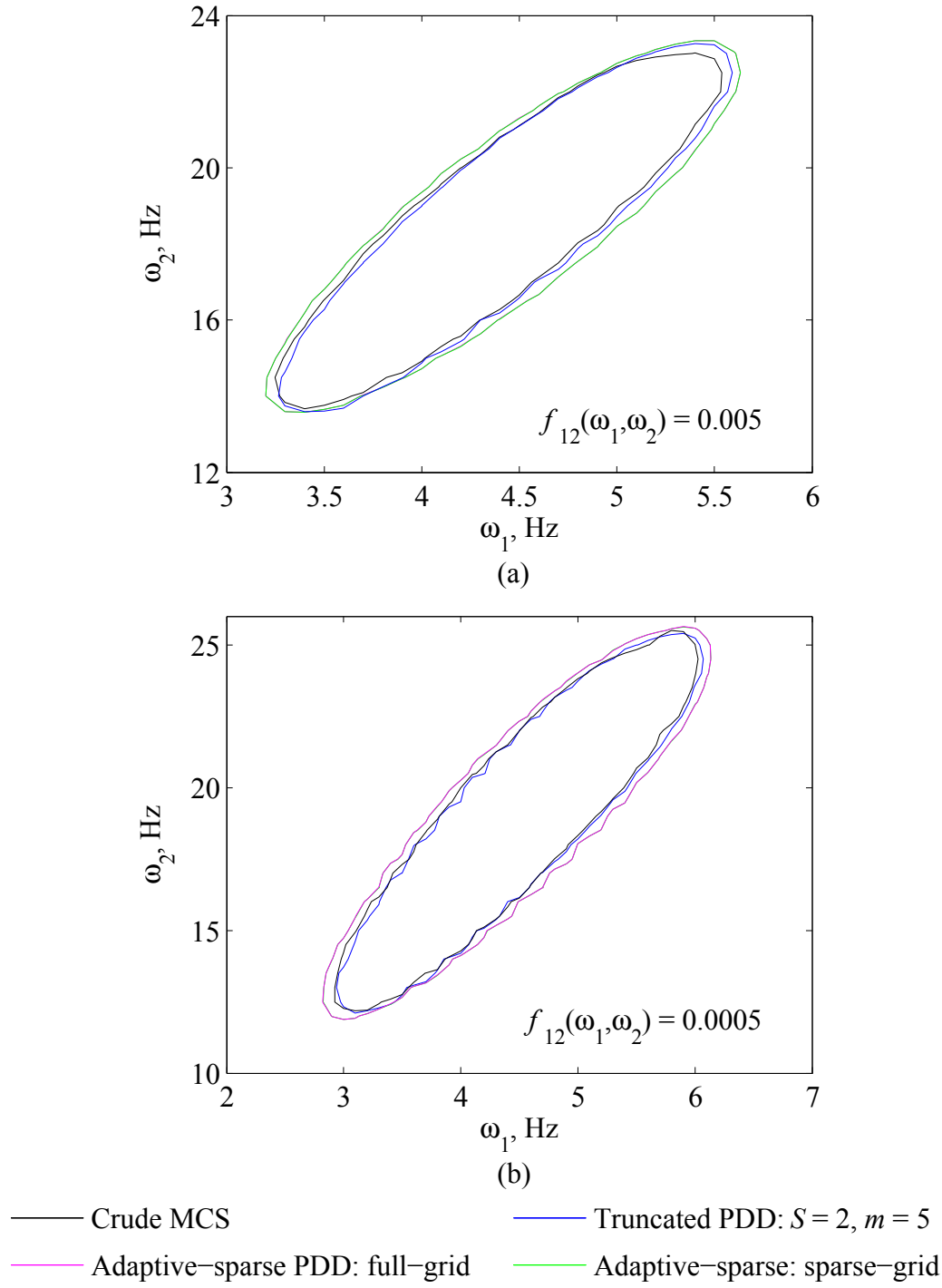

Figure 6.10: Contours of the joint density function of the first and second natural frequencies of the FGM plate by various PDD approximations and crude MCS: (a) $f_{12} = 0.005$; (b) $f_{12} = 0.0005$.

6.6 Application: A Disk Brake System

This section demonstrates the capabilities of the proposed partially adaptive-sparse PDD method in solving a large-scale practical engineering problem. The application comprises of determining instabilities in a disk brake system in terms of statistical analysis of complex frequencies and corresponding mode shapes. The dynamic instabilities in a braking system, emanating from complex frequencies, give rise to the highly undesired phenomenon of brake squeal. When a braking system is subjected to random input parameters, it is imperative to perform a random brake-squeal analysis in order to identify, quantify, and minimize the random dynamic instabilities.

6.6.1 Brake-squeal analysis

A disk brake system, illustrated in Figure 6.11, slows motion of the wheel by pushing brake pads against a rotor with a set of calipers. The brake pads mounted on a brake caliper are forced mechanically, hydraulically, pneumatically, or electromagnetically against both sides of the rotor. Friction causes the rotor and attached wheel to slow or stop. Figure 6.12 presents a simplified FEA model of a disk brake system commonly used in domestic passenger vehicles. The system consists of a rotor of diameter 288 mm and thickness 20 mm. Two pads are positioned on both sides of the rotor. Assembled behind the pads are back plates and insulators. The FEA mesh of the model consists of 26,125 elements and 111,129 active degrees of freedom and was generated using C3D6 and C3D8I elements in the Abaqus computer software (Version 6.12) [131]. The rotor is made of cast iron, and the back plates and insula-

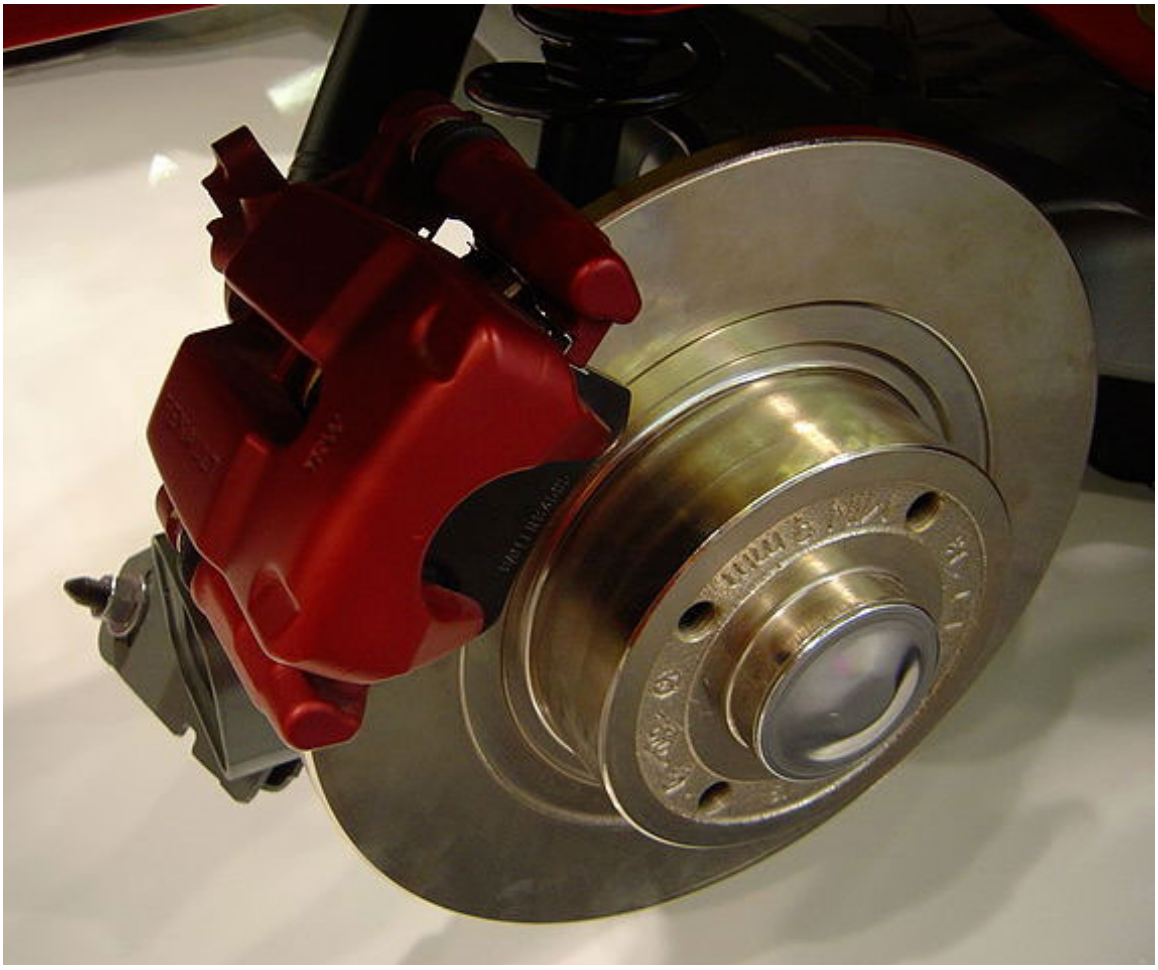

Figure 6.11: Close-up on disk brake system in a passenger vehicle.

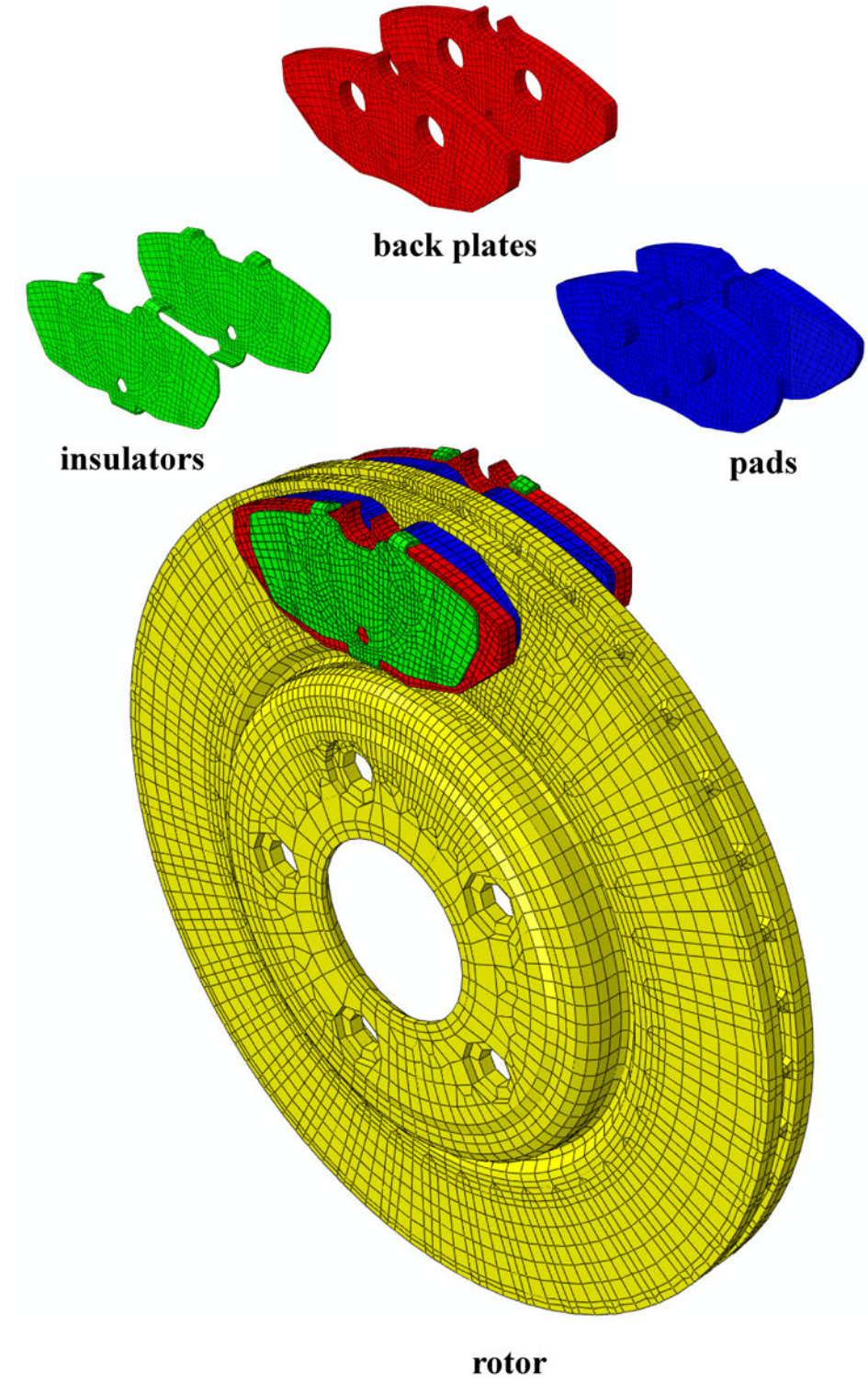

Figure 6.12: A simplified FEA model of a disk brake system with various mechanical components.

tors are made of steel. The two brake pads are made of organic frictional material, which is modeled as an orthotropic elastic material. The mass densities and Young's moduli of the rotor, back-plates, insulators, and pads, along with the shear moduli of the pads, are modeled as random variables with uniform distribution. Along with the random material properties, the brake pressure, the radial velocity of the rotor, and the coefficient of friction between the rotor and pads are modeled as uniform random variables, constituting a total of 16 random variables in this problem. The statistical properties of all random variables are listed in Table 6.4. Apart from the random material properties, the deterministic Poisson's ratio of rotor, back-plates and insulators are 0.24, 0.28, and 0.29, respectively. The three Poisson's ratios of the orthotropic material of pads are $\nu_{12} = 0.06$, $\nu_{23} = 0.41$, and $\nu_{31} = 0.15$.

6.6.2 Results

The dynamic analysis was performed in four steps. In the first step, contact was established between the rotor and the pad by applying brake pressure to the external surfaces of the insulators. Braking at low velocity was simulated in the second step by imposing a rotational velocity on the rotor, accompanied with an introduction of a non-zero friction coefficient between rotor and pad. In the third step, natural frequencies up to 20 kHz were extracted by the eigenvalue extraction procedure in the steady-state condition using the automatic multilevel substructuring method with subspace projection in Abaqus. Finally, in the fourth step a complex eigenvalue analysis was performed up to the first 55 modes.

Table 6.4: Random input variables in disk-brake system with the minimum (a_i) and maximum (b_i) values of their uniform distributions.

Random variables[(a)]	a_i	b_i
ρ_{rotor}, kg/mm^3	5.329×10^{-6}	9.071×10^{-6}
$\rho_{\text{back plate}}$, kg/mm^3	5.788×10^{-6}	9.851×10^{-6}
$\rho_{\text{insulator}}$, kg/mm^3	5.788×10^{-6}	9.851×10^{-6}
ρ_{pad}, kg/mm^3	1.858×10^{-6}	3.162×10^{-6}
E_{rotor}, GPa	92.52	157.5
$E_{\text{back plate}}$, GPa	153.2	260.8
$E_{\text{insulator}}$, GPa	153.2	260.8
$E_{1,\text{pad}}$, GPa	4.068	6.924
$E_{2,\text{pad}}$, GPa	4.068	6.924
$E_{3,\text{pad}}$, GPa	1.468	2.498
$G_{12,\text{pad}}$, GPa	1.917	3.263
$G_{13,\text{pad}}$, GPa	0.873	1.486
$G_{23,\text{pad}}$, GPa	0.873	1.486
P, kg/mm^2	370.1	629.9
ω, rad/s	3.701	6.299
μ	0.50	0.70

[(a)] ρ_{rotor}, $\rho_{\text{back plate}}$, $\rho_{\text{insulator}}$, ρ_{pad}: mass densities of corresponding materials,
E_{rotor}, $E_{\text{back plate}}$, $E_{\text{insulator}}$: elastic modulus of corresponding materials,
$E_{1,\text{pad}}$, $E_{2,\text{pad}}$, $E_{3,\text{pad}}$: elastic modulus associated with the normal directions of pad material,
$G_{12,\text{pad}}$, $G_{13,\text{pad}}$, $G_{23,\text{pad}}$: shear modulus associated with the principal directions of pad material,
P: brake pressure, ω: radial velocity, μ: friction coefficient.

The bivariate partially adaptive-sparse PDD method with tolerances $\epsilon_1 = \epsilon_2 = 10^{-6}$, $\epsilon_3 = 0.9$ was applied to determine the probabilistic characteristics of the dynamic instabilities caused by the first two unstable modes of the disk brake system. Since all input random variables are uniformly distributed, classical Legendre orthonormal polynomials were used as basis functions. The PDD coefficients were calculated using the quasi MCS with 500 samples generated from a 16-dimensional low-discrepancy Sobol sequence. Figure 6.13 displays the first four unstable modes obtained in each quasi Monte Carlo sample. These unstable modes, conveyed by complex frequencies with positive real parts, reflect the dynamic instability caused in the brake system. Each occurrence of the unstable frequency may cause the brake to squeal.

Equations (6.19) and (6.21) were employed to calculate the second-moment statistics of each nodal displacement component of an eigenvector describing the associated mode shape of the disk brake system. Based on these statistics, the $\mathcal{L}_2$-norms, that is, the square root of sum of squares, of the mean and variance of a nodal displacement were calculated. Figures 6.14(a) and 6.14(a) present contour plots of the$\mathcal{L}_2$-norms of the means and variances, respectively, of the first two unstable mode shapes of the disk brake system. Similar results can be generated for other mode shapes, stable or unstable, if desired.

For a disk brake system with complex frequencies, the ith effective damping ratio is defined as $-2\text{Re}\left[\lambda_u^{(i)}(\mathbf{X})\right]/\text{Im}|\lambda_u^{(i)}(\mathbf{X})|$, where $\text{Re}\left[\lambda_u^{(i)}(\mathbf{X})\right]$ and $\text{Im}|\lambda_u^{(i)}(\mathbf{X})|$ are the real part and the imaginary part, respectively, of the ith unstable frequency

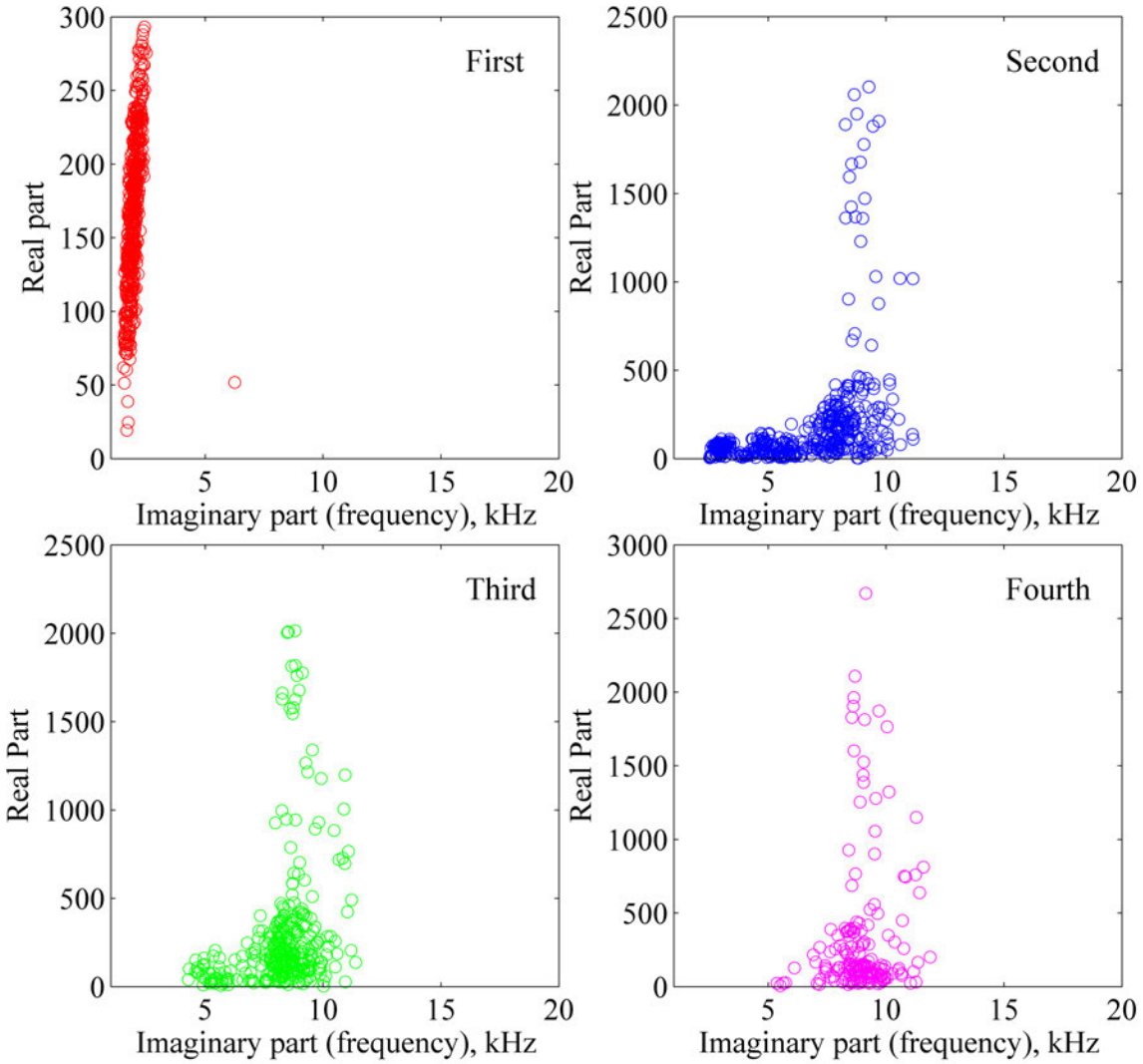

Figure 6.13: Complex eigenvalues of a disk brake system for first four unstable modes

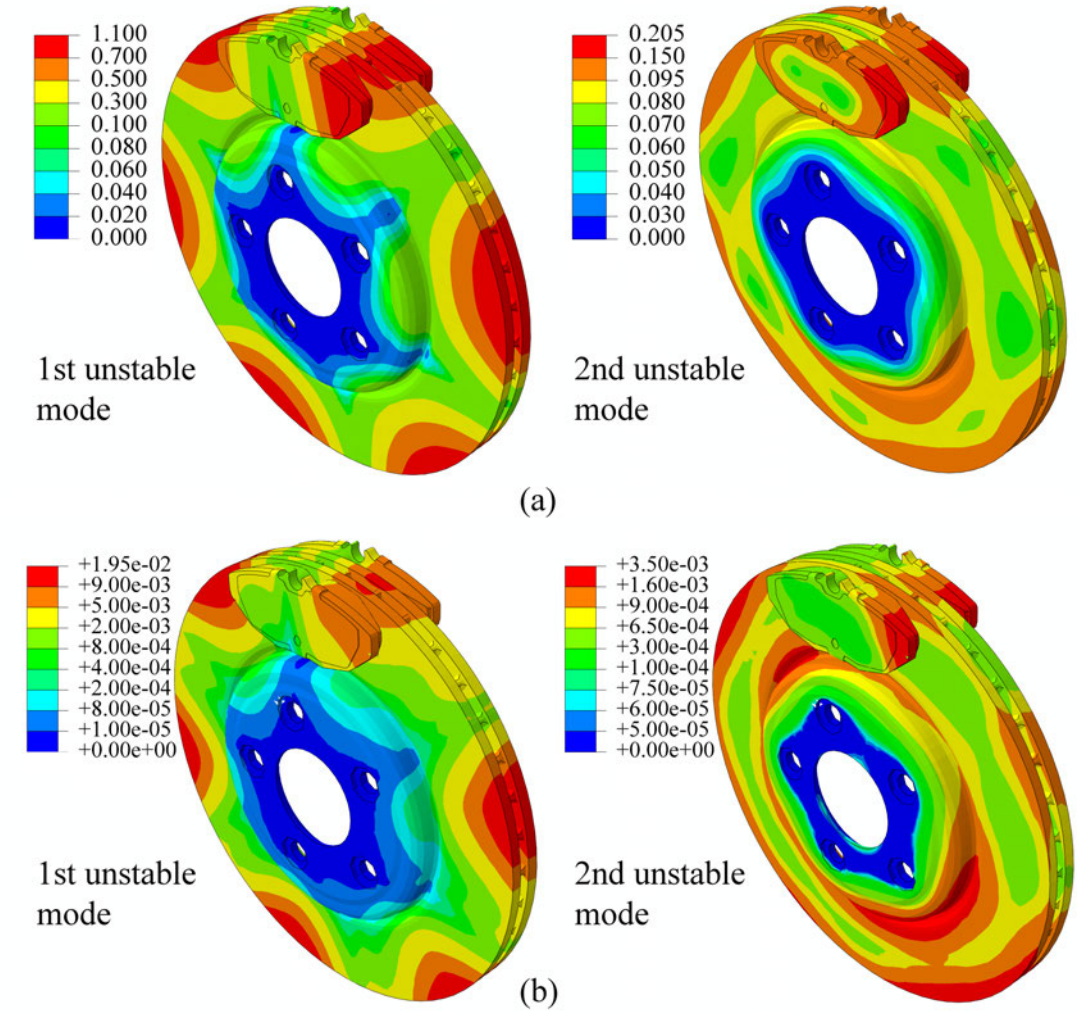

Figure 6.14: Contour plots of the $\mathcal{L}_2$-norm of the first two unstable mode shapes of a disk brake system by the bivariate partially adaptive-sparse PDD method: (a) mean; (b) variance

$\lambda_u^{(i)}(\mathbf{X})$. The magnitude of the damping ratio represents the harshness of brake squeal. The larger the magnitude of the damping ratio, the higher the propensity for brake squeal. Figure 6.15 illustrates the marginal probability density functions of the effective damping ratios corresponding to the first two unstable modes $\lambda_u^{(1)}$, and $\lambda_u^{(2)}$. These probability densities provide a measure of the effect of random input parameters on the dynamic instabilities caused in the disk brake system.

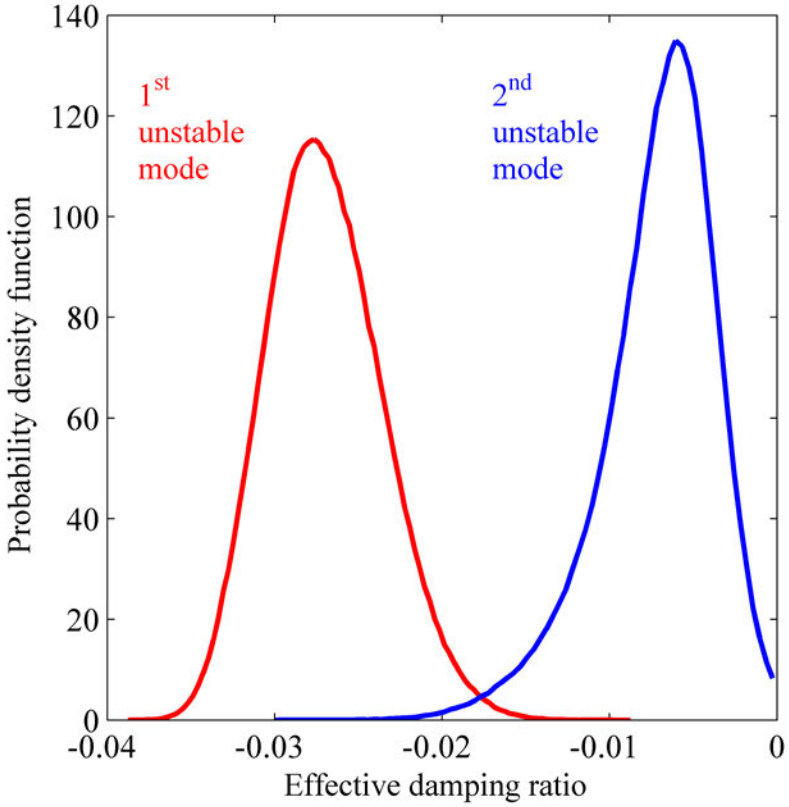

Figure 6.15: Marginal probability density functions of the effective damping ratios of first two unstable modes of a disk brake system by the bivariate partially adaptive-sparse PDD method

It is worth mentioning that a similar brake-squeal analysis with only five input random variables was performed using a univariate RDD method [41]. However, verification or improvement of the univariate solution was not possible due to the inherent limitations of the method used. The adaptive-sparse PDD approximations developed in this work have overcome this quandary even for significantly more input variables.

6.7 Conclusions

Two new adaptive-sparse PDD methods were developed for uncertainty quantification of high-dimensional complex systems commonly encountered in applied sciences and engineering. The methods are based on global sensitivity analysis for defining the relevant pruning criteria, a unified computational algorithm for retaining component functions with largest orders of their orthogonal polynomial expansions, two distinct ranking schemes for grading component functions, and a full- or sparse-grid dimension-reduction integration and quasi Monte Carlo simulation for estimating the expansion coefficients. In the fully adaptive-sparse PDD approximation, PDD component functions of an arbitrary number of input variables are retained by truncating the degree of interaction among input variables and the order of orthogonal polynomials according to specified tolerance criteria. In a partially adaptive-sparse PDD approximation, PDD component functions with a specified degree of interaction are retained by truncating the order of orthogonal polynomials, fulfilling relaxed tolerance criteria. The former approximation is comprehensive and rigorous, leading

to the second-moment statistics of a stochastic response that converges to the exact solution when the tolerances vanish. The latter approximation, obtained through regulated adaptivity and sparsity, is more economical than the former approximation and is, therefore, expected to solve practical problems with numerous variables. A unified computational algorithm was created for solving a general stochastic problem by the new PDD methods. Two distinct ranking schemes − full ranking and reduced ranking − were also developed for grading PDD component functions in the unified algorithm. Compared with past developments, the adaptive-sparse PDD methods do not require truncation parameter(s) to be assigned a priori or arbitrarily. In addition, two numerical techniques, one employing a nested sparse-grid dimension-reduction integration and the other exploiting quasi MCS, were applied for the first time to estimate the PDD expansion coefficients both accurately and efficiently.

The adaptive-sparse PDD methods were employed to calculate the second-moment properties and tail probability distributions in three numerical problems, where the output functions are either simple mathematical functions or eigenvalues of dynamic systems, including natural frequencies of a three-degree-of-freedom linear oscillator and an FGM plate. The mathematical example reveals that the user-defined tolerances of an adaptive-sparse PDD method are closely related to the relative error in calculating the variance, thus providing an effective tool for modulating the accuracy of the resultant approximation desired. Since the adaptive-sparse PDD approximation retains only the component functions with significant contributions, it is also able to achieve a desired level of accuracy with considerably fewer coefficients

than required by existing truncated PDD approximations. The results of the linear oscillator display a distinct advantage of the reduced ranking system over the full ranking system, as the former requires significantly fewer expansion coefficients to achieve results nearly identical to those of the latter. For a required level of accuracy in calculating the tail probabilistic characteristics of natural frequencies of an FGM plate, the new bivariate adaptive-sparse PDD method is more economical than the existing bivariately truncated PDD method by almost an order of magnitude. Finally, the new PDD method was successfully applied to solve a stochastic dynamic instability problem in a disk brake system, demonstrating the ability of the new method in handling industrial-scale problems.

CHAPTER 7
CONCLUSIONS AND FUTURE WORK

7.1 Conclusions

The research conducted in this study analyzed and developed innovative computational methods for solving REPs commonly encountered in high-dimensional, complex dynamic systems. The major conclusions are summarized as follows:

1. **A Rigorous Comparison of PDD and PCE Approximations:** Two stochastic expansion methods stemming from PDD and PCE were investigated for solving REPs. Although the infinite series from PCE and PDD are equivalent, their truncations endow contrasting dimensional structures, creating significant differences between the resulting PDD and PCE approximations in terms of accuracy, efficiency, and convergence properties. When the cooperative effects of input variables on an eigenvalue attenuate rapidly or vanish altogether, the PDD approximation commits smaller error than does the PCE approximation for identical expansion orders. Numerical analyses of mathematical functions or simple dynamic systems reveal markedly higher convergence rates of the PDD approximation than the PCE approximation. From the comparison of computational efforts, required to estimate with the same precision the frequency distributions of dynamic systems, including a piezoelectric transducer, the PDD approximation is significantly more efficient than the PCE approximation.

2. **Multiplicative PDD Methods:** Two new multiplicative versions of PDD, referred to as factorized PDD and logarithmic PDD, were developed for solving high-dimensional stochastic problems. Both versions involve a hierarchical, multiplicative decomposition of a multivariate function, a broad range of orthonormal polynomial bases for Fourier-polynomial expansions of component functions, and a dimension-reduction or sampling technique for estimating the expansion coefficients. Numerical problems involving mathematical functions or uncertain dynamic systems were solved to corroborate how and when a multiplicative PDD is more efficient or accurate than the additive PDD. The results show that, indeed, both the factorized and logarithmic PDD approximations can effectively exploit the hidden multiplicative structure of a stochastic response when it exists. Since a multiplicative PDD recycles the same component functions of the additive PDD, no additional cost is incurred. Finally, the random eigensolutions of a sport utility vehicle comprising 40 random variables were evaluated, demonstrating the ability of the new methods to solve industrial-scale problems.
3. **A Hybrid PDD Method:** A new hybrid PDD method was constructed for uncertainty quantification of high-dimensional complex systems. The method is based on a linear combination of an additive and a multiplicative PDD approximation. When a stochastic response is not endowed with a specific dimensional hierarchy, the hybrid PDD approximation is more appropriate than either the additive or multiplicative PDD approximation. Numerical results indicate that

the univariate hybrid PDD method, which is slightly more expensive than the univariate additive or multiplicative PDD approximations, yields more accurate stochastic solutions than the latter two methods. A successful evaluation of a random eigensolution of a pickup truck, involving coupled acoustic-structural analysis and 53 random variables, illustrates the practical capability of the hybrid PDD method.

4. **Adaptive-Sparse PDD Methods:** Two novel adaptive-sparse PDD methods were developed for solving high-dimensional uncertainty quantification problems in computational science and engineering. The methods entail global sensitivity analysis for defining the relevant pruning criteria, a unified computational algorithm for retaining component functions with largest orders of their orthogonal polynomial expansions, two distinct ranking schemes for grading component functions, and a full- or sparse-grid dimension-reduction integration and quasi Monte Carlo simulation for estimating the expansion coefficients. The fully adaptive-sparse PDD method is comprehensive and rigorous, leading to the second-moment statistics of a stochastic response that converges to the exact solution when the tolerances vanish. A partially adaptive-sparse PDD method, obtained through regulated adaptivity and sparsity, is economical and is, therefore, expected to solve practical problems with numerous variables. Compared with past developments, the adaptive-sparse PDD methods do not require its truncation parameter(s) to be assigned a priori or arbitrarily. The numerical results reveal that an adaptive-sparse PDD method achieves a desired level

of accuracy with considerably fewer coefficients compared with existing PDD approximations. For a required accuracy in calculating the tail probabilistic characteristics of natural frequencies of a functionally graded plate, the new bivariate adaptive-sparse PDD method is more efficient than the existing bivariately truncated PDD method by almost an order of magnitude. Finally, stochastic dynamic analysis of a disk brake system was performed, demonstrating the ability of the new method to tackle practical engineering problems.

7.2 Recommendations for Future Work

Based on the research and development in this study, the following activities are recommended for future efforts:

1. The decomposition methods developed in this work are all based on the fundamental requirement that input random variables be statistically independent. The analytical expressions for determining the PDD component functions, the PDD expansion coefficients, and the second-moment properties are all rooted in a product-type joint PDF of input variables. Further research is required to develop PDD of a stochastic response function for a general non-product type joint PDF, that is, when the input random variables are statistically dependent.
2. The new adaptive-sparse PDD methods developed in this work are limited to additive PDD expansions. The efficient global-sensitivity-based approach to creating a smart PDD method can be naturally applied to multiplicative and hybrid PDD approximations as well. With a modest devotion of resources,

an adaptive-sparse PDD method stemming from the multiplicative and hybrid PDD can also take shape in the near future.

3. A major assumption prior to creating any PDD approximation of a response function is that the function must be continuous and differentiable. However, encountering discontinuity and non-smoothness in random functions is a distinct possibility in engineering and applied sciences. Further research is needed to extend PDD methods for discontinuous and non-smooth functions.

APPENDIX A
PIEZOELECTRIC ANALYSIS: GOVERNING EQUATIONS

The piezoelectric effect is governed by coupled stress and electrical field and requires the solution of the mechanical equilibrium

$$\int_V \boldsymbol{\sigma} : \delta\boldsymbol{\epsilon} dV = \int_S \boldsymbol{t} \cdot \delta\boldsymbol{u} dS + \int_V \boldsymbol{f} \cdot \delta\boldsymbol{u} dV \tag{A.1}$$

and the electric flux equation

$$\int_V \boldsymbol{q} : \delta E dV = \int_S q_S \cdot \delta\varphi dS + \int_V q_V \cdot \delta\varphi dV \tag{A.2}$$

simultaneously, where $\boldsymbol{\sigma}$ is the Cauchy stress tensor, $\boldsymbol{t}$ is the traction vector with surface area S, $\boldsymbol{f} = -\rho\ddot{\boldsymbol{u}}$ is the d'Alembart force vector with ρ denoting mass density of the body with volume V, $\delta\boldsymbol{u}$ is the virtual displacement, $\delta\epsilon$ is the virtual strain, $\boldsymbol{q}$ is the electric flux (electrical displacement) vector, q_S is the electric flux per unit area entering the body, q_V is the electric flux per unit volume entering the body, $\delta\varphi$ is the virtual electric potential, and δE is the virtual potential gradient (electrical field). The constitutive behavior of the piezoelectric media is described by

$$\sigma_{ij} = D_{ijkl}\epsilon_{kl} - e_{mij}E_m \tag{A.3}$$

and

$$q_i = e_{ijk}\epsilon_{jk} + D_{ij}E_j \tag{A.4}$$

where D_{ijkl}, e_{mij}, and D_{ij} are the elastic moduli, piezoelectric stress coefficients, and dielectric constants, respectively, and the subscripts indicate appropriate components.

Consider a finite element discretization, where $\boldsymbol{U}$ and $\boldsymbol{\Phi}$ denote vectors of displacements and electric potentials at the nodal locations. Then, the approximate system of matrix equations becomes

$$\boldsymbol{M}\ddot{\boldsymbol{U}} + \boldsymbol{K}_{uu}\boldsymbol{U} + \boldsymbol{K}_{\varphi u}\boldsymbol{\Phi} = \boldsymbol{P} \tag{A.5}$$

and

$$\boldsymbol{K}_{\varphi u}\boldsymbol{U} - \boldsymbol{K}_{\varphi\varphi}\boldsymbol{\Phi} = -\boldsymbol{Q} \tag{A.6}$$

where $\boldsymbol{M}$ is the mass matrix, $\boldsymbol{K}_{uu}$ is the displacement stiffness matrix, $\boldsymbol{K}_{\varphi u}$ is the piezoelectric coupling matrix, $\boldsymbol{K}_{\varphi\varphi}$ is the dielectric stiffness matrix, $\boldsymbol{P}$ is the mechanical force vector, and $\boldsymbol{Q}$ is the electrical charge vector. These coefficient matrices, which comprise elastic moduli, coupling constants, and dielectric constants, also depend on the shape function of an element. Further details are available elsewhere [144].

APPENDIX B
AN EIGENSOLUTION FOR K-L EXPANSION

Consider a homogeneous Gaussian random field $\alpha(x)$ defined on $0 \leq x \leq L$, such that it has *zero* mean and exponential autocovariance function $\Gamma(\xi) = E[\alpha(x)\alpha(x+\xi)] = \exp[-c|\xi|]$, where $\xi = x_2 - x_1$, and c is the correlation parameter. The K-L representation of $\alpha(x)$ is [122]

$$\alpha(x) = \sum_{i=1}^{\infty} V_i \sqrt{\beta_i} g_i(x), \tag{B.1}$$

where $V_i, i = 1, \ldots, \infty$ is an infinite sequence of uncorrelated random variables, each of which has *zero* mean and *unit* variance, and $\{\beta_i, g_i(x)\}$, $i = 1, 2, \ldots, \infty$, are eigenvalues and eigenfunctions of $\Gamma(x, x+\xi)$ satisfying the following integral eigenvalue problem:

$$\beta_i g_i(x) = \int_0^L \Gamma(x, x+\xi) g_i(x+\xi) d\xi, \ \forall i = 1, 2, \ldots, \infty. \tag{B.2}$$

Differentiating Equation B.2 twice, with respect to x, the integral equation can be transformed into the following ordinary differential equation (ODE)

$$g_i''(x) + \omega_i^2 g_i(x) = 0, \ 0 \leq x \leq L, \tag{B.3}$$

and the associated boundary conditions (BCs)

$$\begin{aligned} c g_i(L) + g_i'(L) &= 0, \\ c g_i(0) - g_i'(0) &= 0, \end{aligned} \tag{B.4}$$

where $\omega_i^2 = (2c - c^2\lambda_i)/\lambda_i$. The solution of ODE in Equation B.3 subject to BCs in Equation B.4 is [46]:

$$g_i(x) = \begin{cases} \dfrac{\cos(\omega_i x)}{\sqrt{\dfrac{L}{2} + \dfrac{\sin(\omega_i L)}{2\omega_i}}}, & i \text{ is odd}, \\ \dfrac{\sin(\omega_i x)}{\sqrt{\dfrac{L}{2} - \dfrac{\sin(\omega_i L)}{2\omega_i}}}, & i \text{ is even}. \end{cases} \tag{B.5}$$

The corresponding eigenvalues are

$$\beta_i = \frac{2c}{\omega_i^2 + c^2}. \tag{B.6}$$

The parameter ω_i is determined by solving the transcendental equations

$$\begin{aligned} c - \omega_i \tan(\omega_i L/2) &= 0, \ i \text{ is odd}, \\ \omega_i + c \tan(\omega_i L/2) &= 0, \ i \text{ is even}. \end{aligned} \tag{B.7}$$

APPENDIX C
WEIGHTS AND EXCITATION FREQUENCIES

Table C.1 presents weights and excitation frequencies for calculating the vertical component of the weighted RMS acceleration.

Table C.1: Frequencies and weights as listed in International Standard ISO 2631 [1].

Frequency (ω_j), Hz	Weight (α_j) $\times 1000$	Frequency (ω_j), Hz	Weight (α_j) $\times 1000$
0.1	31.2	6.3	1054
0.125	48.6	8	1036
0.16	79.0	10	988
0.2	121	12.5	902
0.25	182	16	768
0.315	263	20	636
0.4	352	25	513
0.5	418	31.5	405
0.63	459	40	314
0.8	477	50	246
1	482	63	186
1.25	484	80	132
1.6	494	100	88.7
2	531	125	54
2.5	631	160	28.5
3.15	804	200	15.2
4	967	250	7.90
5	1039	315	3.98

APPENDIX D
COUPLED ACOUSTIC-STRUCTURAL ANALYSIS: GOVERNING EQUATIONS

A coupled acoustic-structural analysis involves solution of the acoustic variational equation

$$\begin{aligned}
&\int_{V_f}\left[\delta p\left(\frac{1}{K_f}\ddot{p}+\frac{\gamma}{\rho_f K_f}\dot{p}\right)+\frac{1}{\rho_f}\frac{\partial\delta p}{\partial\mathbf{x}}\cdot\frac{\partial p}{\partial\mathbf{x}}\right]dV-\int_{S_{ft}}\delta pT_0dS\\
&+\int_{S_{fr}}\delta p\left(\frac{\gamma}{\rho_f c_1}p+\left(\frac{\gamma}{\rho_f k_1}+\frac{1}{c_1}\right)\dot{p}+\frac{1}{k_1}\ddot{p}\right)dS\\
&+\int_{S_{fi}}\delta p\left(\frac{1}{c_1}\dot{p}+\frac{1}{a_1}p\right)dS-\int_{S_{fs}}\delta p\mathbf{n}^-\cdot\ddot{\mathbf{u}}^m dS\\
&+\int_{S_{frs}}\delta p\left(\frac{\gamma}{\rho_f c_1}p+\left(\frac{\gamma}{\rho_f k_1}+\frac{1}{c_1}\right)\dot{p}+\frac{1}{k_1}\ddot{p}-\mathbf{n}^-\cdot\ddot{\mathbf{u}}^m\right)dS=0, \qquad \text{(D.1)}
\end{aligned}$$

and the structural virtual work equation

$$\begin{aligned}
&\int_V\delta\epsilon:\sigma dV+\int_V\alpha_c\rho\delta\mathbf{u}^m\cdot\dot{\mathbf{u}}^m dV+\int_V\rho\delta\mathbf{u}^m\cdot\ddot{\mathbf{u}}^m dV\\
&+\int_{S_{fs}}p\delta\mathbf{u}^m\cdot\mathbf{n}dS-\int_{S_t}\delta\mathbf{u}^m\cdot\mathbf{t}dS=0 \qquad \text{(D.2)}
\end{aligned}$$

simultaneously for the structural displacement $\mathbf{u}^m$ and the acoustic "displacement" or pressure p. In Equations (D.1) and (D.2) K_f is the bulk modulus of the fluid acoustic medium of volume V_f; γ is the volumetric drag, or force per unit volume per velocity, in the fluid; ρ_f is the mass density of the fluid; δp is the pressure variation in the fluid; $\mathbf{x}$ is spatial position of the fluid particle; T_0 is the prescribed boundary traction over S_{ft}, the acoustic boundary subregion where the normal derivative of the acoustic medium is prescribed; $1/c_1$ and $1/k_1$ are the proportionality coefficients between the pressure and velocity, and the pressure and displacement, respectively,

normal to the surface of the fluid; S_{fr} is the reactive acoustic boundary subregion; S_{fi} is the radiating acoustic boundary subregion; S_{frs} is the acoustic boundary subregions where the displacements are linearly coupled but not necessarily identically equal due to the presence of a compliant or reactive intervening layer; $\mathbf{n}^-$ is the outward normal to the structure; σ is the stress at a point on the structure; $\delta\epsilon$ is the strain variation in structure; α_c is the mass proportional damping factor; ρ is mass density of the structure, and $\mathbf{t}$ is the surface traction applied over the surface S_t of the structure. Further details are available elsewhere [145, 146].

REFERENCES

[1] ISO-2631. *Guide for the evaluation of human exposure to whole-body vibration*. International Organization for Standardization, Geneva, Switzerland, 1974.

[2] P. J. Forrester, N. C. Snaith, and J. Verbaarschot. Developments in random matrix theory. *Journal of Physics A: Mathematical and General*, 36:R1–R10, 2003.

[3] J. Wishart. The generalised product moment distribution in samples from a normal multivariate population. *Biometrika*, 20A(1/2):pp. 32–52, 1928.

[4] E. P. Wigner. On the statistical distribution of the widths and spacings of nuclear resonance levels. *Proceedings of the Cambridge Philosophical Society*, 47(4):790, 1950.

[5] E. P. Wigner. Statistical properties of real symmetric matrices with many dimensions. In *Proceedings of 4th Canadian Mathematics Congress*, pages 174–184. Princeton University, 1957.

[6] M. L. Mehta. On the statistical properties of the level-spacings in nuclear spectra. *Nuclear Physics*, 18(0):395 – 419, 1960.

[7] F. J. Dyson. Statistical theory of the energy levels of complex systems i, ii, and iii. *Journal of Mathematical Physics*, 3(1):166–175, 1962.

[8] M. L. Mehta. *Random Matrices*, volume 142. Elsevier, 2004.

[9] F. J. Dyson. The threefold way. algebraic structure of symmetry groups and ensembles in quantum mechanics. *Journal of Mathematical Physics*, 3(6):1199–1215, 1962.

[10] M. Gaudin. Sur la loi limite de l'espacement des valeurs propres d'une matrice ale'atoire. *Nuclear Physics*, 25(0):447 – 458, 1961.

[11] E. P. Wigner. Characteristics vectors of bordered matrices with infinite dimensions. *The Annals of Mathematics*, 65(2):pp. 203–207, 1957.

[12] H. L. Montgomery. The pair correlation of zeros of the zeta function. In *Proceedings of 1972 St. Louis Symposium*, pages 181–193, 1973.

[13] A. M. Odlyzko. On the distribution of spacings between zeros of the zeta function. *Math. Comp*, 48:273–308, 1987.

[14] F. Mezzadri and N. C. Snaith. *Recent perspectives in random matrix theory and number theory*. London Mathematical Society lecture note series. Cambridge University Press, 2005.

[15] A. G. Constantine. Some non-central distribution problems in multivariate analysis. *The Annals of Mathematical Statistics*, 34(4):pp. 1270–1285, 1963.

[16] A. T. James. Distributions of matrix variates and latent roots derived from normal samples. *The Annals of Mathematical Statistics*, 35(2):pp. 475–501, 1964.

[17] R. J. Muirhead. *Aspects of multivariate statistical theory*. Wiley series in probability and mathematical statistics: Probability and mathematical statistics. Wiley-Interscience, 2005.

[18] M. D. Mckay, R. J. Beckman, and W. J. Conover. A comparison of three methods for selecting values of input variables in the analysis of output from a computer code. *Technometrics*, 42(1):pp. 55–61, 2000.

[19] S. Smale. On the efficiency of algorithms of analysis. *Bull. Am. Math. Soc., New Ser.*, 13:87–121, 1985.

[20] P. Viswanath, D. N. C. Tse, and V. Anantharam. Asymptotically optimal water-filling in vector multiple-access channels. *Information Theory, IEEE Transactions on*, 47(1):241 –267, jan 2001.

[21] L. Zheng and D. N. C. Tse. Diversity and multiplexing: a fundamental tradeoff in multiple-antenna channels. *Information Theory, IEEE Transactions on*, 49(5):1073 – 1096, may 2003.

[22] V. Plerou, P. Gopikrishnan, B. Rosenow, L. A. N. Amaral, and H. E. Stanley. A random matrix theory approach to financial cross-correlations. *Physica A: Statistical Mechanics and its Applications*, 287(34):374 – 382, 2000.

[23] M. Potters, J. P. Bouchaud, and L. Laloux. Financial applications of random matrix theory: Old laces and new pieces. *Matrix*, 36(4):129–132, 2005.

[24] M. B. Eisen, P. T. Spellman, P. O. Brown, and D. Botstein. Cluster analysis and display of genome-wide expression patterns. *Proceedings of the National Academy of Sciences*, 95(25):14863–14868, December 1998.

[25] S. Adhikari and M. I. Friswell. Random matrix eigenvalue problems in structural dynamics. *International Journal for Numerical Methods in Engineering*, 69(3):562–591, 2007.

[26] J. V. Scheidt and W. Purkert. Random eigenvalue problems. berlin, akademie-verlag 1983. 271 s., 50 abb., m 48,. bn 7632056 (6747). *ZAMM - Journal of Applied Mathematics and Mechanics / Zeitschrift fr Angewandte Mathematik und Mechanik*, 65(6), 1985.

[27] H. Benaroya. Random eigenvalues, algebraic methods and structural dynamic models. *Applied Mathematics and Computation*, 52(1):37 – 66, 1992.

[28] H. Benaroya and M. Rehak. Finite element methods in probabilistic structural analysis: A selective review. *Applied Mechanics Reviews*, 41(5):201–213, 1988.

[29] W. E. Boyce. Random eigenvalue problems. In A.T. Bharucha-Reid, editor, *Probabilistic Methods in Applied Mathematics I*, number v. 3. Academic Press, 1968.

[30] M. Grigoriu. A solution of the random eigenvalue problem by crossing theory. *Journal of Sound and Vibration*, 158(1):69–80, 1992.

[31] M. Grigoriu. *Stochastic calculus: applications in science and engineering.* Birkhauser, 2002.

[32] R. A. Ibrahim. Structural dynamics with parameter uncertainties. *Applied Mechanics Reviews*, 40(3):309–328, 1987.

[33] C. Lee and R. Singh. Analysis Of Discrete Vibratory Systems With Parameter Uncertainties, Part I: Eigensolution. *Journal of Sound Vibration*, 174:379–394, July 1994.

[34] C. S. Manohar and R. A. Ibrahim. Progress in structural dynamics with stochastic parameter variations: 1987-1998. *Applied Mechanics Reviews*, 52(5):177–197, 1999.

[35] S. Mehlhose, J. Vom Scheidt, and R. Wunderlich. Random eigenvalue problems for bending vibrations of beams. *ZAMM, Z. Angew. Math. Mech*, 14, 1998.

[36] P. B. Nair and A. J. Keane. An approximate solution scheme for the algebraic random eigenvalue problem. *Journal of Sound and Vibration*, 260(1):45–65, 2003.

[37] M. Shinozuka and C. J. Astill. Random eigenvalue problems in structural analysis. *AIAA Journal*, 10(4):456–462, 1972.

[38] J. Zhang and B. Ellingwood. Effects of uncertain material properties on structural stability. *Journal of structural Engineering*, 121(4):705–714, 1995.

[39] H. J. Pradlwarter, G. I. Schuëller, and G. S. Szekely. Random eigenvalue problems for large systems. *Computers & Structures*, 80:2415–2424, 2002.

[40] S. Rahman. A solution of the random eigenvalue problem by a dimensional decomposition method. *International Journal for Numerical Methods in Engineering*, 67:1318–1340, 2006.

[41] S. Rahman. Stochastic dynamic systems with complex-valued eigensolutions. *International Journal for Numerical Methods in Engineering*, 71:963–986, 2007.

[42] S. Rahman. Probability distributions of natural frequencies of uncertain dynamic systems. *AIAA Journal*, 47(6):1579–1589, 2009.

[43] International association for structural safety and reliability. http://www.civil.columbia.edu/iassar/. IASSAR.

[44] N. Wiener. The homogeneous chaos. *American Journal of Mathematics*, 60(4):897–936, 1938.

[45] R. V. Hogg, J. W. McKean, and A. T. Craig. *Introduction to mathematical statistics*. Pearson Education, 2005.

[46] R. Ghanem and P. D. Spanos. *Stochastic finite elements: a spectral approach*. World Publishing Corp., 1991.

[47] S. Rahman and H. Xu. A meshless method for computational stochastic mechanics. *International Journal for Computational Methods in Engineering Science and Mechanics*, 6(1):41–58, 2005.

[48] S. Rahman. *Meshfree Methods in Computational Stochastic Mechanics*, volume 11, pages 187–211. World Scientific Publishing Co., Singapore, 2005.

[49] K. J. Bathe. *Finite element procedures in engineering analysis*. Prentice-Hall civil engineering and engineering mechanics series. Prentice-Hall, 1982.

[50] A. Chopra. *Dynamics of structures*. Prentice-Hall, 1995.

[51] R. W. Clough and J. Penzien. *Dynamics of structures*. McGraw-Hill, 1975.

[52] R. R. Craig. *Structural dynamics: an introduction to computer methods*. Wiley, 1981.

[53] L. Meirovitch. *Fundamentals of Vibrations*. Waveland Press, Inc., 2010.

[54] I. Gohberg, P. Lancaster, and L. Rodman. *Matrix Polynomials*. Classics in Applied Mathematics. Society for Industrial and Applied Mathematics, 2009.

[55] P. Lancaster. *Lambda-Matrices and Vibrating Systems*. Dover Books on Mathematics Series. Dover Publications, 2002.

[56] J. S. Przemieniecki. *Theory of matrix structural analysis*. Dover books on engineering. Dover, 1985.

[57] P. Lancaster. Strongly stable gyroscopic systems. *The Electronic Journal of Linear Algebra*, 5:53–66, 1999.

[58] T. M. Hwang, W. W. Lin, and V. Mehrmann. Numerical solution of quadratic eigenvalue problems with structure-preserving methods. *SIAM J. Sci. Comput.*, 24:1283–1302, April 2002.

[59] T. Apel, V. Mehrmann, and D. Watkins. Structured eigenvalue methods for the computation of corner singularities in 3d anisotropic elastic structures. *Computer Methods in Applied Mechanics and Engineering*, 191(39):4459 – 4473, 2002.

[60] T. Apel, A. M. Sändig, and S. I. Solov'ev. Computation of 3d vertex singularities for linear elasticity: Error estimates for a finite element method on graded meshes. *ESAIM: Mathematical Modelling and Numerical Analysis*, 36(06):1043–1070, 2002.

[61] D. Leguillon and E. Sanchez-Palencia. On 3d cracks intersecting a free surface in laminated composites. *International Journal of Fracture*, 99:25–40, 1999. 10.1023/A:1018366720722.

[62] H. Schmitz, K. Volk, and W. Wendland. Three-dimensional singularities of elastic fields near vertices. *Numerical Methods for Partial Differential Equations*, 9(3):323–337, 1993.

[63] A. Hilliges. Numerische losung von quadratischen eigenwertproblemen mit anwendungen in der schienendynamik. Master's thesis, TU Berlin, Berlin, 2004.

[64] A. Hilliges, C. Mehl, and V. Mehrmann. On the solution of palindromic eigen-

value problems. In *Proceedings of the 4th European Congress on Computational Methods in Applied Sciences and Engineering*, Jyvaskyla, Finland, 2004.

[65] D. S. Mackey, N. Mackey, C. Mehl, and V. Mehrmann. Palindromic polynomial eigenvalue problems: Good vibrations from good linearizations. Technical report, DFG Research Center Matheon, Mathematics for, 2005.

[66] V. Mehrmann and H. Voss. Nonlinear eigenvalue problems : A challenge for modern eigenvalue methods. *GAMM Mitteilungen*, 27(1):1–44, 2004.

[67] H. Voss. A new justification of finite dynamic element methods. In Albrecht et al., editors, *Numerical Treatment of Eigenvalue Problems*, volume 4, pages 232–242. Birkauser Verlag, 1987.

[68] K. Rothe. Least squares element method for boundary eigenvalue problems. *International Journal for Numerical Methods in Engineering*, 33(10):2129–2143, 1992.

[69] L. Mazurenko and H. Voss. On the number of eigenvalues of a rational eigenproblem, 2003.

[70] H. Voss. An error bound for eigenvalue analysis by nodal condensation. In Albrecht et al., editors, *Numerical Treatment of Eigenvalue Problems*, volume 3, pages 205–214. Birkauser Verlag, 1984.

[71] H. Voss. Initializing iterative projection methods for rational symmetric eigenproblems, 2003.

[72] C. Conca, J. Planchard, and M. Vanninathan. Existence and location of eigenvalues for fluid-solid structures. *Computer Methods in Applied Mechanics and Engineering*, 77(3):253 – 291, 1989.

[73] J. Planchard. Eigenfrequencies of a tube bundle placed in a confined fluid. *Computer Methods in Applied Mechanics and Engineering*, 30(1):75 – 93, 1982.

[74] P. Hager. *Eigenfrequency Analysis: FE-Adaptivity and a Nonlinear Eigenvalue Problem*. PhD thesis, Chalmers University of Technology, Goteborg, 2001.

[75] I. Dumitriu and A. Edelman. Matrix models for beta ensembles. *Journal of Mathematical Physics*, 43(11):5830–5847, 2002.

[76] W. Hoeffding. A class of statistics with asymptotically normal distribution. *The Annals of Mathematical Statistics*, 19(3):pp. 293–325, 1948.

[77] A. B. Owen. The dimension distribution and quadrature test functions. *Statistica Sinica*, 13(1):118, 2003.

[78] I. M. Sobol. Multidimensional quadrature formulas and haar functions. *Nauka, Moscow*, 1969. In Russian.

[79] I. M. Sobol. Theorems and examples on high dimensional model representation. *Reliability Engineering & System Safety*, 79(2):187 – 193, 2003.

[80] B. Efron and C. Stein. The jackknife estimate of variance. *The Annals of Statistics*, 9(3):pp. 586–596, 1981.

[81] A. B. Owen. Monte carlo variance of scrambled net quadrature. *SIAM Journal on Numerical Analysis*, 34(5):pp. 1884–1910, 1997.

[82] F. J. Hickernell. Quadrature error bounds with applications to lattice rules. *SIAM J. Numer. Anal*, 33:1995–2016, 1996.

[83] H. Rabitz and O. Alis. General foundations of high dimensional model representations. *Journal of Mathematical Chemistry*, 25:197–233, 1999. 10.1023/A:1019188517934.

[84] S. Rahman and H. Xu. A univariate dimension-reduction method for multidimensional integration in stochastic mechanics. *Probabilistic Engineering Mechanics*, 19(4):393–408, 2004.

[85] H. Xu and S. Rahman. A generalized dimension-reduction method for multidimensional integration in stochastic mechanics. *International Journal for Numerical Methods in Engineering*, 61:1992–2019, 2004.

[86] H. Xu and S. Rahman. Decomposition methods for structural reliability analysis. *Probabilistic Engineering Mechanics*, 20(3):239 – 250, 2005.

[87] S. Rahman. A polynomial dimensional decomposition for stochastic computing. *International Journal for Numerical Methods in Engineering*, 76:2091–2116, 2008.

[88] W. Gautschi. *Orthogonal polynomials: computation and approximation*. Numerical mathematics and scientific computation. Oxford University Press, 2004.

[89] S. Rahman. Statistical moments of polynomial dimensional decomposition. *Journal of Engineering Mechanics*, 136(7):923–927, 2010.

[90] S. Rahman. Extended polynomial dimensional decomposition for arbitrary probability distributions. *Journal of Engineering Mechanics*, 135(12):1439–1451, 2009.

[91] D. Xiu and G. E. Karniadakis. The wiener-askey polynomial chaos for stochastic differential equations. *SIAM Journal of Scientific Computing*, 24:619–644, 2002.

[92] D. Ghosh. *On the Characterization and Analysis of the Random Eigenvalue Problem*. PhD thesis, John Hopkins University, Baltimore, 2005.

[93] Debraj Ghosh and Roger Ghanem. Stochastic convergence acceleration through basis enrichment of polynomial chaos expansions. *International Journal for Numerical Methods in Engineering*, 73(2):162–184, 2008.

[94] R. Y. Rubinstein and D. P. Kroese. *Simulation and the Monte Carlo method*. Wiley series in probability and mathematical statistics. Probability and mathematical statistics. John Wiley & Sons, 2008.

[95] K. Entacher. Quasi-monte carlo methods for numerical integration of multivariate haar series. *BIT37*, 4:845–860, 1997.

[96] H. Niederreiter. *Monte Carlo and Quasi-Monte Carlo methods 1996*. Lecture notes in statistics. Springer, 1998.

[97] I. M. Sobol. On quasi-monte carlo integrations. *Mathematics and Computers in Simulation*, 47(25):103 – 112, 1998.

[98] S. Engelund and R. Rackwitz. A benchmark study on importance sampling techniques in structural reliability. *Structural Safety*, 12(4):255 – 276, 1993.

[99] R. E. Melchers. Importance sampling in structural systems. *Structural Safety*, 6(1):3 – 10, 1989.

[100] P. Bjerager. Probability integration by directional simulation. *Journal of Engineering Mechanics*, 114(8):1285–1302, 1988.

[101] J. Nie and B. R. Ellingwood. Directional methods for structural reliability analysis. *Structural Safety*, 22(3):233 – 249, 2000.

[102] W. R. Gilks, S. Richardson, and D. J. Spiegelhalter. *Markov chain Monte Carlo in practice*. Interdisciplinary statistics. Chapman & Hall, 1996.

[103] B. L. Nelson and B. W. Schmeiser. Decomposition of some well-known variance reduction techniques. *J. Stat. Comput. Simul.*, 23:183–209, January 1986.

[104] M. Stein. Large sample properties of simulations using latin hypercube sampling. *Technometrics*, 29(2):pp. 143–151, 1987.

[105] Visual Numerics Corporate Headquarters. *IMSL Numerical Libraries, User's Guide and Theoretical Manual*, 2005.

[106] J. G. F. Francis. The qr transformation a unitary analogue to the lr transformation part 1. *The Computer Journal*, 4(3):265–271, 1961.

[107] J. G. F. Francis. The qr transformation part 2. *The Computer Journal*, 4(4):332–345, 1962.

[108] Dassault Systems Simulia Corp. *ABAQUS Standard, Version 6.9*, 2010.

[109] Dassault Systems Simulia Corp. *ABAQUS Standard, Version 6.11*, 2011.

[110] J. K. Bennighof and C. K. Kim. An adaptive multi-level substructuring method for efficient modeling of complex structures. In *33rd Structural Dynamics and Materials Conference, Dallas, TX*. American Institute of Aeronautics and Astronautics, 1992.

[111] J. K. Bennighof, M. F. Kaplan, M. B. Muller, and M. Kim. Meeting the nvh computational challange: Automated multi-level substructuring. In *18th International Modal Analysis Conference, San Antonio, Texas*, 2000.

[112] J. K. Bennighof and R. B. Lehoucq. An automated multilevel substructuring method for eigenspace computation in linear elastodynamics. *SIAM Journal on Scientific Computing*, 25(6):2084–2106, 2004.

[113] H. Rutishauser. Solution of eigenvalue roblems with the lr transformation. In *Further Contributions to the Solution of Simultaneous Linear Equations and the Determination of Eigenvalues*, volume 49 of *Applied Math Series*, page 921. National Bureau of Standards.

[114] J. H. Wilkinson. *The algebraic eigenvalue problem.* Monographs on numerical analysis. Clarendon Press, 1988.

[115] V. N. Kublanovskaya. On some algorithms for the solution of the complete eigenvalue problem. *USSR Computational Mathematics and Mathematical Physics*, 1(3):637 – 657, 1962.

[116] B. Sudret. Global sensitivity analysis using polynomial chaos expansions. *Reliability Engineering and System Safety*, 93(7):964–979, 2008.

[117] T. Ishigami and T. Homma. An importance quantification technique in uncertainty analysis for computer models. In *First International Symposium on Uncertainty Modeling and Analysis*, pages 398–403. University of Maryland, 1990.

[118] F. Y. Kuo, I. H. Sloan, G. W. Wasilkowski, and H. Wozniakowski. On decompositions of multivariate functions. *Mathematics of Computation*, 79:953–966, 2011.

[119] S. Rahman. Approximation errors in truncated dimensional decompositions. *submitted to Mathematics of Computation*, 2011.

[120] M. A. Tunga and M. Demiralp. A factorized high dimensional model representation on the nodes of a finite hyperprismatic regular grid. *Applied Mathematics and Computation*, 164:865–883, 2005.

[121] W. J. Morokoff and R. E. Caflisch. Quasi-monte carlo integration. *Journal of Computational Physics*, 122:218–230, 1995.

[122] W. B. Davenport and W. L. Root. *An Introduction to the Theory of Random Signals and Noise*. McGraw-Hill, New York, NY, 1958.

[123] J. K. Cullum and R. A. Willoughby. *Lanczos Algorithms for Large Symmetric Eigenvalue Computations: Theory*. Classics in applied mathematics. Society for Industrial and Applied Mathematics, 2002.

[124] J. K. Bennighof and M. F. Kaplan. Frequency window implementation of adaptive multi-level substructuring. *Journal of Vibration and Acoustics*, 120(2):409–418, 1998.

[125] H. Niederreiter. *Random Number Generation and Quasi-Monte Carlo Methods*. CBMS-NSF Regional Conference Series in Applied Mathematics. Society for Industrial and Applied Mathematics, 1992.

[126] J.H. Halton. On the efficiency of certain quasi-random sequences of points in evaluating multi-dimensional integrals. *Numerische Mathematik*, 2(1):84–90, 1960.

[127] Henri Faure. Discrépances de suites associées à un système de numération (en dimension un). *Bulletin de la Société Mathématique de France*, 109:143–182, 1981.

[128] I. M. Sobol. On the distribution of points in a cube and the approximate evaluation of integrals. *U.S.S.R. Comput. Math. Math. Phys.*, 7:86–112, 1967.

[129] I.H. Sloan and S. Joe. *Lattice Methods for Multiple Integration*. Oxford science publications. Clarendon Press, 1994.

[130] Xiaoqun Wang. Improving the rejection sampling method in quasi-monte carlo methods. *Journal of Computational and Applied Mathematics*, 114(2):231 – 246, 2000.

[131] Dassault Systems Simulia Corp. *ABAQUS Standard, Version 6.12*, 2012.

[132] ISO-5128. *Acoustics - Measurement of noise inside motor vehicles*. International Organization for Standardization, Geneva, Switzerland, 1980.

[133] Xiang Ma and Nicholas Zabaras. An adaptive high-dimensional stochastic model representation technique for the solution of stochastic partial differential equations. *Journal of Computational Physics*, 229(10):3884 – 3915, 2010.

[134] Xiu Yang, Minseok Choi, Guang Lin, and George Em Karniadakis. Adaptive anova decomposition of stochastic incompressible and compressible flows. *Journal of Computational Physics*, 231(4):1587 – 1614, 2012.

[135] S. Rahman and V. Yadav. Orthogonal polynomial expansions for solving random eigenvalue problems. *International Journal for Uncertainty Quantification*, 1:163–187, 2011.

[136] Sharif Rahman. Decomposition methods for structural reliability analysis revisited. *Probabilistic Engineering Mechanics*, 26(2):357 – 363, 2011.

[137] I.M. Sobol. Global sensitivity indices for nonlinear mathematical models and their monte carlo estimates. *Mathematics and Computers in Simulation*, 55(13):271 – 280, 2001.

[138] Sharif Rahman. Global sensitivity analysis by polynomial dimensional decomposition. *Reliability Engineering & System Safety*, 96(7):825 – 837, 2011.

[139] Xuchun Ren and Sharif Rahman. Polynomial dimensional decomposition for stochastic sensitivity analysis. *submitted to International Journal of Numerical Methods in Engineering*, 2013.

[140] Alan Genz. Fully symmetric interpolatory rules for multiple integrals. *SIAM Journal on Numerical Analysis*, 23(6):pp. 1273–1283, 1986.

[141] Alan Genz and B.D. Keister. Fully symmetric interpolatory rules for multiple integrals over infinite regions with gaussian weight. *Journal of Computational and Applied Mathematics*, 71(2):299 – 309, 1996.

[142] Erich Novak and Klaus Ritter. Simple cubature formulas with high polynomial exactness. *Constructive Approximation*, 15(4):499–522, 1999.

[143] Vaibhav Yadav and Sharif Rahman. Uncertainty quantification of high-dimensional complex systems by multiplicative polynomial dimensional decompositions. *International Journal for Numerical Methods in Engineering*, 94(3):221–247, 2013.

[144] T. Ikeda. *Fundamentals of piezoelectricity*. Oxford science publications. Oxford University Press, Incorporated, 1996.

[145] H. Allik. The application of finite and infinite elements to problems in structural acoustics. In *Computational Mechanics '91: Proceedings of the International Conference on Computational Engineering Science*. ICES Publications, 1991.

[146] P. Morse and K. Ingard. *Theoretical Acoustics*. McGraw-Hill, 1968.

[147] D. Ghosh and R. G. Ghanem. Analysis of eigenvalues and modal interaction of stochastic systems. *AIAA Journal*, 43(10):2196–2201, 2005.

[148] S. Adhikari. Random eigenvalue problems revisited. *Sadhana*, 31:293–314, 2006. 10.1007/BF02716778.

[149] R. Bellman. *Dynamic Programming*. Princeton University Press: Princeton, NJ, 1957.

[150] D. Brendan and McKay. The expected eigenvalue distribution of a large regular graph. *Linear Algebra and its Applications*, 40(0):203 – 216, 1981.

[151] Michael Griebel and Markus Holtz. Dimension-wise integration of high-dimensional functions with applications to finance. *J. Complex.*, 26(5):455–489, October 2010.

[152] M. Griebel. *Sparse Grids and Related Approximation Schemes for Higher Dimensional Problems*. Sonderforschungsbereich 611, Singuläre Phänomene und Skalierung in Mathematischen Modellen. SFB 611, 2006.

[153] Manas K. Deb, Ivo M. Babuška, and J.Tinsley Oden. Solution of stochastic partial differential equations using galerkin finite element techniques. *Computer Methods in Applied Mechanics and Engineering*, 190(48):6359 – 6372, 2001.

[154] Baskar Ganapathysubramanian and Nicholas Zabaras. Sparse grid collocation schemes for stochastic natural convection problems. *Journal of Computational Physics*, 225(1):652 – 685, 2007.